

Universidade do Minho  
Escola de Engenharia

Ângelo Rafael Gomes de Araújo

Experimental procedures for the identification  
of material properties of intervertebral  
disc - a contribution for the development  
of biomimetic substitutes for the nucleus  
pulposus



Universidade do Minho  
Escola de Engenharia

Ângelo Rafael Gomes de Araújo

Experimental procedures for the identification  
of material properties of intervertebral  
disc - a contribution for the development  
of biomimetic substitutes for the nucleus  
pulposus

Tese de Doutoramento  
Programa Doutoral em Engenharia Mecânica

Trabalho efectuado sob a orientação de  
Professor Doutor Nuno Ricardo Maia Peixinho  
Professor Doutor António Costa Marques Pinho

Ângelo Rafael Gomes de Araújo

**Título da tese**

Experimental procedures for the identification of material properties of intervertebral disc - a contribution for the development of biomimetic substitutes for the nucleus pulposus

**Orientadores**

Professor Doutor Nuno Ricardo Maia Peixinho

Professor Doutor António Costa Marques Pinho

**Ano de conclusão**

2015

**Designação do Doutoramento:**

Programa Doutoral em Engenharia Mecânica

É AUTORIZADA A REPRODUÇÃO INTEGRAL DESTA TESE APENAS PARA EFEITOS DE INVESTIGAÇÃO, MEDIANTE DECLARAÇÃO ESCRITA DO INTERESSADO, QUE A TAL SE COMPROMETE.

Universidade do Minho, 28 de Outubro de 2015

Assinatura: \_\_\_\_\_

## STATEMENT OF INTEGRITY

I hereby declare having conducted my thesis with integrity. I confirm that I have not used plagiarism or any form of falsification of results in the process of the thesis elaboration.

I further declare that I have fully acknowledged the Code of Ethical Conduct of the University of Minho.

University of Minho, \_\_\_\_\_

Full name: Ângelo Rafael Gomes de Araújo

Signature: \_\_\_\_\_



“For the ones who are always here”



## ACKNOWLEDGEMENTS

The process of earning a doctorate and writing a dissertation is a long and hard journey. During this time, moments of joy are sprinkled with some reluctance. In fact, a project like this could not be done singlehandedly. First and foremost, I have to say a huge thanks to all my supervisors, namely to Prof. Nuno Peixinho and Prof. Marques Pinho for all the meaningful advices and insightful discussions about the intricacies of the experimental testing. You were always present when I need and your technical and practical suggestions were essential for my doctorate. In fact, you were great supervisors.

I also need to say a big thanks to Prof. Pimenta Claro for all the important considerations about the work, as well as the continuous presence, support and good mood during this period. Even though you were not my official supervisor, I consider you as so. You were definitely a key-person for the accomplishment of my experimental work.

To professors Paulo Flores and Luis Alves I also want to thank the availability and gentleness given when I needed some technical advices. P.S. I am pretty sure Paulo Flores is today a little bit more “red” than four years ago.

I also want to express my gratitude to all the members of NP Mimetic Project, for the technical discussions and the meetings that helped me to perform the experimental tests. I also want to express my gratitude to *Indústria de Carnes do Minho (ICM) - Primor Group* - for the possibility of collecting spine column samples in their facilities and to all the University’s technicians that helped in the experimental testing.

To all CT2M and non-CT2M researchers and the people I worked/meet during this period, I have to definitely thank for all the good mood and atmosphere. Together with you, these four years were undoubtedly full of unforgettable moments, moments I will carry with me forever. It



was an indescribable pleasure to work/meet all of you. You guys definitely belong to one of the most remarkable chapters of my life. You know who you are and what I am talking about.

“Last but not the least”, I would like to thank all my family and friends for all the patience, support and strength they gave me, especially in the hardest moments. I know you are not here for today or tomorrow, but for my entire life. A special thanks to my sister Daniela and to my parents, Maria and António. They were undoubtedly the best emotional support during this period. To them I have to thank for all the patience, care and energy and, in the worst moments, for push my forward. I do not have words to describe what you represent for me.

Thank you very much to all of you. I hope to count on you for the rest of my life, wishing you all the best!

## ABSTRACT

The degenerative disc disease is among the promoters of low back pain, being normally associated with sciatica and disc herniation. Several experimental works have studied the intervertebral disc and proven that it presents poroelastic, osmotic, viscoelastic and anisotropic characteristics. However, the information about the mechanical loading on the IVD and its relation with the degenerative disc disease remains unclear.

This work aimed to provide new insights about the mechanical properties of the intervertebral disc, as well as to contribute for selection and characterization of a new implant, developed by research partners at Nicast®, Lod, Israel. In order to better understand the biomechanical behavior of the intervertebral disc, a new set of experimental techniques for mechanical characterization, mechanical testing protocols and benchmark results that allows establishing specifications for the new nucleus pulposus implants were addressed and performed. The experimental approach included mechanical tests in the overall structure of a porcine intervertebral disc: axial compressive tests at the motion segment (composed by the two adjacent vertebrae and the intervertebral disc) and annulus fibrosus level, as well as pressurization tests on nucleus pulposus. Moreover, it comprised several tests for the selection and mechanical characterization of the developed implant.

The outcomes demonstrated that porcine motion segments are valid model to provide valuable information about the mechanical behavior of the human intervertebral disc, for the axial compressive tests. This study also proved that the rupture of the intervertebral disc could be reached at intradiscal pressure levels that are normally reported as physiological. Moreover, the compressive tests on the reinforced-ground matrix of the annulus fibrosus strengthened the idea, previous reported in the literature, that this structure presents an inhomogeneous behavior. Finally, the implant as revealed to have a satisfactory behavior under the set of experimental tests performed: while the *ex-situ* tests revealed promising characteristics in what concerns to the

capacity to replace the nucleus pulposus, the stress relaxation tests *in-situ*, performed during the placement of the implants in the nuclear cavity of the motion segment, revealed no significant differences between the behavior of intact structures and the ones with the implants placed in the inner region of the intervertebral disc.

The intervertebral disc is an intricate structure, with a “multi-factors dependent” biomechanical behavior, being extremely hard to design an efficient solution to replace its damaged structures. The experimental procedures of this work gave valuable information about the mechanical properties of the intervertebral disc, contributing for the advance of the knowledge on the biomechanics of its compounds. Furthermore, it helps to clarify the suitability of the new developed implant in the partial replacement of the damaged intervertebral disc.

## RESUMO

A doença degenerativa do disco intervertebral é uma das principais causas de dor lombar, estando intimamente associada à dor ciática e à herniação discal. Nos últimos anos têm sido realizados diversos trabalhos experimentais, os quais demonstraram que o disco apresenta características poro-elásticas, viscoelásticas e anisotrópicas. No entanto, a relação entre as cargas aplicadas no disco intervertebral e a degeneração do disco intervertebral não é clara.

Este trabalho tem por objectivo providenciar informação relevante sobre as propriedades mecânicas do disco intervertebral, bem como contribuir para a seleção e caracterização de um novo implante, desenvolvido pela Nicast®, localizada em Lod, Israel - associado ao projeto no qual este trabalho se inseriu, o NP Mimetic. Para tal, no âmbito deste trabalho foram desenvolvidas e produzidas protocolos e técnicas experimentais para a caracterização mecânica e material, tendo sido obtidos valores *standard* importantes, que permitem, por um lado, o melhor conhecimento sobre o comportamento biomecânico do disco intervertebral, e por outro lado, definir as especificações relevantes para novos implantes de substituição do núcleo pulposo. A abordagem experimental incluiu testes mecânicos na estrutura do disco intervertebral de suínos, nomeadamente testes de compressão axial em unidades funcionais da coluna, constituídas por um disco intervertebral entre duas vértebras adjacentes, e no anel fibroso, bem como testes de pressurização na cavidade nuclear do disco. Além disso, este trabalho apresenta ainda diversos testes complementares para a seleção, caracterização e validação mecânica do implante desenvolvido.

Os resultados obtidos demonstraram que as unidades funcionais da coluna de suínos apresentam-se como um modelo válido para a obtenção de informações relevantes sobre o comportamento mecânico do disco intervertebral humano, em testes de compressão. Este trabalho mostrou ainda que a rotura do disco intervertebral pode ser atingida para valores de pressão interna discal que são normalmente considerados como fisiológicos. No que diz respeito

aos testes de compressão estática e dinâmica na matriz do anel fibroso, estes reforçaram a ideia previamente descrita na literatura, de que esta estrutura apresenta um comportamento não-homogêneo. Por último, os implantes apresentaram um comportamento muito satisfatório nos testes a que foram submetidos: enquanto os testes de avaliação do implante *ex-situ* revelaram características bastante promissoras no que concerne à capacidade de substituição do núcleo, os testes de relaxação de tensões *in-situ*, realizados aquando da colocação dos implantes na cavidade nuclear das unidades funcionais da coluna, revelaram a inexistência de diferenças significativas entre o comportamento dessas mesmas estruturas antes e após a colocação do implante na cavidade nuclear.

O disco intervertebral é uma estrutura intrincada, apresentando um comportamento biomecânico de dependência multifactorial. Como tal, o desenvolvimento de implantes que possam substituir total ou parcialmente o disco intervertebral degenerado é uma tarefa de elevada complexidade. Este trabalho providencia um conjunto de dados relevantes sobre a resposta mecânica dos discos intervertebrais, contribuindo para o avanço do conhecimento do comportamento biomecânico dos seus componentes. Mais ainda, permite clarificar a adequabilidade de um novo implante na substituição do núcleo pulposo do disco intervertebral.

# INDEX

<b>Acknowledgements</b> .....	iii
<b>Abstract</b> .....	v
<b>Resumo</b> .....	vii
<b>Index</b> .....	ix
<b>List of Figures</b> .....	xv
<b>List of Tables</b> .....	xxiii
<b>Nomenclature</b> .....	xxvii
<b>List of Acronyms</b> .....	xxx
<b>1. INTRODUCTION</b> .....	<b>1</b>
1.1. Motivation.....	1
1.2. Objectives.....	4
1.2.1. Contributions .....	5
1.3. Thesis Structure.....	6
<b>2. THE SPINE AND THE INTERVERTEBRAL DISC</b> .....	<b>9</b>
2.1. Anatomy and Function of the Spine Column .....	9
2.2. Anatomy, Function and Physiology of the Intervertebral Disc .....	12
2.2.1. Nucleus Pulposus .....	12
2.2.2. Annulus Fibrosus .....	13
2.2.3. Cartilaginous Endplate .....	15
2.3. Disc Biomechanics .....	17
2.3.1. Nucleus Pulposus Mechanics .....	18

2.3.2. Annulus Fibrosus Mechanics .....	22
2.3.3. Motion Segment Mechanics .....	26
2.3.4. The Internal Disc Pressure .....	28
2.3.5. Relation between Internal Disc Pressure and External Loading .....	30
2.3.6. Annular Failure Strength due to Internal Disc Pressure.....	34
2.4. Disc Degeneration.....	37
2.4.1. Nutrient Failure on Intervertebral Disc .....	38
2.4.2. Genetic Factors.....	38
2.4.3. Mechanical Factors.....	39
2.5. Disc Treatment .....	41
2.5.1. Discectomy/Arthrodesis (or Fusion).....	41
2.5.2. Intervertebral Disc Replacement.....	42
<b>3. EFFECT OF QUASI-STATIC AND CYCLIC COMPRESSIVE LOADING ON THE MECHANICAL RESPONSE OF PORCINE INTERVERTEBRAL DISCS .....</b>	<b>51</b>
3.1. Introduction .....	51
3.2. Materials and Methods.....	54
3.2.1. Motion Segment Collection and Preparation.....	54
3.2.2. Testing Equipment and Motion Segment Positioning.....	54
3.2.3. Quasi-Static Axial Compressive Test.....	55
3.2.4. Cyclic Compressive Tests.....	56
3.2.5. Five-Parameter Rheological Model for Creep Response Analysis.....	56
3.3. Results .....	58
3.4. Discussion .....	62
<b>4. MECHANICAL AND STRUCTURAL RESPONSE OF THE INTERVERTEBRAL DISC TO ALTERATIONS IN THE INTERNAL DISC PRESSURE: AN EXPERIMENTAL APPROACH ...</b>	<b>69</b>
4.1. Introduction .....	69

4.2. Materials and Methods.....	72
4.2.1. Motion Segment Collection and Preservation .....	72
4.2.2. Configuration of the Pressurization Apparatus to Assess the Effect of the Intradiscal Pressure Increment on the Load Relaxation Rate .....	72
4.2.3. Pressurization Apparatus used to determine the Failure Intradiscal Pressure .....	74
4.2.4. Motion Segment Attachment .....	75
4.2.5. Experimental Procedure .....	77
4.2.6. Statistical Analysis.....	79
4.3. Results .....	80
4.3.1. Visual Inspection of a Pressurized Motion Segment.....	80
4.3.2. Comparison between Relaxation Rates at different Internal Disc Pressures .....	80
4.3.3. Failure Pressure on the Motion Segment .....	82
4.4. Discussion of the Effect of the Intradiscal Pressure on the Mechanical Behavior of the Intervertebral Disc.....	86
4.4.1. Relation between the External Loads applied on Motion Segment and the Intradiscal Pressure .....	86
4.4.2. Failure Strength on the Intervertebral Disc due to Disc Inflation .....	88
<b>5. UNIAXIAL COMPRESSIVE LOADING RESPONSE OF THE PORCINE ANNULUS FIBROSUS: A REINFORCED-GROUND MATRIX STUDY .....</b>	<b>91</b>
5.1. Introduction .....	91
5.2. Materials and Methods.....	95
5.2.1. Motion Segment Collection and Preservation .....	95
5.2.2. Specimens Preparation .....	95
5.2.3. Uniaxial Static Compressive Test .....	96
5.2.4. Dynamic Mechanical Testing.....	99
5.2.5. Data Analysis .....	102
5.3. Results .....	103



5.3.1. Uniaxial Compressive Loading.....	103
5.3.2. Dynamic Mechanical Testing.....	106
5.4. Discussion of Regional Variations on the Mechanical Behavior of the Annulus Fibrosus in both Static and Dynamic Conditions .....	112
5.4.1. Static Uniaxial Compressive Tests .....	113
5.4.2. Dynamic Mechanical Testing.....	116
<b>6. SELECTION AND CHARACTERIZATION OF A NEW ENCAPSULATED HYDROGEL FOR NUCLEUS PULPOSUS REPLACEMENT.....</b>	<b>121</b>
6.1. Introduction .....	121
<b>A. Complementary Tests for the Selection of the Geometrical Characteristics of the Implant.....</b>	<b>127</b>
6.2. Methods .....	127
6.2.1. Analysis of the “Ravioli’s” Free-Swelling.....	128
6.2.2. Axial Quasi-Static Compressive Tests .....	128
6.2.3. Biaxial Tensile Tests.....	130
6.3. Results .....	131
6.3.1. “Ravioli’s” Free-Swelling Analysis .....	131
6.3.2. Quasi-Static Axial Compressive Tests .....	132
6.3.3. Biaxial Tensile Tests.....	134
6.4. Discussion on the Experimental Results for the Selection of the Geometrical Characteristics of the “Ravioli” .....	135
<b>B. Assessment of the Mechanical and Material Parameters of the Final “Ravioli” Configuration .....</b>	<b>137</b>
6.5. Methods .....	137
6.5.1. Uniaxial Tensile Testing.....	137
6.5.2. Cyclic Compression Tests and Percentage of Water Retention.....	138

6.5.3. Stress Relaxation Tests .....	140
6.6. Results .....	144
6.6.1. Uniaxial Tensile Testing of the “Envelope” .....	144
6.6.2. Cyclic Compression Tests and Percentage of Water Retention.....	146
6.6.3. Stress Relaxation Tests .....	147
6.7. Discussion of the Mechanical and Material Parameters of the Final “Ravioli” Configuration .....	149
<b>7. EFFECT OF THE IMPLANT INSERTION ON A MOTION SEGMENT: A LOAD RELAXATION STUDY .....</b>	<b>153</b>
7.1. Introduction .....	153
7.2. Methods .....	156
7.2.1. Motion Segment Collection and Preparation.....	156
7.2.2. Method for Insertion of the Implant on the Nucleus Pulposus Cavity.....	156
7.2.3. Testing Equipment and Motion Segment Positioning. ....	158
7.2.4. Uniaxial Compressive Relaxation Tests .....	159
7.2.5. Data Analysis .....	160
7.2.6. Statistical Analysis.....	162
7.3. Results .....	163
7.4. Discussion of the Effect of the Implant Insertion on a Motion Segment in terms of Load Relaxation.....	167
<b>8. GENERAL CONCLUSIONS .....</b>	<b>173</b>
8.1. Concluding Remarks .....	173
8.2. Future Works and Recommendations .....	178
<b>BIBLIOGRAPHY.....</b>	<b>181</b>
<b>ANNEXES .....</b>	<b>203</b>

Annex A: Calculation of the constants of the Table 2.4.....	203
Annex B: The engineering drawings for the testing devices that were designed and manufactured to carry out the experimental testing detailed in Chapter 4.....	206
Annex C: The material and mechanical characteristics of the “Ravioli”, provided by the manufacturer - Nicast Ltd.).....	212
Annex D: Publications and Communications.....	214

## LIST OF FIGURES

Figure 1.1. The structure of the IVD is composed by a layered structure, the Annulus Fibrosus, limited by the two Cartilaginous Endplates at the top and bottom and a gelatinous core in its center, the Nucleus Pulposus.....	2
Figure 2.1. Lateral view of spine column, with its different regions. ....	10
Figure 2.2. Fibres orientation in the annulus fibrosus. Adapted from Neumann et al. (2010). ...	14
Figure 2.3. Representation of the relative position and the compositional features of the NP, AF and CEP in healthy IVDs. The black arrows indicate the nutrition pathways. ....	16
Figure 2.4. Typical stress-strain curve for AF, under uniaxial tensile tests, where $E_{toe}$ represents toe-region modulus; $E_{lin}$ is linear region modulus; $\epsilon^*$ represents transition point and $E_y$ represents yield point (adapted from (Nerurkar et al., 2010)). ....	23
Figure 2.5. Representation of the motion segment preparation. This structure is highlighted by the dashed rectangle. To obtain a motion segment, two vertebrae are cut parallel and transversely, obtaining an assemble composed by two half vertebra with a disc in between.....	27
Figure 2.6. Intradiscal pressure (IDP) exerted by the NP is omnidirectional and varies with applied load.....	28
Figure 2.7. Schematic representation of the pressure transducer used by Wilke et al. (1999)...	32
Figure 2.8. Schematic representation of the system used to inject coloured hydrogel on NP, via vertebrae (adopted from Schechtman et al. (2005)). ....	35

Figure 2.9. Test performed by Menkowitz et al. (2005). During the pressurization test, the structure was not confined or axially loaded. .... 35

Figure 3.1. Generic example of the quasi-static axial compressive test input, used for the disc 1. .... 55

Figure 3.2. Linear regression performed in a motion segment sample, at a load rate of 16 mm/min, for a 0-50 N increment. The slope of this regression represents the static stiffness coefficient,  $K_s$ , which is defined as the slope of each loading increment (from both 0-50 N and 50-500 N increments). .... 58

Figure 3.3. Bar chart representing the  $K_s$  for two different strain rates: 4 mm/min and 16 mm/min. Two different phases were also distinguished: phase 1 represents the  $K_s$  for the increasing from 0 until the pre-load (50 N), while phase 2 represents the increasing of load until reaching 500 N, for the two strain rates. .... 59

Figure 3.4. Comparison between the creep responses of the experimental obtained with PLIVD and the five parameter rheological model. The values were fit by the inferior and superior limits, with a confidence interval of 95%. .... 60

Figure 4.1. Schematic representation of pressure apparatus, containing: SP - Pressurized air source; RV - Balancing valve; M - Manometer; PC - Pneumatic cylinder; HC – Hydraulic cylinder; T - Tap; SB - Spherical axial bearing; ER – Epoxy resin; MS - Motion segment. .... 73

Figure 4.2. Schematic representation of the pressurization apparatus ( above) and the real image of the failure pressure tester without coupling the motion segment (below). The apparatus is composed by: SB - Spherical Axial Bearing; ER – Epoxy resin; MS - Motion Segment; CPU – Personal Computer; DM – Digital Manometer; T – Tap; HC – Hydraulic cylinder (with manual pump); FE – Fluid Entrance; SSB – Stainless steel basis. .... 74

Figure 4.3. Motion segment attachment. A) The MS was placed between two plates of Instron® 8874, being subjected to compression. The bottom plate is drilled, allowing the fluid passage from pressure apparatus to the hollowed screw. The attachment is done on epoxy resin (yellow region), to provide a better adhesion of the screw; B) Top vision of a drilled MS, with the presence of the self-tapping screw on the vertebral body. .... 77

Figure 4.4. Input used to assess the behavior of IVD under a set  $\Delta$ IDP. The blue line characterizes the displacement imposed to each IVD. The green line represents an approximation of the pressure increments (in steps of 0.1 MPa) applied on the disc, at each 5 minutes of loading. .... 77

Figure 4.5. Images of MS sawed transversally after testing. It is visible the presence of a cavity in the NP region, indicating the pressurizing zone. .... 80

Figure 4.6. Graphical representation of the mechanical test obtained with the present setup. The blue line represents the relaxation curve for a representative sample (MS 1). The red line represents the time of duration of each  $\Delta$ IDP (with steps of 0.1 MPa). In addition, it is visible a slight peak of load at each IDP change. .... 81

Figure 4.7. Absolute mean of relaxation rate for discs (n=5) for the range of  $\Delta$ IDP monitored during the relaxation test and for the control (n=2). The  $\Delta$ 1,  $\Delta$ 2,  $\Delta$ 3 and  $\Delta$ 4 represent the relaxation rate after each the  $\Delta$ IDP (0-0.1 MPa, 0.1-0.2 MPa, 0.2-0.3 MPa, 0.3-0.4 MPa, respectively). C1, C2, C3 and C4 represent the control test for the same period of testing time for the samples after each  $\Delta$ IDP. The error bars represent the standard deviation. .... 82

Figure 4.8. An example of the MS response after the insertion of an IDP magnitude that leads to IVD rupture (in MPa), as function of Time (in seconds). .... 83

Figure 4.9. Representative images of different configurations of failure in motion segments, during the inflation procedure. A) Leakage of fluids from the annular region. Two motion segments failed in this manner. B) Severe leakage around the screw region in the vertebrae

(bottom vertebrae) and in the annular region; slight leakage around the spinal cord (fluid outflowing from the spinal cord channel). One motion segment failed in this manner. C) Moderate leakage around the screwed region in the vertebrae (bottom vertebrae). Two motion segments failed in this manner. D) Little tears formed on the top and bottom parts of annular region (cartilaginous endplate region). One motion segment failed in this manner. .... 85

Figure 5.1. Schematic representation of the process of specimen preparation. A) An intervertebral disc was sectioned and isolated from the lumbar porcine spine. On each sectioned IVD, four regions were clearly defined (posterior, anterior, lateral left and lateral right). B) Six cylindrical samples, with 5 mm diameter, were taken from each region of the isolated porcine IVDs; C) Both CEPs, from bottom and upper region of the IVD were removed, avoiding the fibres linkage between the superior and the inferior CEP. The testing samples presented a variable height, depending on AF region..... 96

Figure 5.2. Submersible compression plates. It allows placing a continuous hydration state on a sample while a compression test is performed. The sample (light grey) is placed on the bottom compression plate and it is possible to submerge the sample with a fluid. .... 100

Figure 5.3. Regression curves of engineering stress-strain of the RGM under uniaxial compressive loading, for initial test (Cycle 1) and for the subsequent tests (Cycles 2-5). The four graphs represent the four distinct regions sectioned in the AF: A) Anterior; B) Posterior; C) Lateral Right; D) Lateral Left; E) Global response of the AF regions. .... 105

Figure 5.4. Static compressive modulus ( $E_s$ , in MPa) for the each RGM region. This parameter was obtained dividing the engineering stress by the engineering strain, for the linear region of the stress-strain curve - from 0 to 15% of strain. .... 106

Figure 5.5. Dynamic mechanical properties (mean  $\pm$  S.D.) for the different annular regions (anterior, left, right and posterior), at three different frequencies: 1, 5 and 10 Hz. A) Storage modulus; B) Loss modulus; C) Internal friction ( $\tan \delta$ ) and D) Dynamic compressive modulus. 107

Figure 5.6. Percentage of water loss (mean  $\pm$  S.D.) immediately after test and after 24 hours, for all the RGM regions (Posterior, Left, Anterior and Right)..... 111

Figure 6.1. A) The swelled “Raviolis”; B) The schematic representation of the “Ravioli”: on the left, the upper view; on the right, the side view. .... 123

Figure 6.2. On the left side, due to the folding of the “Ravioli” ring (detail highlighted with a circle), the strictly confined compressive test configuration cannot be achieved; on the right, the unconfined compressive test configuration. .... 125

Figure 6.A.1. Images used for the determination of the volume variation of “Ravioli”. A) The “non-expanded” configuration, previous to fluid contact. B) The expanded configuration, after 24 hours of swelling. .... 128

Figure 6.A.2. Direction of load for the two different load tests performed on the “Raviolis”: A) “Parallel” test; B) “Perpendicular” test..... 129

Figure 6.A.3. Schematic representation for “Envelope” geometry used on biaxial tensile testing, with a highlight of a generic “Envelope” sample placed on the testing machine. .... 130

Figure 6.A.4. Compressive stress-strain curve for four implants (two Rav<sub>1</sub> and two Rav<sub>2</sub>) tested on the parallel and perpendicular configuration. The engineering stress was obtained by dividing the force applied by the initial contact area of “Ravioli”. The engineering strain was given by  $(l-L)/L$ , where L is the initial length and l is the final length of the sample. During this test, the displacement speed was set to 4 mm/min..... 133

Figure 6.A.5. The rupture zone in the “Ravioli”, corresponding to the “normal plane” of the ring region..... 133

Figure 6.A.6. Graphical representation of the results from biaxial tests for each “Envelope” sample (Env<sub>1</sub> and Env<sub>2</sub>). The “Envelope” behaviour was described in two axes of tensile strength:



axis 1 and axis 2. The nominal stress was obtained by dividing the force applied by the initial contact area of “Ravioli”. The engineering strain was given by  $(l-L)/L$ , where L is the initial length and l is the final length of the sample. During this test, the speed the displacement was set to 5 mm/min. .... 134

Figure 6.B.1. Uniaxial tensile test where the  $l$  is the length of the smaller side and the red arrow represents the direction of the “Envelope ‘s” stretch. .... 138

Figure 6.B.2. Cyclic test performed on “Raviolis” (n=4). The curve represents the strain as function of time (in seconds). The positive signal of the engineering strain indicates the direction of load in axial compression..... 139

Figure 6.B.3. Implant tested in the acrylate cubic tank, in hydrated conditions. .... 141

Figure 6.B.4. A) Motion segment mesh; B) Swelled implant mesh. Note: Images not scaled... 143

Figure 6.B.5. Linear regression of the contact area ( $R^2=0.99$ ) as function of the “Ravioli’s” height for a 9 mm diameter implant. This data was determined by a FEM model of “Ravioli”, produced by the CT2M researchers..... 143

Figure 6.B.6. Curves of force (N) as function of the sample elongation (in mm) for both manufacturer (Nicast) and this work (CT2M), truncated at 5 mm elongation. .... 144

Figure 6.B.7. Curves of the nominal stress of the “Envelopes”, in MPa, as function of the engineering strain, for both manufacturer (Nicast) and CT2M work. .... 145

Figure 6.B.8. Load vs time curve of the five loading-unloading cycles for the four “Raviolis” used on the study. .... 146

Figure 6.B.9. A generic example of the experimental curve of the true stress as function of the engineering strain (Rav\_1\_Exp) and the model adjust (Rav\_1\_Sim), with  $R^2 = 0.98$ . .... 147

Figure 7.1. Schematic representation of the setup adopted to perform the mechanical test on the RMS (n=5): A) The motion segment was taken from the lumbar region of a porcine sample; B) After drill a hole in the top of the vertebra and CEP and removing of a prescribed amount of NP, a “Ravioli” in its initial configuration (dried) was inserted in the nuclear cavity using an appropriate rod; C) A cork plug (brown color) was placed in the vertebral hole to retain the “Ravioli” in the NP cavity and silicon (red color) was used on the top of MS to stick it to vertebrae. Moreover, the whole structure was immersed in PBS (blue color in the image) during four hours, to allow the complete swelling of the hydrogel; D) Finally, the MS was placed on the mechanical tester, the Instron® 8874, after suffer a 180° rotation on the sagittal plane, to avoid the collapse of the cork structure. During the axial compressive mechanical test the IVD remained submersed in PBS to allow the “Ravioli” expansion. The control samples were tested in same configuration as the RMS (n=4). ..... 158

Figure 7.2. Load relaxation test input. A displacement of 1 mm at a strain rate of 0.033 s<sup>-1</sup> was imposed to all samples – CMSs and RMSs..... 160

Figure 7.3. Mean value of the coefficient of stiffness ( $K_s$ ), in Newton per meter, for both CMS and RMS..... 164

Figure 7.4. Load-relaxation curves for the experimental tests (green line) and the exponential model adopted (orange line), for a representative sample of both CMS and RMS. .... 165



## LIST OF TABLES

Table 2.1. Vertebral column sections, its constitution and body area.....	9
Table 2.2. Resume of major structural differences among cervical, thoracic, and lumbar region (Adopted from Tortora & Derrickson 2008).....	11
Table 2.3. The type of NP modification and the main findings by author. ....	19
Table 2.4. Summary of native tissue viscoelastic benchmarks related to mechanics of the NP. Legend: $G^*$ = complex shear modulus; $\delta$ = phase shift angle; $E'$ = Storage modulus; $E''$ = Loss modulus; $Tan \delta$ = Coefficient of friction; $WC$ = Water Content; $H_{AO}$ = Aggregate Modulus; $K0$ = Zero-strain permeability; $E_s$ = Static Compressive Modulus; $E_{toe}$ = Toe modulus; $\nu$ = Poisson's Ratio; $K_d$ = Dynamic Stiffness; $DC$ = Damping capacity.....	20
Table 2.5. Summary of native tissue viscoelastic benchmarks related to mechanics of the multi-lamellae AF - adopted from Nerurkar et al. (2010). Legend: $\theta$ indicates angle relative to the prevailing collagen orientation; $z$ , $y$ and $r$ indicate the loading axes along the disc circumferential, axial, and radial directions, respectively. The remaining constants were already described in Table 2.4. ....	25
Table 2.6. Previous studies reporting the IDP according to the type of load/posture adopted, for human IVDs. ....	31
Table 2.7. Surgical approach and the FDA approval for four types of lumbar TDR designs. ....	43
Table 2.8. Clinical features of NPR solutions tested in human.....	47

Table 3.1. Experimental dynamic stiffness coefficient ( $K_d$ ), obtained in this study PLIVDs (n=5; mean and standard deviation), and HLIVDs  $K_d$  (mean) found in a previous study performed by Li et al., (1995), at 1 Hz. .... 59

Table 3.2. Comparison between model parameters obtained with the best fit to the experimental results with PLIVDs (mean, inferior and superior limit with a confidence interval of 95%) and the values obtained by O'Connell et al. (2011) for HLIVDs (mean and interquartile range)..... 61

Table 3.3. Comparison between  $K_s$  and the maximum load applied on HLIVD (obtained in previous studies) and PLIVD (present study). .... 63

Table 4.1. Maximum compressive strain for each MS (n=5). The maximum strain is given by the absolute value of the ratio between the maximum change in disc length during the compressive loading and the original length. .... 80

Table 4.2. Standard deviation (SD) and the coefficient of variation (CV) for each IDP increment.82

Table 4.3. Intradiscal failure pressure (maximum in the curve IDP vs time) for the six motion segments that presents external indicators of rupture, such as sudden pressure drop, leakage in the vertebra region or in spinal cord (fluid outflowing from the spinal cord channel) or tears formed in the annular region or also in the top and bottom parts of annular region (cartilaginous endplate region). .... 84

Table 4.4. Recent data about the failure pressure data for different IVD models. .... 88

Table 5.1. Parameters of the best fit of the cubic polynomial function to the experimental data, including the standard error of the estimate. .... 104

Table 5.2. Differences between each region for each viscoelastic parameter ( $E'$ ,  $E''$ ,  $\tan\delta$  and  $E_d$ ), according to the frequency, determined by the *p-value* of the ANOVA tests. .... 108

Table 5.3. <i>P-values</i> determined with <i>t-student</i> test by the comparison of each region with the remaining ones for each viscoelastic parameter, according with frequency.....	109
Table 5.4. The differences between the viscoelastic parameters ( $E'$ , $E''$ , $\tan\delta$ and $E_d$ ) for the different annular regions with the frequency, determined by the <i>p-value</i> of the ANOVA tests. ..	110
Table 5.5. Comparison between previous experimental findings and the results of the current work.....	114
Table 5.6. Statistical analysis and comparison between the values of viscoelastic parameters for a specific and the remaining RGM regions, according with <i>p-value</i> (significant level of 0.05). The “lowest” and “highest” words indicate that a particular region presents the lowest or the highest values of a defined parameter, at an indicated frequency (n=20). .....	118
Table 6.A.1. Characteristics of the “pre-swelled Raviolis” used on preliminary tests.....	127
Table 6.A.2. The expansion ratio (ratio between swelled and non-swelled configuration) in terms of both volume and weight, for “Raviolis” with two different “Envelope” thickness (n=3).....	131
Table 6.B.1. The static stiffness coefficient, $K_s$ (in N/mm), obtained for the Env <sub>2</sub> by both Nicast Ltd. and CT2M. ....	145
Table 6.B.2. Young modulus of the “Envelopes”, ( $E$ , in MPa) obtained by the Nicast Ltd. and CT2M for the Env <sub>2</sub> , in static conditions.....	146
Table 6.B.3. Percentage of water retention (%WC) for all the samples tested, including the mean and the standard deviation (mean $\pm$ S.D.) .....	147
Table 6.B.4. Mean and (standard deviation) for the unconfined compression equilibrium properties of the NP and several HA-based hydrogels solutions (Cloyd et al., 2007) as well as for the “Ravioli” (this study). .....	148

Table 7.1. Coefficient of stiffness ( $K_s$ , in Newton per meter) for the CMS and RMS, and the presence or absence of “Ravioli” swelling in the nuclear cavity of MS (“Yes” when it reached the minimum swelling, “No” for the cases where “Ravioli” did not expanded). Note: “N.A.” means “Not Applicable” ..... 164

Table 7.2. Relaxation parameters (mean  $\pm$  standard deviation)..... 166

## NOMENCLATURE

Aggregate modulus.....	$H_{AO}$
Applied load .....	$F$
Complex shear modulus .....	$ G^* $
Compressive displacement .....	$d$
Damping capacity.....	$DC$
Dynamic compressive modulus.....	$E_d$
Dynamic stiffness coefficient.....	$K_d$
Elapsed time .....	$t$
Engineering stress .....	$\sigma$
Engineering strain.....	$\varepsilon$
Equilibrium stress.....	$\sigma_e$
Fast constant rate.....	$R_f$
Fast response constant.....	$\tau_f$
“Fast” half-life value.....	$t_{f\frac{1}{2}}$
Final height of the sample.....	$l$
Final weight.....	$W_f$
Fraction of the span.....	$S$



Internal friction .....	$Q^{-1}$
Initial load .....	$F_0$
Initial weight .....	$W_i$
Linear region .....	$E_{lin}$
Load at the end of time.....	$F_{\infty}$
Loss modulus .....	$E''$
Original sample height.....	$L$
Parameters of elastic response of the IVD under loading.....	$S_E$
Parameters of fast response of the IVD under loading.....	$S_1$ and $\tau_1$
Parameters of slow response of the IVD under loading.....	$S_2$ and $\tau_2$
Peak stress.....	$\sigma_p$
Percentage of relaxation.....	$\%R$
Percentage of water content.....	$\%WC$
Permeability .....	$K_0$
Phase shift angle.....	$\delta$
Poisson's ratio.....	$\nu$
Slow constant rate .....	$R_s$
"Slow" half-life value .....	$t_{s^{1/2}}$
Slow response constant .....	$\tau_s$
Standard deviation.....	$S. D.$
Static compressive modulus .....	$E_s$

Storage modulus .....  $E'$

Toe modulus region .....  $E_{toe}$

Transition point.....  $\epsilon^*$

True stress .....  $\sigma_t$

Water content .....  $WC$

Yield point .....  $E_y$

## LIST OF ACRONYMS

Annulus Fibrosus.....	AF
Cartilaginous Endplate.....	CEP
Coefficient of Variation.....	CV
Complex “Ravioli” – Motion Segment.....	RMS
Degenerative Disc Disease.....	DDD
Dynamic Mechanical Analysis.....	DMA
Finite Element Model.....	FEM
Human Lumbar Intervertebral Disc.....	HLIVD
Intact Motion Segment (Control).....	CMS
Intervertebral Disc.....	IVD
Intradiscal Pressure.....	IDP
Intradiscal Pressure Increment.....	$\Delta$ IDP
Motion Segment.....	MS
Nucleus Pulposus.....	NP
Nucleus Pulposus Replacement.....	NPR
Phosphate Buffer Saline.....	PBS
Porcine Lumbar Intervertebral Disc.....	PLIVD
Prosthetic Disc Nucleus.....	PDN

Reinforced-Ground Matrix..... RGM

Standard Deviation ..... SD

Total Disc Replacement ..... TDR

Ultra-High Molecular Weight Polyethylene..... UHMWPE



# 1. Introduction

*This first chapter aims to describe the motivation as well as to define the main objectives and the major contributions of this work. Furthermore, the structure of the thesis is described in detail.*

## 1.1. Motivation

Back pain is widespread in developed societies, with 80% of world population being affected at some point of their lives (Gregory, 2009). In Portugal, it represents one of most common musculoskeletal disorders, occurring in 72.4% of population. Among these cases, 70% of the complaints are related to low back pain, i.e., the lumbar region ache. The low back pain is the reason why around 420.000 Portuguese people are forced to work absent, being the main cause of the attribution of pensions due to disability<sup>i</sup>. Thus, it represents a severe economic problem, which needs to be urgently solved or, at least, minimized. The low back pain could be caused by several etiologies, such as aging, genetic factors, lack of nutrition or overloading on the intervertebral disc (IVD) (Shiri et al., 2010).

The IVD is a complex structure being composed by a layered structure - the annulus fibrosus (AF) - limited by cartilaginous endplates (CEP) at the top and bottom. Both structures surround and confine a soft, elastic and gelatinous core, the nucleus pulposus – NP (Nerurkar et al., 2010; Shankar et al., 2009) - Figure 1.1. While NP is not innervated, the AF and the CEP are only superficially innervated; however, an injury on these structures could induce pain (van der Veen, 2009).

---

<sup>i</sup> A study performed by the “Sociedade Portuguesa de Patologia da Coluna (SPPCV)”, “Sociedade Portuguesa de Ortopedia e Traumatologia (SPOT) and “Sociedade Portuguesa de Neurocirurgia (SPNC)”. More information in: [http://www.in.pt/Paginalnicial/Sociedade/Interior.aspx?content\\_id=1390915](http://www.in.pt/Paginalnicial/Sociedade/Interior.aspx?content_id=1390915)

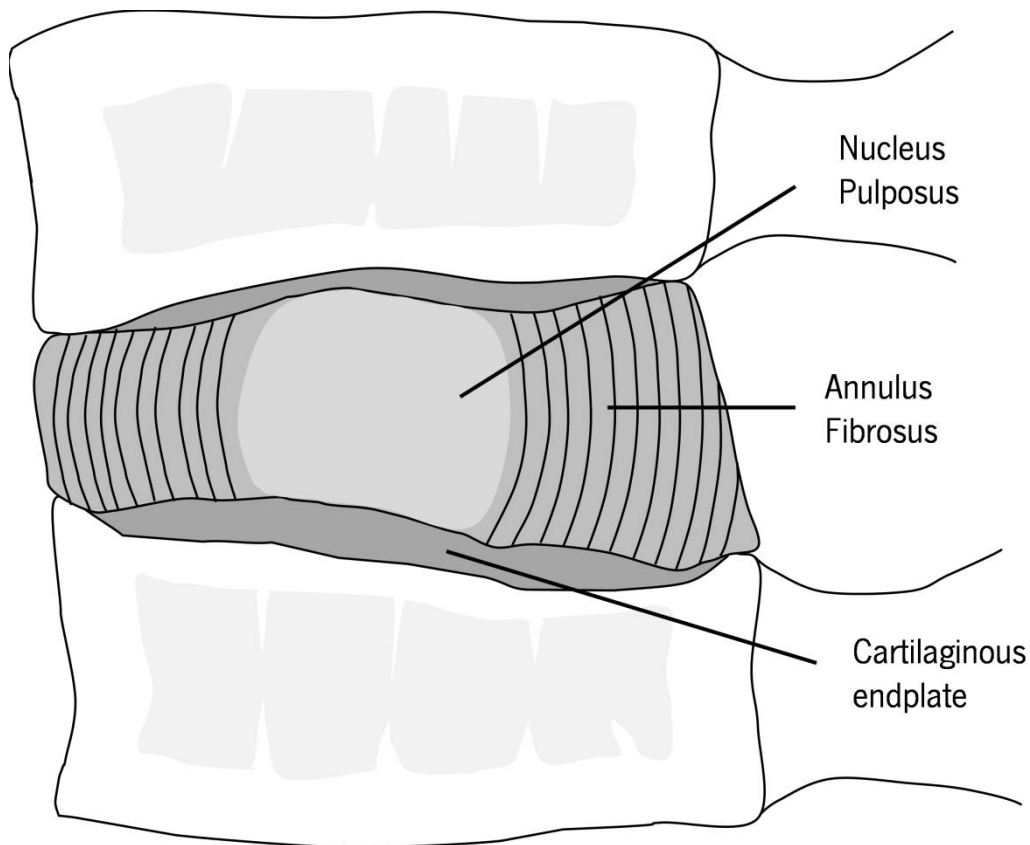


**Figure 1.1.** The structure of the IVD is composed by a layered structure, the Annulus Fibrosus, limited by the two Cartilaginous Endplates at the top and bottom and a gelatinous core in its center, the Nucleus Pulposus.

An example of disc injury is the degenerative disc disease, a condition that alters the IVD height and the mechanics of the entire spinal column, affecting negatively the behaviour of surrounding spinal structures, such as muscles and ligaments (Urban and Roberts, 2003). The degenerative disc disease is among the most important promoters of low back pain, being normally associated with sciatica and disc herniation or prolapse.

Although the relationship between the degenerative disc disease and the low back pain is well-defined, the information about the mechanical properties of the IVD and its relation with the degenerative disc disease is still incomplete. On the one hand, the experimental characterization still needs to be improved in order to explain all the particularities of the IVD. On the other hand, despite the existence of several computational models for the IVD (Schmidt et al., 2013), the definition of better approaches is essential for obtaining more accurate material properties of this structure.

An effective solution for low back pain provoked by a degenerated IVD is considered a challenge by the clinicians. The low back pain could be classified according to its duration (Silva-Correia et al., 2013): acute (for the cases where pain does not last more than 6 weeks); sub-chronic (6 to 12 weeks) or chronic (when pain persists more than 12 weeks). The acute and sub-chronic cases could be treated with a conservative approach, based in analgesics and anti-inflammatories, muscle relaxants, injection of corticosteroids, or local anaesthetic, manipulation therapies and exercise (Urban and Roberts, 2003); however, these techniques are only used as pain relievers, which could not be a definitive solution. In the case of the chronic condition, which evolves e.g. the IVD herniation, surgical intervention is occasionally chosen as treatment option. The surgical procedures for patients with degenerative disc disease include discectomy, spinal fusion and partial or total disc replacement (van der Veen, 2009). Although discectomy and spinal fusion represent definitive solutions for degenerative disc disease, they are not the most desirable solution as they induce limitation in the patient mobility.

An ideal implant should presents certain characteristics such as biocompatibility, durability and ease implantability (Whatley and Wen, 2012). Concerning to the use of implants for partial or total disc replacement, they represent a valid alternative since they reduce the pain, allowing some spinal mobility (Bono and Garfin, 2004; Rousseau et al., 2006; Whatley and Wen, 2012). The total disc replacement solutions presents some advantages such as the maintenance of mobility at the operated disc, reducing the risk of adjacent segment degeneration (Jacobs et al., 2012); however, several drawbacks are related to this prosthesis as they could be linked to loosening, extrusion, infection and cytotoxicity (Cunningham, 2004; Denozière and Ku, 2006; Geisler, 2006; Whatley and Wen, 2012). With respect to the partial disc replacement solutions, which consists on the replacement of the NP, they allow to preserve the remaining disc structures - AF, CEP and ligaments (Shim et al., 2006). In addition, these implants mimick the native tissue physiology, as they normally contain high water volumes, promoting the fluid flowing through disc and consequently the nutrient delivery. Nevertheless, the normal procedure for NP replacement involves the implantation through an incision in the AF, compromising the integrity of the disc. Thus, it is absolutely vital the development of a therapy that restores the NP



functional disc matrix with minimally invasive approach (Goins et al., 2005; Iatridis et al., 1998; Setton et al., 2006)).

The motivation behind this work arises from: (1) the need of additional insights about the mechanical properties of the IVD, through suitable experimental procedures. This experimental approach should allow obtaining the mechanical properties of the IVD and its constituents. These properties would be translated to benchmark values for validate Finite Element Models (FEM), which permits the comparison between the computational response and the experimental values from tests in the IVD; (2) as the present work run in parallel with the European project Npmimetic<sup>ii</sup>, which purposed to develop a biomimetic long-term nano-polymer based gel for minimally invasive IVD regeneration treatment, it is expected a contribution for the progress of this project namely by the design of new experimental techniques for mechanical characterization, mechanical testing protocols and benchmark results that allows stablishing specifications for the new implant.

## **1.2. Objectives**

The mechanical loading experienced by the IVD during daily events is intimately related to its life cycle duration (van der Veen, 2009). The improvement of knowledge about the mechanical response of the IVD to loading was one of the main goals of this work. Thus, the aim of this research is to develop an experimental framework to study the mechanical specificities of IVD, in order to optimize both the accuracy of the Finite Element models and the treatment strategies for back pain. Porcine lumbar discs samples were used for the studies, as the quadruped spine is essentially loaded in the same way as that of a human (Smit, 2002); moreover, these samples also present higher availability and lower cost when compared with human ones, as well as its morphometric data are described in detail (Busscher et al., 2010; Dath et al., 2007), making it a suitable choice for experimental studies on spine column. This work also aims to give a contribution on the selection and the characterization of the long-term biomimetic substitute of

---

<sup>ii</sup> For further information about this project, please visit [www.npmimetic.com](http://www.npmimetic.com)

NP, developed in the scope of project NPmimetic. Therefore, the most relevant objectives addressed in this work are:

- 1) To quantify the mechanical properties of porcine lumbar IVD under quasi-static and cyclic axial compression loading; to define new parameters for pre-existent models of the IVD mechanical behaviour, comparing the parameters obtained for porcine models with the ones reported in the literature for the human IVDs. The suitability of the use of porcine lumbar IVDs will be also detailed discussed.
- 2) To develop and validate a methodology that allows applying increments in the intradiscal pressure, presenting the capacity to determine the compressive load throughout the internal disc pressure variations.
- 3) To obtain the values of internal disc pressure which promote the IVD disruption, by means of pressure insertion in the nucleus pulposus cavity.
- 4) To determine the mechanical behaviour of the annular reinforced-ground matrix using unconfined uniaxial compressive and dynamic mechanical testing and compare the response of AF to the application of both physiological and non-physiological strains
- 5) To contribute for the development of the biomimetic solution for replacement of NP, based in the use of biocompatible polymers and innovative minimal invasive surgical techniques. For that, suitable implant configuration and geometry as well as the mechanical and material parameters of the implant configuration will be studied.
- 6) To propose a method to insert and retain the developed implant in the nuclear cavity, during mechanical testing, allowing the assessment of the implant in a “physiological” condition.

### **1.2.1. Contributions**

This research project was conceived to answer to important questions as the mechanical properties of the tissues that composed the IVD and the design of an efficient biomimetic substitute of injured discs. As first main contribution, this work aims to bring a meaningful addition on overall knowledge about the properties of the IVD, since it introduces new experimental data that allows clarifying its complex mechanical response. For that, it brings to

light the problematic of the use of animal studies as models to study the mechanical behaviour of the IVD. The suitability of the use of porcine lumbar IVDs is clarified and several mechanical properties of these structures are reported. Moreover, the porcine IVD samples are studied concerning to its internal disc pressure. Thus, this work contemplates a methodology that allows applying a prescribed internal disc pressure into NP cavity, helping in the determination of the compressive load throughout the pressure variations, as well as in the definition of the intradiscal pressure values that leads to IVD disruption. A new set of values and its physiological relevance were reported, composing the first major contribution of the present work.

Moreover, the accuracy of the computational and analytical models for the AF are strongly dependent on the material laws determined experimentally, being essential a deep understand about the mechanical behaviour inherent to each AF component. Thus, the second significant contribution of this work is related with the experimental quantification of the particular barely documented mechanical properties of the reinforced-ground matrix of the AF.

The third key contribution of this work is associated with the mechanical and material characterization of a new implant for NP replacement, developed in the scope of the NPmimetic Project. Several testing protocols for both mechanical and material parameters determination were studied. These procedures include complementary tests for the selection of the geometrical characteristics of the implant, the assessment of the mechanical and material parameters of the final “Ravioli” configuration and a load relaxation study to determine the effect of hydrogel insertion in a functional spinal unit.

### **1.3. Thesis Structure**

The present thesis is structured and divided in eight chapters. In **Chapter 1** the motivation and objectives of this work are detailed defined, under the framework of mechanical characterization of the IVD and the definition of material and mechanical properties of the new implant.

A comprehensive description of the specificities of the spine, with special emphasis on the IVD, is described in **Chapter 2**. This chapter encloses the main characteristics of the spine column as well as the complex features of the IVD, from the anatomy, physiology and function to the biomechanical behaviour, including the most significant experimental approaches adopted to determine the relevant properties. Moreover, a critical consideration about the mechanisms that leads to the degenerative disc disease as well as the actual therapies used for the treatment of this condition are also a target of this chapter.

The study of axial loading is essential to determine the properties of intervertebral disc since this structure is predominantly subjected to quasi-static and cyclic axial compressions during daily events. The **Chapter 3** helps to clarify this influence by determining the mechanical properties of porcine lumbar discs under quasi-static and cyclic axial compressive loading. Moreover, it includes the use of a phenomenological model already applied in human lumbar IVDs to fit in experimental compression tests, performed with porcine lumbar discs. The model parameters obtained for the porcine lumbar IVDs is compared with values reported in the literature for the human lumbar discs.

Although a simple axial compressive overload not inducing damage on a healthy disc, some movements such as compression combined with hyperflexion might generate an IDP beyond what the disc could withstands, promoting several spinal injuries. The **Chapter 4** presents the development of a methodology that applies pre-defined pressure increments into NP while the compressive load throughout the intradiscal pressure variations is monitored. Moreover, an adaptation of this apparatus will allow the quantification of the values of internal pressure that lead to rupture in the IVD.

The accuracy of computational and analytical models of the AF is strongly dependent on the material laws determined experimentally. However, these data needs to be better defined, especially the mechanical properties of the reinforced-ground matrix that composes the AF. The **Chapter 5** aims to contribute for the determination of the mechanical behaviour of the reinforced-ground matrix of the AF under unconfined uniaxial static and dynamic compressive

loads and compared the response of AF to the application of both physiological and non-physiological strains.

Moreover, the **Chapter 6** contains a mechanical characterization of a new hydrogel-based solution, developed by Nicast<sup>iii</sup> in the scope of the NPmimetic project. This section complements the manufacturer information about the developed implant, helping in the selection of the most suitable implant configuration. This chapter includes an extensive series of material and mechanical tests of the implant, which allows the determination of its material and mechanical properties; moreover, it aims to compare these properties and the previous mechanical tests reported in the literature, including with the characteristics of a native NP.

After testing the implant in non-physiological conditions, there is also a need in the characterization of the functional and behavioral changes induced by the implant when placed in the disc. Thus, in **Chapter 7** a pioneer method to insert and retain the implant in the nuclear cavity, during mechanical testing was suggested. Moreover, the mechanical response of the whole complex disc-implant to compression was assessed by means of determination of stiffness and load relaxation curves. The load relaxation curve was fit in an exponential model and the parameters from the curve of disc-implant and healthy disc were compared. The goal is to observe if there are significant differences between parameters the disc-implant and the healthy disc.

Finally, the **Chapter 8** comprises the utmost significant considerations about this work as well as the relevant conclusions to retain from the several data reported. In addition, a future perspective on the mechanical testing of IVD and the further iterations to perform in order to fully characterize the developed implant are a target of this section.

---

<sup>iii</sup> A Project partner, responsible for the conception of the new hydrogel-based implant. More information in <http://www.nicast.com/>

---

## 2. The Spine and the Intervertebral Disc

*The present chapter depicts the main characteristics of the spine column together with the complex features of the intervertebral disc, from the anatomy, physiology and function to the biomechanical behavior, including the degeneration and actual therapies for disc degeneration. Special focus will be given to the biomechanical behavior of intervertebral disc, as well as to the most significant experimental approaches adopted to determine its properties.*

### 2.1. Anatomy and Function of the Spine Column

The vertebral column (or spinal column) extends from the skull to the pelvis and is comprised by 33 individual vertebrae. The vertebrae are joined axially on top of each other and can be divided in 4 sections – Table 2.1.

**Table 2.1.** Vertebral column sections, its constitution and body area.

Section	Vertebrae Number	Body Area	Abbreviation
Cervical	7	Neck	C1-C7
Thoracic	12	Chest	T1-T12
Lumbar	5	Low back	L1-L5
Sacrum	5 (fused)	Pelvis	S1-S5
Coccyx	4	Tailbone	None

Each vertebra is connected with the subjacent one by an Intervertebral Disc (IVD). It is important to refer that there are no IVDs between the Atlas (C1), Axis (C2), and Coccyx, which are the fused vertebra – Figure 2.1. The vertebral column presents several functions, according with the section of analysis. Cervical spine normally contains 7 vertebrae joined by IVDs.

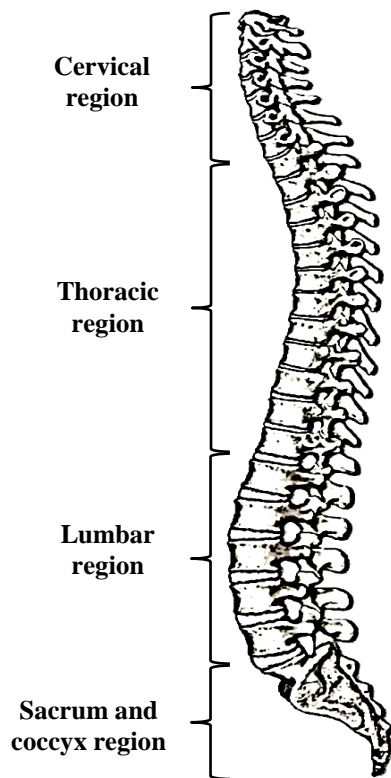





**Figure 2.1.** Lateral view of spine column, with its different regions.

The main functions of cervical region are to contain and protect the spinal cord, support the skull and to enable or/and constrain some head movements, such as rotation and bending. An intricate system of ligaments, tendons and muscles contribute to perform these functions. The ligaments are responsible to constrain the movement that can result in serious injury. In case of muscles, they enable the movement and also help in the regulation of the spinal balance and stability. This kind of regulation is achieved by specific muscles functioning: while some muscles contracts, the remaining relax (Tortora and Derrickson, 2008). The thoracic part is the most stable part of spine and its vertebrae are considerably larger and stronger than cervical ones. Located in the chest region, the thoracic vertebrae present also the longest and the largest transverse processes. The unique feature of the thoracic vertebrae is to articulate the spine column with the ribs. Due to its stiffness and the attachment of the ribs to the sternum, which is a part of the rib cage, this section of the spine presents a very limited range of motion (Tortora and Derrickson, 2008). The lumbar spine is located precisely where spine curves inward toward the abdomen, consisting on five vertebrae alternated with IVDs. The lumbar vertebrae are the

largest and strongest of unfused bones in the spine, conferring them the capacity to withstand the weight of the entire torso (Tortora and Derrickson, 2008). The lumbar IVD plays an important role in this structure: it experiences large deformations, providing the spinal flexibility and allowing the resistance to high loads and the load transmission along the spinal column (Schmidt et al., 2013). The lumbar column bears much of the body weight and the related biomechanical stress: the two lowest spinal segments of lumbar spine, L4-L5 and L5-S1, bear the most weight, being the most predisposed to degradation and damage (Joshi, 2004). Another important detail about the lumbar spine is that spinal cord does not run through it, which makes extremely rare that a lower back problem would result in spinal cord injury or paralysis. The comparison of the major structural differences among cervical, thoracic, and lumbar vertebrae is presented in Table 2.2.

**Table 2.2.** Resume of major structural differences among cervical, thoracic, and lumbar region (Adopted from Tortora & Derrickson 2008).

Characteristic	Cervical	Thoracic	Lumbar
<b>Overall structure</b>			
<b>Body</b>	Small	Small	Large
<b>Articular facets for ribs</b>	Absent	Present	Absent
<b>Size of intervertebral discs</b>	Thick relative to the size of vertebral bodies	Thick relative to the size of vertebral bodies	Largest

In sum, the main biomechanical functions of spine column are to resist to large loads, to allow the load transmission along the spinal column, giving support to the upper body and to



protect the spinal cord from impacts (Hoogendoorn 2008; van der Veen 2009). In the spine structure, the different components give the body freedom to move in three directions: flexion-extension, latero-flexion and axial rotation (van der Veen, 2009). While spinal muscles and intervertebral discs provide the movement capabilities of the spine such as bending or turning, the ligaments of the spine prevent the damage of tissues by inducing restrictions in the spinal movements (Little et al., 2010).

## **2.2. Anatomy, Function and Physiology of the Intervertebral Disc**

As described above, several structures contribute for the several functions played by spinal column. The IVD is a component of utmost importance for the spinal column. The IVD is a fibrocartilage structure located between two vertebral bodies, surrounded by ligaments and muscles (Silva-Correia et al., 2013). They are present from the second cervical vertebra to the sacrum, accounting for about 25% of the total height of the vertebral column (Tortora and Derrickson, 2008).

This structure plays an important role at spinal level: it is responsible for the spine motion, helping the spine in both weight support and load transfer from head and upper torso to the pelvis (Niosi and Oxland, 2004; White and Panjabi, 1990). As referred previously, the IVD is an intricate structure composed by an inner gel-like core - the nucleus pulposus (NP) surrounded by a layered structure, the annulus fibrosus (AF). These structures are limited at the top and bottom by the cartilaginous endplate (CEP).

### **2.2.1. Nucleus Pulposus**

The NP is composed by a proteoglycan-water gel enmeshed in a network of fine randomly organized collagen and radially distributed elastin fibres (up to a length of 150 nm) (Raj, 2008). Both elastin and collagen fibres provide consistence to the central NP region, holding the less dense surrounding area, mainly containing proteoglycan molecules (Castro, 2013). The proteoglycans are glycoproteins containing a protein core linked to, at least, one glycosaminoglycan chain. The amount of proteoglycans corresponds to approximately 50% of NP

dry weight, while the percentage of collagen rounds 25%. The collagen type II is predominant in the NP and its concentration decreases towards the surrounding AF (Cassinelli & Kang 2000). Due to the hydrophilic character of glycosaminoglycans, a large quantity of water is maintained in the IVD (Raj, 2008).

Thus, the main role of NP is to resist to compressive forces, redistributing the forces within the spine: due to the high concentration of glycosaminoglycans the water is captured to the NP, leading to the swelling of the NP. This event creates an osmotic pressure inside the IVD, allowing it to resist to large compressive loads. In fact, a reduction in the amount of glycosaminoglycans will decrease the disc height, promoting the disc degeneration due to a presence of less water content, leading to a more fibrous NP (Whatley and Wen, 2012). The expansion of NP is constrained by the AF and CEPs, which generates a hydrostatic pressure in the absence of external loads (Nerurkar et al., 2010). Moreover, the NP swelling helps to support the AF lamellae, ensuring the maintenance of the AF at its normal pressure.

The NP is thus considered a biphasic tissue that presents both solid and fluid material phases (Iatridis et al., 1997a, 1996). Furthermore, the NP exhibits a complex osmo-poro-visco-hyperelastic behaviour, being also described as an isotropic and almost incompressible gel (Castro, 2013).

### **2.2.2. Annulus Fibrosus**

The AF is the tough outer layer of IVD, mainly composed by a non-fibrous matrix (water, proteoglycans and some non-collagen proteins) and aligned collagen fibre, although some elastin fibres can also be found in the fibrous region (Holzapfel et al., 2005). The transition from the NP to the AF is made by a thin band of tissue. However, comparing to the NP, the AF presents less water content as well as more percentage of collagen fibres. According to this, the AF exhibits a porous matrix with high density of fibrous composite, tissue making the AF stiffer than the NP (Castro, 2013; Raj, 2008).

The AF collagen fibres are presented in multiple concentric layers, between 15 and 25, with consecutive rings disposed in alternating directions. The fibres angle is about  $30^\circ$  or  $150^\circ$  referred to the transverse plane of the spine, with variations in the circumferential and radial directions – Figure 2.2 (Holzapfel et al., 2005; Neumann et al., 2010).

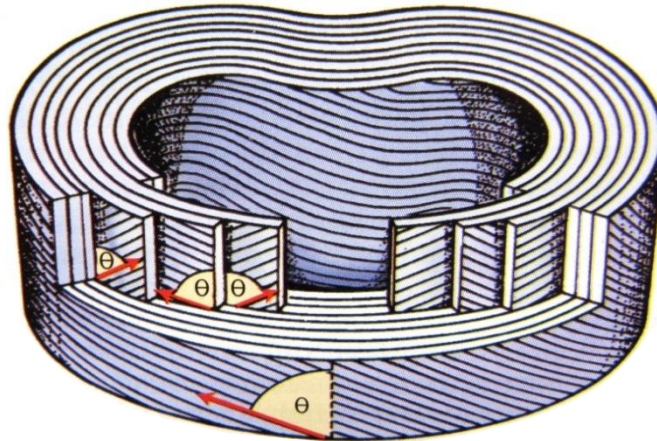


**Figure 2.2.** Fibres orientation in the annulus fibrosus. Adapted from Neumann et al. (2010).

The number of layers is dependent on the circumferential location, the spine level, and the specimen age (Holzapfel et al., 2005; Marchand and Ahmed, 1990)). The region-dependency of AF fibres is noticeable, since the concentration of the collagen fibres increases from the inside to the outside region of the AF, with the outermost AF stiffer than the inner one. Thus, the particular histological and structural disposition of each single layer represents an adaption to the complex loading on IVD: while the outermost AF fibres are well structured and organized, conferring great resistance to radial tensile forces originated by the compression loads acting on the NP, the elastin fibres are more dispersed, helping to IVD structure to return to its initial position (Castro, 2013; Holzapfel et al., 2005).

In sum, this structural inhomogeneity is fundamental for the AF biomechanical functions, which are to contain the intradiscal pressure (pressure exerted by the NP) as well as to mediate the motion of the IVD (Bass et al., 2004; Wagner and Lotz, 2004). On one hand, the complex organization of the AF confers it a non-linear anisotropic behaviour (Holzapfel et al., 2005); on

the other hand, it provides osmotic, porous, viscoelastic and hyperelastic characteristics to the IVD (Castro, 2013; Eberlein et al., 2001).

### **2.2.3. Cartilaginous Endplate**

Each IVD is connected to both the superior and inferior adjacent vertebrae by a thin horizontal layer, with approximately 600  $\mu\text{m}$  thick, called the Cartilaginous Endplate (CEP) - Figure 2.3 (Moon et al., 2013; Roberts et al., 1989). In spite of being attached to the subchondral bone of the vertebrae, the CEP is strongly connected to AF. The CEP is usually compared to articular cartilage as it consists on a hyaline cartilage composed by proteoglycan, collagen and water (Raj, 2008; Urban and Roberts, 2003). According to these structural connections and morphological similarities, there are strong evidences that consider CEP as a part of IVD and not as a constituent of the vertebral body (Castro, 2013). However, this structure presents an inferior amount of water content than those presented by NP and AF, making the CEP the stiffest structure in the IVD (Wilson et al., 2007).

In what concerns to its organization and constitution, the CEP is a non-uniform structure, with the collagen fibres running on the horizontal direction, parallel to the vertebral body (Raj, 2008). Moreover, although the highest cell density is located in the center, the same region represents the thinnest zone of CEP (Castro, 2013). The CEP has an important role at the IVD level: first, it acts as mechanical barrier between the major part of IVD and the vertebral body, since it covers the whole extension of the NP and about one-third of the AF; second, it represents, in addition to the peripheral annulus, a crucial pathway for nutrient exchange from adjacent blood vessels to the disc (Moon et al., 2013; Moore, 2006, 2000; Nachemson and Elfström, 1970; Roberts et al., 1989). Due to the osmotic regulation of proteoglycans, presented by the CEP, the nutrients are captured to the inner region of the IVD by capillarity. Thus, the nutrition is guided by diffusion, through the avascular healthy IVD (Roberts et al., 1989). The nutrition pathways are described in Figure 2.3.

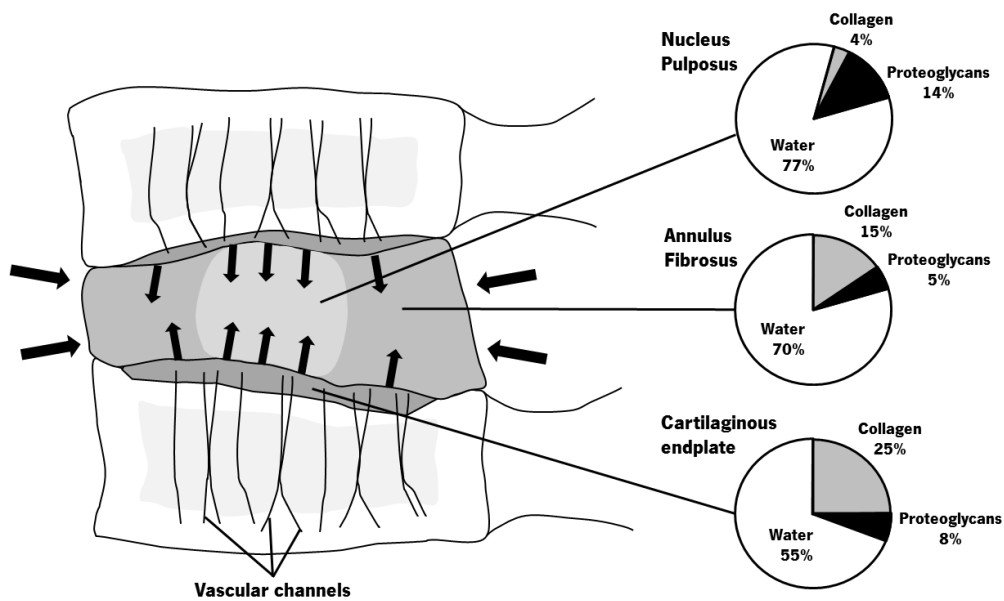


**Figure 2.3.** Representation of the relative position and the compositional features of the NP, AF and CEP in healthy IVDs. The black arrows indicate the nutrition pathways.

The CEP assumes an important role in the IVD as any problem affecting this structure will have effects on the IVD. For example, during the IVD degeneration, the CEP becomes more sclerotic and calcified and the vascular ramifications are suppressed. Consequently, there is a reduction in the permeability of the IVD and a consequent decrease of nutrients diffusion to NP cells, contributing to disc degeneration (Moon et al., 2013; Roberts et al., 1996). However, these events also promote the appearing of cracks, thus increasing the permeability. In this case, the regulation of nutrient diffusion becomes chaotic as well as the CEP could not withstand with the NP pressure, bringing additional problems to the disc (Castro, 2013).

The disc degeneration is also related to the presence of protuberant nodules in the adjacent vertebral body, denominated as Schmorl's nodes. The appearance of these structures are normally linked to pathological conditions in CEP (Adams and Dolan, 2012; Iatridis et al., 2013; Moore, 2006).

### **2.3. Disc Biomechanics**

It is well known that acute mechanical injury and accumulated overloading could induce disc degeneration (Chan et al., 2011). Thus, it is crucial to characterize mechanically the IVD, since the mechanical loads are one of the main causes of degenerative disc disease. An ideal prosthesis should withstand the physiological loads, making the study of the mechanical loading acting on IVD even more important.

The movements of the spinal column occur in segments, which are composed by vertebrae, IVDs, ligaments and vertebral joints. According to this, the main function of IVD is to maintain the flexibility and motion in the spine. Additionally, it is responsible for accommodating the compressive loads that the trunk is subjected. This includes different types of loads and stresses, such as dynamic loads, static loads, tensile and compressive loads, among others. To find a successful replacement of the IVD, it is important to describe to characterize the disc mechanics, establishing discrete functional goals to reach the best NP substitution approach. However, due to the inherent complexity of the IVD and the great variability obtained in mechanical measurements, it is extremely difficult to define exact and coherent values for disc benchmark data. Moreover, the wide range of animals used to obtain this data brings the problem of the variability interspecies, constituting an additional problem for the correct definition of IVD benchmark values.

Thus, this section also describes the complex mechanical behaviour of the different constituents of IVD, namely AF, NP and the complex vertebrae-disc-vertebrae, known as motion segment. In addition, it also contains the concept of internal disc pressure, defining the relation between the inner disc pressure and the external loading as well as the annular failure strength due to inflation method pressurization. Moreover, this section will take as basis of discussion the values reported for several studies using different animal IVDs. It is important to notice that the benchmark values used in this section are all provided by published data.

### **2.3.1. Nucleus Pulposus Mechanics**

Many researchers have studied the mechanical behaviour of the IVD after altering the NP. Some studies investigated the effect of removal or alteration of the NP through surgical and chemical intervention (Iatridis et al., 1996). The studies also included the determination of changes with aging and the consequent degeneration (Iatridis et al., 1997b; Urban and McMullin, 1988), the effect of partial or total nucleotomy (Brinckmann and Horst, 1985; Markolf and Morris, 1974; Vresilovic et al., 2006) and the evaluation of the pressurization effect on the IVD (Andersson and Schultz, 1979; Handa et al., 1997).

The main findings related to these researches are described in Table 2.3. The viscoelastic behaviour of NP is fundamental for IVD behaviour, ensuring the overall flexibility and stability of the spine. On one hand, the glycosaminoglycans provide a high fixed charge density since they produce an internal osmotic pressure, promoting a water gradient in the NP. On the other hand, the AF and the endplates constrained the NP swelling, causing an physiological hydrostatic pressure, even without the presence of external loads (Nerurkar et al., 2010). Taking in consideration these facts, it is clear that mechanical properties of the NP, including the viscoelastic parameters, are important in the determination of the structural response of the IVD.

In Table 2.4 some viscoelastic benchmarks related to mechanics of the NP are reported. The way of calculation of these parameters are presented on Annex A. Concerning to the viscoelastic tests, Iatridis et al. (1997b) aimed to characterize the viscoelastic behaviour of the non-degenerate human lumbar NP in shear, using a mechanical spectrometer. The results showed that NP exhibited significant viscoelastic effects in torsional shear, becoming stiffer with frequency. In addition, under dynamic shearing conditions the NP appears to have a more 'solid-like' rather than 'fluid-like' behaviour, being characterized as a viscoelastic solid. However, although they use 10% strain before shear tests, a potential coupling between compressive and shear stresses could occur. They also used a static cross-sectional area of NP, ignoring the NP bulging. This could be an important limitation since the bulging occurs when the samples are submitted to an initial 10% strain.

**Table 2.3.** The type of NP modification and the main findings by author.

<b>Type of IVD modification</b>	<b>Author (Year)</b>	<b>Main findings</b>
Aging and degeneration	Urban & McMullin (1988)	<ul style="list-style-type: none"> <li>The hydration and swelling pressure are more dependent on IVD's composition than on age or degree of degeneration;</li> </ul>
Aging and degeneration	Iatridis et al. (1997a)	<ul style="list-style-type: none"> <li>The NP undergoes a transition from "fluid-like" behaviour to more "solid-like" behaviour with aging and degeneration.</li> </ul>
Aging and degeneration	Johannessen & Elliott (2005)	<ul style="list-style-type: none"> <li>Swelling is the primary load-bearing mechanism in both non-degenerate and degenerate NP</li> </ul>
Partial or total nucleotomy	Markolf and Morris (1974)	<ul style="list-style-type: none"> <li>↑ in IVD height with saline injection into NP</li> <li>No significant differences in load-deformation</li> </ul>
Partial or total nucleotomy	Brinckmann and Horst (1985)	<ul style="list-style-type: none"> <li>Discectomy ↑ the radial IVD bulging and ↓ the IVD height</li> </ul>
Partial or total nucleotomy	Vresilovic et al. (2006)	<ul style="list-style-type: none"> <li>Cyclic loading did not cause structural damage</li> <li>The recovery after load application is related to fluid flow</li> </ul>
Pressurization of IVD	Andersson and Schultz (1979)	<ul style="list-style-type: none"> <li>IVDs that retained the fluid from saline injection exhibited pronounced differences in mechanical behaviour.</li> <li>Decreased deformations in these IVDs were detected.</li> </ul>
Pressurization of IVD	Handa et al. (1997)	<ul style="list-style-type: none"> <li>At a pressure of 0.3 MPa → may act as anabolic factor for stimulation of proteoglycan synthesis and tissue inhibitor of metalloproteinases-1 production.</li> <li>At 3 MPa or more or 0.1 MPa or less → catabolic effect is predominant; reduction of proteoglycan synthesis rate; increase of matrix metalloproteinase-3 production.</li> </ul>
Pressurization of the IVD	Vergoesen et al., (2014)	<ul style="list-style-type: none"> <li>Prolonged dynamic loading → decreases intradiscal pressure and disc height; increase the compressive stiffness.</li> </ul>



**Table 2.4.** Summary of native tissue viscoelastic benchmarks related to mechanics of the NP. Legend:  $|G^*|$  = complex shear modulus;  $\delta$  = phase shift angle;  $E'$  = Storage modulus;  $E''$  = Loss modulus;  $Tan \delta$  = Coefficient of friction;  $WC$  = Water Content;  $H_{AO}$  = Aggregate Modulus;  $K_0$  = Zero-strain permeability;  $E_s$  = Static Compressive Modulus;  $E_{toe}$  = Toe modulus;  $\nu$  = Poisson's Ratio;  $K_d$  = Dynamic Stiffness; DC = Damping capacity.

Authors	Model	Testing device	Testing Mode	Benchmark Value
Iatridis et al. (1997b)	Human lumbar	Mechanical spectrometer	Torsional Shear	$ G^*  = 7.4\text{--}19.8 \text{ kPa}$ $\delta = 23\text{--}30^\circ$
Leahy & Hukins (2001)	Sheep	DMTA3	Cyclic compression	$E' = 64 \pm 28 \text{ kPa}$ $E'' = 24 \pm 11 \text{ kPa}$ $Tan \delta = 0.33 \pm 0.07$ $WC = 81 \pm 2\%$
Périeré et al. (2005)	Bovine tail	ELF-3200	Confined compression	$H_{AO} = 0.31 \pm 0.04 \text{ MPa}$ , $K_0 = 6.7 \pm 0.9 \text{E-}16 \text{ m}^4/\text{Ns}$
Cloyd et al. (2007)	Human lumbar	Instron 5542	Unconfined compression	$E_s = 5.39 \pm 2.56 \text{ MPa}$ $E_{toe} = 3.25 \pm 1.56 \text{ MPa}$ $\nu = 0.62 \pm 0.15$
Boxberger et al. (2009)	Rat lumbar	Instron 5848	Cyclic compression	$\delta = 5.7 \pm 1.7^\circ$ at 0.05 Hz / $1.7 \pm 1.3^\circ$ at 5 Hz $K_d = 31.52\text{--}64.77 \pm 27.11 \text{ N/mm}$
Vogel and Pioletti (2012)	Bovine	Electropulse E3000	Confined compression	$DC = 18\text{--}36\%$

Another study performed by Leahy & Hukins (2001) investigated the viscoelastic properties of the NP under cyclic compression. The samples were measured immediately in different situations: after slaughter and after defrost. It was found that viscoelastic properties of NP are approximately to linear, which could be correlated to linear viscoelastic behaviour of intact IVD under compression. Additionally, the values of storage and loss modulus increased when a repeated test was performed, likely due to water loss. It was also shown that freezing appears to

increase the storage modulus, but not the loss modulus. Nevertheless, these studies were performed without humid bath, which could promote the NP dehydration. This fact will influence the final results, since NP water content is around 80%.

Later, Périé et al. (2005) determined linear and non-linear material properties of NP and AF. The caudal bovine specimens were tested in confined compression stress-relaxation. The aggregate modulus (or compressive modulus in confined compression) and hydraulic permeability were quantified using linear and nonlinear biphasic models. The results suggested that both confined swelling pre-test condition and non-linear biphasic model provided the better approach for material parameters, since they present lowest relative variance and more representative water content of physiological conditions. In addition, it was visible that a smaller compressive modulus and higher hydraulic permeability were obtained for the NP rather than AF. The results suggested that *in vivo* exposure of IVD tissues to low strain-rate and high-deformation loading conditions may alter its mechanical behaviour, due essentially to a change in the biological conditions. It is also important to refer that this study used samples that were frozen, which may induce a loss of the IVD physiological characteristics.

Cloyd et al. (2007) attempted a different methodology: to assess the characteristics of NP and some materials, under unconfined compression, in order to find the best approach to replace NP. The results showed a complete set of parameters for NP, in agreement with literature (Umehara et al., 1996). However, although it exemplifies an easy way to obtain the behaviour of NP under compression, it is not representative of *in vivo* loading. This method induces the free expansion of NP to lateral sides, a process that is limited *in vivo* by surrounding AF and CEP, which increases the intradiscal pressure, allowing the support of axial spine loads. In addition, the values for Poisson's ratio were obtained from an optical analysis which requires the user definition of diameters; thus, this methodology could induce a large uncertainty in the results.

In a cyclic load experiment using rat lumbar IVDs, Boxberger et al., (2009) found a non-linear behaviour with higher dynamic stiffness at elevated compressive loads regardless of frequency. Thus, dynamic stiffness did not depend on frequency of loading. In addition, it was

verified that the phase angle decreased with increased frequency. These findings are a good approach to understand the effect of equilibrium load and loading frequencies in IVD mechanics.

Two more studies evaluated the viscoelastic behaviour of NP, using a confined compression methodology (Aladin et al., 2010; Vogel and Pioletti, 2012). Aladin et al. (2010) investigated the structure of individual collagen fibres of the NP and assessed its correlation with the bulk mechanical properties of the tissue. It was found a mild linear correlation of mean fibre diameter and the compressive modulus, which is justified by a possible correlation between the decrease of proteoglycans, during an increase of compressive force, and the formation of collagen fibres of large diameters. Vogel and Pioletti (2012) had recently determined that the lowest values of specific damping capacity are found for frequencies corresponding to the dynamics of loads in all day activities such as walking (0.1 to 1 Hz). These values indicate that NP contributes to dissipate energy under physiological large deformations, presenting a minimal damping value for moderate daily activities.

### **2.3.2. Annulus Fibrosus Mechanics**

An injury in the IVD causes a prompt drop in NP pressure. Although values for NP decompression are in average 25%, they can reach the 80% of injury in IVD at ages of 50-70 years old (Adams et al., 2000). Aging is likely the cause of this phenomena: the AF is losing its ability to be deformed along the years, causing the NP decompression (Adams et al., 2009).

Thus, the mechanical characterization of the AF represents a remarkable challenge for the determination of the mechanical behaviour of the IVD. The overall response of the AF, characterized by a non-fibrous matrix with aligned collagen fibres imbibed (Holzapfel et al., 2005), has been initially represented as having a linear elastic behaviour (Kurowski and Kubo, 1986). Moreover, several researchers took in account the material differences in the AF, characterizing the matrix or ground substance of the AF as having linear elastic properties (Goel et al., 1995; Kumaresan et al., 1999; Shirazi-Adl et al., 1986). However, the use of linear elastic laws to characterize the AF is considered as a significant simplification of the tissue behaviour as this structure presents an effective nonlinear response to loading (Little, 2004). The AF is

normally assumed as a fibre-reinforced soft tissue, acting as a non-linear material. The typical behaviour of AF under uniaxial tensile loading is described in Figure 2.4.

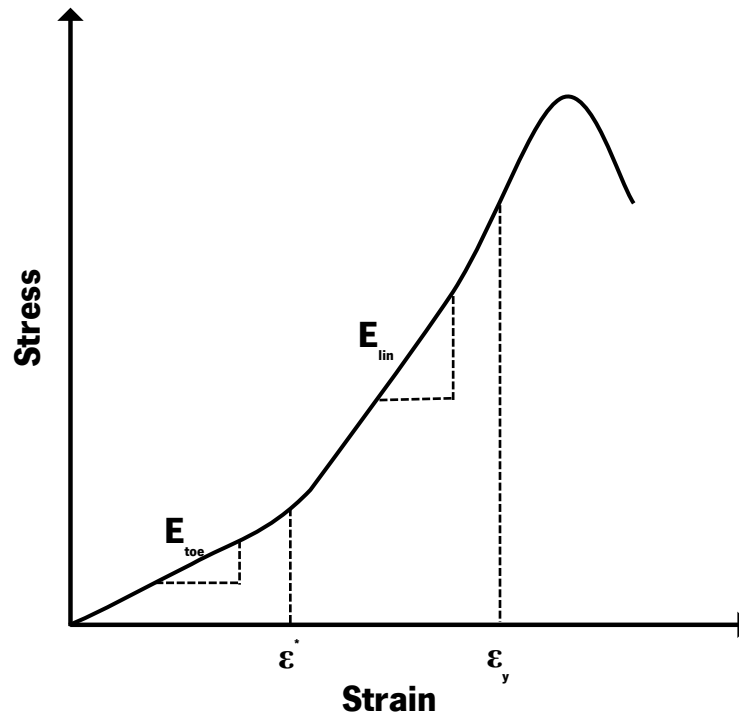


**Figure 2.4.** Typical stress-strain curve for AF, under uniaxial tensile tests, where  $E_{toe}$  represents toe-region modulus;  $E_{lin}$  is linear region modulus;  $\epsilon^*$  represents transition point and  $E_y$  represents yield point (adapted from (Nerurkar et al., 2010)).

Initially, there is a phase of small strain, known as toe-region modulus ( $E_{toe}$ ); then, a linear region is observed ( $E_{lin}$ ). From the observation of the curve of the Figure 2.4 it is evident the presence of a transition point ( $\epsilon^*$ ). This point is quite important, not only for the definition of the behaviour of AF, but also it is a benchmark value to take in account in the IVD replacement: while a low value of transition point could mean a limitation in the motion and overload in the peripheral tissues, high values of  $\epsilon^*$  could result in mechanical instability. Thus, an ideal substitute of AF should withstand large elastic deformations before yielding during its physiological activity (Nerurkar et al., 2010).

Several mechanical tests were performed in the AF in order to evaluate its response. Uniaxial tensile testing, where loads are applied along a single axis, appears to be the easiest way to obtain these important reference-values (Nerurkar et al., 2010). The uniaxial testing

approaches include the isolation of single (Holzapfel et al., 2005; Skaggs et al., 1994) and multi lamellae (Ebara et al., 1996; Fujita et al., 1997; Guerin and Elliott, 2007; Kasra et al., 2004). The single lamellae test presents some advantages relative to AF multi-lamellae: it allows obtaining benchmark properties, such as the nonlinear behaviour of stress-strain curve and the anisotropy, which are “hidden” or “masquerade” in larger length tests of AF fibres. However, tests with single lamellae are extremely difficult to perform due essentially to a complex technical procedure required. Thus, multi-lamellae approach is more common, since it presents the typical benchmark values for AF and it is also easier to prepare and test than single lamellae. The most prominent results of the mechanics of multi-lamellae of the AF are presented in the Table 2.5.

Interestingly, Little et al. (2010) studied the behaviour of native AF using a biaxial test. This test, where loads are applied along two axes, allows submitting the AF sample to a test that replicates the format of constrained boundaries found *in vivo* conditions. Although it generates a large amount of data with a single test, this approach could not determine all the relevant benchmark values needed to characterize the AF. Currently, it is well known that the AF is mainly composed of type I collagen fibres arranged in a unique multi-scale architecture layered, presenting an anisotropic, non-linear and viscoelastic behaviour. This combination of material properties is essential to withstand mechanical loading experienced *in vivo* (McNair and Breakwell, 2010; Nerurkar et al., 2010). The AF is also described as presenting both solid structure and fluid phases. Although a solid or a fluid material is considered as incompressible, a structure that combines both responses behaves as a compressible material. Thus, although a well-defined value for the permeability of the solid matrix is difficult to obtain, the poroelastic models were also adopted to characterize the AF behaviour (Castro et al., 2013; Ferguson et al., 2004; Malandrino et al., 2013).

**Table 2.5.** Summary of native tissue viscoelastic benchmarks related to mechanics of the multi-lamellae AF - adopted from Nerurkar et al. (2010). Legend:  $\theta$  indicates angle relative to the prevailing collagen orientation;  $z$ ,  $y$  and  $r$  indicate the loading axes along the disc circumferential, axial, and radial directions, respectively. The remaining constants were already described in Table 2.4.

Authors	Testing Mode	Benchmark Value
Acaroglu et al. (1995)		$E_{\theta} = 2.5/18-45$ MPa
Fujita et al. (1997)		$E_z = 0.27/0.82$ MPa
Guerin & Elliott (2006)	Uniaxial Tension	$E_r = 0.19/0.45$ MPa
Elliott & Setton (2001)		$\nu_{\theta z} = 1.77$
Kasra et al. (2004)		$\nu_{\theta r} = 0.33$
		Axial Fixed $E_s = 9.8/27.2$ MPa
		Equibiaxial $E_s$
O'Connell et al. (2009)	Biaxial tension	- Circumferential = 16.5/43.3 MPa
		- Axial = 10.7/26.8 MPa
Périé et al. (2005)	Confined compression	$H_{AO} = 440 \pm 750$ kPa, $K_0 = 1.6- 2.3$ E-16 m <sup>4</sup> /Ns

The anisotropic properties of AF also play an important role in the IVD behaviour. Since the tensile behaviour differs according to its orientation, AF is considered as anisotropic material. Moreover, it was found that “uniaxial tensile modulus of the AF is one to two orders higher along the circumferential direction than in the axial and radial directions” (Nerurkar et al., 2010). This means that not only the fibres angle is higher in both radial and axial direction than circumferential one, but fibres are also more able to be stretched in circumferential than in axial or radial directions due to its orientation. The anisotropic behaviour is thus a remarkable characteristic of AF, so that it should be preserved in a total disc substitute, since fibres are only stretched under tensile loads. The fibres also provide the multi-axial response of AF to loading as they are disposed in several directions.

Although several studies on the tensile properties of the annular fibres are presented in the literature, there is a paucity of studies about the mechanical properties of the reinforced-

ground matrix (the ground matrix of AF with fibres imbedded that is not actively bearing the axial load) and its contribution for the complex mechanical response of the AF. In fact, the AF is a viscoelastic tissue with a strain rate dependent behaviour to tensile loads (Kasra et al., 2004; Whatley and Wen, 2012), leading to a need in the deep characterization of the AF in order to better understand the behaviour of this complex structure. Moreover, as the accuracy of the computational and analytical models for the AF is strongly dependent on the material laws determined experimentally, it is necessary to correctly define the mechanical behaviour inherent to each AF component, i.e., the fibres and the reinforced-ground matrix (the ground matrix of AF with fibres imbedded that is not actively bearing the axial load).

### **2.3.3. Motion Segment Mechanics**

Although the large amount of NP and AF studies for the characterization of the IVD mechanics, it was shown that, for cases of severe degeneration, the replacement of only one structure is insufficient. In terms of complexity, the combination of such different structures as AF and NP represents an enormous challenge in the total disc replacement (Nerurkar et al., 2010). First, due to its complex and multiphasic structure; and second, due to the difficulty in the discs isolation as explants for direct assessment of its mechanical properties (MacLean et al., 2007). Thus, in order to improve the knowledge about the mechanical behaviour of the entire intervertebral disc, several researchers used the motion segment. The motion segment is the smallest functional unit of the spine, consisting of two adjacent vertebrae and the intervening disc – Figure 2.5 (Adams et al., 2009; van der Veen, 2009). The mechanical behaviour of motion segment is a result of combined and interactive disc and vertebrae response, since both present time-dependent behaviours associated with flow-dependent and flow-independent viscoelastic properties (MacLean et al., 2007). However some controversy was found among the motion segment researches. Some biomechanical studies reported that vertebral endplates could fracture at higher loads and bulge under axial deformations (Adams et al., 2000; Brinckmann and Horst, 1985), while other works assumed vertebral endplates as rigid and impermeable structures (Shirazi-Adl and Parnianpour, 1993; Spilker et al., 1984; van der Veen, 2009; Zimmerman et al., 1992). This last assumption seems to be reasonable, since the resistance of

the bone is considerably higher than the one of disc tissues; moreover, the disc evaluation in the motion segment closely mimics *in vivo* conditions (MacLean et al., 2007).

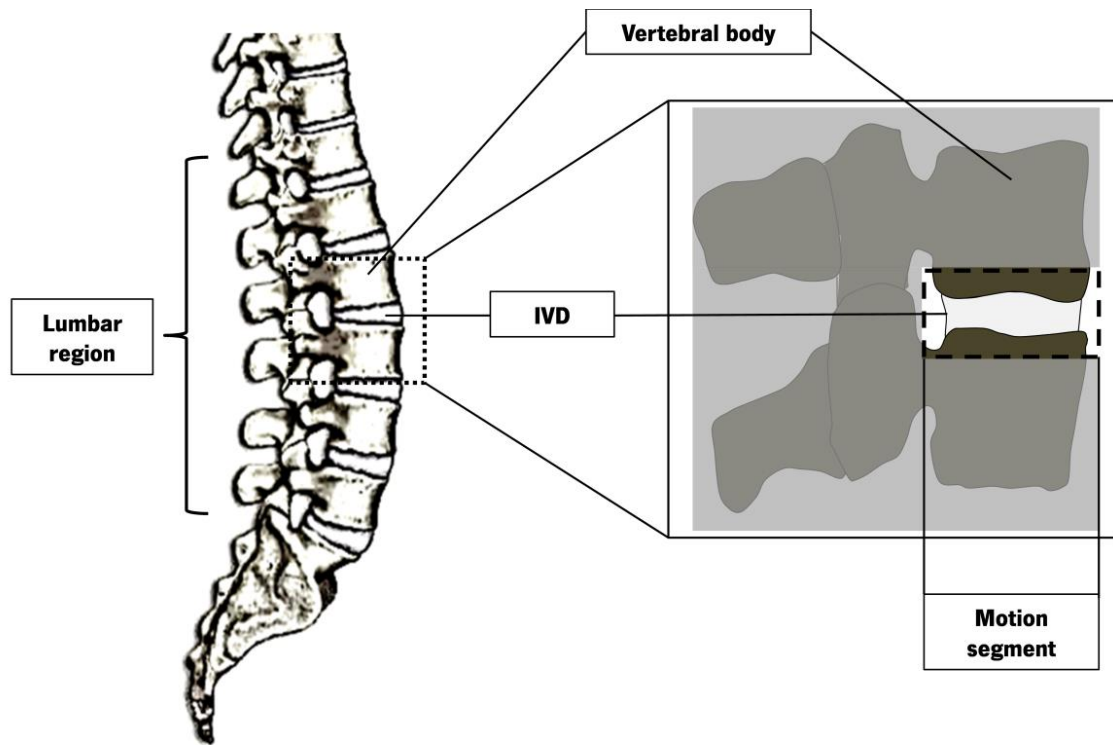


**Figure 2.5.** Representation of the motion segment preparation. This structure is highlighted by the dashed rectangle. To obtain a motion segment, two vertebrae are cut parallel and transversely, obtaining an assemble composed by two half vertebra with a disc in between.

For the characterization of IVDs using motion segments, the model should be carefully chosen. Despite the evident differences in geometry of motion segments, the use of animal models for IVD research is widely accepted and essential for testing specific hypothesis and relationships (Lotz, 2004). The selection of animal models to both study IVD degeneration and to evaluate disc treatment methods is normally based on the availability of the animal tissue, the variability between subjects compared with humans, and the feasibility of performing *in vivo* experiments. However, several features should be included in the selection of particular species as model, such as size, cost, disc geometry, biochemistry, cellularity, and biomechanics. Thus, the knowledge about the similarities and differences between animal and human discs is



important for the choice of a suitable model for interpretation of results with respect to the human disc (Beckstein et al., 2008).

In Chapter 3, a compilation of the reported data about the mechanical properties of the motion segment under compression will be given. Moreover, this Chapter also includes a discussion about the viability of animal models for the motion segment testing.

#### 2.3.4. The Internal Disc Pressure

The IVD is both complex and inhomogeneous, allowing successful load-bearing movements due to the synergy of all components of IVD (Schechtman et al., 2006). However, this structure is subjected to several ranges of loads during the daily routine, including overloading. This kind of phenomenon could induce injuries in IVD, since the internal disc pressure is beyond what IVD could withstand (Wilke et al., 1999). Nonetheless, healthy IVD is capable of sustain stress gradients due to hydrostatic pressure exhibited by NP, normally known as intradiscal pressure (IDP) - Figure 2.6.

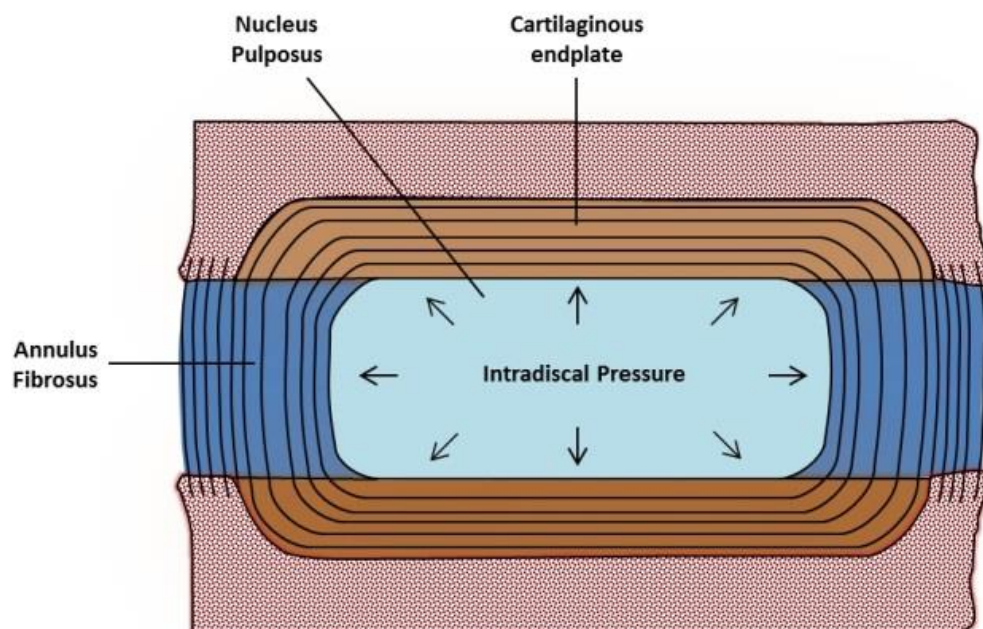


**Figure 2.6.** Intradiscal pressure (IDP) exerted by the NP is omnidirectional and varies with applied load.

The internal disc pressure or intradiscal pressure can be defined as the hydrostatic pressure presented by the NP of a healthy IVD (Claus et al., 2008). The IDP plays a key role on the IVD's ability to withstand the physiological loads (Steffen et al., 1998), being an important parameter to understand the aetiology of the disc degeneration. The IDP data has been essential to clarify the effect of the external loads on the IVD behaviour, helping to recognize the mechanism of IDP drop in disc degeneration. Thus, it represents an outstanding tool to prevent the spinal complaints by forming a basis for clinical advice for the implementation of correct sitting postures (Claus et al., 2008). In addition, this information is the basis for physiotherapy and rehabilitation programs (Wilke et al., 1999).

At a biomechanical point of view, the IDP is highly influenced by the axial spinal load (Sato et al., 1999). According to this, an increase on the compressive load applied to healthy discs is converted into IDP (Schechtman et al., 2006). Since the NP can be considered as incompressible (Castro, 2013; Cloyd et al., 2007; Iatridis et al., 1996), the AF bulges outward due to the stretch of annular fibres (van der Veen et al., 2008), which, together with the osmotic gradient, promote a loss on both disc height and volume.

The importance of IDP is reinforced due to difficulties on the assessment of the disc strength properties. For example, a simple compressive overloading does not induce damage on the disc structure. However, previous studies showed that before occurring any disc disruption, the compressive overloading promotes the vertebral endplate damage and collapse (Schechtman et al., 2006). These phenomena could be explained at a cellular level by the influence of the IDP on the chondroid tissues, characteristic of the IVD (Adams et al., 2009). On one hand, the IDP or gradient pressures could induce the internal disruption on these tissues, causing a progressive structural failure typical on disc degeneration (Adams et al., 2009). On the other hand, the stresses and pressure oscillations also affect the cell metabolism, where the IDP levels influence the matrix synthesis.

The measurement of the IDP is a subject of intense research. Numerous authors have developed experimental methods to determine the relationship between the IDP and the disc mechanics: some authors were focused on the association between the IDP and the external load

applied or posture adopted; others were more involved on the calculation of IDP value that leads to AF disruption. Next subsections will describe with more detail the studies performed under these subjects.

### **2.3.5. Relation between Internal Disc Pressure and External Loading**

Previous studies investigated the relation between external loads applied and IDP on lumbar (Dennison et al., 2008; Heuer et al., 2007; Nachemson and Elfström, 1970; Nachemson, 1965; Sato et al., 1999; Schultz et al., 1982; Wilke et al., 1999) or cervical (Cripton et al., 2001; Hattori et al., 1981; Pospiech et al., 1999) discs.

The magnitudes of pressure and the methodologies developed for measure the IDP are diverse - Table 2.6. The first *in vivo* approaches were performed on the 1960s and 1970s (Nachemson, 1965, 1963; Okushima, 1970), alerting for the importance of IDP on the spinal biomechanics (Claus et al., 2008). A pressure transducer using elastic polyethylene tubing was used in healthy discs for IDP determination. This transducer was threaded over the side of a tip from a hollow liquid-filled needle, connected with an electromanometer. The results showed that a healthy NP could behave hydrostatically and the IDP is dependent on the posture. Even though the interesting findings, this pioneer approach presents a couple of limitations. First, the polyethylene membrane does not present enough sensitivity for dynamic pressure measurements. Second, the fluid-filled needle is not prepared to bend more than 20° (Nachemson, 1965). The evolution of the transducer technology and its increased accuracy leads to a decrease on the IDP measurement (a reduction of 25 and 33%), due to the replacement of liquid-filled sensors by the piezoresistive ones, as well as the set of calibration to body temperature rather than room temperature (Claus et al., 2008). The initial approach using a transducer was developed by Nachemson & Elfström (1970): a piezoresistive semiconductor strain gauge was imbedded in a rigid resin into a tip of a 0.8 mm diameter transducer needle. This sensor allows bending until 40° without affecting the IDP measurement, thus increasing the IDP measurement accuracy (Claus et al., 2008).

**Table 2.6.** Previous studies reporting the IDP according to the type of load/posture adopted, for human IVDs.

<b>Author (Year)</b>	<b>Number of tests; Donor 's Age (years) (Mean <math>\pm</math> S.D.)</b>	<b>Transducer Type</b>	<b>IDP evaluation</b>	<b>Mean IDP [MPa]</b>
<b>Lumbar spine</b>				
Nachemson (1963-65)	n=8; 40 $\pm$ 8	Liquid-filled	Relaxed standing	0.70
			Relaxed sitting	1.13
Nachemson & Elfstrom (1970)	n=9; 28 $\pm$ 13	Piezoresistive	Relaxed standing	0.72
			Relaxed sitting	1.00
Schultz et al. (1982)	*	Piezoresistive	2400 N axial load	1.60
Sato et al. (1999)	n=8; 25 $\pm$ 2	Piezoresistive	Relaxed standing	0.53
			Relaxed sitting	0.63
Wilke et al. (1999)	n=1; 45	Piezoresistive	Relaxed standing	0.50
			Relaxed sitting	0.46
			Lifting a 20-kg weight with round flexed back	2.30
Heuer et al. (2007)	n=7; 48 (range:38-58)	Piezoresistive	500 N axial load	0.49
Dennison et al. (2008)	n=5; 69 $\pm$ 12	Fibre Gratings	800 N axial load	2.40 - 3.50
<b>Cervical spine</b>				
Hattori et al. (1981)	*	Piezoresistive	53 N axial load	0.31
			75 N axial load	0.45
			100 N axial load	0.59
			155 N axial load	0.91
Pospiech et al. (1999)	n=7	Piezoresistive	<b>Muscular inactivation</b>	
			- Flexion/Extension	0.23 - 0.32
			<b>Muscular activation</b>	
			- Flexion/Extension	0.36 - 0.64
Cripton et al. (2001)	** ; n=4	Piezoresistive	1000 N axial load	3.5

\* No access to donor 's age

\*\* One donor with 80 years, other one with 83; No data for the remaining two donors.

In early 80's, Schultz et al. (1982) tried to validate a biomechanical model lumbar spine by monitoring the IDP and the myoelectric signals, using a piezoresistive transducer for IDP measurement. This study pointed to 1.6 MPa of mean IDP, for a compressive load as much as 2.4 kN. The main finding of this study was that overloading could be a promoter of low back disorders.

In the late 90s, two important studies were published: Sato et al. (1999) developed an *in vivo* new approach using a piezoresistive sensor to determine the IDP in young patients. The innovative principle of this method was the sensor positioning: the sensing diaphragm was mounted laterally on the transducer needle (1.2 mm diameter); Wilke et al. (1999), studied the IDP *in vivo*, in one volunteer, with 45 years old, performing various daily life activities. To measure the IDP, a piezoelectric pressure transducer, with 1.5 mm diameter and 7 mm length, was implanted in the NP of a healthy L4–L5 disc - Figure 2.7.

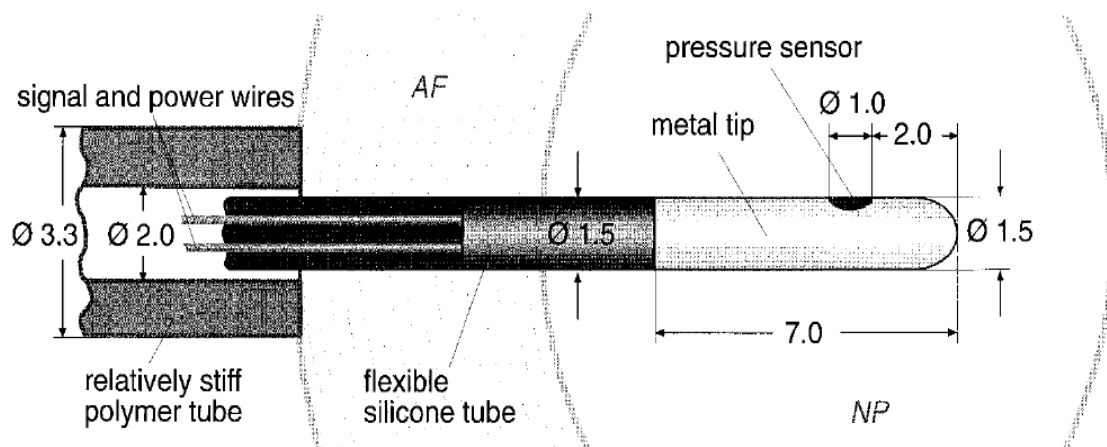


**Figure 2.7.** Schematic representation of the pressure transducer used by Wilke et al. (1999).

However, in this case, the IDP was recorded telemetrically, avoiding the problem of having a needle *in situ*. These studies reported similar IDP for standing position and reinforced the idea that *in vivo* IDP varies accordingly to the adopted position of the body and the compressive force applied. Interestingly, Wilke et al. (1999) revealed that pressure increases during sleeping, which presumably occurs due to rehydration of the IVD. Nevertheless, even though the work provides useful data about the magnitude of IDP for different human positions, the test was performed in only one subject, which is not statistically significant.

Although the accuracy of piezoelectric sensors, they are not able to characterize pressure profiles within disc (Dennison et al., 2008). With the advances on the sensor technology, new sensors were adapted for IDP measurement. Dennison et al. (2008) used small diameter (125  $\mu\text{m}$ ) Fibre-Bragg grating, which consist on an optical fibre with a Bragg grating embedded into a fibre core. These sensors are known to be biocompatible, mechanical compliant and insusceptible to electromagnetic interference. This work points to linear response of disc pressure as function of compressive load applied.

Heuer et al. (2007) also quantified the IDP *ex vivo* introducing a piezoresistive sensor into the NP by the lateral side of IVD and correlated it with the 3D contour variation, determined with a non-contact laser scanning. The mechanical test consisted on the application of 15 minutes of a 500 N static compression. This work showed that these loads result in an IDP of 0.49 MPa (range: 0.36–0.53 MPa), decreasing linearly to 0.48 MPa (0.36–0.52 MPa) during a continuous disc compression. It was also revealed that the disc bulging was around a few tenth of millimeters, meaning that this methodology could be useful to detect the variation of IVD geometry during different loading and IDP fluctuations. A deep analysis in Table 2.6 allows observing that, in the tests performed on lumbar spine, there is a wide discrepancy of results for similar test conditions. For example, while Dennison et al. (2008) reported a minimum of 2.4 MPa for an axial loading of 800 N, Schultz et al. (1982) had previously reported 1.6 MPa for 2400 N. These divergences can be explained by different patient's age or even the accuracy of the techniques. Thus, it is essential a standardization of the test conditions in order to access the correct value of human IDP (Vergroesen et al., 2014).

In contrast to the extensive experimental work on lumbar IDP, the data related to cervical pressure is particularly scarce. The measurements on the cervical are challenging due to the small size and anatomy of the cervical IVDs. Hattori et al. (1981) was the first study recording the cervical IDP *in vivo*. A needle-based pressure transducer was used, during common neck movements. The results showed no differences among the cervical IVDs, detecting the values of 0.31 MPa and 0.91 MPa for 53 N and 155 N of axial load, respectively. Later, Pospiech et al. (1999) studied the IDP of cervical spine *in vivo* using a specially developed spine tester. This device allowed not only testing intact specimens and after discectomy and fusion in C4-C5, but

also simulating the muscle forces acting on both test conditions. The IDP was measured using a pressure transducer mounted on a 1.3 mm-diameter needle. The results showed significant increase in IDP when the musculature was activated and a marked increase in IDP in both segments adjacent to fused vertebrae.

Although the importance of these findings, the cervical IDP measurement presents additional difficulties, since the cervical annular fibres can disrupt with the needle-tip insertion, due to its rigidity and its large diameter (over 1mm) (Cripton et al., 2001). To minimizing the AF disruption and reduce the distortion of the IDP signals or specimen kinematic behaviour, (Cripton et al., 2001) tested *ex vivo* the cervical IDP response to external loads, using with a 0.26 mm diameter flexible electric wires passing through AF. They found a maximum of 3.5 MPa for cervical IDP under a 1000 N axial load. These values are comparable with those reported for the lumbar region by (Dennison et al., 2008), indicating that cervical and lumbar spine present a similar IDP value for this particular loading magnitude.

### **2.3.6. Annular Failure Strength due to Internal Disc Pressure**

Despite the panoply of mechanical tests intending to elucidate the contribution of loads to annular tear or disruption, the effect of the IDP fluctuation on the AF injury remains unknown. The measurement of the IDP value that leads to AF disruption is a subject of extreme interest, not only to understand the mechanisms of IVD failure but also for the IVD replacement design, since new implants should withstand the daily routine activities without collapsing.

Previous studies have determined the maximum value of IDP that annular fibres support before failure (Iencean, 2000; Menkowitz et al., 2005; Schechtman et al., 2006; Veres et al., 2010). Schechtman et al. (2005) investigated the intrinsic failure strength of the intact bovine caudal disc by a process of inflation promoted by a hydraulic actuator - Figure 2.8. In this work, a colored gel was injected into the NP, under monitored pressure. It was found a mean hydrostatic failure pressure of  $18 \pm 3$  MPa. This method allowed understanding the alterations of the intrinsic disc strength associated with prior loading history or degeneration. However, it does not give information about the microstructural behaviour of the inner annular fibres after the inflation.



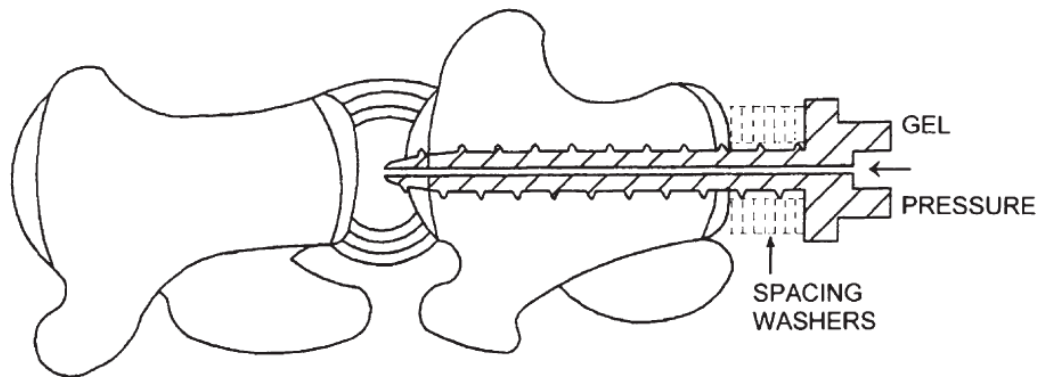


**Figure 2.8.** Schematic representation of the system used to inject coloured hydrogel on NP, via vertebrae (adopted from Schechtman et al. (2005)).

Later, Veres et al. (2010) used the same technique performed by Schechtman et al. (2005) to investigate the role of high IDP on annular fibres disruption in ovine lumbar IVDs. This team included the analysis of the AF damage after insertion of pressure into NP by a microstructural investigation. The main findings showed that posterior annular region is more susceptible to disruption than any other disc region, due to inability of the disc to distribute the hydrostatic pressures circumferentially.

Menkowitz et al. (2005) documented a mean intradiscal rupture pressure of 0.28 MPa on the cervical spine (range 0.1-1.18 MPa), using a 25G needle for the insertion of a contrast dye, with IDP monitoring during time - Figure 2.9.



**Figure 2.9.** Test performed by Menkowitz et al. (2005). During the pressurization test, the structure was not confined or axially loaded.



This study indicated that rupture of cervical annular fibres could occur for IDPs within the physiological range on the lumbar spine (see Table 2.6), showing that the injury on cervical spine could be induced at significantly lower pressures. In addition, the authors did not detect a measurable IDP change in any of the adjacent IVD levels, for the maximum IDP. Moreover, lencean (2000) inflating human lumbar IVD with compress air via CEP access, reported a rupture pressure up to 1.3 MPa, demonstrating that the injury on human lumbar spine could be also induced at significantly lower pressures. Furthermore, this divergence could be also caused by the experimental approach: on the one hand, the interspecies dissimilarities could explain the discrepancies, since each animal IVD presents their own particularities; on the other hand, the differences between the methods used to measure the failure IDP could be related to these differences as the researchers used different methods to assess the failure IDP.

All of these methodologies helps to generate valuable data, useful for a pre-clinically evaluation of spinal implants and disc injuries in further biomechanical *in vitro* experiments. However, the development of a device which allows monitoring the IDP, after nucleotomy, is desirable. Thus, more tests should be performed in order to clarify the magnitude of the annular failure strength for human discs.

## **2.4. Disc Degeneration**

The degenerative disc disease (DDD), is the most significant cause of back pain. The process of DDD cannot be really called a disease but it represents a term used to describe the changes in disc structure and composition which give rise to mechanical and physiological dysfunction and failure (Adams and Roughley, 2006).

The development of DDD is normally associated to a decrease on water concentration of the disc with ageing and degeneration, which induces irreversible changes on the mechanical behaviour of IVD. This process leads to a less effectiveness of NP as a cushion and consequently the weakening of the AF. Thus, when NP is subject to a higher pressure, the rupture of AF can occur by pouring out the gelatinous NP through damaged zone of AF.

However, the detailed study of disc degeneration is a difficult process, mainly because it is a diffuse definition, due to a line of associated parameters that are extremely hard to quantify. To overcome this problem, the use of animal models is suggested on the study of DDD. However, the use of these samples is quite controversial. On one hand, the animal samples present several anatomical variations. A great difference is visible on NP, where the majority of mammals present notochordal cells during all life. On human, these cells disappear during infancy (van der Veen, 2009). Moreover, while in humans the CEP acts as a growth plate for the vertebral body, on animals there are two growth plates within the vertebral body and CEP much thinner than found on humans (Urban and Roberts, 2003). On the other hand, although they are important to obtain a first insight on the aetiology of disc degeneration in animal samples, the most relevant information of the aetiology of disc degeneration is provided by human studies (Urban and Roberts, 2003).

The factors that involved on DDD process remains the same after several decades of research. However the degree of importance of each factor is changing with last researches (Shankar et al., 2009).

#### **2.4.1. Nutrient Failure on Intervertebral Disc**

Among the theories behind the cause of disc degeneration, one of the most consensual is the failure of the nutrient supply to the IVD cells. As it is known by common sense, all cells types require nutrients in order to perform their normal activity and to remain alive (Adams et al., 2000). Thereby, a decrease in nutrient supply, namely in oxygen levels and pH, could disturb the normal metabolism of cells. IVD cells are not an exception: the nutrients are diffused through several pathways, as both capillaries in CEP and AF (Sélard et al., 2003).

Numerous factors could affect the normal nutrient supply in the IVD. Despite the mechanism of nutrient supply blockage remains unknown, it is suggested that both long term and the absence of exercise could affects the capillaries pathways. Some diseases such as atherosclerosis sickle cell anemia, Caisson disease and Gaucher's disease are also linked to the increasing of DDD by nutrients supply failure (Urban and Roberts, 2003). The nutrients suppression is also related to the calcification of CEP (scoliotic discs). In this case, although blood supply remains undisturbed, the nutrients did not reach the disc cells. Thus, even though the scant information about the nutrients supply in the disc, it was found that there is a reduction in nutrient transport in scoliotic IVDs (Urban and Roberts, 2003). All these evidences support the idea that a lack in nutrient supply could eventually induce the DDD state.

An additional particularity that contributes to IVD degeneration is the fact that this structure is not supplied with healing nutrients and oxygen, not presenting self-repair capacity when damaged. This limitation potentiated the appearance of several treatment options comprise either or both pain management, by plaster jacket, pain reducing drugs and physiotherapy, or invasive surgical interventions, like vertebral interbody fusion or spinal arthroplasty. However, to restore the normal physiology of nutrient supply in the IVD represents complex challenge, since it can be associated to an irreversible anatomical injury.

#### **2.4.2. Genetic Factors**

In the last years, several researches showed that genetic factors could be behind the process of DDD. This fact was demonstrated by recent studies, which indicate that the heritability of DDD

exceeds 60% (Urban and Roberts, 2003). Recent findings demonstrated that mutations in two collagen type IX genes, namely COL9A2 and COL9A3 (Shankar et al., 2009) are related with DDD. Moreover, some polymorphisms were also related with a risk increment for DDD (Ala-Kokko, 2002), representing a strong evidence of genetic predisposition for the DDD. Polymorphisms in the aggrecan gene are also linked to DDD, leading to a lower chondroitin sulfate concentration in IVD. This absence results in discs with similar characteristics to the degenerated ones. A quick progress of DDD is also linked to a polymorphism in the promoter region of the matrix metallo-proteinase gene, MMP-3 (Hoogendoorn, 2008).

Interestingly, the majority of genetic mutations related to DDD, are normally associated to the production of molecules evolved in structure and function of extracellular matrix. Nevertheless, there is a need of different approaches in DDD genetic research. In spite of the importance of these studies, there is a lack on the genetic research for other systems, such as the metabolic pathways. In addition, they only recognize the locus responsible for IVD herniation, but the gene directly associated to DDD remains still unknown (Urban and Roberts, 2003). Moreover, since there is only a gene-environment interaction, genetic studies in isolation are not indicated to define the various pathways of IVD degeneration.

### **2.4.3. Mechanical Factors**

As referred previously, mechanical overload is considered as one of the main causes of DDD. These abnormal loads are known to origin low back injury, which is normally linked to DDD

Although intense exercise does not appear to affect discs adversely and they are reported to respond to some long-term loading regimens by increasing proteoglycan content, experimental overloading or injury to the IVD can induce the DDD. Furthermore, the support for the influence of abnormal mechanical forces in the development of DDD comes from the conclusion that the IVDs adjacent to a fused segment had suffered a quick degeneration (Urban and Roberts, 2003).

The loading also affects also the IVD cell metabolism (Hsieh and Twomey, 2010). When the matrix is subjected to a direct mechanical stimulation, several phenomena such as cell and

NP deformation, change in both membrane and volume of the cells and cytoskeletal strain could occur in the IVD (Chan et al., 2011).

This influence of mechanical factors is also supported by many epidemiological studies that have found associations between environment factors and development of disc degeneration. Changes in physical environment around cells caused by loading, such as the concentration of fluids and proteoglycans, pH, osmolarity and fixed charge density, affects the nutrients concentration and metabolic products in the IVD (Chan et al., 2011). Thus, as it was previously referred, it is important to analyze the mechanical behaviour of IVD in order to understand the influence of load/overload in the DDD evolution.

## **2.5. Disc Treatment**

The low back pain implicated by a degenerated IVD is considered a problem of difficult resolution by the clinicians. Several procedures have been developed in order to treat the DDD state (Whatley and Wen, 2012). Currently, it is common the use of non-surgical therapies such as analgesia, muscle relaxants, injection of corticosteroids, or local anaesthetic, manipulation therapies and exercise (Urban and Roberts, 2003). However, these techniques are only used as pain relievers, which could not be considered a long-term solution. When these techniques are not well-succeeded, surgery is required. Among the surgical solutions, the discectomy or arthrodesis and the disc replacement are normally adopted.

### **2.5.1. Discectomy/Arthrodesis (or Fusion)**

The most common surgical procedures for patients with DDD are discectomy and arthrodesis (van der Veen, 2009). While discectomy characterizes the process of excision or removal of the degenerated portion of the IVD, the arthrodesis (normally referred as spinal fusion) represents the process of fusing two adjacent vertebral bodies together (Bohlman et al., 1993). This method, largely used worldwide, allows to restore stability and weight bearing in the IVD (Hoogendoorn, 2008).

The clinicians normally adopt the spinal fusion as typical procedure after a discectomy, in order to promote the patient comfort, reducing the motion and instability in the spine column. In addition, it is expected that the reduction in the mobility decreases the pain for the patients (Rousseau et al., 2006). However, although it shows good short-term results as pain relief, it usually leads to a loss in IVD height due to negative biomechanical changes and anatomical problems. The problems associated to the spinal fusion include limitation in the motion of a segment or joint and failure of the effective immobilization (Whatley and Wen, 2012). Moreover, the motion segments that are adjacent to a fused vertebrae, suffer an increment on the stress concentrations (Goto et al., 2003), leading to pathologies in these segments.

Due to the problems associated to discectomy and spinal fusion, such as loss of spinal function and the possible adjacent disc degeneration, new solutions are being developed (Whatley and Wen, 2012).

### **2.5.2. Intervertebral Disc Replacement**

As definitive solutions, the discectomy and spinal fusion are not the most desirable solution for low back pain or DDD. Consequently, the IVD replacement is presented as a valid alternative, since it presents some advantages when compared with previous solutions. While the discectomy and spinal fusion induce limitation in patient mobility, the IVD replacement ensures some spinal mobility (Bono and Garfin, 2004), as well as it reduces the pain (Rousseau et al., 2006; Whatley and Wen, 2012).





The selection of features for a disc implant is essential for the development of an efficient replacement of the disc. Concerning to its general characteristics, the implant should be biocompatible, durable and easily implantable (Whatley and Wen, 2012). In addition, it should take in account the design, the patient and the spine level where should be introduced (Bono and Garfin, 2004).

Thus, a replacement of disc must be prepared to remove the diseased tissue, to reduce the pain and to restore the disc function. Currently, there are two different approaches for disc replacement: the Total Disc Replacement (TDR) and the Nucleus Pulposus Replacement (NPR).

#### **2.5.2.1. Total Disc Replacement**

In recent years, the TDR has received increasing attention as DDD treatment. This methodology allows the maintenance of mobility in an operated disc, which could also reduce the possibility of adjacent segment degeneration (Jacobs et al., 2012), helping to re-establish flexibility of the spine. In addition, this technique is normally recommended for later stages of DDD, where the integrity of the native AF has been compromised or associated to pain in the patient (Joshi, 2004). Some FDA approved TDR solutions are presented in Table 2.7.

**Table 2.7.** Surgical approach and the FDA<sup>iv</sup> approval for four types of lumbar TDR designs.

Name	Maverick®	Mobidisc®	ProDisc L®	SB Charité®
<b>Design</b>				
<b>Surgical approach</b>	Under development	Retroperitoneal	Transperitoneal or retroperitoneal	Anterior and retroperitoneal
<b>FDA approval</b>	Approved for FDA study	Clinical trials	Yes	Yes

Among the artificial discs proposed for TDR, the SB Charité III® undergone in the longest clinical trials. This device consists on an ultra-high molecular weight polyethylene (UHMWPE) sliding core positioned between two cobalt-chromium alloy endplates. The UHMWPE core was designed to allow unlimited axial rotation, but only 20° flexion (Joshi, 2004; McCullen and Yuan, 2003). To stimulate the osteointegration in the adjacent vertebrae, the cartilaginous endplate were coated with titanium and hydroxyapatite (Joshi, 2004). However, the center of rotation of the SB Charité III® was considered as too anterior and the polyethylene core would undergo on cold flow in about four years. The clinical tests performed in humans showed that 92% of patients had complained about preoperative back pain, while 40-50% noticed a reduction in the pain (Joshi, 2004). Latest studies indicated that the use of this device produced results similar or superior to fusion (Guyer et al., 2012; Whatley and Wen, 2012).

One of most known TDR solutions for IVD replacement is the Pro-Disc®. It consists of endplates composed of cobalt chrome molybdenum (CoCrMo) alloy articulation with a fixed

<sup>iv</sup> FDA – USA Food and Drug Administration – More details on the webpage [www.fda.gov/](http://www.fda.gov/)



UHMWPE bearing surface, articulated on metal. During the surgical procedure, a central keel provides an immediate secure fixation to vertebral bodies (Delamarter et al., 2005). The bone ingrowth is also promoted by the porous coatings or screws, contained in the metal implants (Whatley and Wen, 2012). Concerning to the clinical results, patients who received this device instead of fusion had a significant improvement in pain and functional condition in the early postoperative period (Delamarter et al., 2005). In addition, the Pro-Disc® presented a decrease in operative time, blood loss and length of hospitalization when compared with spinal fusion (Whatley and Wen, 2012).

Another option for TDR is the Maverick® artificial disc (Maverick TDR, Medtronic Inc., Memphis, TN, USA). It consists of an all metal disc implant containing a ball and socket that presents high fatigue strength, presenting the same principle used by the Pro-Disc® - the device rotation is limited to a fixed center (Whatley and Wen, 2012). Whereas the upper articulating surface is a thinner and matched dome-shaped concavity, built into the end plate component, the lower articulating surface is a dome-shaped protrusion from the CEP (Bono and Garfin, 2004). However, the Maverick® and the Pro-Disc® can be distinguished by its kinematic responses. While the Pro-Disc® possesses an articulating surface with a curvature radius of 9 mm, the Maverick® presents a radius of 8.1 mm. In addition, when the devices were placed in the spine, the location of the Pro-Disc® center of rotation is 5 mm anterior to the one of the Maverick® (Whatley and Wen, 2012). A study performed by Le Huec et al. (2005) revealed that an increment in the degeneration of the extensor muscles was associated to a worse clinical outcome. This study also reported a degree of mobility close to normal as well as a degree of improvement equivalent to that obtained with anterior fusion cages using the mini-invasive technique. In addition, it was also demonstrated that the surgical technique is safe, since the intra- and postoperative complication rates are low (Le Huec et al., 2005).

The varied rate of long-term success of the SB Charité® III gave rise to a second generation of TDR approaches. These new devices aim to reduce UHMWPE wear debris, optimize the device implantation and improve implant stability (Austen et al., 2012). The Mobidisc® (LDR Spine, Troyes, France) belongs to these “second generation TDR solutions”. The Mobidisc® consists of two polished cobalt-chromium endplates with a UHMWPE core, which presents a

spherical domed superior surface and a flat inferior surface. In addition, it is articulated by two lateral wings within lateral capture mechanisms in the inferior cartilaginous endplate. In terms of clinical results, it was reported an improvement in the mobility and in both Visual Analog Scale<sup>V</sup> and Oswestry index<sup>VI</sup> in 149 patients. However, in 149 patients analyzed, 12 complications had appeared, resulting in three revision surgeries (Villarraga and Ianuzzi, 2009). In addition, a study performed by Austen et al. (2012) revealed the presence of UHMWPE particles and inflammatory cells in the device.

All these TDR solutions showed significant improvements for patients when compared to conventional treatments, such as spinal fusion. However, current implants present also some relevant drawbacks, including loosening, extrusion, infection and cytotoxicity (Cunningham, 2004; Denozière and Ku, 2006; Geisler, 2006; Whatley and Wen, 2012). These problems could appear in all the approaches described: (1) metal-on-metal devices interaction could generate toxic wear debris and large compliance mismatch, leading to foreign body reaction and, eventually, to a destruction of the tissue implant interface. In this case, the metal endplates may dislocate or even drift out of the bone, since the interface implant-vertebral body is affected (Whatley and Wen, 2012); (2) the polyethylene, normally used in both SB Charité® and ProDisc®, could also experience loosening and wear, or even incur in creep or fracture (Rawlinson et al., 2007; van Ooij et al., 2003; Whatley and Wen, 2012).

Due to the described complications, some revision surgeries are required. These operations aim to remove the implant followed by a spinal fusion to immobilize the affected area. However, this kind of surgeries is dangerous for the patient, since the surrounding scar tissue makes it hard for the surgeon to operate near the spine (Whatley and Wen, 2012). Thus, more studies are needed in order to evaluate the long term survival and integrity of the current TDR solutions.

---

<sup>V</sup> Visual Analog Scale is the psychometric response used to measure subjective characteristics that cannot be directly measured.

<sup>VI</sup> The Oswestry Disability Index represents a low back pain questionnaire used by clinicians to quantify disability for low back pain.

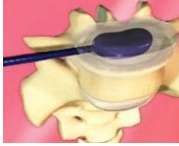


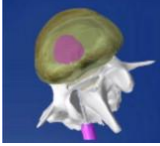

In spite of these solutions representing a great improvement in DDD therapy, current methodologies did not demonstrate to be a complete success in the ability to regenerate the injured disc. TDR techniques cannot reestablish the physiological motion and stability (Ross, 2009) as well as they could induce divergencies in loading absorption (mainly in compressive forces) and compliance mismatch between the implant and the native spine (Gloria et al., 2007), which could induce degeneration at other disc levels (Rousseau et al., 2006). Finally, the clinical results of TDR cannot be considered as effectively reproducible, since they did not represent a general solution for all the patients (Whatley and Wen, 2012).

### **2.5.2.2. Nucleus Pulposus Replacement**

In opposition to the total disc replacement, the NPR preserves the disc structures (AF, CEP and ligaments) with exception for NP (Shim et al., 2006). In addition, NPR solutions normally contains high water contents, promoting the fluid flowing through disc and consequently the nutrient delivery, mimicking the native tissue physiology. The NPR solutions are also less invasive, helping to preserve the natural forces acting on the spine (McCullen and Yuan, 2003). Several NPR designs are currently being developed, on clinical trials or even being commercialized (Bao and Yuan, 2002). Among the NPR solutions, several devices were already implanted in humans, being these described in Table 2.8.

The DASCOR Disc Arthroplasty System (Disc Dynamics, Inc., Eden Prairie, Minnesota), has recently been introduced. It consists of a catheter-based polyurethane balloon, with an in situ cured polyurethane core. The balloon presents an important mechanical function, since it only lies on the device during the implementation stage (Tsantrizos et al., 2008). To implant the device, the balloon is injected under pressure with the in situ-curable polyurethane by a system specially designed for the effect. Since polyurethane cures, the balloon adheres to it, acquiring both the disc space size and shape (Lewis, 2012; Tsantrizos et al., 2008). Although good results were presented by this device in humans, some deposition of wear particles were observed, especially along the most anterior and posterior edges (Tsantrizos et al., 2008), which could induce an immune response.

**Table 2.8.** Clinical features of NPR solutions tested in human.

Features	DASCOR	Newcleus	NuBac	Nucore	PDN
<b>Design</b>					
<b>Types</b>	In situ curable polymer	One-piece mechanical	Two-piece mechanical	In situ curable polymer	Composite polymer
<b>Composition</b>	A polyurethane core and a balloon	A memory-coiling polycarbonate urethane	Poly-etheretherketone (PEEK-on-PEEK)	A protein polymer hydrogel, with the polymer chains	Flexible preformed hydrogel core encased in a jacket
<b>Surgical Approach</b>	Retroperitoneal, mini-anterior lumbar interbody fusion or anterolateral transpoas	Microdiscectomy	Posterior or extreme lateral	Posterior	Posterior
<b>Patients Tested</b>	85	5	39	14	-
<b>Devices implanted</b>	-	-	-	14	423
<b>Results</b>	Substantial decreases in ODI and VAS scores	Substantial decreases in ODI and VAS scores; No complications	Substantial decreases in ODI and VAS scores; No complications	No complications; decrease in leg pain VAS, back-pain VAS, and ODI scores; central and posterior IVD height reach 93% of preoperative value	10% explanted; complications: endplate failure (extrusion and subsidence); marked decreases in ODI scores

ODI: Oswestry Disability Index; VAS: Visual Analog Scale.

Another NPR solution already tested in humans was Newcleus (Centerpulse Orthopaedics, Winterthur, Switzerland). The implant is based in a polymer that was manufactured with a memory that, once inserted into the nucleus of the disc, it curls into a preformed spiral (Di Martino et al., 2005; Lewis, 2012). This feature allows the minimization of the annulotomy, reducing the potential for implant dislocation. The novelty of this implant is that that it does not function in a fixed axis, being resistant to compressive forces while allowing motion, even if the

component is not placed in the optimal position (Di Martino et al., 2005). Pre-clinical results have revealed adequate biocompatibility and optimum biomechanical behavior (Plasencia-Arriba and Maestre-García, 2007). Tests with human patients have confirmed that no migration of the implant and no neurologic complications associated with implant were found (Lewis, 2012).

The NuCore developed by Spine Wave (Shelton, CT) was also presented as solution for NPR. After mixing it with crosslinking agent, the polymer is injected in liquid state into the disc space and the cure takes place in few minutes. The implantation is performed posteriorly. As Newcclus, it also presents good results when implanted in both animal and human (Lewis, 2012).

A different approach was developed by Pioneer Surgical Technology (Marquette, MI): the Nubac. This device presents special features that give it a unique design. On one hand, it presents two pieces with an oval outer surface with a large contact area; on the other hand, the inner articulation of the device was designed in a *ball-and-socket* format. The results of pre-clinical tests demonstrated that the polymer is biocompatible, biodurable, presenting an excellent biomechanical behaviour. In addition, Nubac restored disc height and the typical range of motion of a segment, as well as low risk of implant rejection in human models (Bao et al., 2007).

Finally, the Prosthetic Disc Nucleus, normally known as PDN (Raymedica, Minneapolis, MN, USA), is also one of NPR solutions already approved according FDA guidelines, as it demonstrated good results in terms of cytotoxicity and biomechanical fatigue tests (Ray, 2002). The device consists of a hydrogel (polyacrylonitrile) encapsulated by a biodegradable woven polyethylene fibre mesh, in a kind of “pillow cover”, that increases in thickness and height when hydrated (Plasencia-Arriba and Maestre-García, 2007), being also prepared to prevent the excessive hydrogel swelling (Ray, 2002). The third generation of this implant is already in usage and its placement is performed by specific instruments. A minimum disc height of 5 mm is required as well as the annular ring should be unbroken to avoid the PDN migration (Goins et al., 2005). The insertion technique consists on the placement of two pillows transversely within the disc space. To preserve the annulus as much as possible, the device is introduced mediolaterally in the disc space, through a posterior laminotomy and standard discectomy approach (Bono and

Garfin, 2004; Plasencia-Arriba and Maestre-García, 2007). This approach ensures that posterior AF remains intact, minimizing the device migration (Bono and Garfin, 2004). The clinical results confirmed that PDN is effective in patients with DDD who present chronic back pain. However, the clinical improvement is very slow, as well as the postoperative pain is substantial and the PDN extrusion still remains a problem (McCullen and Yuan, 2003).

Although the use of a NP replacement appears to have a great future due essentially to be a less invasive procedure, is not as widespread as the use of total disc replacement. Moreover the NP replacements are normally implanted through incisions in the AF, compromising the integrity of the operated disc. According to this, the process of NPR could result in an inflammatory response that may at last drive to a DDD process (Whatley and Wen, 2012). Thus, it is absolutely vital the development of a therapy that restores the NP functional disc matrix with minimally invasive approach (Iatridis et al., 1998; Goins et al., 2005; Setton et al., 2006).



# **3. Effect of Quasi-Static and Cyclic Compressive Loading on the Mechanical Response of Porcine Intervertebral Discs**

*The present chapter provides information about the mechanical response of the porcine intervertebral disc to static and cyclic compressive loading. The experimental methodology evolves static and dynamic axial compressive tests and a posterior fitting in a rheological model previous described in the literature as suitable to be applied in compressive tests on the intervertebral disc. The outcomes from the experimental procedure are also discussed and contextualized in the light of previous studies about the mechanical behavior of the disc.*

## **3.1. Introduction**

The intervertebral disc (IVD) is comprised by a peripheral angle-ply laminated ring, the annulus fibrosus (AF), with the nucleus pulposus (NP) in its center, bounded by the cartilaginous endplate. This intricate and inhomogeneous IVD structure allows six degrees of freedom load-bearing movement, load transfer and energy dissipation to the spine (Nerurkar et al., 2010; O'Connell et al., 2011).

The mechanical response of the disc to loading is time-dependent, presenting a complex behaviour (Stokes et al., 2011): while the short time response is governed by viscoelastic phenomena (Campana et al., 2011; Ellingson and Nuckley, 2012), the long term response is guided by osmotic events - the fluid flows through NP, AF and endplate, ruled by fixed proteoglycans charges (Schroeder et al., 2006; Stokes et al., 2011). During daily routine events, this structure is subjected to several ranges of loads, where the quasi-static and cyclic axial compressions are the predominant ones. Several studies showed that compressive loads are



responsible for great oscillations in the intradiscal pressure (Wilke et al., 1999), disc height (Korecki et al., 2008) and disc volume (Masuoka et al., 2007). In terms of intradiscal pressure, an increase in the compressive load applied to healthy discs promotes an upturn in the NP pressure (Stokes et al., 2011). Since the NP can be considered as incompressible, the AF bulges outward (van der Veen et al., 2008), which, together with osmotic phenomenon, lead to a loss in both disc height and volume. Thus, the disc hydration influences the disc mechanics, namely the stiffness and creep properties during axial loading (Costi et al., 2002; Johannessen et al., 2004; O'Connell et al., 2011).

To assess the mechanical properties of the IVD, several samples of animal spines are widely used, namely the smallest functional unit of the spine, the motion segment (Li et al., 1995; MacLean et al., 2007; O'Connell et al., 2011; van der Veen et al., 2008). The animal disc samples are commonly used since they present higher availability and lower cost when compared with human tissues. Among disc animal models, rat (Ching et al., 2004; MacLean et al., 2007), bovine (Périé et al., 2005; Ryan et al., 2008; Vogel and Pioletti, 2012), goat (Cheung et al., 2003; Zhang et al., 2011) and porcine (Callaghan and McGill, 2001; Keller et al., 1990; Kuo and Wang, 2010) are widely used in both *in vivo* and *in vitro* studies (Korecki et al., 2008). They can be prepared directly and gripped to perform motion segment studies and surgical techniques (Cho et al., 2011).

Although the common use of these animal models, data extrapolation from different animal tests to human IVD properties should be carefully done, since benchmark values are normally not significant due to interspecies variability (Nerurkar et al., 2010). Among the animal models, porcine cervical IVDs are widely used to test the human biomechanical spine function, due to its similarity in terms of mechanical characteristics and resulting injuries (Yingling et al., 1999). In case of the porcine lumbar intervertebral discs (PLIVD), they present morphological and biological differences such as the size and the presence of notochord cells in adult pig IVDs, which did not appear in adult human ones (van der Veen, 2009). In spite of these differences, several authors used the PLIVD as model for studying human lumbar injury (Indahl et al., 1997; van der Veen, 2009). However, there is a lack of information about the differences between the

mechanical properties of PLIVD and human lumbar intervertebral discs (HLIVDs) (Ryan et al., 2008).

Thus, the first aim of this work is to quantify the mechanical properties of PLIVD under quasi-static and cyclic axial compressive loading. Consequently, the coefficient of static stiffness, ( $K_s$ ) and the coefficient of dynamic stiffness ( $K_d$ ) of PLIVDs will be experimentally determined and compared. The acquired values will be also correlated with those reported on literature for HLIVDs, to check if PLIVDs are a good model to study the mechanical properties of human samples under compression.

In addition, to numerically describe the viscoelastic behaviour of IVDs, several rheological mathematical models were used (Johannessen et al., 2006; Keller et al., 1987; Li et al., 1995; O'Connell et al., 2011; Pollintine et al., 2010). The formulation adopted to model the creep behaviour of the disc results from the combination of parallel springs and dashpots sets (viscoelastic solid Voigt model) with a spring in serial, representing the initial elastic behavior (Johannessen et al., 2006; Keller et al., 1987; Li et al., 1995; O'Connell et al., 2011; Pollintine et al., 2010). These mathematical models are very useful since they allow the state prediction of the IVD after a certain time (O'Connell et al., 2011), being also used to test differences between study groups, such as comparing the behavior of human and animal samples.

As second goal, this work proposes to compare the model parameters obtained for the PLIVD with the values reported in the literature for the HLIVD. To achieve it, a phenomenological model (O'Connell et al., 2011) was used to fit in experimental creep data for PLIVDs. This study considered that the adjacent vertebral bodies are incompressible, for the range of loads applied. Consequently, the IVD is the only structure subjected to deformation in the MS.

In this study, the optimized set of model parameters was determined and compared with those found in literature, for HLIVDs. The premise is that the parameters values may help understanding the differences between the HLIVDs and PLIVD behavior.

## **3.2. Materials and Methods**

### **3.2.1. Motion Segment Collection and Preparation**

Two porcine lumbar spines, from young cadavers (with approximately eighteen months), were collected from an abattoir. Motion segments (IVD and half of both the adjacent vertebral bodies, without posterior elements) were cut from the spines, parallel to the mid-transverse plane of the disc. In addition, all specimens were visually inspected before and immediately after the mechanical test. Care was taken to remove the surrounded tissues during dissection. The segments were stored at 4°C before testing, which were performed within 24 hours after dissection, in accordance with a protocol approved by the Institutional Human Tissue Committee (Campbell-Kyureghyan et al., 2011).

The specimens were immersed in a phosphate saline solution (PBS 1X) before, during and after the mechanical test, to prevent the dehydration. The degeneration grade was assessed by Thompson five-category grading scheme (Thompson et al., 1990), after testing. All discs presented a level I of this degeneration scale.

### **3.2.2. Testing Equipment and Motion Segment Positioning**

The testing equipment consists of a servo hydraulic testing system, Instron 8874. This machine tester presents axial and torsion axes, as well as quasi-static and dynamic loading modes, being equipped with a 25 kN load cell (the Dynacell™, class of precision 1, patented by Raymond et al. (2003)). The samples were placed on compression grips and aligned to minimize the effects of bending/extension that could occur on a compression test with a misaligned sample. Thus, the samples were positioned in a centre of a cast aluminium pot, parallel to the base. This pot was filled with PBS in order to keep the samples completely submersed. All tests were carried out at room temperature.

### 3.2.3. Quasi-Static Axial Compressive Test

During quasi-static axial compressive tests, the samples (n=7) were first submitted to a pre-load of 30 N, during 10 minutes, to ensure the contact with loading platen, helping to minimize errors due to post-mortem effects, such as the super hydration (Adams et al., 1996; Campbell-Kyureghyan et al., 2011). Then, load and displacement were set to zero and each sample was submitted to 50 N load (Phase 1). The displacement reached for 50 N load was maintained during 7.5 minutes and, subsequently, the samples were loaded until reach 500 N (Phase 2) Finally, the displacement, reached at 500 N, was kept during 12 minutes. A generic example of the quasi-static axial compressive test input is shown in Figure 3.1.

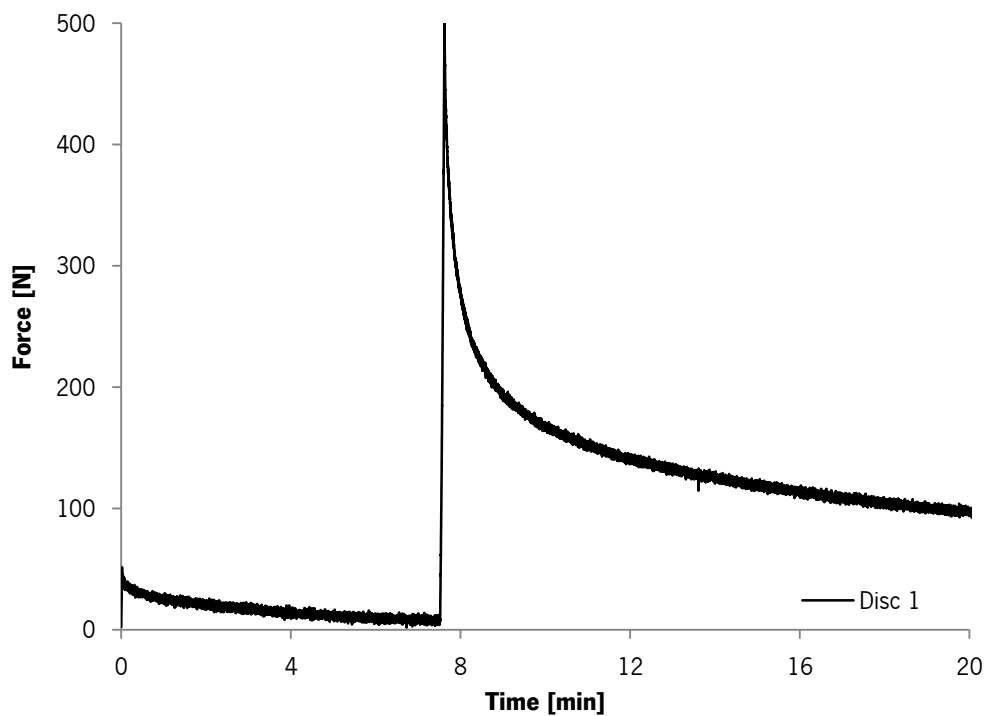


**Figure 3.1.** Generic example of the quasi-static axial compressive test input, used for the disc 1.

This kind of loading was applied in order to understand the effect of loading magnitudes on  $K_s$  of lumbar porcine IVDs. In this work, it was adopted a range of loading considered as an appropriate estimation for the PLIVDs axial loading experienced in daily life (Ryan et al., 2008). In addition, the displacement rates were set to 4 mm/min and 16 mm/min, which correspond to the physiological load rates, experimented by a human when submitted to an inclination of 30

degrees and when a human is getting up, respectively. The displacement rates were determined from the curves presented in the database OrthoLoad (Bergmann, 2008), from which the slope of the load-time curves, for these movements, was converted into displacement rates. The displacement rates used in this work are considered as quasi-static. Thus, the static stiffness coefficient,  $K_s$ , was defined as the slope of each loading increment (from both 0-50 N and 50-500 N increments), being determined using a linear trend in the curve load-displacement.

In terms of statistical analysis, the four groups of  $K_s$  values (phase 1 at 4 mm/min; phase 1 at 16 mm/min; phase 2 at 4 mm/min and phase 2 at 16 mm/min) were compared by a 2-factor ANOVA. According to this analysis, a *t-student* test with two-sample was used to characterize the significant differences between each phase and displacement rate. All statistical analyses were performed with Microsoft Excel® and significance level  $p < 0.05$ .

#### **3.2.4. Cyclic Compressive Tests**

An initial 30 N compressive load was applied, in order to ensure the contact loading platen. Each motion segment ( $n=5$ ) was subjected to 1200 cycles of axial compressive loading, at a frequency of 1 Hz. The mean load was 500 N, with amplitude of 125 N.

The data from cyclic load phase was used to determine the dynamic stiffness coefficient -  $K_d$ , which was calculated dividing the peak-to-peak load applied by the peak-to-peak displacement, for each loading cycle (Li et al., 1995). The final  $K_d$  value was determined by the arithmetic mean of dynamic stiffness coefficients obtained for each cycle.

#### **3.2.5. Five-Parameter Rheological Model for Creep Response Analysis**

To compare the creep behaviour of LPIVD with HPIVD, the experimental data were fitted into a phenomenological model, using Equation 3.1, developed by O'Connell et al. (2011). This model allows the prediction of the displacement that occurs in human IVDs, as a function of time. It consists on a five-parameter rheological model, composed by two Voigt solids and a spring in series (Johannessen et al., 2006; O'Connell et al., 2011) and it is used to determine the

displacement ( $d$ , in millimetres), as a function of time ( $t$ , in seconds) and applied load ( $F$ , in Newton). The model is mathematically described as:

$$d(t = t_i \rightarrow t_{i+1}) = F^* \left[ \left( \frac{1}{S_1} \left( 1 - e^{-\frac{t}{\tau_1}} \right) \right) + \left( \frac{1}{S_2} \left( 1 - e^{-\frac{t}{\tau_2}} \right) + \frac{1}{S_E} \right) \right] \quad \text{Equation 3.1}$$

Where  $S_1$  and  $\tau_1$  are related to the fast response,  $S_2$  and  $\tau_2$  to the slow response and  $S_E$  the elastic response. In addition,  $i$  and  $i + 1$  represents the start and the end time for the creep test.

The experimental displacement-time curve was traced considering the average displacement for each compression cycle. The objective was to minimize the noise resulting from a cyclic curve. A mean force of 500 N was adopted as the  $L$  value as this loading magnitude is recognized as within the normal physiological values (Castro, 2013). The minimization of the sum of the squared error between the predicted and the experimental displacement during creep test allows the determination of the constants of the five-parameter model for the IVDs. The parameters acquired experimentally were compared directly with reported literature for human samples.

### 3.3. Results

Previous studies showed that IVDs from the lumbar zone present a non-linear load-deflection curve in quasi-static conditions (Izambert et al., 2003). However, in this study the  $K_s$  values were obtained from a linear regression with  $R^2 > 0.92$  (Figure 3.2), indicating this approach presents a good fit for the experimental data.

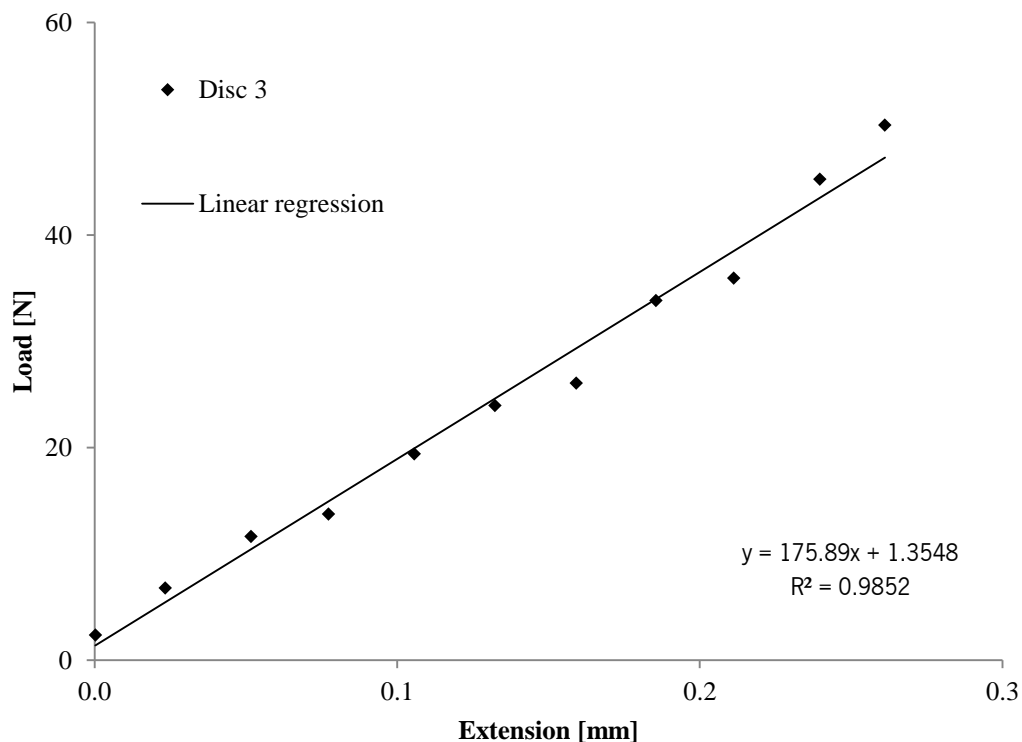


**Figure 3.2.** Linear regression performed in a motion segment sample, at a load rate of 16 mm/min, for a 0-50 N increment. The slope of this regression represents the static stiffness coefficient,  $K_s$ , which is defined as the slope of each loading increment (from both 0-50 N and 50-500 N increments).

In this study, for the first slope (0 until 50 N), the values of stiffness coefficient were lower  $0.485 \pm 0.127$  MN/m (Mean  $\pm$  S.D.) than those found in the load slope (until 500 N), where the  $K_s$  is  $1.215 \pm 0.248$  MN/m (Figure 3.3). The ANOVA test showed that there are significant differences between the mean values of the data groups analysed. Then, the *t-student* test revealed that there are significant differences in  $K_s$  according to the magnitude of the load applied (between phase 1 at 4 mm/min and phase 2 at 4 mm/min; between phase 1 at 16 mm/min and phase 2 at 16 mm/min;  $p < 0.05$ ), while non-significant differences were found

when different displacement rates were applied (between phase 1 at 4 mm/min and phase 1 at 16 mm/min; between phase 2 at 4 mm/min and phase 2 at 16 mm/min;  $p < 0.05$ ).

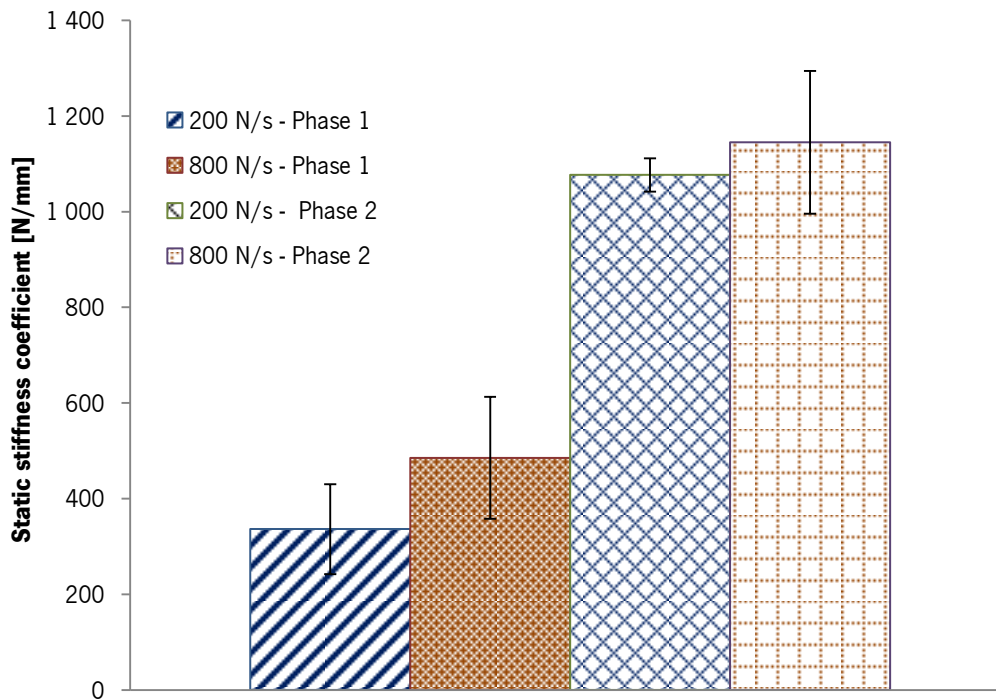


**Figure 3.3.** Bar chart representing the  $K_s$  for two different strain rates: 4 mm/min and 16 mm/min. Two different phases were also distinguished: phase 1 represents the  $K_s$  for the increasing from 0 until the pre-load (50 N), while phase 2 represents the increasing of load until reaching 500 N, for the two strain rates.

In terms of  $K_d$ , the results indicated an oscillation of values between specimens, for the five IVDs. The comparison of the  $K_d$  results with those obtained in a previous study for human IVDs - Table 3.1 - revealed that the dynamic stiffness coefficient is, at least, two times higher than the values presented for human samples. In addition, the magnitude of  $K_d$  values is between four and ten times higher than those obtained for  $K_s$ , depending on load applied.

**Table 3.1.** Experimental dynamic stiffness coefficient ( $K_d$ ), obtained in this study PLIVDs (n=5; mean and standard deviation), and HLIVDs  $K_d$  (mean) found in a previous study performed by Li et al., (1995), at 1 Hz.

	Li et al., (1995)	Present study
$K_d$ [MN/m]	2.42 ± 0.51	5.41 ± 0.05



The five-parameter model presented an average relative error of 0.2% for the fitting to the experimental data - Figure 3.4.

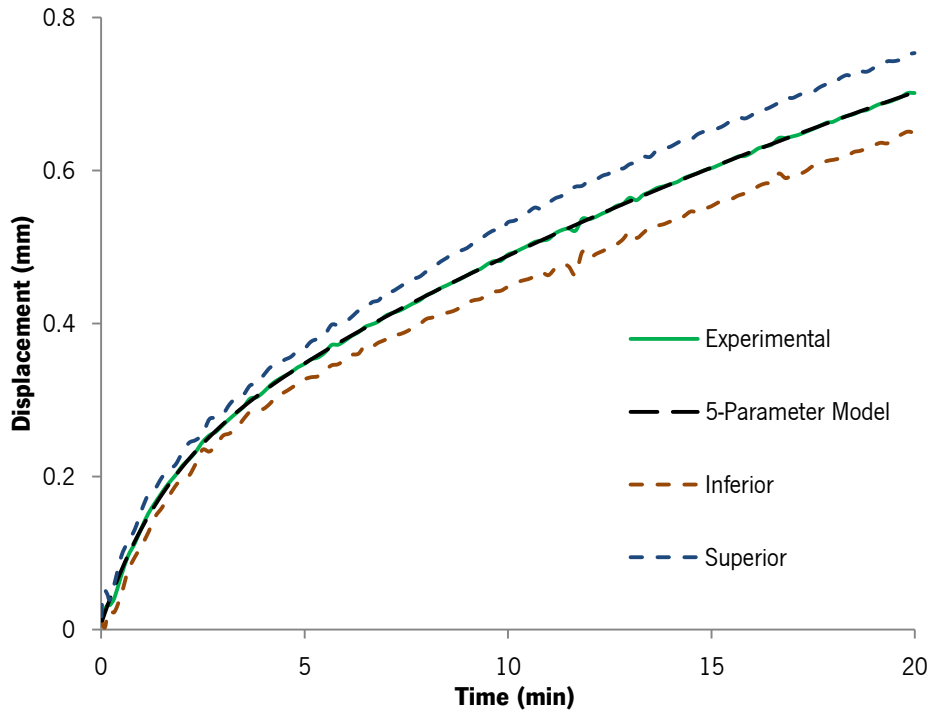


**Figure 3.4.** Comparison between the creep responses of the experimental obtained with PLIVD and the five parameter rheological model. The values were fit by the inferior and superior limits, with a confidence interval of 95%.

Thus, the rheological model presented a good fit for the set of parameters found during this study (Table 3.2). The time constants are approximately four times higher (in case of  $\tau_1$ ) and seventeen times lower (for  $\tau_2$ ) than those found by O'Connell et al. (2011). The porcine displacement parameters  $F/S_2$  and  $F/S_E$  (that correspond to slow displacement and elastic displacement, respectively) presented lower values than those obtained for human IVDs ( $F/S_2$  is six times lower and  $F/S_E$  is around ninety times). Contrarily,  $F/S_1$ , which is a parameter of fast response, is around four times higher than previous values (O'Connell et al., 2011).

**Table 3.2.** Comparison between model parameters obtained with the best fit to the experimental results with PLIVDs (mean, inferior and superior limit with a confidence interval of 95%) and the values obtained by O'Connell et al. (2011) for HLIVDs (mean and interquartile range).

	<b>Present study</b>	<b>O'Connell et al. [2011]</b>
$\tau_1$ (min)	32.04 (23.23, 47.13)	8.09 (6.12, 11.75)
$F/S_1$ (mm)	1.16 (0.91, 1.61)	0.29 (0.21, 0.44)
$\tau_2$ (h)	0.18 (0.17, 0.31)	3.07 (2.96, 3.43)
$F/S_2$ (mm)	0.27 (0.23, 0.31)	1.51 (1.31, 1.72)
$F/S_E$ (mm)	0.016 (0.016, 0.016)	1.44 (1.08, 1.71)

### 3.4. Discussion

In this study the mechanical properties of PLIVD were evaluated under quasi-static and dynamic conditions and the obtained data were compared with published values for HLIVD. Moreover, the experimental data were fitted into a phenomenological model - Equation 3.1 - developed by O'Connell et al. (2011). The results documented in this paper lead to important considerations, in both quasi-static and dynamic conditions.

A linear regression was used to calculate the  $K_s$ , with a minimum R-square of 0.92, indicating a good fit to experimental data. However, the values of  $K_s$  are lower for PLIVDs than for human samples (Table 3.3), which can be explained by the fact of PLIVDs derived from young animal specimens and so, it is expected that they behave more elastically and compliant than the human samples used in the previous studies. Since the load was applied on fresh thawed lumbar spines, the  $K_s$  magnitude should be significantly lower for smaller loads. Thus, a lower value of  $K_s$  for the Phase 1 (0-50 N load) is an expectable value. In addition, a higher value of  $K_s$  was obtained on this PLIVD during the application of the second loading phase (from 50 N to 500 N), since this is stiffer than the first loading phase (from 0 to 50 N).

These data are confirmed by earlier studies (Table 3.3), where it is reported that  $K_s$  presents a high dependency on load or displacement imposed on the specimen (Race et al., 2000). This phenomena is even more evident by the highest value for  $K_s$  documented for human IVDs (Virgin, 1951), which is not mechanically representative, since 4.5 kN is above the maximum physiological values (forces that did not induce irreversible deformation in the discs) for humans (Castro, 2013). For the first slope (until 0.5 mm of displacement and 50 N of load), the values present the same magnitude of the ones reported by Asano et al. (1992); the results for phase two (slope until reach 500 N) are also close to the ones documented in the literature, namely for those obtained for Markolf and Morris (1974) and Asano et al. (1992). This information indicates that the magnitude of load applied and the method of stiffness calculation (Izambert et al., 2003) are likely the causes for the divergence found between human data.

**Table 3.3.** Comparison between  $K_s$  and the maximum load applied on HLIVD (obtained in previous studies) and PLIVD (present study).

Authors	$K_s$ [MN/m]	Maximum Load [N]
Virgin (1951)	2.5	4500
Hirsch & Nachemson (1954)	0.7	1000
Brown et al. (1957)	0.1 - 1.5 (initial slope)	450-900
	2.1 - 3.6 (major slope)	
Markolf & Morris (1974)	1.23 - 3.32 (tangent at max. load)	220-670
Asano et al. (1992)	0.49 (0.04) (0 – 0.5 mm)	1500
	0.73 (0.06) (0.5 – 1 mm)	
	1.18 (0.09) (1 – 1.5 mm)	
Izambert et al. (2003)	0.05 (0.02) (until 0.5 mm)	400
	0.64 (0.1) (until 1.5 mm)	
	0.60 - 0.94 (tangent at max. load)	
Present study	0.49 (0.13) (until 0.5 mm – 50 N)	500
	1.215 (0.248) (from 0.5 mm – 50 N until 1.5 mm – 500 N)	

No significant differences were detected in the magnitude of the  $K_s$  found in human and porcine samples, for both load-displacement slopes, indicating that PLIVD can be useful for the determination of quasi-static behaviour of HLIVD. Moreover, the values of  $K_s$  of the IVDs did not

reveal significant differences for different physiological displacement rates, meaning that changes in displacement rate, during the daily routine movements, do not have an important effect on the  $K_s$  of PLIVDs. It is important to refer that several options could be considered for the calculation of the elastic stiffness response of the IVD, since it presents an elastoplastic behavior, i.e., some of the mechanical work (or energy) is irreversibly dissipated into heat, in a way that it cannot be recovered as such again (Luczynski et al., 2013). However, in this study, the  $K_s$  was calculated using a simplified approach referenced in the literature (O'Connell et al., 2011), i.e., the slope of the linear-region of the force-displacement curve.

The comparison of the  $K_d$  results with those obtained in previous study for HLIVDs (Li et al., 1995), showed that porcine  $K_d$  is two times higher than the human one. Furthermore, the  $K_d$  is between four and ten times higher than  $K_s$ , which is in opposition with what is referred in literature, where  $K_d$  and  $K_s$  appear to present the same range of values, for low frequencies (Izambert et al., 2003). The differences between these results and the literature could be justified by the choice of the viscoelastic model, which affects the mode of  $K_d$  calculation (Izambert et al., 2003), and the different experimental setups adopted (Kasra et al., 1992). Here, the  $K_d$  calculation came directly from experimental data, and not from any model estimation. In addition, this work revealed a small variation (in the case visible by the low standard deviation values) when compared to the data presented by Li et al. (1995). Since the samples were originating from different porcine lumbar motion segments of the same specimen, this could indicate that there is a minimal  $K_d$  difference for different intra-specimen PLIVDs samples.

Concerning to the IVD fluid flow and transport, it represents a complex three-dimensional problem, evolving several questions such as the strain-dependent permeability, anisotropy and inhomogeneity (Galbusera et al., 2011; Schmidt et al., 2013). Recent findings also evidenced a local viscous sliding of microstructural components without a major fluid mass exchange (Shahidi et al., 2014). Thus, although the use of sophisticated models to understand the mechanisms of IVD flow and transport under load (Castro et al., 2014; Ferguson et al., 2004; Malandrino et al., 2014, 2011; Yao and Gu, 2006), this process remains still unclear. Consequently, the development of optimized constitutive models and experiments is essential in order to better understand the process of fluid flow.

However, the viscoelastic models can be used as simplified tool to understand the mechanics of fluid flow in the IVD (Johannessen et al., 2004; O'Connell et al., 2011; Pollintine et al., 2010). These models provide parameters that can be useful to describe the time-dependent mechanics and the viscoelasticity of IVD, as well as to identify the fluid flow differences between animal and human IVDs (Johannessen and Elliott, 2005; Keller et al., 1987; Li et al., 1995; Pollintine et al., 2010).

For the parameters of the viscoelastic model adopted in this study (Table 3.2), the authors associated the differences in time constants  $\tau_1$  and  $\tau_2$  to the changes in the fluid flow pathway, while the displacement amplitude constants ( $F/S_1$ ,  $F/S_2$  and  $F/S_E$ ) were related to the quantity of fluid exchange in that pathway (O'Connell et al., 2011). The difference between human and porcine time constants are likely linked to the influence of fluid flow pathway and strain-dependent permeability (Johannessen et al., 2006; van der Veen et al., 2008). Previous studies proposed that parameters of fast response ( $\tau_1$  and  $F/S_1$ ) are more connected to the fluid flow through NP or endplate, and the slow response,  $\tau_2$  and  $F/S_2$ , is more related to AF fluid flow (Johannessen et al., 2006; O'Connell et al., 2011).

Earlier studies also showed that  $\tau_1$  increases with nucleotomy, in a compressive cyclic loading (Johannessen et al., 2006), resulting on a both lower NP and endplate permeability. However, it is also known that NP presents an increased permeability with severe degeneration, resulting on an easier and faster flow (Johannessen and Elliott, 2005). Therefore, the higher porcine  $\tau_1$  is presumably caused by a lower NP and endplate permeability, which could be explained by the age and condition of PLIVDs: they were taken from young animals and were not frozen, allowing keeping a good physiological condition in the IVD, in a non-degenerated state. In addition, while the test executed by O'Connell et al. (2011) was performed along 5 hours, the present experiment took around 30 minutes. Thus, the poroelastic response, which is normally a slow response event, was minimized (Castro et al., 2013). Consequently, the parameters of slow response reported in this work are not relevant, since their effect is only visible in the magnitude of hours.

The displacement parameters,  $F/S_2$  and  $F/S_E$ , whose correspond to slow displacement and elastic displacement, respectively, indicate that the volume and distance of fluid flowing in the pathway is likely higher during the fast response and lower for slow response. This is expectable, since this study is focused on the fast response due to a short time of test applied on IVD, being predictable that the fluid flow occurs predominantly during the fast response.

The major displacement due to fluid flow occurs during the fast response. This suggests that after the load application, even though the AF fluid outflow normally occurs during slow response, in case of PLIVDs it may also occur during fast response, overwhelming the low permeability of NP and endplate. This is supported by Ellingson and Nuckley (2012), who noticed that AF has a significant role in the IVD's fast response, whereas the NP may have a minor intervention during this phase.

Even though the load has been normalized by the viscoelastic model, these assumptions can be influenced by the magnitude of the load applied. Previous studies had reported that 1000 N load on human IVD samples (used by O'Connell et al. (2011)) correspond to a load limit on the IVD (Castro, 2013), which is a force magnitude that could lead to a dramatic change in the osmotic pressure in the IVD, promoting a quick expel of the fluid out of the system (Schroeder et al., 2006). In this study 500 N of creep load was applied, which corresponds, even in PLIVDs, to a loading range (0–800 N) considered as an appropriate estimation for the axial loading experienced in daily life (Ryan et al., 2008).

There are obviously many aspects to consider when an animal model is chosen and these differences must be considered in both experimental design and data interpretation (Dath et al., 2007). However, it is unarguable the existence of striking similarities between the spines of human and quadrupeds: the quadruped spine is essentially loaded in the same way as that of a human (Smit, 2002); in addition, the curvature of the spine does not influence the way a motion segment or an intervertebral disc is loaded (Patwardhan et al., 1999). In the particular case of the lumbar porcine models, they are readily available and not subject to stringent regulations. Moreover, the morphometric data for both porcine vertebrae and disc are described in detail, helping the researchers to choose the most appropriate experimental procedure (Busscher et al.,

2010; Dath et al., 2007). All of these facts help to justify the use of these animals as model for the study of human spine behavior.

Moreover, the viscoelastic model applied can be considered as simplification of a complex mechanical and physiological process, bringing important parameters to better understand the fluid flowing in the IVD. This model presents an excellent agreement between experimental and predicted displacements for the time interval considered, showing that it is well suited to analyze a short-time response of a motion segment. However, it presented some limitations, including the fact that the parameters of the simple viscoelastic model did not represent invariant materials properties since they could vary with testing conditions (Pollintine et al., 2010). Still, this model showed that care must be taken on the direct mechanical behaviour comparison between PLIVDs and HLIVD: they present different anatomical and physiological properties (Ryan et al., 2008), as well as relevant differences in terms of quasi-static and dynamic response.





## **4. Mechanical and Structural Response of the Intervertebral Disc to Alterations in the Internal Disc Pressure: an Experimental Approach**

*This chapter presents an experimental methodology that allows applying pressure increments into nucleus pulposus while the compressive loading response of the disc is evaluated. Moreover, it aims to determine the values of internal disc pressure that leads to disc disruption. A pressurization apparatus is presented and the comparison of the relaxation rate after the increment of internal disc pressure with the normal relaxation of disc is performed. The disc disruption tests were performed using a hydraulic cylinder that inflates the intervertebral disc with glycerin, while disc is compressed. The results are analyzed and discussed according with the current knowledge about the intervertebral disc biomechanics.*

### **4.1. Introduction**

The intervertebral disc (IVD) is a complex and inhomogeneous structure that allows successful load-bearing movements due to a synergetic effect of all components. The loads applied on the disc, during its normal daily activities, are responsible for variations of the internal disc pressure (IDP) in the nucleus pulposus - NP (Schechtman et al., 2006). At a biomechanical point of view, the IDP is highly influenced by the axial loads acting on the spine (Sato et al., 1999). In fact, an increase on the compressive load applied to healthy discs is “converted” into IDP (Schechtman et al., 2006). Since the NP can be considered incompressible, the annulus fibrosus (AF) bulges outwardly due to the stretch of annular fibres (van der Veen et al., 2008) which, together with osmotic phenomenon, promotes a loss in both IVD height and volume.

Although a simple axial compressive overload might not induce damage in a healthy disc, some movements such as compression combined with hyperflexion might generate an IDP beyond what the disc could withstands, promoting several injuries (Nachemson and Elfström, 1970; Schechtman et al., 2006). In addition, the importance of IDP is reinforced due to the difficulty in the assessment of the disc strength properties. Previous studies have demonstrated that before occurring any disc disruption the compressive overloading promotes the vertebral endplate damage and collapse (Dolan et al., 2013; Schechtman et al., 2006). Thus, the study of the IDP is a subject of deep interest in order to determine its contribution for IVD injury.

The methodology used experimentally to determine the IDP is typically sensor based: some approaches used needle sensors (Lisi et al., 2006; Nachemson, 1965; Okushima, 1970), while piezoresistive (Cripton et al., 2001; Pospiech et al., 1999; Sato et al., 1999; Wilke et al., 1999) and fibre optic (Dennison et al., 2008) were also considered as an option. These sensors are accurate on the recordings, helping to generate valuable data for pre-clinically evaluation of spinal implants and disc injuries in further biomechanical *in vitro* experiments. However, these approaches present some drawbacks, such as spinal fluid leakage or the use of AF access, which causes irreversible damage in the annular fibres (Moore et al., 2009). Moreover, these studies are commonly focused on IDP analysis for different postures. Less is known about the compressive loading response of intervertebral disc after the increment in the IDP. As the development of replacement or regeneration/repair technologies must be in concordance to the natural mechanical response of the NP, the IDP monitoring should be emphasized and improved.

Interestingly, the determination of the magnitude of IDP that is responsible for disc failure is also essential as it represents a potential parameter for the evaluation of the mechanisms that promote the weaken and the disruption of the annular fibres (Iencean, 2000). Once combined with the traditional provocative discography, the IDP monitoring represents an important way to determine the clinical significance internal disc disruption (Menkowitz et al., 2005). However, few studies include the determination of the failure pressure in the IVDs (Iencean, 2000; Menkowitz et al., 2005; Schechtman et al., 2006; Veres et al., 2010) and their results are widely disperse, as presented in Chapter 2.

Therefore, the objectives of the present section are (1) to develop and validate a methodology that allows applying IDP increments into NP, presenting the capacity to determine the compressive load throughout the IDP variations; (2) to determine the values of IDP that promotes the IVD disruption. To achieve the first goal a new combined apparatus, consisting on a pneumatic device that applies a pressure in the hydrostatic system by cartilaginous endplate access, was designed. In addition its validation was undertaken by the comparison of the relaxation rate after the increment of intradiscal pressure ( $\Delta$ IDP) with the normal relaxation of IVD, throughout the same compression test conditions. Concerning to the disc disruption tests, these were performed using a hydraulic cylinder that inflates the IVD with glycerin, while disc is compressed. The pressure was monitored by a digital manometer and the maximum point of pressure was considered as the rupture point.

## **4.2. Materials and Methods**

### **4.2.1. Motion Segment Collection and Preservation**

After being collected, the young porcine lumbar spines from, with 18 months-old, were immediately sectioned into motion segments - MSs (Campbell-Kyureghyan et al., 2011). Posteriorly, the MSs were sealed in plastic bags and frozen at -20°C, until the day prior to mechanical testing, minimizing the tissue dehydration. This procedure was adopted since dead and frozen storage presents a negligible effect in mechanical properties of the spine (Adams et al., 1996). Before start any mechanical test, samples were hydrated with 12 hours with phosphate buffer saline solution (1X) in order to prevent segment desiccation.

### **4.2.2. Configuration of the Pressurization Apparatus to Assess the Effect of the Intradiscal Pressure Increment in the Load Relaxation Rate**

The developed device is relatively simple and can be used for hold the MS, as well as for increase and measure the intradiscal pressure. The schematic representation of the apparatus is presented in Figure 4.1. The apparatus is divided in two parts: a pneumatic and a hydraulic one. The pressurizing mechanism consists in a pneumatic device that applies a prescribed pressure to a hydrostatic system, forcing a fluid to flow into the lumbar motion segment.

On the pneumatic segment, the pressure is exerted by the application of external pressurized air source - up to 0.6 MPa of pressure - which acts on a pneumatic double-acting cylinder (a Camozzi® minicylinder, series 16, 10 mm of diameter, 100 mm of stroke). The pressure is controlled in the pneumatic cylinder by a balancing valve. Then, the inner stem of the cylinder pushes an internal nylon piston (with two O-rings to avoid the reflow) of a larger stainless steel hydraulic cylinder, specially designed for the scope of this application (the technical drawings of both nylon piston and the stainless steel hydraulic cylinder are presented in Annex B). The pressure, applied on the hydraulic cylinder, was transmitted to the fluid poured in the hydraulic system. This system consisted on a graduated manometer up to 1 MPa, connected with a tube with 50 cm of length and 2 cm and 1.5 cm of outer and inner diameter, respectively.

This tube allowed the introduction of fluid in the stainless-steel basis of the MS – the technical drawing is presented in the Annex B.

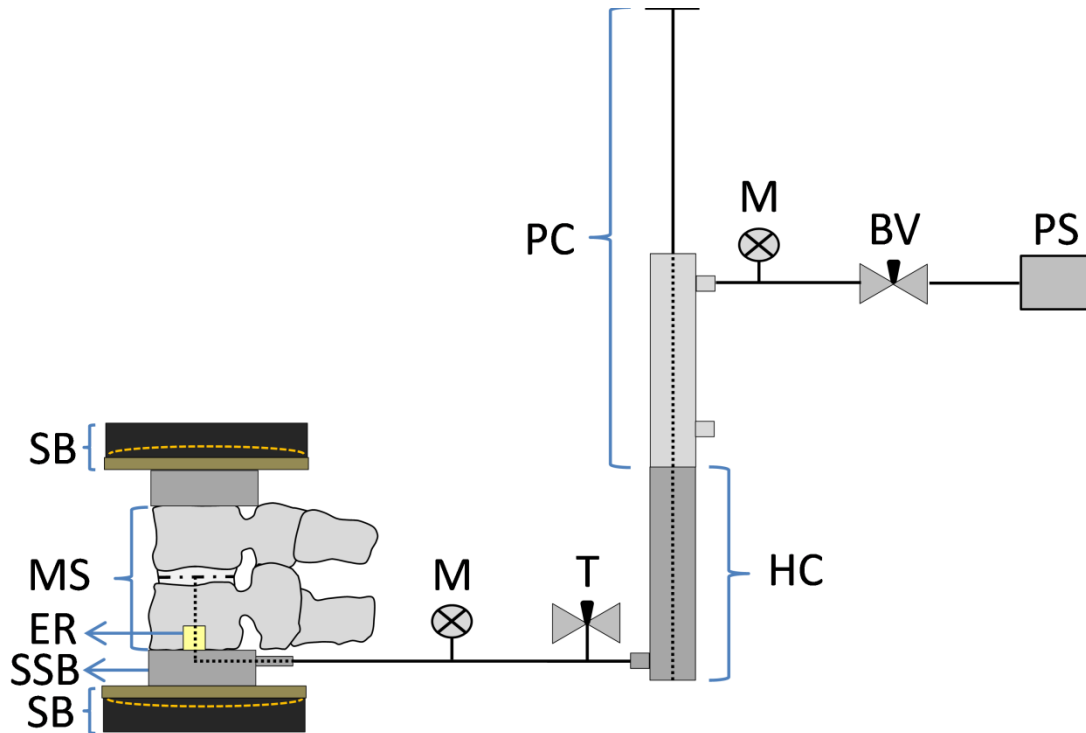


**Figure 4.1.** Schematic representation of pressure apparatus, containing: SP - Pressurized air source; RV - Balancing valve; M - Manometer; PC - Pneumatic cylinder; HC – Hydraulic cylinder; T - Tap; SB - Spherical axial bearing; ER – Epoxy resin; SSB – Stainless steel basis; MS - Motion segment.

The inflow was promoted by the tap opening. When the hydraulic system was entirely filled with fluid, the tap was closed. During the filling process, care was taken to prevent the presence of air in the tubes. After tap closing, the MS was ready to be pressurized. The pressure in the hydraulic segment was monitored immediately upward the fluid insertion in the IVD by the graduated manometer. Finally, the fluid was injected in the IVD through the hole in the top of the motion segment.

### 4.2.3. Pressurization Apparatus used to determine the Failure Intradiscal Pressure

For the failure IDP tests, the pressure generating apparatus was modified. The schematic representation of the apparatus responsible for the inducement of intradiscal pressure is presented in Figure 4.2.

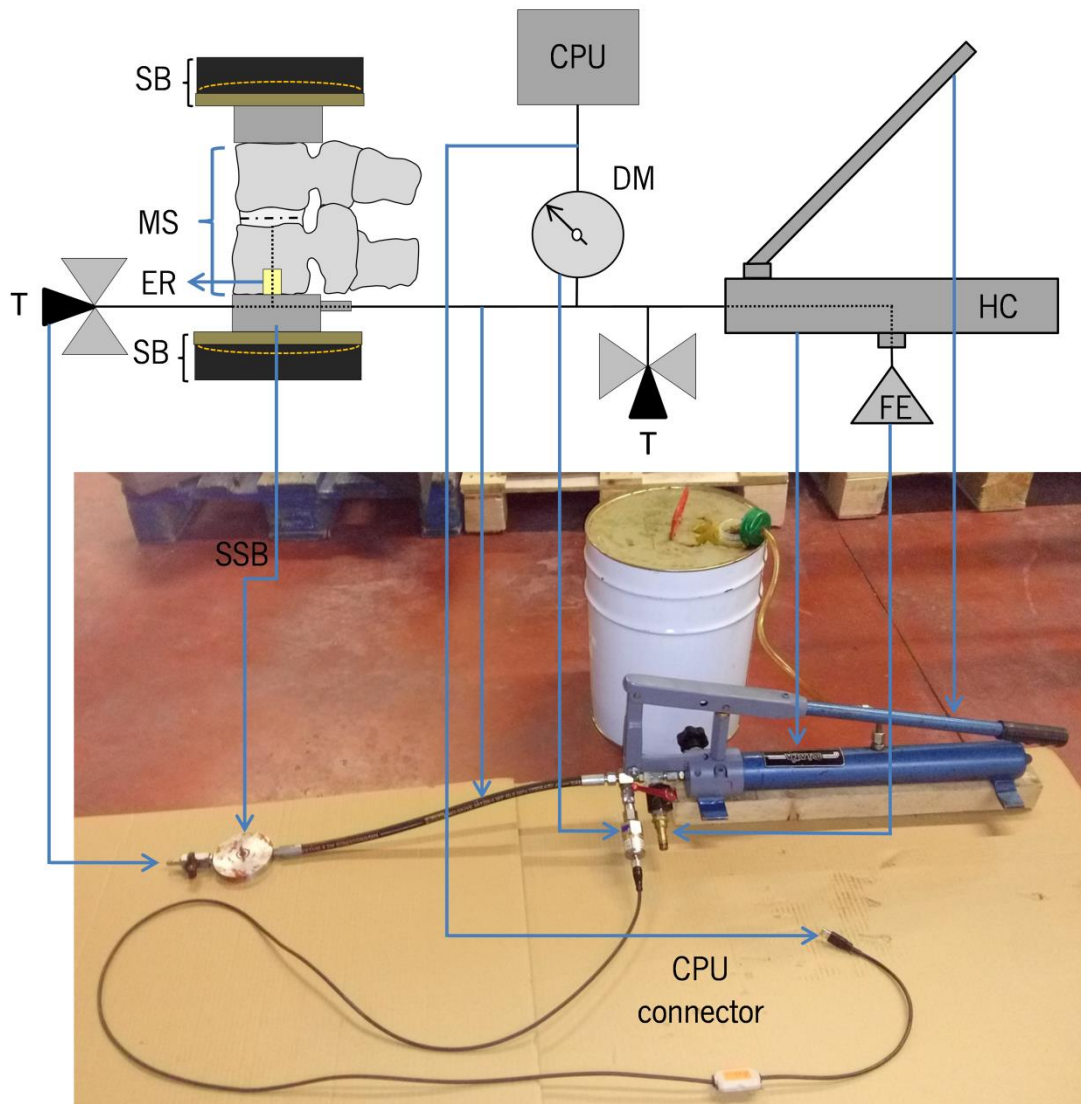


**Figure 4.2.** Schematic representation of the pressurization apparatus ( above) and the real image of the failure pressure tester without coupling the motion segment (below). The apparatus is composed by: SB - Spherical Axial Bearing; ER – Epoxy resin; MS - Motion Segment; CPU – Personal Computer; DM – Digital Manometer; T – Tap; HC – Hydraulic cylinder (with manual pump); FE – Fluid Entrance; SSB – Stainless steel basis.

In this configuration, the pressure was inserted in the inner disc region using exclusively a hydraulic cylinder. The pressure generating apparatus consisted on a hydraulic cylinder, with a coupled lever that allowed controlling the pressure exerted in the system. The injected pressure was assessed by a digital manometer incorporated in the system - the electronic pressure sensor PP7553, from IFM®. This manometer was connected with the LineRecorder® software that allowed registering the pressure acting in the IVD as function of time.

The principle of function of each failure pressure test is simple. First, the entire system was filled with glycerin, which was inserted in the system by the pressure exerted when the lever of the hydraulic cylinder is moved. The glycerin was selected as testing fluid since it presents relative higher density and viscosity than water (1.261 g/cm<sup>3</sup> and 1499 cP at 20°C, respectively). To certify that the entire system was filled with the liquid, and so, the value of failure pressure was not affected by air bubbles in the tubes, a “bleeding” tap was included in the stainless steel basis. The procedure for air bubbles removal was simple: after the placement of the motion segment in the system; the tap was opened and the glycerin was forced to enter into the system by the suction effect promoted by the lever movement of the manual pump. Then, the fluid was poured by the tap until ensuring that the system presents no air bubbles. Finally, the tap was closed and the system was ready to be submitted to test.

#### **4.2.4. Motion Segment Attachment**

The vertebral bone is a highly porous structure, in which the fluids easily outflow from its inner region to the outer one (Bronner et al., 2010), being extremely hard to tight a screw on it. To effectively overcome this obstacle, a 9 mm diameter and 2 mm height hole as drilled in the top vertebra hole of the MS, in order to fill it with an epoxy resin with fast curing. Consequently, a 4 mm pilot hole was carefully drilled longitudinally through the resin and vertebrae until a sudden change in the structure resistance. This change of resistance indicates the point of contact between cartilaginous endplate and the NP.

The MS was then attached to pressure apparatus, in case to a homemade cylindrical stainless steel bottom plate, by a self-tapping steel screw - Figure 4.3. The self-tapping screw was



20 mm length (the technical drawing is presented in the Annex B), presenting two threads: a section of 10 mm height and 7 mm diameter drywall screw thread to a drill in the vertebra and a region of 10 mm height and 5 mm diameter to attach to the stainless steel plate. This screw also presents a drilled hole along its entire length, with an internal bore of 1.5 mm diameter that allows the fluid passage. Then, the screw was tightened until reaching the contact point between cartilaginous endplate and the IVD. An O-Ring was placed on a cylindrical stainless steel bottom plate (around the self-tapping screw), in order to prevent fluid leakage. The compressive loading on the system was then exerted in the top of the other vertebral body. The MS samples were carefully aligned according a pre-defined XY system of axis, using spherical axial bearing system. This alignment ensures that all discs are placed in the horizontal and vertical planes. In the case of failure pressure tests, preliminary trials have failed in containing the insertion of glycerin in the nuclear cavity. During initial tests (using only fast curing resin as interface between the screw and the MS), the fluid flowed out from the drilled vertebrae motion segment, by the screw insertion. Six motion segments were used during preliminary trials the failure IDP. Then, the approach was improved by using a thin film of silicone in the interface vertebrae-stainless steel base.

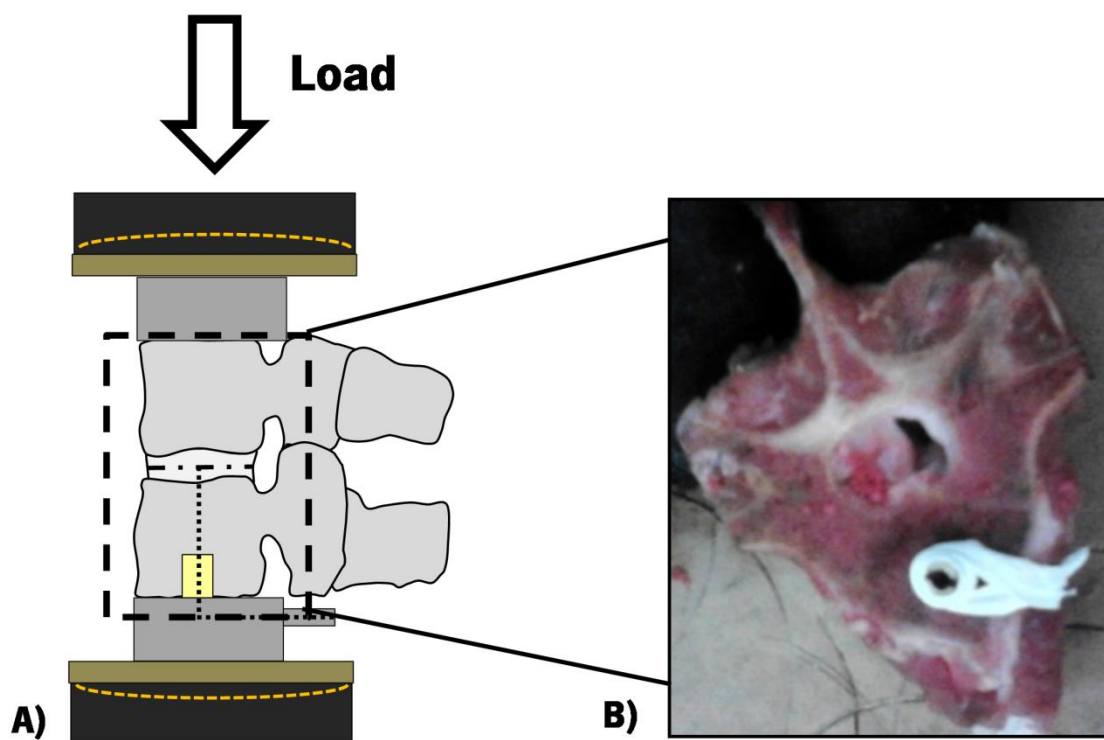


**Figure 4.3.** Motion segment attachment. A) The MS was placed between two plates of Instron® 8874, being subjected to compression. The bottom plate is drilled, allowing the fluid passage from pressure apparatus to the hollowed screw. The attachment is done on epoxy resin (yellow region), to provide a better adhesion of the screw; B) Top vision of a drilled MS, with the presence of the self-tapping screw on the vertebral body.

#### 4.2.5. Experimental Procedure

For both the assessment of the effect of the  $\Delta$ IDP in the load relaxation rate and the determination of the failure IDP, the samples ( $n=5$ , for each test) were first positioned in the same way before testing, according with a XY coordinate system. When placed on the Instron® 8874, the MS was subjected to a pre-load of 50 N, during 5 min, to ensure the contact with loading platen and to minimize errors due to post-mortem effects (Campbell-Kyureghyan et al., 2011).

For the evaluation of the effect of the IDP increment on the load relaxation rate, each MS was submitted to 2 mm displacement, during 30 minutes. During this period, the IDP suffered increments of 0.1 MPa, as presented in Figure 4.4.

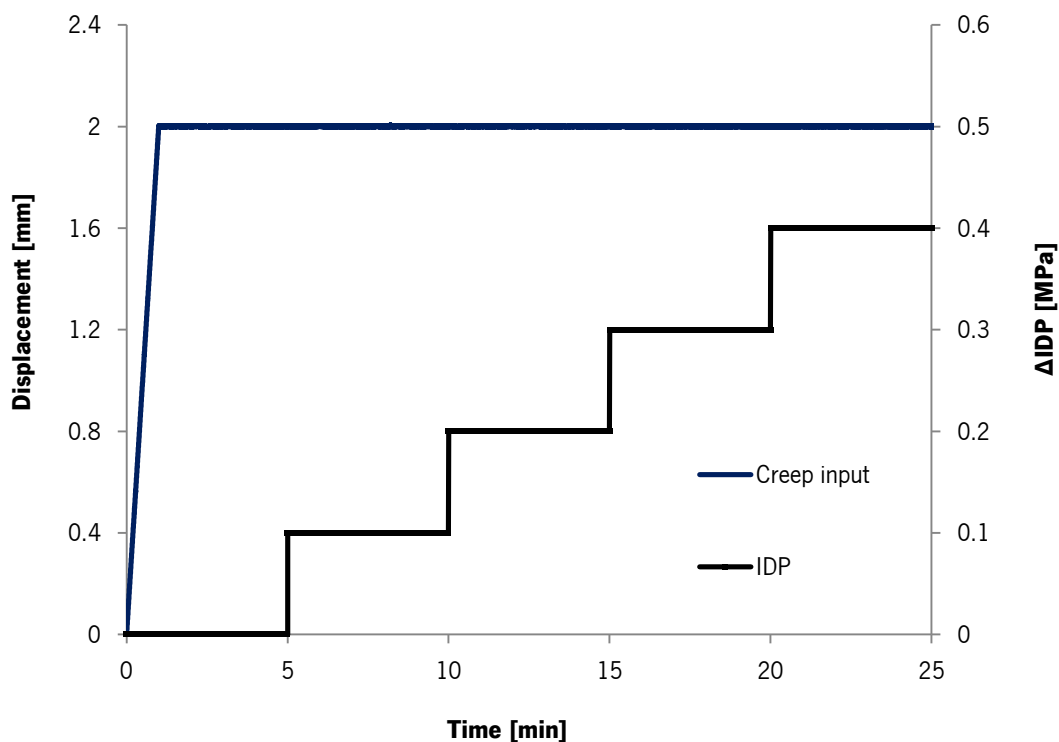


**Figure 4.4.** Input used to assess the behavior of IVD under a set  $\Delta$ IDP. The blue line characterizes the

displacement imposed to each IVD. The green line represents an approximation of the pressure increments (in steps of 0.1 MPa) applied on the disc, at each 5 minutes of loading.

The pressure was monitored and the load values were recorded using the Instron® 8874 software BlueHill ®. In addition, the curve of the load as function of time was traced and the relaxation rate was measured as the slope of load relaxation over time, for all pressurization periods. The goal was to compare the relaxation rate at same  $\Delta$ IDP, using the values of standard deviation (SD) to evaluate the dispersion in the values of the relaxation rate. Two control tests were used to compare the values of the normal relaxation rate and the one obtained for the  $\Delta$ IDPs. These control tests consist on the application of the same mechanical test to intact MSs, i.e., MSs without insertion of an external source of IDP. Concerning to the IDP failure tests, a compressive axial displacement of 1 mm was imposed on the top of MS in order to either avoid the longitudinal expansion of the IVD during the pressurization test and to simulate the *in-vivo* confined conditions (Schechtman et al., 2006). This methodology also allows controlling the loading conditions ex-vivo. In fact, limiting the longitudinal expansion of IVD using the Instron 8874 allows determining not only the internal pressure of the disc using the digital manometer, but also the loading variation during this process. After impose this displacement, the MS is pressurized by the descendent movement of the lever. These samples were pressurized during a period of approximately 10 seconds, which represents the maximum time that all samples needed to reach failure after the application of an external pressure source. During this period, the LineRecorder® software allowed to monitored and save the values of IDP as function of time. Ten motion segments were used for the monitoring of the failure IDP. This study neglected the effect of the pressure drag in the walls during the fluid passage on both tubes and screws. Thus, it is assumed that the pressure read in the pressure sensor corresponds to the real inflation pressure of the IVD. After all tests, each MS was sectioned transversally in the IVD region, in order to assess if it was pressurized in nuclear region. The segmented disc was photographed and the final area of each IVD determined using the image processor Image Pro Plus 4.6®.

#### **4.2.6. Statistical Analysis**

The effect of the  $\Delta$ IDP on the load relaxation rate was reached by comparing the relaxation rate obtained for each period of pressurization. First, the standard deviation (SD) between tests was determined and compared to evaluate the dispersion of results. Then, the coefficient of variation (CV) was calculated as the ratio between the SD and the mean (Moroney et al., 1988) between each increment (0-0.1; 0.1-0.2; 0.2-0.3; 0.3-0.4 MPa). The Shapiro–Wilk test was used to determine if the data follow a Normal distribution (Holzapfel et al., 2005). To test the equality of the variances between the relaxation rates, the F-test was undertaken, for each relaxation period of pressurized samples and the same period in the control sample. According with the F-test result, the appropriate *t-student* test for unequal sample sizes was applied in order to analyze if the relaxation rate values for the pressurized samples are significantly different from the control test. All statistical analyses were performed with Microsoft Excel® and significance level  $p < 0.05$ .

### 4.3. Results

#### 4.3.1. Visual Inspection of a Pressurized Motion Segment

The tests were performed to assess the functionality of the pressurizing system and, in addition, to validate the results. All specimens were pressurized in the NP region, which is visible for example, in Figure 4.5. The specimens that not detected a signal of NP pressurizing were discarded. The average disc area and height were  $917.2 \pm 107.0 \text{ mm}^2$  and  $5.97 \pm 0.63 \text{ mm}$ , respectively.

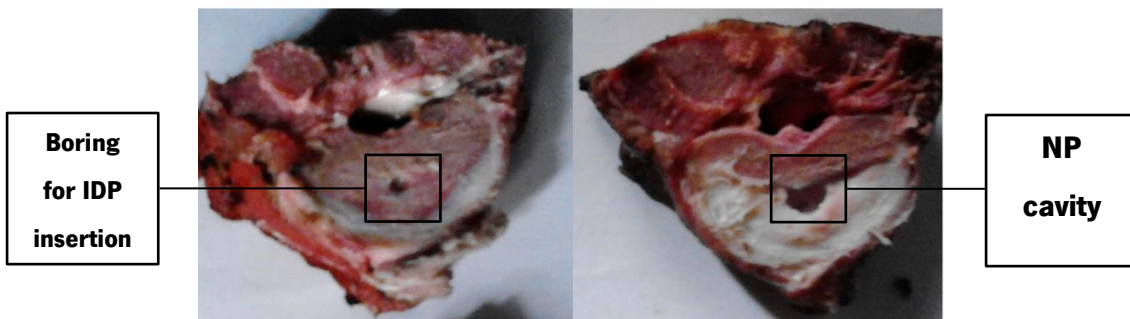


**Figure 4.5.** Images of MS sawed transversally after testing. It is visible the presence of a cavity in the NP region, indicating the pressurizing zone.

#### 4.3.2. Comparison between Relaxation Rates at different Internal Disc Pressures

For a detailed analysis of the relaxation rate, it is important to document the compressive strain applied on the MS for each relaxation test. This value allows understanding the relation between the MS relaxation rate and strain applied on the disc. The maximum load applied and the average areas of the tested samples are reported in Table 4.1.

**Table 4.1.** Maximum compressive strain for each MS (n=5). The maximum strain is given by the absolute value of the ratio between the maximum change in disc length during the compressive loading and the original length.

	MS 1	MS 2	MS 3	MS 4	MS 5
<b>Maximum compressive</b>	0.29	0.31	0.37	0.39	0.33

**engineering strain**

An example of the output of the mechanical test performed during this work is presented in Figure 4.6. This curve clearly demonstrated the effect of the  $\Delta$ IDP in the relaxation load: at each  $\Delta$ IDP, it is noticeable a slight load peak. Furthermore, the peak increases with IDP change - for instance, the peak is higher for a 0.2 - 0.3 MPa change than from 0.1 - 0.2 MPa increment.

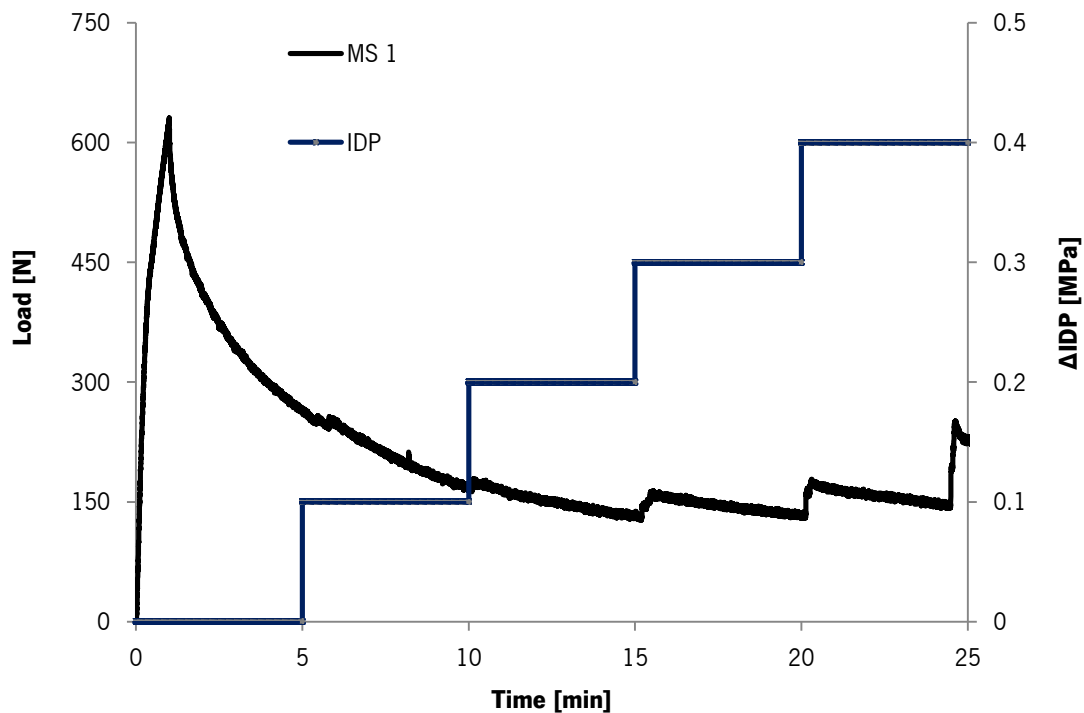


**Figure 4.6.** Graphical representation of the mechanical test obtained with the present setup. The blue line represents the relaxation curve for a representative sample (MS 1). The red line represents the time of duration of each  $\Delta$ IDP (with steps of 0.1 MPa). In addition, it is visible a slight peak of load at each IDP change.

The relaxation rate showed a linear response, with a very good correlation, with  $R^2 \geq 0.9205$  for all the tests. The results for each relaxation period, at different  $\Delta$ IDPs are presented in Figure 4.7. The Shapiro-Wilk test confirmed that the data is normally distributed. Therefore, the *t-student* test indicates there were no significant differences between the relaxation rate for pressurized samples and for control ( $p < 0.05$ ). The relevant values of the statistical analysis are presented in Table 4.2. The SD values range from 0.016-0.027 N/s, while the coefficient of variation is comprised between 16.9 and 22.1%. However, for the first increment of 0.1 MPa the

coefficient of variation is 6%. This value indicates low data dispersion for the first increment, while more significant dispersion is evident in remaining tests.

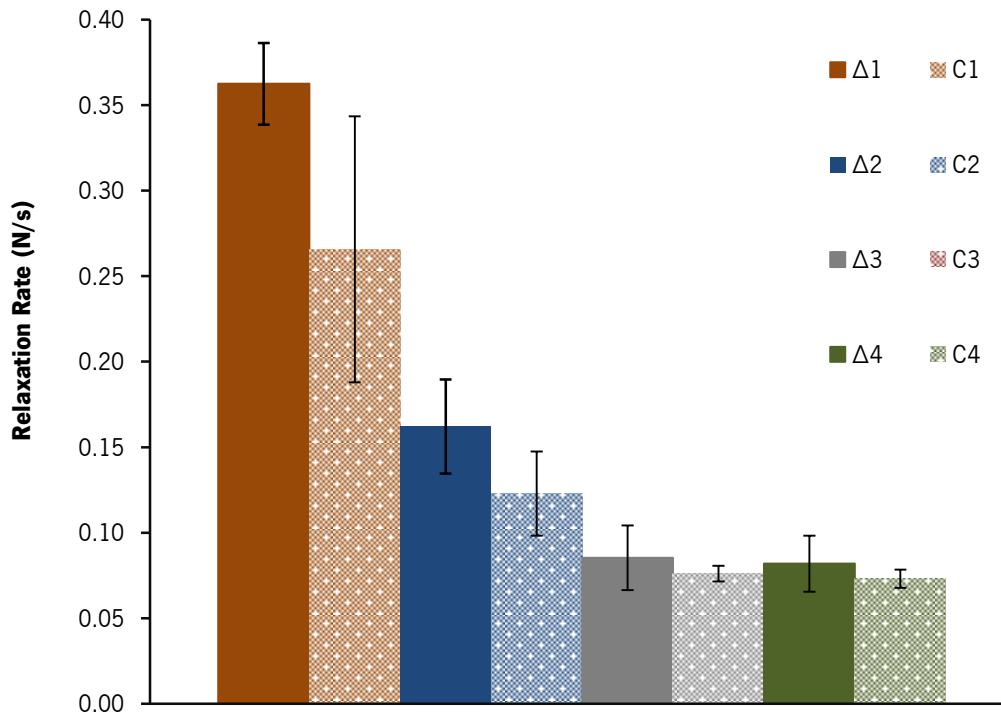


**Figure 4.7.** Absolute mean of relaxation rate for discs (n=5) for the range of  $\Delta$ IDP monitored during the relaxation test and for the control (n=2). The  $\Delta$ 1,  $\Delta$ 2,  $\Delta$ 3 and  $\Delta$ 4 represent the relaxation rate after each the  $\Delta$ IDP (0-0.1 MPa, 0.1-0.2 MPa, 0.2-0.3 MPa, 0.3-0.4 MPa, respectively). C1, C2, C3 and C4 represent the control test for the same period of testing time for the samples after each  $\Delta$ IDP. The error bars represent the standard deviation.

**Table 4.2.** Standard deviation (SD) and the coefficient of variation (CV) for each IDP increment.

IDP value	0.1 MPa	0.2 MPa	0.3 MPa	0.4 MPa
<b>SD</b>	0.024	0.027	0.019	0.016
<b>CV [%]</b>	6.6	16.9	22.1	20.0

#### 4.3.3. Failure Pressure in the Motion Segment

The criteria of failure in the MS structure, due to the insertion of IDP using an external source, comprises two evident phenomena: (1) the flood of the glycerin from any motion segment region, with exception for the top region of both vertebral bodies, and (2) a significant drop in the

pressure detected by the digital manometer. A representative example of the curve of a failure IDP curve as function of time is presented in Figure 4.8.

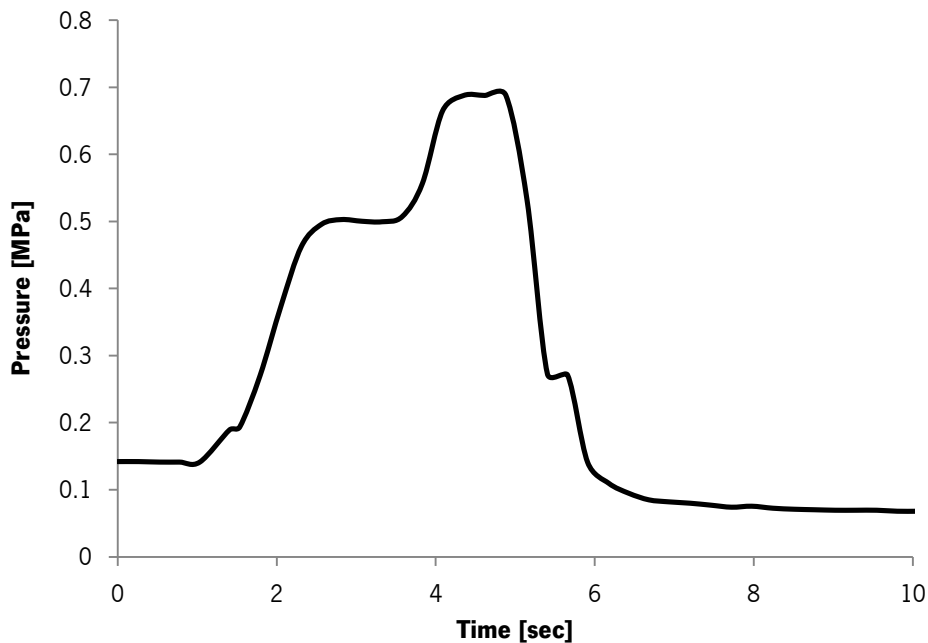


**Figure 4.8.** An example of the MS response after the insertion of an IDP magnitude that leads to IVD rupture (in MPa), as function of Time (in seconds).

The values of IDP that leads to disc failure, together with the description of the failure in the specimen after visual inspection of the six motion segments that matched the criteria for failure are described in Table 4.3.

In all the cases a substantial drop of pressure was visible after reaching the maximum value of IDP that corresponds to the failure pressure. Several events can be identified during the process of MS failure due to the insertion of an external pressure source. In all discs, an immediate glycerin leakage was visible after reaching the maximum value of pressure. Moreover, there was not possible to identify a pattern between the IDP failure and the place of glycerin outflow, being visible a wide range of rupture regions in the motion segment instead. In Figure 4.9 are exposed several examples of MS failure due to NP inflation. The images document the different type of rupture occurring in each MS submitted to failure IDP values.



**Table 4.3.** Intradiscal failure pressure (maximum in the curve IDP vs time) for the six motion segments that presents external indicators of rupture, such as sudden pressure drop, leakage in the vertebra region or in spinal cord (fluid outflowing from the spinal cord channel) or tears formed in the annular region or also in the top and bottom parts of annular region (cartilaginous endplate region).

<b>Motion segment</b>	<b>Failure pressure [MPa]</b>	<b>Description of the failure in the specimen after visual inspection</b>
1	0.58	- Moderate leakage around the screw region in the vertebra - A little tear formed in the annular region
2	0.69	- Leakage of fluids from the annular region
3	0.69	- Moderate leakage around the screw region in the vertebra - Slight leakage around the spinal cord (fluid outflowing from the spinal cord channel)
4	0.69	- Leakage of fluids from the annular region
5	0.55	- Slight leakage around the screw region in the vertebra - Tears formed on the top and bottom parts of annular region (cartilaginous endplate region)
6	0.50	- Slight leakage around the spinal cord (fluid outflowing from the spinal cord channel) - Moderate leakage in annular region and around the screw region in the vertebra
Mean ± S.D:	0.62 ± 0.08	

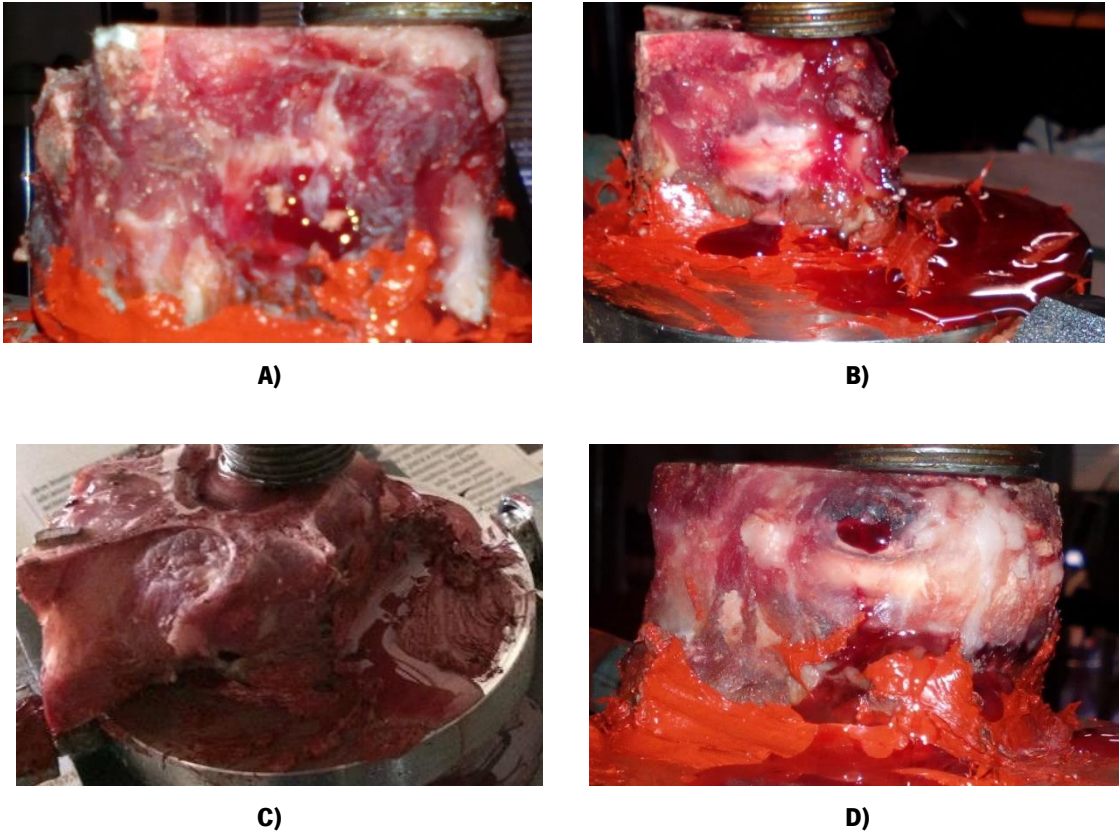


**Figure 4.9.** Representative images of different configurations of failure in motion segments, during the inflation procedure. A) Leakage of fluids from the annular region. Two motion segments failed in this manner. B) Severe leakage around the screw region in the vertebrae (bottom vertebrae) and in the annular region; slight leakage around the spinal cord (fluid outflowing from the spinal cord channel). One motion segment failed in this manner. C) Moderate leakage around the screwed region in the vertebrae (bottom vertebrae). Two motion segments failed in this manner. D) Little tears formed on the top and bottom parts of annular region (cartilaginous endplate region). One motion segment failed in this manner.

#### **4.4. Discussion of the Effect of the Intradiscal Pressure on the Mechanical Behavior of the Intervertebral Disc**

Previous studies indicate that there is a strong relation between the external loads applied and the IDP (Schmidt et al., 2013). However, less is known about the effect of the changes of IDP on disc behaviour. This information is even more important for the patients that undergo on surgical procedures, since the success of this process could be affected by IDP variation.

The evaluation of the influence of the IDP variation in the IVD mechanics, normally determined by an AF access (Dennison et al., 2008; Nachemson and Elfström, 1970; Nachemson, 1965; Okushima, 1970; Pospiech et al., 1999), could be also valuable in order to design appropriate NP substitutes that are able to restore the normal IVD functions.

Moreover, despite the panoply of mechanical testing intending to elucidate the contribution of loads to MS collapse, the magnitude of IDP that led to the MS rupture remains still unclear. The measurement of the IDP values for MS collapse is a subject of extreme interest, not only to understand the mechanisms of IVD failure but also for the designing of new implants for IVD replacement as they should withstand the daily routine activities without MS subsiding.

##### **4.4.1. Relation between the External Loads applied on Motion Segment and the Intradiscal Pressure**

Based on the method developed by Schechtman et al. (2006) to measure the failure strength on bovine caudal disc, this work suggested a new combined hydraulic and pneumatic apparatus to study IDP effect on load relaxation, without disrupting the AF fibres. This new method allows to monitor and to pressurize the nuclear region of the IVD, accessing the NP by a perforation through cartilaginous endplate.

From the first groups of results, where the relation between the external loads applied on MS and the IDP was compared, it was clear that this approach is effectively able to increment the IDP, remaining with the same IDP value during a prescribed time. In addition, the results presented in Figure 4.5 show that pressure acts directly in the NP, meaning that the method of

pressure insertion is valid. After submitting the MSs to a compressive strain between 29 and 39%, it is verified that the relaxation rate is higher for the initial relaxation time, decreasing until reaching a “constant” value (approximately 0.10 N) after 20-25 minutes of loading (Figure 4.4). This is characteristic of a normal load relaxation test for MS (Johannessen et al., 2004), where the slope of load relaxation curve decreases over time. Therefore, the inexistence of significant differences between the relaxation rate for pressurized samples and control tests means that an increment of 0.1 MPa has a minimal effect on the intervertebral disc relaxation rate. This is an expected result as the increments are within physiological values (Wilke et al., 1999) and so, they are quickly dissipated by the viscous response of the IVD. Thus, a slight IDP increment promotes a slight peak on compressive loads, which is rapidly dissipated during each relaxation time.

This approach was able to measure the effect of IDP increments on relaxation rate of MS, with a maximum of 22% for the coefficient of variation – visible in Table 4.2. Interestingly, the coefficient of variation for the first IDP increment was 6%, showing that an increment of 0.1 MPa in pressure during the initial relaxation period affects the relaxation rate in the same way for several tests. The lower divergence in the initial phase could be explained by a theoretical assumption: for higher stresses the effect of an IDP increment should be lower, since the IDP increases as much as the compressive stress applied on disc rises (Wilke et al., 1999). Moreover, it evidenced that this approach presents a good accuracy for the measurement of the relaxation rate. However, this is the time interval where the effect of the IDP increment on relaxation rate is minimal; in the remaining increments, the effect on load is more evident. For that reason, the higher dispersion of results for the subsequent IDP increments reflects the instability on the peaks of load after the IDP increment. In the remaining increments, the relaxation rate presents a considerable oscillation (with a coefficient of variation between 19 and 22%). The high value of the coefficient of variation is likely related to (1) the origin of the MS samples, as they were taken from the same porcine lumbar spine and consequently, they could present some anatomical differences (Moore et al., 2009) and (2) the low loads acting on MS during this period. Thus, during these increments, a small increment in IDP promotes a great variation in load, inducing severe oscillation in RR. Nevertheless, some limitations could be attributed to this procedure as the experiments were conducted without submerging the IVD in

saline solution and this absence could influence the disc mechanics, in particular the transient stiffness and creep properties (O’Connell et al., 2011). Nevertheless, the time of mechanical testing can be considered as short, reducing the effects of dehydration.

#### 4.4.2. Failure Strength in the Intervertebral Disc due to Disc Inflation

The failure strength of the porcine MSs under an imposed IDP was also determined using a hydraulic cylinder and the same cartilaginous endplate access. The definition of failure of the present work contemplates the flood of the glycerin from any region motion segment together with a significant drop in the pressure detected by the digital manometer. This consideration arises from the fact that, when a failure pressure is imposed in a MS, a chaotic effect is detectable in the whole MS structure. No localized region was detected or identified as a typical region of disc rupture after the insertion of an external pressure, indicating that there was a redistribution of the IDP in the inner region of the multilayered AF, i.e. , in the contact zone between NP and AF. Thus, the collapse of the IVD structure is not a local but a generalized event.

Regarding to quantitative results, this study reports a mean pressure failure of  $0.62 \pm 0.08$  MPa for lumbar porcine samples. The comparison between these results with the failure pressure of the annular fibres reported in previous studies for several MS models - Table 4.4 – reveals that the values documented in this report are appreciably lower than the more recent studies, performed by Schechtman et al. (2006) and Veres et al. (2010).

**Table 4.4.** Recent data about the failure pressure data for different IVD models.

Author (Year)	Models	Mean failure pressure (MPa)
Iencean (2000)	Lumbar human	0.75 to 1.3
Menkowitz et al. (2005)	Cervical human	0.28 (min-máx:0.1 - 1.18)
Schechtman et al. (2006)	Caudal bovine	$18 \pm 3$
Veres et al. (2010)	Lumbar ovine	$14.1 \pm 3.9$
Present study (2015)	Lumbar porcine	$0.62 \pm 0.08$

Schechtman et al. (2006) investigated the intrinsic failure strength of the intact bovine caudal disc under inflation, injecting a colored gel with a hydraulic actuator: the mean hydrostatic failure pressure was found to be  $18 \pm 3$  MPa. Later, Veres et al. (2010), using the same technique performed by Schechtman et al. (2006) to investigate the role of high IDP on annular fibres disruption in ovine lumbar IVDs, reported a the mean failure pressure of  $14.1 \pm 3.9$ . According with the latest developments about the failure pressure of disc, it would be expectable a higher value for the rupture of porcine discs, as the magnitudes presented by these authors are decidedly superior from those documented in this work.

However, several studies reported the magnitude of the rupture values obtained in this study as within the normal range of physiological IDP for human samples (Iencean, 2000; Menkowitz et al., 2005). The results of the present study are within the magnitude of values documented in these human lumbar (Iencean, 2000) and human cervical (Menkowitz et al., 2005) studies. Iencean (2000) reported a rupture pressure up to 1.3 MPa after inflating the IVD with compress air through a tunnel drilled in the body of the subjacent vertebra via cartilaginous endplate access; Menkowitz et al. (2005) claimed a mean intradiscal rupture pressure of 0.28 MPa (range 0.1-1.18 MPa), using a 25G needle for the insertion of a contrast dye, with IDP monitoring along the pressurization time. These studies indicates two important facts: (1) the potential for iatrogenic disc injury may exist at low pressures and volumes for lumbar porcine IVDs when compared with samples presented in Table 4.4; (2) the rupture of human cervical and porcine lumbar annular fibers could occur for IDPs within the physiological range, showing that the injury in these structures could be induced at significantly lower pressures.

The disparities in the failure pressure, presented in Table 4.4, could be related to several phenomena. This study had limited the expansion of the MS in terms of height, imposing a permanent 1 mm displacement to each disc sample while the pressurization test occurred. The particular case of the use of caudal discs as model for the human lumbar disc is an option that has been questioned at several levels: they present different mechanical loading during daily events relative to human lumbar spine together with different composition, metabolism and anatomy (Alini et al., 2008). The caudal bovine samples present a nearly cylindrical shape (Schechtman et al., 2006), neglecting the possible existence of critical point of the hydrostatic

pressures distribution in the IVD. This misassumption could lead to divergent values concerning to which is expected for human discs. Thus, the present work was conducted with lumbar porcine samples since they were considered was geometrically and morfologically more similar to the human ones, and so, a more suitable choice for mechanical studies on the IVD (Alini et al., 2008). Moreover, the different techniques used to quantify the failure pressure may compromise the reliability of the results. Several approaches were analyzed and their weaknesses should not be neglected when a comparison is made.

This work itself present some limitations as the cadaveric study was limited by sample size or the criteria defined for MS failure. In fact, in this study the real values of rupture could be hidden by the flood of glycerin from the screwed vertebra. However, the samples where the rupture had only occurred on the screwed vertebra were discarded and, for the quantitative analysis, only the samples with an additional point of rupture were considered. Moreover, it does not contemplate the microstructural analysis of the failure mechanisms. The rupture occurred in the cited articles, neglected the shape differences on samples concerning to the critical points of failure, that are different between specimens.

# **5. Uniaxial Compressive Loading Response Of the Porcine Annulus Fibrosus: a Reinforced-Ground Matrix Study**

*The purpose of this chapter is to present the mechanical behaviour of the annular reinforce-ground matrix under unconfined uniaxial compressive loading and compared the response of the annulus fibrosus to the application of both physiological and non-physiological strains. The loading profiles are divided in static and dynamic tests. In the static tests, a polynomial model is used to fit in all the loading cycles applied on the samples; during dynamic tests, the water content of the samples was also determined. Finally, the outcomes were analyzed and discussed taking in account the most recent advances on the mechanical procedures of the annulus fibrosus testing.*

## **5.1. Introduction**

The annulus fibrosus (AF) of the intervertebral disc (IVD) presents a highly organized structure and composition, comprised essentially by concentric lamellae of type I collagen fibres. Within lamellae, collagen fibres are aligned in a cross-ply manner at  $\pm 30^\circ$  to the transverse plane, with changes in the predominant fibre direction between adjacent lamellae (Cassidy et al., 2009; Sen et al., 2012). These fibres are embedded in a proteoglycan rich network, the ground matrix, formed by a network of interconnected negatively charged macromolecules (Cegoñino et al., 2014; Little et al., 2010). The ion concentration disproportion created between the AF and the surrounding fluids due to the presence of proteoglycans is responsible for the hydration state in this tissue (Cortes and Elliott, 2012).



The AF fibre network, together with the extrafibrillar matrix, presents nonlinear, viscoelastic and anisotropic properties (Ambard and Cherblanc, 2009; Castro et al., 2014; Elliott and Setton, 2001; Sen et al., 2012), which undergoes an intricate combination of loads from several orientations during the daily routine, including bending, torsion and axial compression (Cortes and Elliott, 2012; O'Connell et al., 2009). The mechanical response of the ground matrix to loading is ruled by a combination of several phenomena, including the osmotic pressure and the elastic solid part. A deep analysis in the elastic solid part revealed that the mechanical response of AF to multidirectional loading is governed by the interaction between the annular ground matrix, that resists to compression and tension stresses due to its predominant proteoglycan composition, and the collagen fibres that are essential to withstand to tensile loads (Little et al., 2010). Previous studies indicates that the AF mechanical behaviour also depends on the particular frictional interaction between the ground matrix and the collagen fibres, together with the cross-linking between the fibres embedded in the matrix (Pezowicz et al., 2006; Schollum et al., 2009; Wagner and Lotz, 2004).

As the AF is typically submitted to uniaxial quasi-static loading tests (Acaroglu et al., 1995; Ebara et al., 1996; Elliott and Setton, 2001; O'Connell et al., 2009), neglecting the effect of the rate-dependent viscous on the determination of the mechanical properties of the AF. However, it is well known that the IVD also experiences dynamic loading *in vivo* at a wide range of frequencies. In fact, the loading frequency is reported to be higher than the characteristic frequency of the AF, leading to a significant increase in the interstitial fluid pressure and the stiffness of the tissues (Soltz and Ateshian, 2000, 1998; Yao et al., 2002). Previous studies had demonstrated that an increment in the cyclic strain lead to a decrease in the hysteresis and an increment in the linear region dynamic modulus in axial tests using ovine AF, suggesting that at higher strain rates the dissipated energy decreases (Kasra et al., 2004). Thus, it is clear that the rate dependent viscous effects may play an important role in the disc's ability to dissipate energy. However, the dynamic behaviour of the ground matrix was not been studied on the circumferential region of the AF, which is a recognized loading zone in the AF.

Recently, several analytical and computational models have been developed or optimized in order to simulate the mechanical response of the AF (Castro, 2013; Cegoñino et al., 2014;

Malandrino et al., 2013; Wagner and Lotz, 2004). However, since the accuracy of the computational and analytical models for the AF is strongly dependent on the material laws determined experimentally, it is crucial to define the mechanical behaviour inherent to each AF component, i.e., the fibres and the reinforced-ground matrix (the ground matrix of AF with fibres embedded, which is not actively bearing the axial load). In fact, even though the existence of several studies reporting the properties of annular stresses (Iatridis et al., 2005; Kasra et al., 2004; Little et al., 2010), the current computational models used to predict the IVD response are not completely validated against experimental data. The constitutive laws that describe the mechanical behaviour of the AF need to be in consonance with the particular response and reorganization of AF when submit to loading. However, while the tensile behaviour of the AF, i.e., when loads are applied parallel to lamellae, is nonlinear and described by the use of analytical models, such polynomial and exponential functions (Ambard and Cherblanc, 2009; Cortes and Elliott, 2012; Eberlein et al., 2001; Klisch and Lotz, 1999; O'Connell et al., 2009; Wagner and Lotz, 2004), the experimental tests perpendicular to the lamellae or to evaluate the reinforced-ground matrix (RGM) are scarce in the literature.

Thus, the purpose of this study is to determine the mechanical behaviour of the RGM under unconfined uniaxial static and dynamic compressive loads. Moreover, it aims to compare the response of the RGM tissues under the application of both physiological and non-physiological strains. Test specimens were taken from porcine AF and its geometry was such that there were no continuous collagen fibres coupling the cartilaginous endplate (CEP). To determine the regional inhomogeneity AF mechanics, the samples were taken from four different annular regions (anterior, posterior, lateral right and lateral left). In what concerns to the static uniaxial compressive response, it was determined after submitting the samples to an initial pre-load and then to repeated loading. The maximum strain applied on tissues overstepped the damage strain, in order to define the effect of overstrain on the annular tissue. In addition, to inhibit fluid outflow from the AF care was taken in the strain rate selection. The best fit for the curves of engineering stress as function of the engineering strain for the initial and repeated loading was determined for each annular region. The curves were compared in order to examine the existence of local stiffness differences.

Regarding to the determination of the dynamic mechanical properties, a Dynamic Mechanical Analysis (DMA) was used to obtain the typical viscoelastic parameters - the storage modulus, the loss modulus, the internal friction and the dynamic compressive modulus, in frequency sweep tests. The aim is to better understand the loading support mechanisms of the different annular regions under unconfined axial compression. During the compression tests, the hydration level of each sample was determined in order to determine a possible correlation between the water content in the samples and its mechanical behaviour.

## **5.2. Materials and Methods**

### **5.2.1. Motion Segment Collection and Preservation**

As discussed previously, the young porcine discs have been demonstrated to exhibit similar response, in terms of kinematic and biochemical properties, to human discs. After being collected from a common source, the lumbar spines from 18 months-old pigs were immediately sectioned into motion segments. The posterior elements, together with the spinal cord and the surrounding musculature were removed.

The motion segments were stored at 4°C before testing, which were performed within 24 hours after dissection, in accordance with a protocol approved by the Institutional Human Tissue Committee (Campbell-Kyureghyan et al., 2011).

### **5.2.2. Specimens Preparation**

From the previous sectioned motion segments, six samples were selected for the preparation of the testing specimens. The process of samples preparation is detailed described in Figure 5.1.

The IVDs from the porcine motion segments were sectioned and isolated using precision thin-cutting saw blade. As the AF is anisotropic, i.e., its physical properties are direction and, consequently, region dependent (Castro, 2013; Cavalcanti et al., 2013; Elliott and Setton, 2001; Fujita et al., 1997), each disc was divided in four regions (posterior, anterior, lateral left and lateral right) and six cylindrical AF samples, with 5 mm diameter, were taken from each region (Figure 5.1 - B). The cuts were performed on the sagittal and frontal planes through the disc and its height was variable, oscillating between 3 to 6 mm.

Previous studies reported that it is desirable the tests on RGM should be performed without including the CEP and the vertebral bodies; in addition, the attachment of the specimens should not cause any limitation on the mechanical test performed on the sample (Little, 2004).

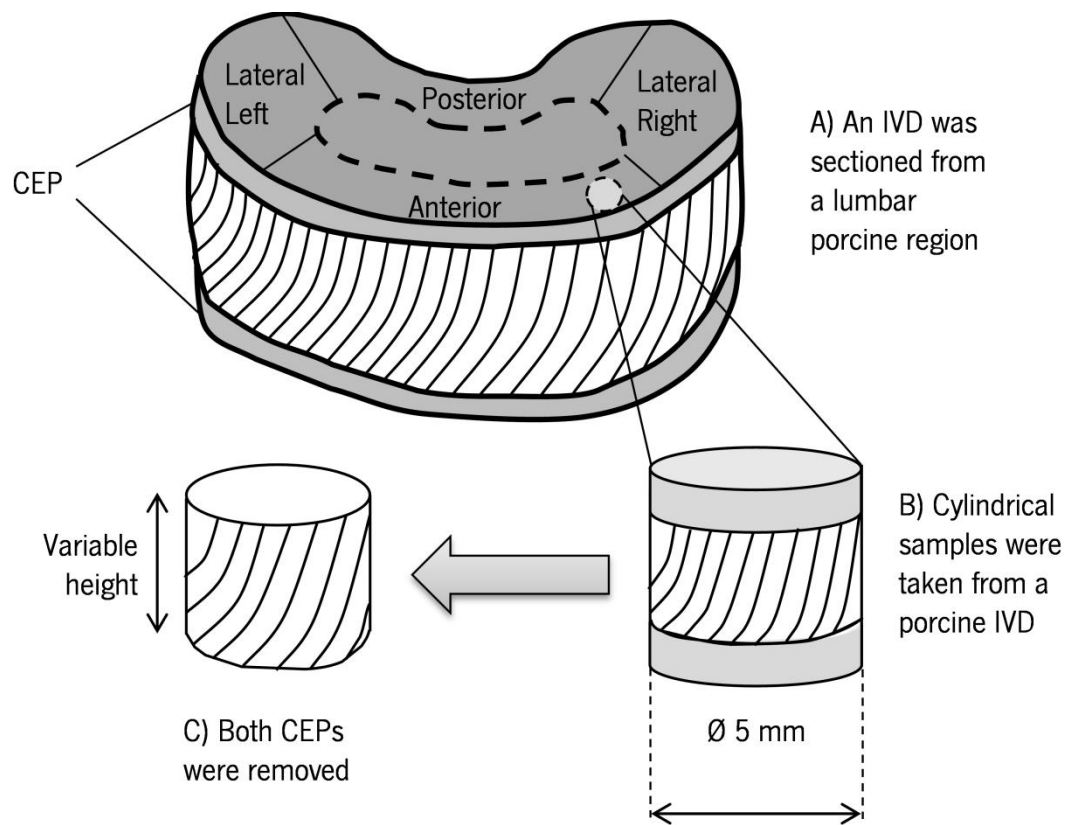


**Figure 5.1.** Schematic representation of the process of specimen preparation. A) An intervertebral disc was sectioned and isolated from the lumbar porcine spine. On each sectioned IVD, four regions were clearly defined (posterior, anterior, lateral left and lateral right). B) Six cylindrical samples, with 5 mm diameter, were taken from each region of the isolated porcine IVDs; C) Both CEPs, from bottom and upper region of the IVD were removed, avoiding the fibres linkage between the superior and the inferior CEP. The testing samples presented a variable height, depending on AF region.

Thus, either CEP layers presented in motion segments were removed (Figure 5.1 - C). This detail is fundamental as for the determination of the mechanical properties of reinforced-annulus ground matrix, no continuous fibres must be coupled to the endplates (Marchand & Ahmed, 1990). Here, the mechanical response of the reinforced-annulus ground matrix was defined as response of the ground matrix with the fibres embedded but not actively bearing a load (Little et al., 2010). Each sample was then processed and submitted to non-confined uniaxial compressive tests in both static and dynamic conditions.

### 5.2.3. Uniaxial Static Compressive Test

After prepared and labelled according with disc positions, the samples for the uniaxial static compressive tests were isolated in a plastic box and kept in phosphate buffer saline solution (PBS

1X) for a maximum of 12 hours prior testing, at 4°C .The remaining material, including the nucleus pulposus and CEPs were discarded. The AF samples were then submitted to unconfined uniaxial compressive tests with a single axis Hounsfield Materials Tester (H5KS, Tinius Olsen Ltd, Surrey, UK, class of precision 1),,, with a 500 N load cell. The loading was oriented in the vertical direction and there was no risk of specimen slippage between the platens.

Due to the scarcity of experimental studies on the reinforced-annulus ground matrix, a considerable effort was performed into the definition of parameters for the mechanical testing of this structure. As the main goal of this work was to observe the physiological response of the AF to strain, the selection of the range of strains that reflects the daily events acting on AF was fundamental. Little (2004) indicated that the strain needed to promote an injury in the AF ground substance ranged between 20 and 27% under uniaxial loading. However, it is widely recognized that the ground matrix can withstand higher strains during physiological events (Kasra et al., 1992; Little et al., 2010, 2007). Thus, the experiments of repeated loading could be important to clarify the role of load support normally attributed to RGM prior to injury initiation.

In what concerns to the loading protocol, this work was based on the loading method developed by Little et al. (2010). Thus, prior to compressive tests, each sample was preconditioned with five cycles at 0.4 Hz. The test procedure consist on the evaluation of the mechanical response of the RGM to initial and repeated loads. As so, each specimen was loaded five times until a maximum strain of 60%, with a relaxation period of five minutes between each load application. The samples were always kept hydrated between tests with PBS (1X).

The characteristic response of RGM to both initial and repeated loading is non-linear. Thus, several equations were used to fit the experimental results. The optimum set of parameters was obtained using a simple cubic polynomial regression - Equation 5.1.

$$\sigma = Y_0 + \varepsilon A + \varepsilon B^2 + \varepsilon C^3 \quad \text{Equation 5.1}$$

Where  $\sigma$  represents the engineering stress in MPa,  $\varepsilon$  the engineering strain, being  $Y_0$ ,  $A$ ,  $B$  and  $C$  the specific material parameters. For this type of materials that present a nonlinear elastic stress-strain behaviour, the curve slope in the linear region could be used to estimate the

change in strain for a specified range in stress, and so to assess the compliance of these materials<sup>vii</sup>. Thus, the linear region of the stress-strain curve for the samples submitted to initial loading regime (for a strain interval between 0 and 15%) was defined as the static compressive modulus ( $E_s$ , in MPa) of the RGM. This material parameter was determined by dividing the stress by the strain for the pre-defined interval of strain. In addition, the strain rate of each sample should be optimized as it represents a critical point in biological tissues testing. The dimensions of all specimens were determined before testing, in order to calculate of the engineering stress and strain (Little et al., 2010).

### **5.2.3.1. Strain Rate Selection**

The bulk response of the ground substance is governed by a combination of pore fluid flowing and the elastic matrix. In detail, the elastic matrix allows the embedment of the pore fluid, establishing the boundaries of the pores, which confers a very specific mechanical response to the RGM. The resistance of this complex structure to loading is defined by two different phenomena: (1) the mechanical resistance of the elastic matrix and (2) the increment of the pore pressure, inherent to the fluids retention in the pores of the elastic matrix (Little, 2004). Thus, an adequate selection of the magnitude of the strain rate is essential for the evaluation of the RGM properties. In fact, while lower strain rates are responsible for the inhibition of fluid drag in the elastic matrix and, consequently, for either the outflow of the fluid from and volume loss in tissue, higher strains are associated to the fluid retention in pores leading to increment in the loads resistance due to the rise of pressure in pore fluid (Kasra et al., 2004; Little, 2004; Little et al., 2010).

The application of a loading protocol that insures a residual fluid loss from tissue during loading is essential to test the RGM's physiological conditions. Previous studies focused on the selection of the low strain rates, ranging between  $0.0001 \text{ s}^{-1}$  and  $0.0005 \text{ s}^{-1}$ , aiming to promote the fluid outflow from the AF (Acaroglu et al., 1995; Ebara et al., 1996; Fujita et al., 1997; Skaggs et al., 1994; Wu and Yao, 1976). As such, their methodologies did not allow the

---

<sup>vii</sup> <http://www.astm.org/Standards/E111.htm>

determination of the AF mechanical properties under physiological conditions. However, it was also reported that higher strain rates, such as  $0.1 \text{ s}^{-1}$  have a dramatic effect on the pore fluid pressure levels, creating an excessive drag pressure from the pores (Little, 2004). In the scope of this work a strain rate of  $0.01 \text{ s}^{-1}$ , such as used by (Little et al., 2010) appears to be a reasonable value to understand the mechanical response of RGM to uniaxial compressive loading.

#### **5.2.4. Dynamic Mechanical Testing**

The annular RGM is known by exhibit deformation characteristics that are a combination of both solids (elasticity) and liquids (viscosity), being referred as viscoelastic. Thus, the application of an oscillating force, with a non-steady deformation, is a common technique used to determine the degree of elasticity and viscosity of this structure.

##### **5.2.4.1. Dynamic Compressive Test**

The determination of the viscoelastic behaviour was performed by DMA (TA DMA Q-800). This instrument has several design features which make it particularly useful for dynamic characterization of biological samples. Presenting a wide variety of probe tips, it is capable of operating in a compression cycling mode, with the specimen in air or immersed in water. In the scope of this study, it was selected the submersible uniaxial compression configuration - Figure 5.2.

The operating principle of the DMA consists on the application of an oscillating stress/strain to a sample of known geometry as a function of frequency or temperature. The sample can be subjected by a controlled stress or a controlled strain. The process of application of a known stress, where the sample deforms a certain amount, is done sinusoidally by a force motor, being transmitted via a drive shaft. In this case, one plot the modulus versus frequency as they provide useful information about viscous properties of biological samples, namely about the flowing.



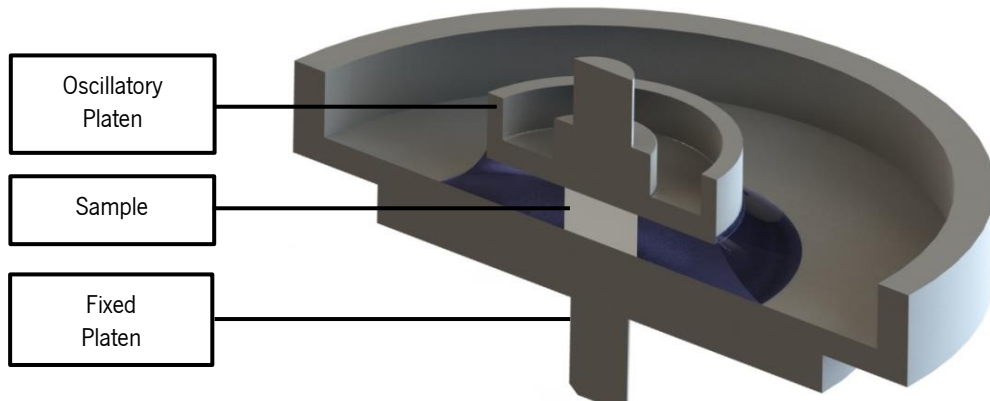


**Figure 5.2.** Submersible compression plates. It allows placing a continuous hydration state on a sample while a compression test is performed. The sample (light grey) is placed on the bottom compression plate and it is possible to submerge the sample with a fluid.

From the compressive test with DMA, two basic quantities were directly obtained as function of frequency: the dynamic modulus ( $E_d$ ) and the phase shift ( $\delta$ ). While  $E_d$  is defined as the ratio between the amplitudes of the sinusoidal curves of the stress and strain, the  $\delta$  represents the phase angle between the same sinusoidal curves. Moreover, the viscoelastic parameters, storage modulus ( $E'$ ) and loss modulus ( $E''$ ) of the samples were calculated directly from the dynamic modulus and the phase shift, by Equation 5.2. and Equation 5.3 respectively.

$$E' = E_d \cos \delta \quad \text{Equation 5.2}$$

$$E'' = E_d \sin \delta \quad \text{Equation 5.3}$$

In a first stage, the samples placed in a rigid plate, were solicited with a sinusoidal 1 N load, to ensure their osmotic balance in the fluid of the clamps. This procedure was repeated until the monitored variation between the initial and final thickness of the samples was less than 10%. When the osmotic balance between the sample and the fluid in the clamps was reached, the pre-load was maintained and an isothermal DMA test (Room Temperature) was performed by the application of a 0.5  $\mu\text{m}$  displacement amplitude, while imposing a frequency sweep of 1, 5 and 10 Hz. In an ovine explant mode it was found that a 10 Hz frequency resulted in increased

number of apoptotic cells, while a frequency higher than 5 Hz of 1 MPa intermittent hydrostatic pressure had led to impaired collagen synthesis (Chan et al., 2011). The option for this range of frequencies, from a normal physiological value (1 Hz) to an ultra-high frequency (10 Hz), is thus justified by the possibility of the assessment of the AF behavior under physiological and non-physiological frequencies. Additionally, the Dynamic Compressive Modulus ( $E_d$ ) and Internal Friction ( $Q^{-1}$ ) were determined, using the Equation 5.4 and the Equation 5.5, respectively.

$$E_d = \sqrt{E'^2 + E''^2} \quad \text{Equation 5.4}$$

$$Q^{-1} = \tan(\delta) = \frac{E''}{E'} \quad \text{Equation 5.5}$$

It is important to mention that although the storage modulus and the Young's modulus, which is determined from the slope of the initial part of a stress-strain curve, are conceptually similar, they do not represent the same amount. Just as shear, bulk and compressive modulus for a material will differ, the dynamic compressive modulus will not have the same value as the storage modulus.

#### **5.2.4.2. Water Content**

The water content was determined in order to understand its relation with the dynamic behaviour of the RGM. The AF samples were not completely immersed and water during the dynamic tests to avoid the overhydration; instead of that, to ensure an adequate tissue hydration, each sample was immersed in a drop of 1mL PBS (1X). Then, each sample was immediately weighted using an analytical balance (Gibertini®, E425-B). This weight was considered as the initial weight of the samples. Then, each sample was submitted to the axial compressive test. After the test, the samples were weighted again in order to assess the effect of the effect of the test in water content. Each sample was left in a controlled conditions room, with 24°C temperature and approximately 0% humidity during 24 hours. The objective was to obtain the dry weight of each RGM sample.

The water content of each sample was determined by the Equation 5.6.

$$\%WC = \frac{W_i - W_f}{W_i} \times 100 \quad \text{Equation 5.6}$$

Where  $\%WC$  represents the percentage of water content,  $W_i$  the initial weight or the weight before testing and  $W_f$  is the final weight or dry weight. The results of water content were compared to the dynamic behaviour of each sample, in order to understand if there is some correlation between the dynamic loading and the water content of the RGM samples.

### 5.2.5. Data Analysis

In what concerns to the static compressive tests, the best fitting curves for the initial and the repeated loading tests were determined using specific software, the GraphPad Prism 6 (Graphpad Software, California). In order to analyze the curve fitting, the coefficient of determination,  $R^2$ , together with the standard error of the estimate was obtained for the regression lines applied to each sample. Moreover, a 1-factor ANOVA test was applied to compare the initial and repeated regression curves in each disc region. The goal was to define if repeated and initial tests were significantly different from each other and if significant differences were found between AF regions. The 1-factor ANOVA regression analysis was also applied to compare the static compressive modulus of the several AF samples.

Regarding to DMA tests, the dependency of the viscoelastic parameters ( $E'$ ,  $E''$ ,  $\tan \delta$  and  $E_d$ ) with the frequency was evaluated for each AF region. The differences between the viscoelastic parameter for each region under the same frequency were also assessed. All statistical tests were performed with a 1-factor ANOVA, with a significance level of  $p < 0.05$ .

In addition, the percentage of water loss for different AF regions was analyzed and compared. 1-factor ANOVA was used to assess if significant differences in terms of water content are detected between samples. The *t-student* test was applied to compare the percentage of water content of each region with the remaining values.

## 5.3. Results

### 5.3.1. Uniaxial Compressive Loading

After inspect the samples collected from each AF region, two posterior, one lateral left and one lateral right sample were discarded from the study due to irregularities in its geometry.

The parameters of Equation 5.1 and the standard error of estimate for the curves of best fit to the experimental data are reported in Table 5.1. The  $R^2 \geq 0.995$  indicated an excellent fit of the polynomial curves to the compressive behaviour of the RGM. The standard error of estimate, i.e., the standard deviation of the prediction errors, presents a relative low magnitude, reinforcing the idea that the adopted model presents a good fit to the experimental data. The data from Table 5.1 also highlights that the response of AF samples to initial loading does not present a solid pattern, while the repeated loading is highly reproducible between successive cycles.

The analysis of the stress vs strain curves - Figure 5.3, reveals interesting observations. Until 30% strain, the initial loading cycles present a stiffer response than the ones exhibited by the repeated loading cycles (cycles 2 to 5). This stiffness difference is more evident for the posterior and lateral right samples - Figure 5.3 - B) and C).

The comparison between the regional values of  $E_s$ , for a strain up to 15% in the initial tests, showed that the anterior RGM is the most compliant - Figure 5.4.. In fact,  $E_s$  for the anterior samples was significantly different from the remaining RGM regions ( $p < 0.006$ ). No significant differences were observed between the posterior, lateral left and lateral right RGM samples ( $p > 0.63$ ), which reveals a similar stiffness between specimens. Interestingly, no significant differences were observed between the samples stiffness in the repetitive tests, for a strain up to 25% ( $p > 0.05$ ) (Figure 5.3 - E)).

**Table 5.1.** Parameters of the best fit of the cubic polynomial function to the experimental data, including the standard error of the estimate.

<b>Coefficients</b>		<b>Y<sub>0</sub></b>	<b>A</b>	<b>B</b>	<b>C</b>	<b>Standard error of the estimate</b>		
<b>Region</b>	<b>Anterior</b>	-0.017	0.655	-4.010	8.906	7.0E-03		
		Initial	±	±	±		±	
		4.507	0.026	0.354	3.619			
		-0.023	0.812	-5.715	12.050		8.3E-03	
		Repeated	±	±	±			±
		0.001	0.036	0.214	0.369			
	<b>Posterior</b>	-0.001	0.238	-0.469	3.725	4.4E-03		
		Initial	±	±	±		±	
		0.010	0.144	0.758	2.082			
		-0.0181	0.6917	-5.0103	11.126		8.1E-03	
		Repeated	±	±	±			±
		0.0071	0.1752	1.0049	1.1890			
<b>Lateral Left</b>	-0.009	0.328	-1.508	3.840	3.7E-03			
	Initial	±	±	±		±		
	0.006	0.179	0.722	1.075				
	-0.008	0.232	-1.746	4.779		2.6E-03		
	Repeated	±	±	±			±	
	0.001	0.021	0.157	0.242				
<b>Lateral Right</b>	0.010	0.400	-1.774	2.874	5.43E-03			
	Initial	±	±	±		±		
	0.006	0.127	5.547	1.295				
	-0.019	0.670	-4.808	10.10		8.12E-03		
	Repeated	±	±	±			±	
	0.004	0.120	0.643	0.739				

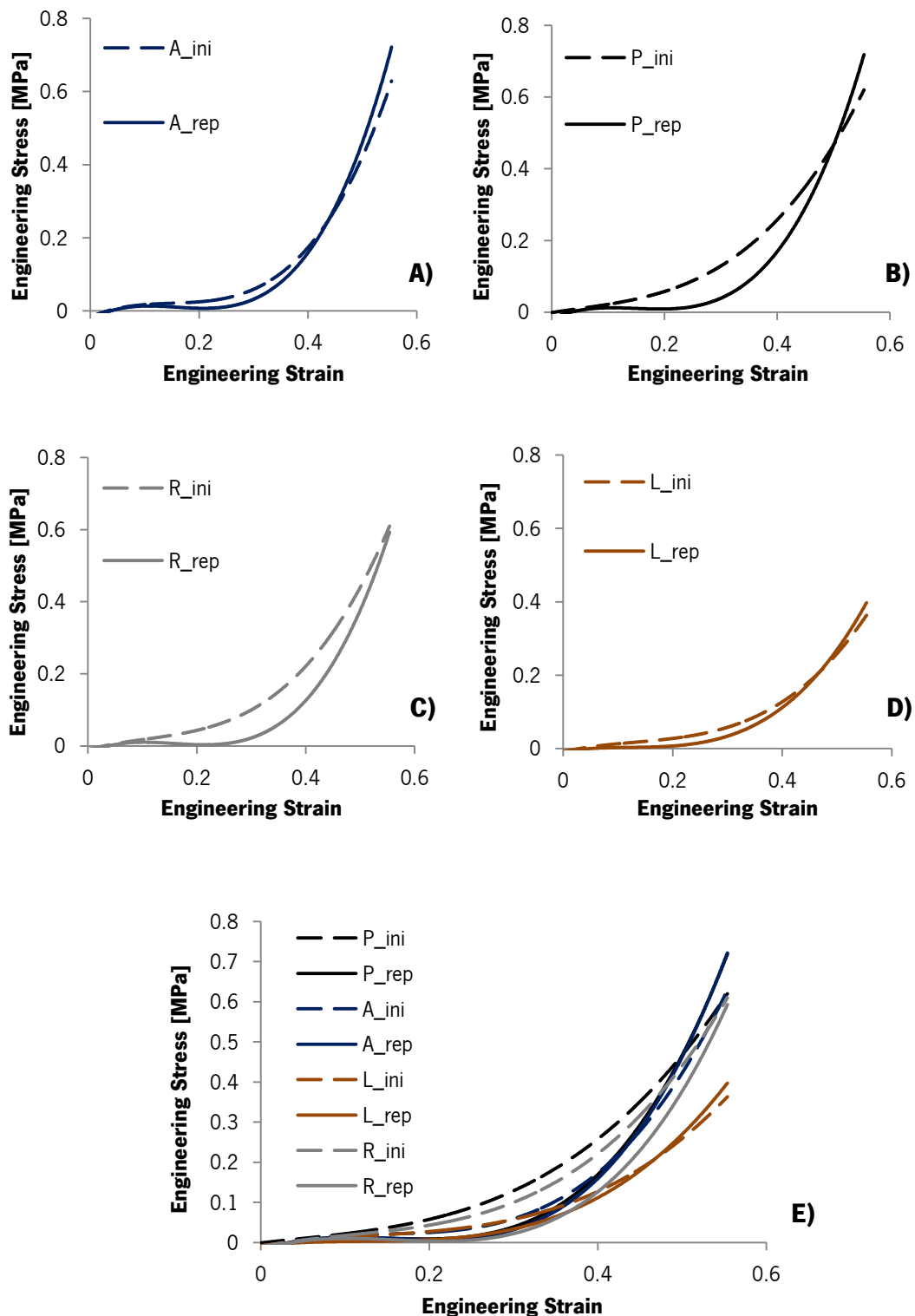


**Figure 5.3.** Regression curves of engineering stress-strain of the RGM under uniaxial compressive loading, for initial test (Cycle 1) and for the subsequent tests (Cycles 2-5). The four graphs represent the four distinct regions sectioned in the AF: A) Anterior; B) Posterior; C) Lateral Right; D) Lateral Left; E) Global response of the AF regions. Legend: ini – Initial loading; rep – Repeated loading; A – Anterior region; P - Posterior region; L – Lateral left region; R – Lateral right region.

The ANOVA carried out on the regression lines for the uniaxial compression tests had indicated significant differences between the initial and repeated loading cycles for all regions ( $p < 0.03$ ), with exception for the anterior one ( $p > 0.70$ ). The repeated loading tests also revealed a more significant variation with increased strain: for strains above 40%, the repeated loading response is generally stiffer than the initial loading, which is detectable by the trend of the stress-strain curve.

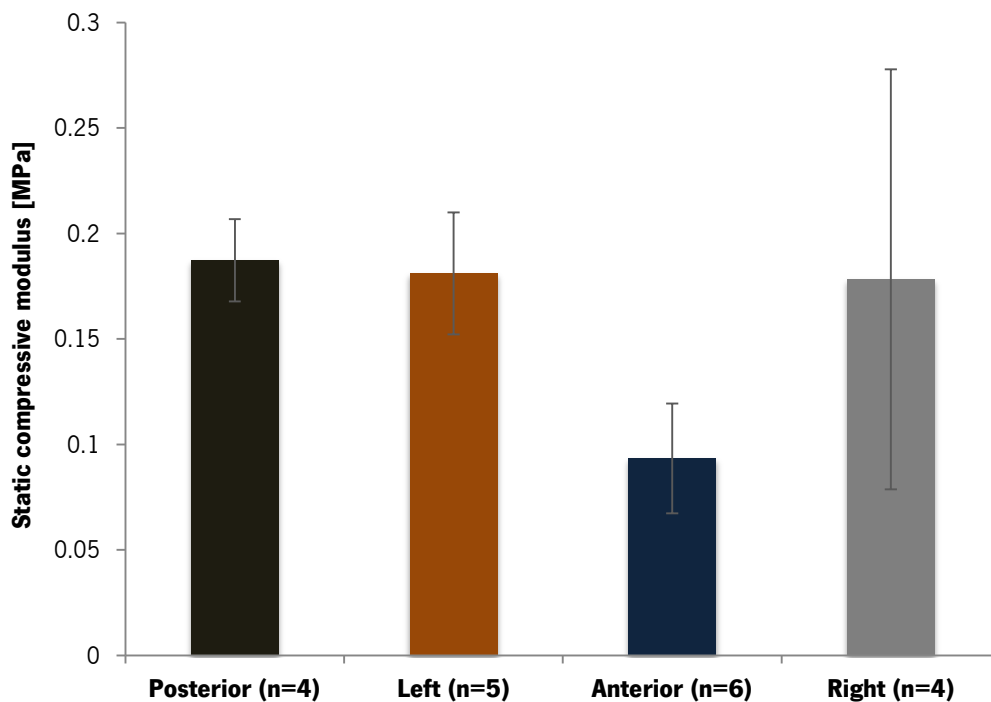


**Figure 5.4.** Static compressive modulus ( $E_s$ , in MPa) for the each RGM region. This parameter was obtained dividing the engineering stress by the engineering strain, for the linear region of the stress-strain curve - from 0 to 15% of strain.

### 5.3.2. Dynamic Mechanical Testing

The viscoelastic parameters ( $E'$ ,  $E''$ ,  $\tan \delta$  and  $E_d$ ) of the RGM are presented in Figure 5.5. As shown, the loss modulus was much lower than the storage modulus, in all the groups. In addition, significant differences ( $p < 0.05$ ) were detected for the values of the viscoelastic parameters for the different annular regions (Table 5.2), with exception for the loss modulus and the internal friction, at 1 Hz ( $p > 0.4$ ). Each ANOVA test that revealed significant differences

between the parameters was submitted to a *t*-test, in order to detail the significant differences for each viscoelastic parameter, at a set frequency, according to each region.

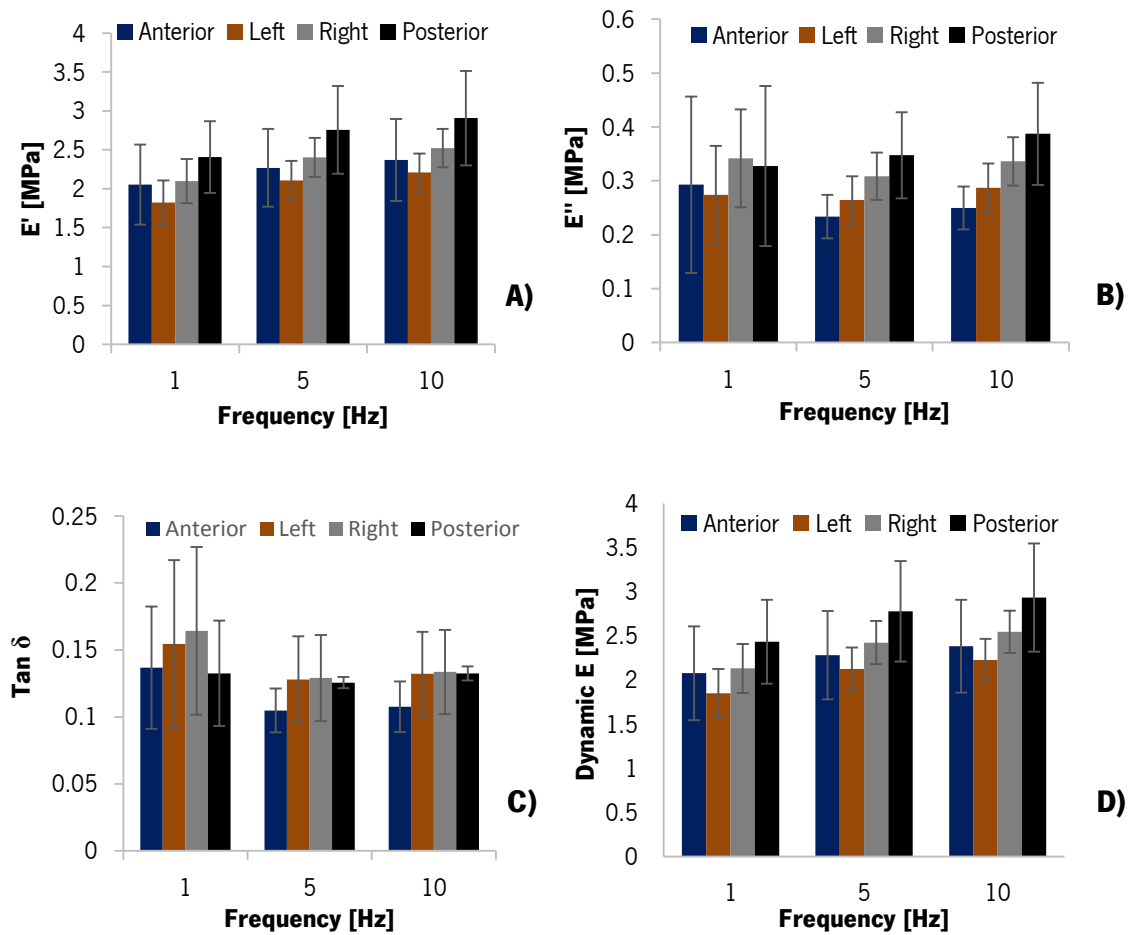


**Figure 5.5.** Dynamic mechanical properties (mean  $\pm$  S.D.) for the different annular regions (anterior, left, right and posterior), at three different frequencies: 1, 5 and 10 Hz. A) Storage modulus; B) Loss modulus; C) Internal friction ( $\tan \delta$ ) and D) Dynamic compressive modulus.



**Table 5.2.** Differences between each region for each viscoelastic parameter ( $E'$ ,  $E''$ ,  $\tan \delta$  and  $E_d$ ), according to the frequency, determined by the  $p$ -value of the ANOVA tests.

Parameter	Frequency [Hz]	<i>P-value</i>	Difference <sup>viii</sup>
<b>E'</b>	1	1.7E-04	Significant
	5	8.8E-06	Significant
	10	4.7E-06	Significant
<b>E''</b>	1	5.9E-01	Not Significant
	5	2.3E-07	Significant
	10	3.3E-08	Significant
<b>tan <math>\delta</math></b>	1	4.3E-01	Not Significant
	5	2.6E-03	Significant
	10	7.7E-04	Significant
<b>E<sub>d</sub></b>	1	2.5E-04	Significant
	5	7.4E-06	Significant
	10	3.8E-06	Significant

The results, presented in Table 5.3, revealed that, when compared with the remaining regions, there was no significant differences for both the storage modulus and dynamic compressive modulus of anterior and lateral right regions, for all the frequencies ( $p > 0.05$ ). Conversely, for the same parameters, significant differences were registered between the posterior and lateral left regions, when compared with the remaining samples ( $p < 0.05$ ). In fact, while the storage modulus in the posterior region is significantly higher than other AF regions, the lateral left presented lower values, indicating that the values of these parameters are dependent on the annular region.

<sup>viii</sup> For a significant level of 0.05

**Table 5.3.** *P-values* determined with *t-student* test by the comparison of each region with the remaining ones for each viscoelastic parameter, according with frequency.

	<b>Frequency</b>	<b>Anterior</b>	<b>Left</b>	<b>Right</b>	<b>Posterior</b>
<b>E'</b>	1 Hz	4.9E-01	2.1E-04	8.0E-01	6.7E-04
	5 Hz	1.2E-01	2.8E-05	9.9E-01	5.0E-04
	10 Hz	9.6E-02	9.0E-03	9.9E-01	4.1E-04
<b>E''</b>	1 Hz	-	-	-	-
	5 Hz	2.0E-07	3.3E-02	1.7E-01	5.9E-02
	10 Hz	2.5E-08	4.2E-09	2.0E-01	1.0E-04
<b>Tan Delta</b>	1 Hz	-	-	-	-
	5 Hz	2.0E-05	3.2E-01	1.7E-01	1.6E-01
	10 Hz	1.8E-05	3.2E-01	1.8E-01	3.7E-02
<b>E</b>	1 Hz	4.8E-01	2.0E-04	8.7E-01	9.3E-04
	5 Hz	1.1E-01	2.2E-05	9.4E-01	4.9E-04
	10 Hz	8.2E-02	1.1E-05	9.5E-01	4.1E-04

Regarding to the loss modulus and the internal friction, the *p-values* demonstrated that anterior region presents significant lower values than those reported for remaining samples ( $p < 0.05$ ). However, no significant differences were found between lateral right samples and the other regions ( $p > 0.05$ ), for the range of frequencies tested.

Interestingly, the lateral left samples revealed significant differences between the values of the internal friction ( $p < 0.05$ ), whereas no differences were detected between the values of loss modulus compared to the remaining RGM regions ( $p > 0.05$ ). Furthermore, posterior region was the only group of samples showing a dependency on the frequency: while for 5 Hz testing, no significant differences were found between regions ( $p > 0.05$ ), for a frequency of 10 Hz both loss modulus and internal friction ( $p < 0.037$ ) were significant higher for the posterior region than for the remaining regions.

In Table 5.4 is shown the statistical differences between the viscoelastic parameters for the different annular regions with the frequency. The ANOVA demonstrated that loss modulus is not dependent on the frequency, for all annular regions ( $p > 0.2$ ). Moreover, the internal friction has also revealed to be not dependent on the frequency, with exception for the anterior region. Conversely, the storage modulus and the dynamic compressive modulus presented significant regional dependency with frequency ( $p < 0.05$ ), excluding for anterior region.

**Table 5.4.** The differences between the viscoelastic parameters ( $E'$ ,  $E''$ ,  $\tan \delta$  and  $E_d$ ) for the different annular regions with the frequency, determined by the  $p$ -value of the ANOVA tests.

Parameter	Annular Region	<i>P</i> -value	Difference*
<b>E'</b>	Anterior	9.7E-02	Not Significant
	Left	1.2E-04	Significant
	Right	1.5E-13	Significant
	Posterior	6.7E-03	Significant
<b>E''</b>	Anterior	2.1E-01	Not Significant
	Left	7.8E-01	Not Significant
	Right	5.7E-01	Not Significant
	Posterior	2.9E-01	Not Significant
<b>Tan <math>\delta</math></b>	Anterior	2.4E-02	Significant
	Left	3.0E-02	Not Significant
	Right	5.6E-02	Not Significant
	Posterior	3.2E-01	Not Significant
<b>E<sub>d</sub></b>	Anterior	1.2E-01	Not Significant
	Left	1.4E-04	Significant
	Right	2.9E-13	Significant
	Posterior	1.4E-04	Significant

### 5.3.2.1. Water Content

The quantification of the water content allows the better understanding of the material composition, the temporal performance and water maintenance of the RGM. The results,

<sup>ix</sup> For a significant level of 0.05 in the ANOVA test.

presented in Figure 5.6, showed that the posterior region presented lower water loss, during the mechanical test, for both after test and after 24 hours period. Significant differences were found between the posterior and the remaining regions in both after mechanical test and after 24 hours at drying conditions ( $p=5.5E-06$  and  $p=0.04$ , respectively;  $n=4$ ). No significant differences were found between the remaining samples.

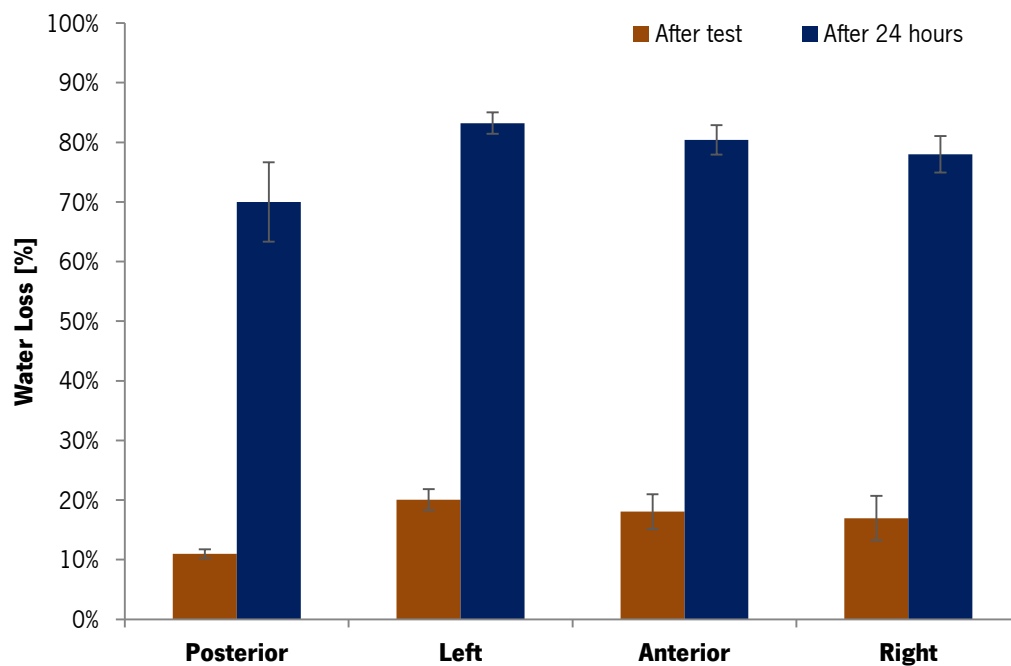


**Figure 5.6.** Percentage of water loss (mean  $\pm$  S.D.) immediately after test and after 24 hours, for all the RGM regions (Posterior, Left, Anterior and Right).

#### **5.4. Discussion of Regional Variations in the Mechanical Behavior of the Annulus Fibrosus in both Static and Dynamic Conditions**

The contribution of RGM for the mechanical behaviour of the AF structure is a matter of deep interest concerning to the whole response of the IVD to loading. The RGM, composed by a matrix with embedded collagen fibres that do not actively withstand the axial loads, contributes considerably for the resistance of the AF to applied strains, due essentially to the interaction fibre-fibre together with the friction on the interface fibre-surrounding matrix (Little et al., 2010).

Moreover, the computational and analytical constitutive models of the AF need to quantify the contribution of the relationship between the ground matrix with its embedded fibres to the mechanical response of the IVD. Thus, the experimental characterization of the RGM by means of an appropriate and special defined protocol should be executed to provide additional information about this structure.

The objective of this study was to investigate and assess the mechanical response of the annular RGM under unconfined compressive tests. With that purpose, RGM samples from porcine IVDs were isolated and carefully manipulated according with their specific characteristics. An earlier study reported that the excision of the RGM samples should be performed in a specific way that ensures no continuous collagen fibres linked to the vertebral endplates (Little et al., 2010). The adjacent bony constituents were removed in all the samples, allowing the determination of the compressive response of the RGM.

Previous studies were focused on the characterization of the structural mechanisms of the ground matrix that are responsible for the cohesion between the concentric groups of fibre that composed the AF, under tensile loading tests (Adams and Green, 1993; Pezowicz et al., 2006). However, the experimental quantification of the contribution of each interaction type to AF mechanics is a complex process, where the value of the parameters could be strongly concealed due the significant errors associated to the measurements of biological samples. The compressive behaviour of the AF was studied by previous researchers aiming to determine both the stress relaxation (Best et al., 1994) and the biphasic properties (Iatridis et al., 1998). However, these tests were carried out under lower strain rates which can lead to inhibition of

fluid drag in the elastic matrix (Little et al., 2010). Recently, the study of the mechanical response of the ground matrix was divided into the contribution of the osmotic pressure and the elastic solid phase of the extra-fibrillar matrix, in both tension and compression tests (O'Connell et al., 2009; Périé et al., 2005). However, both approaches neglect the contribution of the non-activate fibres, embedded in ground matrix during compressive loads.

The proposal of this study is to determine the response of RGM to loading considering the contributions of the each type of RGM interaction. The quantified parameters can be included into a constitutive model that, together with a fibre-reinforced composite approach, may allow the representation of the mechanical behaviour of the AF in computational models of the IVD (Little et al., 2010; Wagner and Lotz, 2004).

The typical methodology to measure the behaviour of biological samples under compressive loading is to submit the specimens to a confined test (Cortes and Elliott, 2012; Ellingson and Nuckley, 2012; Périé et al., 2005). However, this work reported the determination of the mechanical properties of the AF under non-confined compressive tests, as it was considered that physiologically, the AF is not as constrain as a confined test presuppose. In fact, the RGM could expand laterally under physiological conditions, indicating that the concept of confining the compressive tests also presents some limitations in its approach.

#### **5.4.1. Static Uniaxial Compressive Tests**

Regarding to the static compressive tests, the results of the Table 5.1 indicated that the analytical model presents an excellent fit to all the loading cycles applied on the samples ( $R^2 \geq 0.995$ ). As expected, the material parameters for the initial tests  $Y_0$ ,  $A$ ,  $B$  and  $C$  present a wide standard deviation when compared to the repeated tests. In fact, during the initial tests, the RGM still presents its normal structure, with its particular features such as inhomogeneity, anisotropy and osmolarity that contribute for the results dispersion. The reduction of the microspaces in the interfaces matrix-fibres and fibres-fibres after the application of damaging strain, combined to a less water content in the AF (a significant part flows out of its structure during initial test) and consequently, a prevalence of the solid phase of the RGM during repeated tests, leads to a more

predictable and “standardized” set of results. Remarkably, no significant differences were detected between the initial and the repeated test in the anterior RGM region. This fact indicated that the anterior region does not suffer a significant change in its mechanical behaviour after suffering a compressive damaging strain.

The results provided in this work were quantitatively compared with the previously reported in the literature for the four annular regions - Table 5.5. The stiffness of the RGM samples was determined as the elastic modulus in the linear region of the compression tests, for the initial loading cycle tests.

**Table 5.5.** Comparison between previous experimental findings and the results of the current work.

<b>Mechanical Test</b>	<b>Source of data</b>	<b>Animal Model</b>	<b>“Highest stiffness” region of Annulus</b>	<b>“Lowest stiffness” region of annulus</b>
Uniaxial confined compression	Best et al. (1994)	Human lumbar	The mean values of posterior region are higher than the anterior; however, the mechanical response of the solid phase of the AF, i.e. the aggregate modulus (HA) had revealed no significant differences between the anterior and posterior AF.	
Uniaxial unconfined compression	Little et al. (2010)	Ovine lumbar	Posterior	Lateral
Uniaxial unconfined compression	Present Study	Porcine lumbar	-	Anterior

From the comparison of the results of the current work with previous experimental studies, it is clear that the posterior region is stiffer than the anterior. Interestingly, the present study revealed no significant differences were found between both lateral and the posterior regions, while the anterior region presented the lower stiffness. This evidences support the idea that the anterior RGM is more prepared to damaging compressive strains than the remaining regions. Conversely, the study performed by Little et al. (2010) points out the lateral region as the lowest stiffer region in the AF.

The divergences between the studies are likely related to several factors such as the sample preparation and manipulation, the calculation of the elastic static modulus, the strain rate

applied and the use of different animal models in the study. First, in opposition to the work of Little et al. (2010), the present work does not include any segment of the vertebral bones in order to avoid the presence of continuous fibres that could act in the tension mode. Second, in the present study, the elastic modulus was determined by the linear regression in the stress-strain curve; in the work performed by Little et al. (2010), it is not clear the method applied to calculate this material parameter, while Best. et al (1994) have determined the mechanical response of the solid phase of the AF in confined compression tests. This last configuration is probably associated to differences in stiffness, as the fibres are not able to freely expand in any direction during the compression test. Thus, the fibre-matrix interaction is quite different in confined and unconfined approaches. In addition, the strain rate, that is an important factor for the analysis of compressive behaviour of the AF, was not referred in the Best. et al (1994) tests. Finally, these comparisons involve the use of different models: Little et al. (2010) used ovine IVD samples, while the tests performed by Best. et al (1994) used human samples. All this variety of models is also a source of differences in terms of values, namely when compared to porcine ones. However, and despite all limitations of the comparisons, the results of the current study reinforced the idea that the AF presents an inhomogeneous structure concerning to its stiffness.

In what concerns to the repeated loading tests, the current study also demonstrated that the RGM shows a significant drop in stiffness. This is a predicted phenomena, already described by Little et al. (2010): under tissue damage strains, an increment in the interlaminar separations is observable, being likely the cause for the loss of stiffness between the initial and repeated loading. However, previous studies also referred that the AF presents the mechanisms to promote tissue repairing after this type of aggressions, leading to the maintenance of the tissue stiffness even for damage strains (Iatridis et al., 2005).

A remarkable event emerges from the repeated loading on the RGM: although the samples also revealed to be able to withstand the applied load, a different mechanical behaviour is evident when damaging strains are applied to RGM. In fact, all the RGM samples upon repeated compressive loading revealed an initial high compliant behaviour at low strains (up to 30%), followed by an increased stiffness at higher strains. This behaviour is similar to the uniaxial compressive tests performed by Little et al. (2010), where the stiffness of the samples exceeds in



all the cases the one demonstrated in the initial loading cycle. These results indicated that the AF tissue damaging is likely preceded by a decrease in the stiffness of the RGM and a consequent change on its mechanical behaviour.

#### **5.4.2. Dynamic Mechanical Testing**

The Dynamic Mechanical Analysis (DMA) is one of the most recognized techniques for the characterization of the viscoelastic properties of biological materials. In the particular case of AF, it is remarkable the influence of the viscoelasticity of the solid matrix on the overall response of AF (Cegoñino et al., 2014; Wang et al., 1997). Nevertheless this influence, the studies about the dynamic behaviour of the RGM are scarce in the literature. Thus, this research allowed a better comprehension about the dynamic behaviour of this structure.

During compression loading on the disc, the viscoelastic properties of the disc structures, such as annular ground matrix or nucleus, enable the disc to absorb the applied energy, dissipating it into the surrounding tissues by changes in shape. When the load is removed, the shape is recovered due to the release of energy and consequently dissipation in the surrounding tissues. Several material parameters such as storage modulus, loss modulus and the internal friction ( $\tan \delta$ ) are known to be an important tool for the evaluation of the viscoelasticity of biological tissues and biomaterials (Zhou et al., 2014). While the storage modulus represents the elasticity of a material, the loss modulus reflects the viscosity and the  $\tan \delta$  is the ratio between storage and loss modulus. All of these parameters allow presenting a mathematical description of the dynamic experiment under physiological strains. In this study, these viscoelastic parameters were obtained by a dynamic compression test, being analyzed in order to assess the variations on the RGM viscoelasticity according to the annular region and frequency.

Regarding to the results, the loss modulus was revealed to be much lower than the storage modulus in all the RGM regions, suggesting that there is more prominent contribution of the elastic component for the mechanical response of the RGM than of the viscous one. These results are in line with the recent assumptions taken by Cegoñino et al. (2014), where in spite of neglecting the intrinsic viscoelasticity of the matrix and collagen fibres in its numerical model, it

was recognized that the viscoelastic nature of the solid matrix can affect the overall response of the tissue. Thus, although the magnitude of the viscous component being lower than the elastic one, it should be included in the constitutive models of the AF.

The comparison between the values of the viscoelastic parameters for a specific and the remaining RGM regions (Table 5.6) revealed interesting facts. Recent models of the annulus fibrosus have included the fibre matrix interaction in its formulation (Guerin and Elliott, 2007). Thus, it is important to quantify the influence of internal interactions on the AF matrix to optimize the accuracy of the current models. A better understand on the inner interactions in the RGM could be given by the internal friction (or  $\tan \delta$ ). Analytically, this amount is given by the ratio between the storage and loss modulus or, by other words, the ratio between the energy dissipated and the energy stored. Physically, the internal friction represents the frictional interaction between adjacent portions in the interior of the RGM due to viscous deformation or flow. Concerning to the experimental values of loss modulus and internal friction, they revealed to be not dependent on frequency. However, while the mean values of loss modulus and internal friction were found to be significantly lower in the anterior region of the RGM than the remaining samples (for higher frequencies – 5 Hz and 10 Hz), a statistically greater value of loss modulus was found in the posterior region for a frequency of 10 Hz. For the particular case of the RGM, the results suggest that the anterior region is the viscous region of the AF, being mainly involved in the energy storage than in the energy dissipation function of the IVD.

Furthermore, although no significant differences were detected in terms of global value of the internal friction with frequency, the results indicate that the local fibres-matrix or fibres-fibres interactions on the posterior and anterior regions of RGM is dependent on the frequency. In fact,  $\tan \delta$  is higher than remaining samples for higher frequencies on posterior region, while is lower for anterior specimens at higher frequencies. A possible explanation arises from the fact that a loading frequency higher than the characteristic frequency of the tissue could drive to a significant increase in the interstitial fluid pressure (Yao et al., 2002), which likely induces a structural “reorganization” of AF in order to withstand the high loading frequencies.

**Table 5.6.** Statistical analysis and comparison between the values of viscoelastic parameters for a specific and the remaining RGM regions, according with *p-value* (significant level of 0.05). The “lowest” and “highest” words indicate that a particular region presents the lowest or the highest values of a defined parameter, at an indicated frequency (n=20).

Parameter	Frequency [Hz]	Anterior	Left	Right	Posterior
<b>E'</b>	1	-	Lowest	-	Highest
	5	-	Lowest	-	Highest
	10	-	Lowest	-	Highest
<b>E''</b>	1	-	-	-	-
	5	Lowest	Significant	-	-
	10	Lowest	Significant	-	Highest
<b>Tan Delta</b>	1	-	-	-	-
	5	Lowest	-	-	-
	10	Lowest	-	-	Significant
<b>E</b>	1	-	Lowest	-	Highest
	5	-	Lowest	-	Highest
	10	-	Lowest	-	Highest

Regarding to the storage and a dynamic compressive modulus, they are significant higher for the posterior region and the lower for the lateral left, for all the frequencies of test. Interestingly, the Table 5.4, where the differences between the viscoelastic parameters for each annular region were analyzed, showed that, with exception for the anterior region, the values of storage modulus and dynamic compressive modulus are statically different between the AF regions. These results strengthened the idea of the heterogeneity in the elastic component structure of AF. However, concerning to the viscous component, the loss modulus, no significant differences were found between regions. A similar behaviour was found for the internal friction, with the exception for the anterior region, presenting a statistically lower value of internal friction than the remaining regions.

All these results revealed that the viscoelastic properties are also different according with the annular region. Thus, in parallel to the dynamic mechanical tests, it is important to understand the role of the annular hydration on the response of the RGM to loading. Skaggs et al. (1994) found that, in the circumferential region of the AF, there was no significant variation in both the collagen content and hydration. However, the present study revealed that the posterior region presented statistical higher water loss than the remaining samples, for both immediately after test and 24 hours after the loading. In addition, it also indicated that the propensity to imbibe fluid is different according to the annular regions. Thus, the highest values of elastic parameters for the posterior specimens could be related to a lower amount of water content in the posterior ground substance.

The microstructure of the ground matrix could also explain this variation. An investigation on the laminated structure of the AF taken by Marchand & Ahmed (1990) reported that the thinnest region in the AF is the posterior one and thickest is the lateral one, demonstrated that the AF is not only inhomogeneous in terms of response to loading, but also in what concerns to its structure. Furthermore, they found that the largest number of incomplete lamellae is present in the posterolateral region of the AF, while the least amount occurred in the anterior AF. In the present study, the annular region was divided in four regions. Thus, the posterolateral region reported by Marchand & Ahmed (1990) is similar to the posterior region of this study, and so, the posterior specimens would contain the most incomplete layers together with the thinnest lamellae. According to this, the posterior regions would contain more lamellae than the anterior and lateral specimens since the lamellae were thinner in the posterior region. Consequently, a greater number of interlamellar interfaces are present in the posterior specimens, indicating that a greater amount of elastin fibres is presented in the posterior rather than the anterior and the lateral regions (Little, 2004). Thus, the highest values of elastic parameters in the posterior annulus could be linked to the higher concentration of elastin fibres, contributing to the highest value of the storage modulus and dynamic compressive modulus on the dynamic compressive tests.

Concerning to the limitations, these samples came from pigs, whose discs are a little different from human discs. However, porcine samples are widely used (Balkovec et al., 2013;

Hongo et al., 2008; Ryan et al., 2008; Yingling et al., 1997), being recognized as good biomechanical model for the study of IVD behaviour. Moreover, the test was performed in unconfined conditions, which could promote a reorganization of the microstructure of the RGM, leading to test conditions that are quite different from the physiological state. Nevertheless, as explained previously, the confined conditions are also an ideal condition of loading on the RGM, as in physiological state these fibres are not completely confined by the surrounding tissues. Thus, the unconfined compression tests are considered a valuable approach for the determination of the mechanical properties of the AF under compression, being widely used for the characterization of the IVD structures under compression (Cloyd et al., 2007; Little et al., 2010). Finally, the hydration state is not considered as the typical procedure for simulate the *in vivo* conditions. However, the adopted approach allowed controlling and standardizing the experimental procedure, leading to more accurate results. Notwithstanding the influence of these limitations on the biomechanical response of the AF under compression, it is clear that this study largely contributes to a better understand about the inhomogeneity and viscoelastic properties of the RGM.

## **6. Selection and Characterization of a New Encapsulated Hydrogel for Nucleus Pulposus Replacement**

*This chapter aims to complement the manufacturer information about an innovative nucleus pulposus implant. Firstly, the description of the parameters already determined by the implant 's manufacturer is presented. Then, complementary tests were performed for the determination of the more suitable characteristics for the preliminary implants; by means of several mechanical tests. Finally, relevant material and mechanical properties of final configuration of the implant are assessed. The outcomes of these tests are compared and discussed according with the literature.*

### **6.1. Introduction**

The Nucleus Pulposus (NP) is limited axially by the superior and inferior cartilaginous endplates and circumferentially by the Annulus Fibrosus (AF). During axial compressive loading, the NP distends radially, transferring the load to the AF. In addition, the osmoregulation processes also intervene in the variation of the NP volume as function of time. Thus, it is considered that the NP behaves physiologically in an environment that is neither completely confined nor totally unconfined (Cloyd et al., 2007). However, as referred in Chapter 2, the degenerative disc disease affects decisively the normal function of the NP. In order to solve this problem, NP replacement therapies have shown to be very promising, since they are thought to delay the degenerative disc disease, to reduce the pain and/or to restore the spinal mobility (Boyd and Carter, 2006; Cloyd et al., 2007; Di Martino et al., 2005; Huang et al., 2005; Klara and Ray, 2002). The main goal of any NP replacement solutions is to mimic the function of native NP. Nonetheless, the use of

these techniques is not so common than the TDR solutions, mainly because the NP replacements are generally implanted through annular incisions, which injures irreversibly this region.

The process of finding a replacement material mechanically similar to NP is a difficult task since it presents complex mechanical properties, with a biphasic (Iatridis et al., 1996; Johannessen and Elliott, 2005), poroelastic (Castro et al., 2013; Galbusera et al., 2011) and incompressible (Cloyd et al., 2007; Iatridis et al., 1996; LeRoux et al., 1999) behaviour. Moreover, actual NP replacement solutions could also induce an inflammatory response, which could for last, result on a degenerative disc disease process (Whatley & Wen, 2011). Consequently, it is absolutely vital the development of a therapy that restores the NP functional disc matrix with minimally invasive approach (Iatridis et al., 1998; Goins et al., 2005; Setton et al., 2006).

Hydrogels are widely used in biomedical applications, such as contact lenses (Stapleton et al., 2006), ocular surgery (Xi et al., 2014), suture coatings (Pedley et al., 1980), artificial internal organs (Colton, 1995), drug delivery systems (Ashley et al., 2013), scaffolds for tissue engineering (Strange and Oyen, 2012) or prostheses (Balkovec et al., 2013). A prominent case of the usage of hydrogel-based solution as a prosthetic is the NP replacement, with several patents already published (Bao and Higham, 2001; Vresilovic et al., 2012a, 2012b). In fact, a panoply of advantages are addressed by hydrogels as a biomedical solution: it retains the surrounding water, presenting a low frictional coefficient and biocompatibility (Bao and Higham, 1993; Bao and Yuan, 2002). An ideal hydrogel-based NP replacement solution should also include some other requisites such as the ability to be implanted with a minimal invasive procedure; to retain large amount of water, providing an adequate swelling pressure under physiological loadings and; to withstand the complex mechanical loading acting on NP (Chan and Gantenbein-Ritter, 2012). Thus, the mechanical characterization of hydrogel-based solution, as well as its swelling pressure and the capacity to retain water after loading are therefore critical for the selection of the proper option for NP replacement.

This work presents a mechanical study of a new hydrogel-based NP replacement solution, the “Ravioli”, developed by Nicast Lda<sup>x</sup>, in the scope of the NPmimetic project. The “Ravioli” is mainly composed by two materials: 1) A nano-polymer based gel, the HydroMed, with high water absorbing capacity and consequently, with swelling behaviour; 2) A nano-fibre based, biocompatible, biodegradable, synthetic scaffold with high osmotic capacity used in the exterior as a container for the hydrogel expansion, developed using electrospinning technology, the “Envelope” - Figure 6.1.

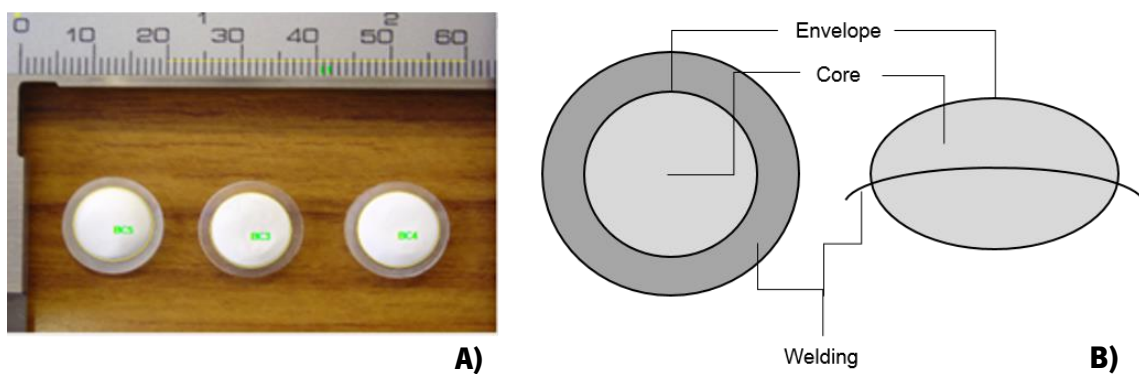


**Figure 6.1.** A) The swelled “Raviolis”; B) The schematic representation of the “Ravioli”: on the left, the upper view; on the right, the side view.

Discovered in the early 1900’s, electrospinning is a polymer processing technique that has been widely used. It allows the creation of nanofibres that can be collected to form a non-woven fabric (Nicast Ltd.). Basically, the “Ravioli” is made by a central core with swelling behavior, confined by two “Envelope”, that are welding to each other in an outside ring - Figure 6.1- in order to completely confine the HydroMed core.

The detailed chemical properties and fabrication process of each implant material are a matter of Nicast Ltd. responsibility, subjected to industrial confidentiality. Thus, none of this material characteristics and methods is addressed in this work. The preliminary tests performed in the scope of the NPmimetic project had revealed that the “Ravioli’s” core presents great cell viability and delivery (e.g. injectability, gel setting behaviour) properties. However, the filled

---

<sup>x</sup> Company responsible for the development of the NP implant, the “Ravioli”. More information on <http://www.nicast.com/>



“Ravioli’s” produced by Nicast Ltd. implants must be validated in terms of both material and mechanical behaviour, as the “Ravioli” should be able to withstand mechanical loading states experienced under physiological conditions (Joshi et al., 2006).

The assessment of the mechanical behaviour of the “Ravioli’s Envelope” is thus essential for the understanding of the behaviour of this structure during the swelling of the inner hydrogel. Moreover, the characterization of the mechanical behaviour of these implants should include confined and unconfined compressive tests. However, in the particular case of the “Ravioli”, a confined configuration could not be achieved. Due to the geometrical properties of these implants, i.e. the welding, the confined configuration was not assessed. Therefore, the mechanical tests only contemplate the unconfined configuration, through the placement of the structure inside a punch structure - Figure 6.2. Several material and mechanical tests were already performed by the Nicast Lda. More information is presented in Annex C.

Thus, the objective of this study is to complement the manufacturer information about the developed implant, helping to select the most suitable configuration among several options. Thus, this chapter includes: (1) the set of parameters already determined by the manufacturer; (2) the determination of most appropriate “Envelope” for the HydroMed core encapsulation; (3) once selected the “Envelope”, the obtainment of several material and mechanical properties of “Ravioli” and the comparison between these properties and the previous mechanical tests reported in the literature, and also with the performance of a native NP. During the phase of configuration selection, two kinds of “Raviolis”,  $Rav_1$  and  $Rav_2$ , with the “Envelopes”,  $Env_1$  and  $Env_2$  respectively - the  $Env_2$  presents twice of the  $Env_1$ ’s thickness - were submitted to mechanical testing.

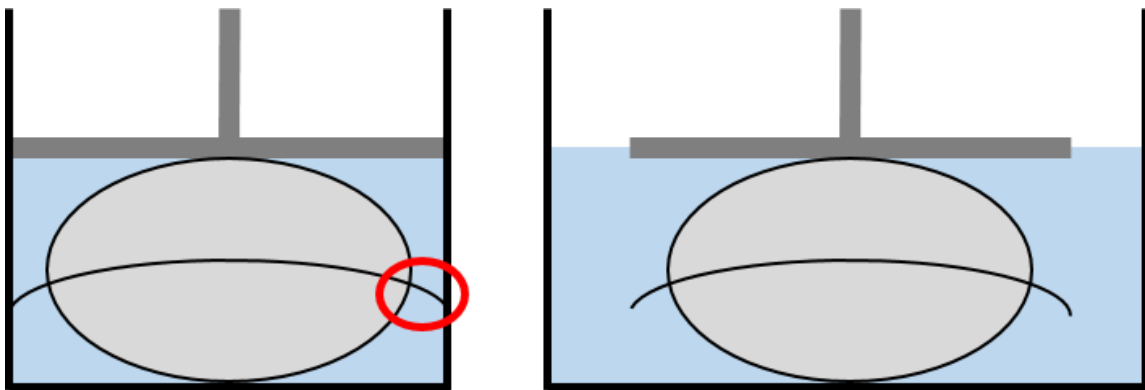


**Figure 6.2.** On the left side, due to the folding of the “Ravioli” ring (detail highlighted with a circle), the strictly confined compressive test configuration cannot be achieved; on the right, the unconfined compressive test configuration.

This work was then divided in three main topics: (1) the “Ravioli’s” characteristics, provided by the manufacturer; (2) selection of the implant’s configuration, based on mechanical features; (3) complementary tests for determination of additional properties of “Ravioli”, performed in the current study. In what concerns to the topics 2 and 3, an extensive series of tests were performed. In terms of configuration’s selection, the experimental procedure started with the quantification of core expansion: both implants were immersed in water and its volume and weight variation, in dry and wet (after immersing in water) conditions, were compared. The second step was to submit the different “Envelope” configurations to biaxial tensile tests, in order to define the most appropriate “Envelope’s” thickness. A biaxial test was performed to characterize the directional dependency of the material as well as to determine benchmark values. The quasi-static compression tests were also performed for both “Ravioli” configuration to assess the resistance of the “Envelope” as well as to check if there is any influence or critical point in the “Envelope’s” welding region on the “Ravioli” rupture.

Concerning to the topic 3, the assessment of the mechanical configuration of the “Raviolis”, it started with the determination of the “Envelope’s” tensile characteristics. The obtained values were compared with the ones reported by the manufacturer; moreover, cyclic compressive loading was applied to the implants in order to assess its ability to retain water and how the “Ravioli” behaves after the application of several loading cycles. Finally, the “Raviolis” were subjected to unconfined compressive test in order to determine the equilibrium toe-region and linear-region modulus. The obtained values were compared with several synthetic HA-based

hydrogels reported as presenting potential to replace NP as well as with the values documented for human NP samples. These tests bring an important input data for the software used for structural analysis and the determination of the stress distribution in the structure. It is hypothesized that the “Raviolis” produced by Nicast Lda. are mechanically suitable for replacing a damaged NP.

## A. Complementary Tests for the Selection of the Geometrical Characteristics of the Implant

The selection of the more suitable characteristics of an implant is essential for its performance. In this subsection, several configurations of the nucleus pulposus implant, the “Ravioli”, developed by Nicast®, were tested. These tests include the analysis of the free swelling of the HydroMed core, compressive tests on the “Ravioli” and biaxial tests of the “Envelope” that encloses the core. The discussion will be based on the selection of the geometrical configuration of the “Ravioli”, according with the most suitable characteristics to replace the nucleus pulposus.

### 6.2. Methods

The “Envelope” constrains the HydroMed core expansion, and limits the deformation of the gel, both in shape and in volume. One of the problems of the “Ravioli” design was thus the “Envelope’s” thickness. For the preliminary studies, the implants were produced in two different configurations –  $Rav_1$  and  $Rav_2$  - Table 6.A.1.

**Table 6.A.1.** Characteristics of the “pre-swelled Raviolis” used on preliminary tests.

---

	<b>Core A height [mg]</b>	<b>Inner Diameter [mm]</b>	<b>“Envelope’s” thickness [mm]</b>
<b><math>Rav_1</math></b>	9	10	0.1
<b><math>Rav_2</math></b>	9	10	0.2

---

Three kinds of tests were subsequently performed on both configurations: the “Ravioli’s” free-swelling analysis, the biaxial tensile tests and the axial quasi-static compressive tests.

### 6.2.1. Analysis of the “Ravioli’s” Free-Swelling

To understand the behavior of  $Rav_1$  and  $Rav_2$  when hydrated, the “Ravioli” was left in phosphate buffer saline solution (1X), under free-swelling conditions during 24 hours, to allow the complete osmotic equilibrium in the system. To evaluate the hydrogel swelling, the expansion of this structure was determined as the ratio between the final and the initial measurements of both volume and weight.

The volume measurements were performed using the software Image Pro Plus 4.6, where the measurements of “Raviolis” were made on both dried and hydrated conditions. An example of the analyzed images is visible in Figure 6.A.1. In terms of weight, the variation of expansion ratio was measured with a precision scale.

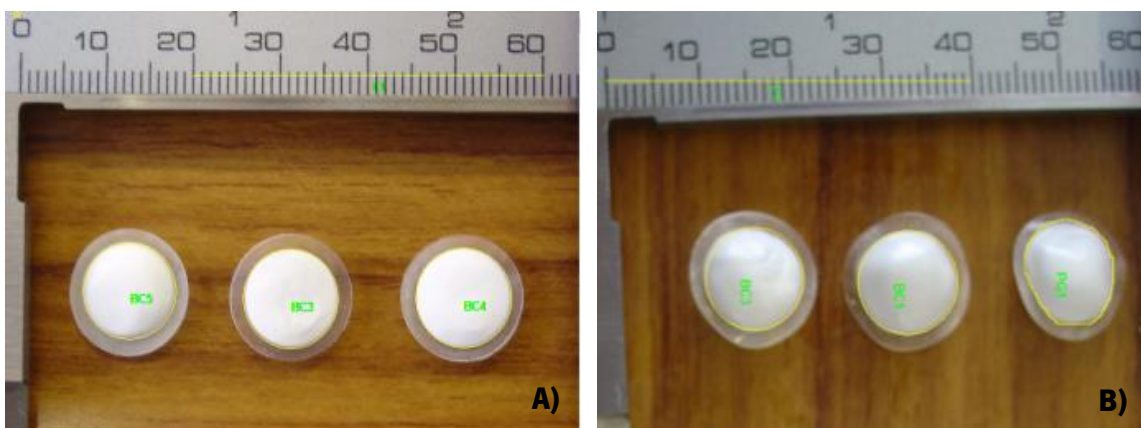


**Figure 6.A.1.** Images used for the determination of the volume variation of “Ravioli”. A) The “non-expanded” configuration, previous to fluid contact. B) The expanded configuration, after 24 hours of swelling.

### 6.2.2. Axial Quasi-Static Compressive Tests

Both “Ravioli’s” configurations were evaluated under non-confined conditions, by quasi-static axial compressive tests. For that purpose, a flat and non-porous plunger was attached to a Hounsfield Materials Tester (H5KS, Tinius Olsen Ltd, Surrey, UK, class of precision 1), fitted with a 10 N load cell (HBM®, Model 1-S2M/10N-1). The plunger was lowered to make contact with the platform on the basis. When 0.1 N load was visible on the load detection software (minimum load detected by the software), the reset was made. Thus, the contact point was marked as the point of zero-displacement. The plunger was then elevated to allow the placement of the

specimens on the platform. Finally, the initial height of the “Ravioli” was defined as the point of contact. The tests were divided in two configurations: the first one placing the compression plates in parallel with “Ravioli” ring (“parallel” tests) and the second one testing the implant with the its ring perpendicular to the compression plate (“perpendicular” tests) - Figure 6.A.2. The compressive test was performed until a deformation of 70% was reached, at a low displacement rate - 0.67 mm/s.

The “perpendicular” tests were performed in hydrated conditions while “parallel” tests were made at environmental conditions. This difference in the test configuration was required since it was experimentally impossible to keep the “vertical” position of “Ravioli” under water, since there is a re-adjust of the implant by sliding, leading to a return of the sample to the horizontal position. Thus, the absence of water prevented the slippage. Nevertheless, the water absence does not fully avoid the misalignment of the implant in relation to the ordinate axis, during the “parallel” tests. The special configuration of the “Ravioli”, with its ring is, in fact, an intricate limitation for the desirable execution of these tests. Consequently, it was considered an admissible misalignment of 10%, in relation to the ordinate axis.

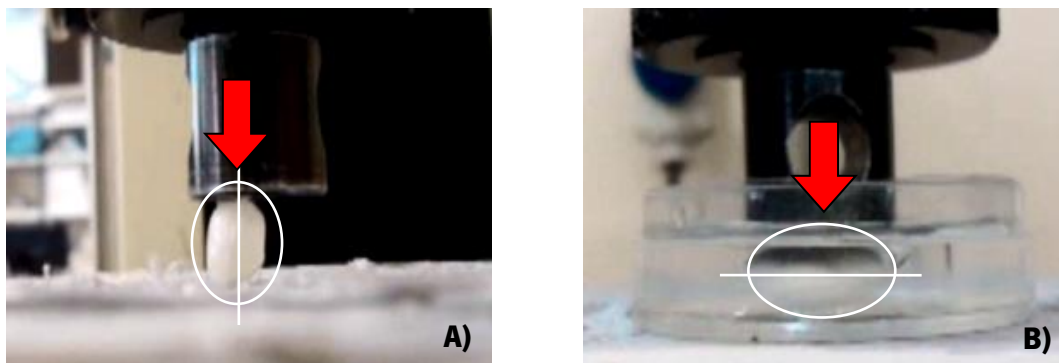


**Figure 6.A.2.** Direction of load for the two different load tests performed on the “Raviolis”: A) “Parallel” test; B) “Perpendicular” test.

### 6.2.3. Biaxial Tensile Tests

Biaxial tensile tests were performed in order to determine the load-displacement curve of both “Envelopes” ( $Env_1$  and  $Env_2$ ). The samples of “Envelope” were designed to present a cross format, compatible with the biaxial tensile tester. The biaxial tensile tester consisted on an Instron 4507, with specially designed automatic biaxial extensometers - Figure 6.A.3 - presenting a 50 N load cell with a 0.1 N resolution.

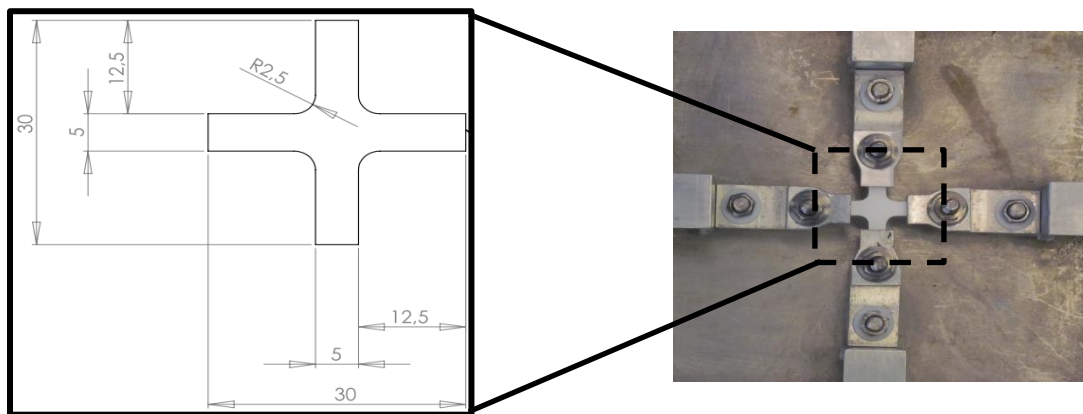


**Figure 6.A.3.** Schematic representation for “Envelope” geometry used on biaxial tensile testing, with a highlight of a generic “Envelope” sample placed on the testing machine.

The samples were attached using mechanical wedged grips with double-sided tape on the end zones to reinforce the samples gripping. Previous tests performed by Nicast Lda revealed no significant differences between wet and dry tests in the “Envelope”. The biaxial tensile test was carried out at a displacement rate of 1mm/min, until a maximum of 200% of the initial sample length.

The objective of the test was to apply a tensile loading to the sample in both axes simultaneously, thus creating a state of equibiaxial tensile state, which allows assessing the resistance of this material under “working” loads. Moreover, this test aims to study the symmetry of the mechanical response to loading, in order to understand the directional dependency of the “Envelope”. The force and displacement applied on the samples, in both axes, were registered and analyzed and the curves “engineering strain - engineering stress” were traced and compared.

### 6.3. Results

#### 6.3.1. “Ravioli’s” Free-Swelling Analysis

The quantification of “Ravioli’s” swelling is presented in Table 6.A.2. The results have revealed that the “Ravioli” presents a significant expansion in free swelling conditions. Concerning to the weight variation, the expansion ratio was reported to be between 4.80 and 6.42, which could be considered as the same magnitude to the value reported by the manufacturer for the “Ravioli’s” expansion, which is approximately 9 - Annex C. Moreover, it was showed that weight of the the  $Rav_1$  expansion ratio is higher than  $Rav_2$ , presuming that the  $Rav_1$  absorbs more water than  $Rav_2$ . Both “Ravioli” presented the same volumetric expansion, which is approximately 3, when placed in a hydrated environment. For this reason, the volumetric expansion was assumed to be the same for the two types of “Ravioli”.

**Table 6.A.2.** The expansion ratio (ratio between swelled and non-swelled configuration) in terms of both volume and weight, for “Raviolis” with two different “Envelope” thickness (n=3).

---

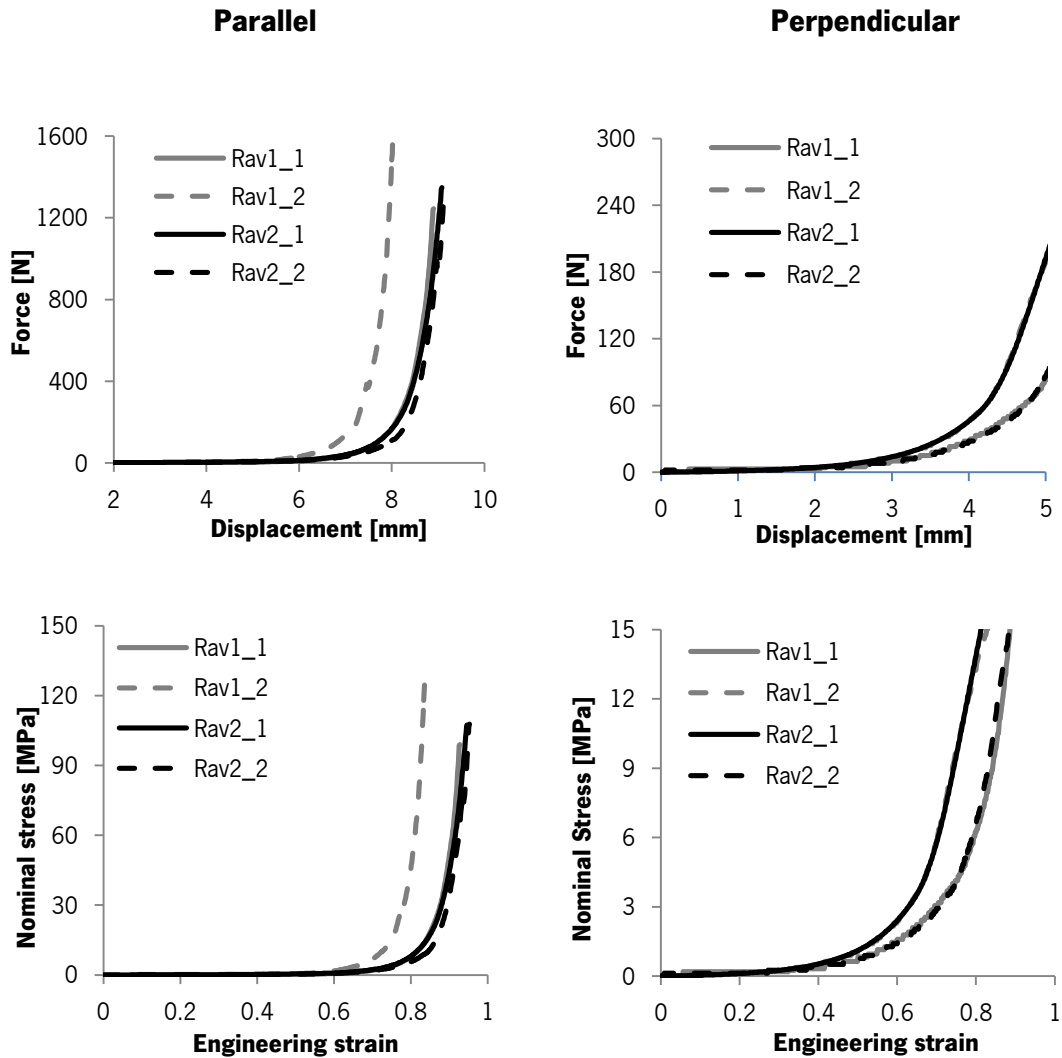
Ratio	Volume	Weight
$Rav_1$	$2.98 \pm 0.42$	$6.42 \pm 0.16$
$Rav_2$	$2.98 \pm 0.22$	$4.80 \pm 0.03$

---

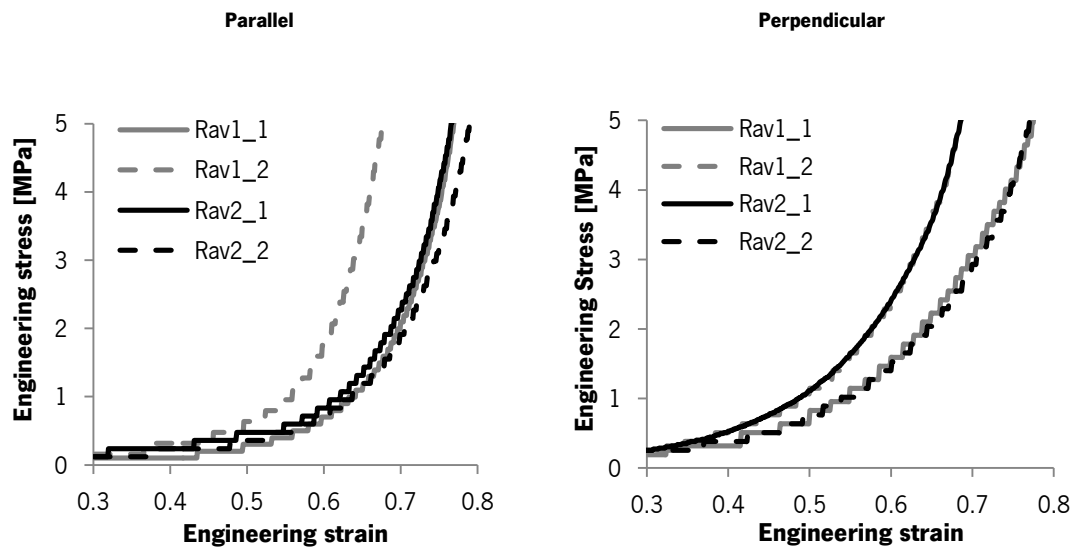


### 6.3.2. Quasi-Static Axial Compressive Tests

Concerning to the simple compression tests, the results are presented in Figure 6.A.4.



A) Load-displacement and stress strain curves for the tested samples.



B) Curves truncated at 5 MPa (biomechanical range)

**Figure 6.A.4.** Compressive stress-strain curve for four implants (two Rav<sub>1</sub> and two Rav<sub>2</sub>) tested on the parallel and perpendicular configuration. The engineering stress was obtained by dividing the force applied by the initial contact area of “Ravioli”. The engineering strain was given by  $(l-L)/L$ , where L is the initial length and l is the final length of the sample. During this test, the displacement speed was set to 4 mm/min.

During parallel tests, three of four samples bursted under vertical compression at different rupture points, occurring at higher strains; these strains corresponds to a range of non-working values of the “Ravioli”, i.e, to deformation magnitudes that are not applied in physiological conditions. No rupture was observed for the range of physiological values. Furthermore, the rupture point was, in all the cases, detected on the plane normal to the ring zone - Figure 6.A.5.



**Figure 6.A.5.** The rupture zone in the “Ravioli”, corresponding to the “normal plane” of the ring region.

### 6.3.3. Biaxial Tensile Tests

The curves of nominal stress (i.e. the loads calculated using the initial area of the sample) as function of the engineering strain for the biaxial tensile tests in the two “Ravioli” samples ( $Rav_1$  and  $Rav_2$ ) are presented in Figure 6.A.6.

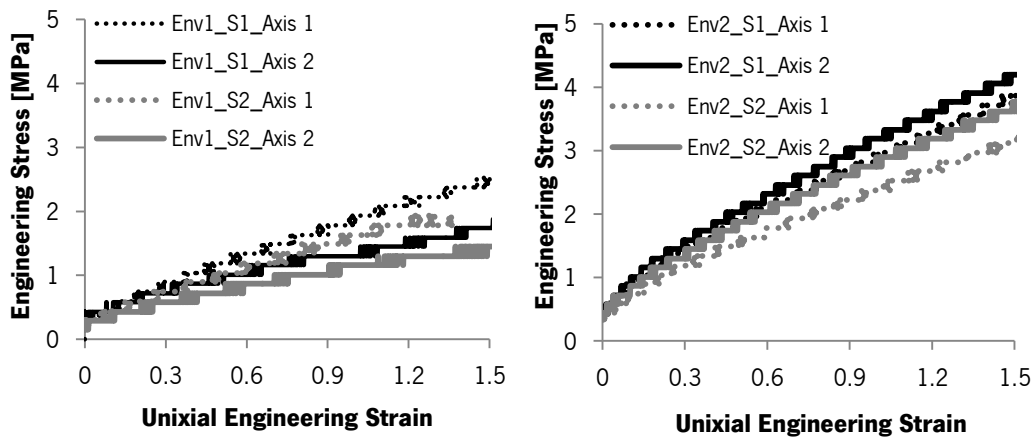


**Figure 6.A.6.** Graphical representation of the results from biaxial tests for each “Envelope” sample ( $Env_1$  and  $Env_2$ ). The “Envelope” behaviour was described in two axes of tensile strength: axis 1 and axis 2. The nominal stress was obtained by dividing the force applied by the initial contact area of “Ravioli”. The engineering strain was given by  $(l-L)/L$ , where  $L$  is the initial length and  $l$  is the final length of the sample. During this test, the speed the displacement was set to 5 mm/min.

These results indicate that for an engineering strain of 1.5, there was no rupture in the “Envelope” samples. However, the stress applied to impose a 1.5 of strain in the  $Env_2$  was approximately two times higher than the one applied on  $Env_1$ .

#### **6.4. Discussion on the Experimental Results for the Selection of the Geometrical Characteristics of the “Ravioli”**

In terms of weight, the  $Rav_1$  expansion ratio is higher than  $Rav_2$ , presuming that the  $Rav_1$  absorbs more water than  $Rav_2$ . The differences registered in weight could be explained by two events: first, a simple drop of water which would induce variations on “Ravioli” weight; second, the osmotic potential of the  $Rav_1$  is likely higher than for  $Rav_2$  due probably to the presence of a thinner “Envelope”.

The reports of the manufacturer have revealed a free swelling of 900% for the “Ravioli” - Annex C. The present work determined a maximum of 642% of weight expansion (in case for the  $Rav_1$ ), when the implant was placed in a hydrated environment. Thus facts support the idea that the “Ravioli” presents different swelling ratio depending on the amounts of hydrogel in its core, as well as the type of the “Envelope” adopted. In addition, it was also obtained a volumetric expansion of 300% for both “Ravioli” configurations, indicating that volumetrically there is no effect of the “Envelope” on the hydrogel swelling. The volumetric expansion is thus independent on the “Envelope’s” thickness. These results indicate that “Envelope” is dependent on the amount of expansion required: if the goal is a higher swelling  $Env_1$  should be selected, while for more efficiency on the “Ravioli” expansion constraint the  $Env_2$  should be adopted. In fact, the “Envelope” is absolutely vital for the structure of the implant since it constrains the HydroMed expansion, limiting the deformation of the gel, both in shape and in volume.

The quasi-static axial compressive tests on the “Ravioli” revealed the presence of a toe region, typical of the biological tissues. The toe region corresponds to a zone where a minimum load corresponds to a significant deformation on the sample; moreover, it does not represent a property of the material: it is normally an artefact probably caused by the take-up of slack or seating of the specimen<sup>xi</sup>. In the specific case, the toe region is likely caused by the specimen seating. However, it was not perceptible the typical linear region of a compressive test. The tests also indicate that both “Envelope” are able to withstand with a 5 MPa static stress, which is

---

<sup>xi</sup> More information on: <http://www.astm.org/Standards/D882.htm>

highly superior to normal stress acting on intervertebral disc during a moderate effort - as example, the lifting of a 20-kg weight with round flexed back is 2.3 MPa (Wilke et al., 1999). Thus, both implants are able to support the physiological compressive loads.

During parallel tests, three of four samples bursted at non-physiological loads under vertical compression in different rupture points. These points were not easily detected, even using typical approaches: first, no noticeable change was detected in the stress-strain curves; second, the camera record was not able to acquire the rupture point since it is an undistinguishable event due to the absence of contrast colour between hydrogel and “Envelope”. Furthermore, the rupture point was, in all cases, detected in the normal plane to ring zone - Figure 6.A.5 - demonstrating that the ring region is not the critical zone in terms of rupture. Interestingly, no rupture was observed for the range of “working” or “physiological” loads. These data corroborate the report for parallel tests, since this stress is much higher than the maximum stress acting on human disc during daily events.

Concerning to the results of the biaxial tests, no significant differences were found between each axis for both  $Env_1$  and  $Env_2$ , indicating that both “Envelopes” present an isotropic behaviour, i.e., the reaction of the “Envelope” to loading is uniform in all orientations. According to the scope they were designed, this homogeneous response to loading is an important characteristic since the “Envelope” must restrain the HydroMed core omnidirectionally, avoiding its protrusion. Furthermore, it was found that for an engineering strain of 1.5, there was no rupture in “Envelope” samples. However, the stress applied to impose a strain of 1.5 on “Envelope”  $Env_2$  was approximately two times higher than applied in the  $Env_1$ . This fact showed that the “Envelope”  $Env_2$  is able to withstand higher loads without breaking than the thinner sample. This statement reinforces the idea that if the requirements are to constrain, under physiological loads, the inner pressure imposed by the HydroMed core expansion, the 0.2 mm-thickness “Envelope” is the most appropriate choice.

## **B. Assessment of the Mechanical and Material Parameters of the Final “Ravioli” Configuration**

After the selection of the adequate “Envelope” to confine the HydroMed core, the determination of the material and mechanical properties of the “Raviolis” is essential to predict how the implant behaves when inserted in the NP cavity. Moreover, it will provide a comprehensive overview of the parameters needed to analyze computationally the geometrical characteristics and the mechanical properties of the “Raviolis”.

To complement the manufacturer information, this work contains several mechanical and material tests, relevant for the implant characterization. The experimental procedure included the response of the “Raviolis” to static compressive tests, compressive load relaxation test, the evaluation of the mechanical response and the percentage of water retained after cyclic compressive tests.

### **6.5. Methods**

#### **6.5.1. Uniaxial Tensile Testing**

The characterization of the “Envelope’s” behaviour under tensile loading is crucial since the “Ravioli’s” swelling is highly dependent on how this structure reacts to the application of this kind of loading. Therefore, uniaxial tensile tests were performed to characterize the “Envelope” that would wrap the hydrogel, produced to substitute the NP.

The configuration was selected in order to analyze and to evaluate the properties of the “Envelopes” under uniaxial tensile testing. For testing, the same height x length relation was

selected, as reported by the manufacturer's (Nicast Ltd.) – Figure 6.B.1. The dimensions of these “Envelopes” are 10 mm x 5 mm x 0.2 mm.

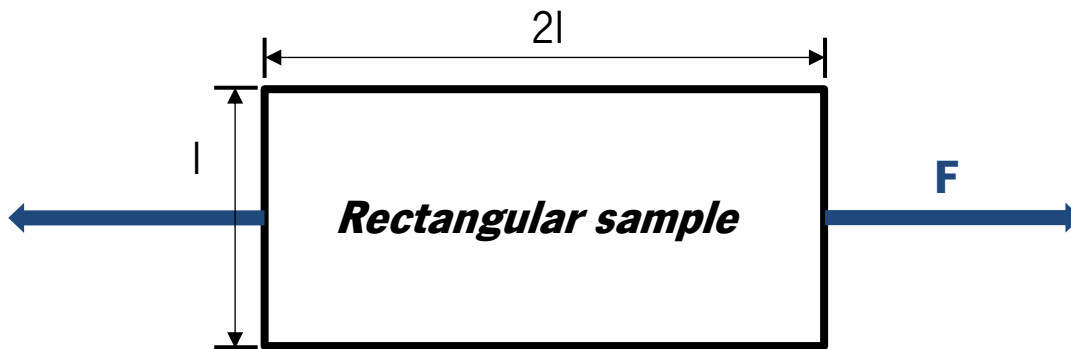


**Figure 6.B.1.** Uniaxial tensile test where the  $l$  is the length of the smaller side and the red arrow represents the direction of the “Envelope’s” stretch.

The gripping process must properly fit the specimens (or vice versa), and they must have sufficient force capacity so that they are not damaged during testing. Each sample was placed in a Hounsfield Materials Tester (H5KS, Tinius Olsen Ltd, Surrey, UK, class of precision 1), using pneumatic tensile testing grips and equipped with 500 N load cell, provided by the tester machine’s manufacturer. The uniaxial tensile test was carried out at a displacement rate of 1mm/min, until a maximum of 200% of the initial “Envelope” length. The goal was to assess the resistance of this material within the physiological conditions, as under these conditions the “Envelope” will not suffer a tensile strain of more than four times of its original length. The force and displacement applied on each sample were registered and analyzed to trace and compare the load-displacement curves. Finally, the stress-strain curves were compared with those reported by the manufacturer.

### **6.5.2. Cyclic Compression Tests and Percentage of Water Retention**

The quantification of water retention after loading is essential to understand how the “Ravioli” behaves under physiological loading. To determine this property, four implants were left in distilled water. The manufacturer tests showed that the complete swelling of the “Raviolis” was reached after four hours. Here, the implants were left in distilled water bath overnight, in order to swell freely. Then, the “Raviolis” were weighted just before the mechanical test

accomplishment. For the cyclic compressive test, a flat and non-porous plunger was attached to Hounsfield Materials Tester (H5KS, Tinius Olsen Ltd, Surrey, UK, class of precision 1), with an integrated 10 N load cell (HBM®, Model 1-S2M/10N-1). The plunger was lowered to make contact with the platform base to zero the instrument displacement. The specimens were then placed on the platform. The mechanical test consisted on five cycles of compression, with cycles of 2 mm displacement and a displacement rate of 25 mm/min - Figure 6.B.2.

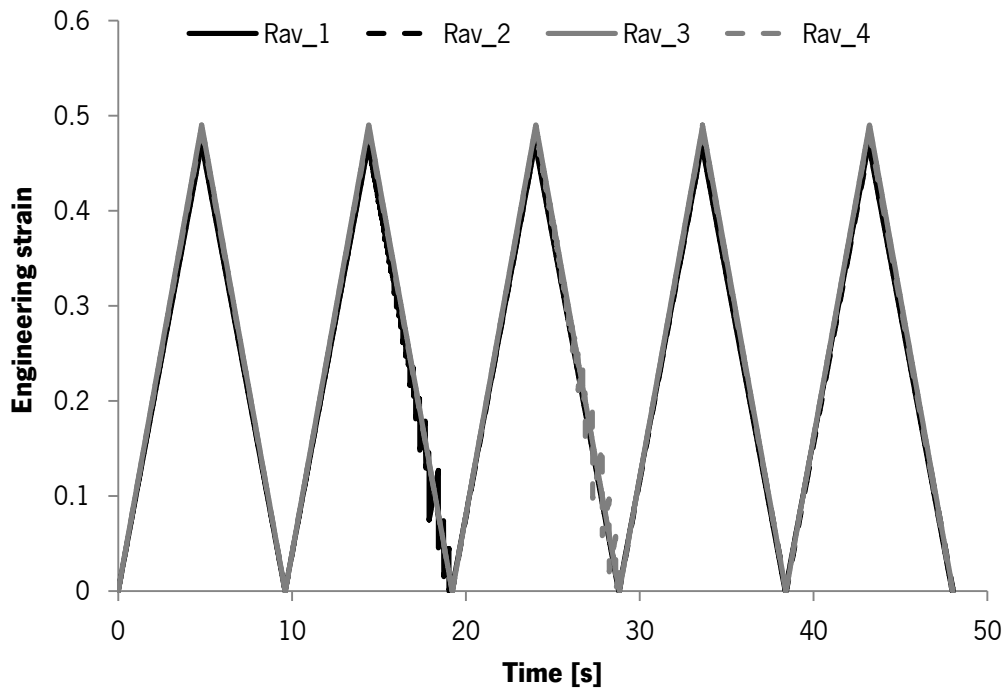


**Figure 6.B.2.** Cyclic test performed on “Raviolis” (n=4). The curve represents the strain as function of time (in seconds). The positive signal of the engineering strain indicates the direction of load in axial compression.

Then, the engineering strain was determined using Equation 6.B.1.

$$e = \frac{l-L}{L} \quad \text{Equation 6.B.1}$$

Where  $e$  represents the engineering strain,  $L$  is the original “Ravioli” height and  $l$  represents the final height of the implant. Immediately after each test, the “Raviolis” were weighted again. The water retention was determined using Equation 6.B.2.



$$\%WC = \frac{W_f}{W_i} \times 100 \quad \text{Equation 6.B.2}$$

Where  $\%WC$  represents the percentage of water retained by the “Ravioli” after the mechanical test, while  $W_i$  and the  $W_f$  are the initial and the final weight of the “Ravioli”, i.e, the weight before and after the mechanical test, respectively.

### **6.5.3. Stress Relaxation Tests**

The stress relaxation test was made in order to understand if the “Ravioli” could keep an osmotic pressure after loading application. To assess this property, this structure was submitted to several increments of strain. Between each increment, the samples relaxed during five minutes, which is considered as sufficient to allow complete relaxation (<0.001 kPa/s of change in stress) (Cloyd et al., 2007).

#### **6.5.3.1. Mechanical Testing**

The test configuration was developed to directly determine relevant mechanical properties of the implants, such as the toe modulus, the linear modulus and the percent relaxation. For that, a custom-built clear acrylate cubic tank, with the 5 cm edge, was constructed. All samples were tested in an aqueous environment – the samples were immersed in distilled water during testing - Figure 6.B.3.

Then, an even and non-porous plunger was attached to the previously described Hounsfield Materials Tester, with 10 N load cell. The plunger was lowered to make contact with the platform base, in order to reset the instrument displacement. The specimens were placed on the platform for the relaxation tests.

The mechanical test protocol was already described by Cloyd et al. (2007). Briefly, a pre-load of 0.05 was applied during 10 min. The load was then removed and the samples were left under an unloading state to ensure the osmotic equilibrium during 5 min. Then, a stress-relaxation test was performed, consisting of 5% strain increments at a rate of 5%/s. Among each

increment interval, the samples relaxed during 5 min. This relaxation time is reported as enough to allow the complete relaxation of the implant, which analytically represents a change of <0.001 kPa/s in stress (Cloyd et al., 2007). The increments in strain were repeated to 25% strain and the load and displacement were recorded at 1 Hz.

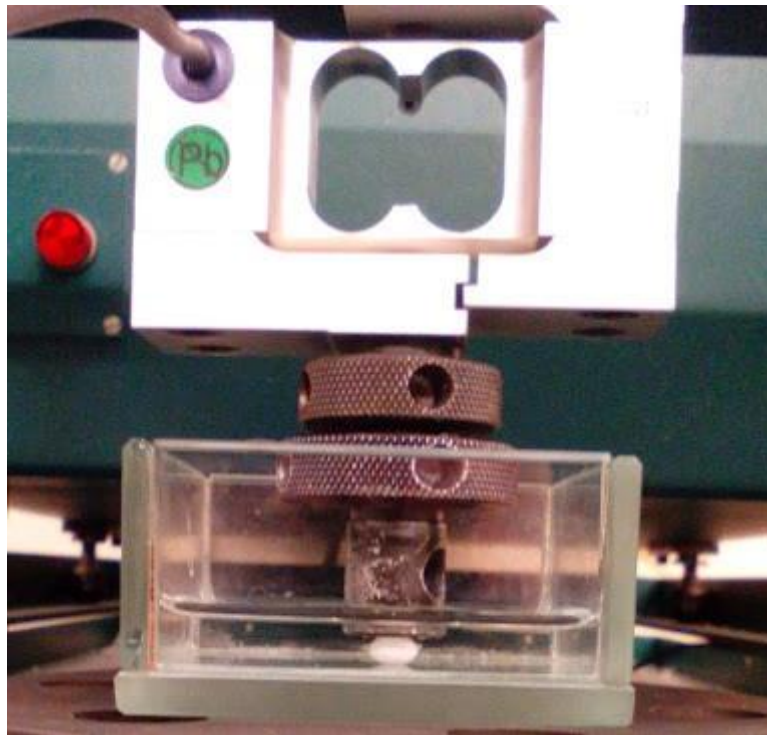


**Figure 6.B.3.** Implant tested in the acrylate cubic tank, in hydrated conditions.

### 6.5.3.2. Data Analysis

The stress-relaxation was fit to Equation 6.B.3, using Graph Quad 6.0.

$$\sigma_t = A(e^{\beta\varepsilon-1}) \quad \text{Equation 6.B.3}$$

Where  $\sigma_t$  represents the true stress, while  $\varepsilon$  represents the strain; moreover, the  $A$  and  $\beta$  represents constants related to the material properties. In addition, the toe modulus was defined as the slope of the relaxation curve at 0% strain, while the slope of the stress-strain curve at 20% strain was defined as the linear-region modulus. Finally, the percentage of relaxation was calculated with Equation 6.B.4:

$$\%R = \frac{\sigma_e}{\sigma_p} \times 100$$

**Equation 6.B.4**

where  $\sigma_e$  is the equilibrated stress and  $\sigma_p$  is the peak stress. The contact area of these implants is difficult to define due to the change of configuration during the compressive test. Thus, according to the reported manufacturer parameters, the “Ravioli” was defined by the manufacturer as incompressible material, so the Poisson’s Ratio was defined as 0.45.

The contact area was estimated using a Finite Element model (FEM), developed by for the swelling of the “Ravioli”. The software developed by the CT2M researchers<sup>xii</sup> was used to compute the desired parameters: volume, contact area (with the punch) and internal pressure evolution according to the Ravioli’s height, applying uniform incremental internal pressure steps to mimic the internal osmotic pressure.

In short, this FEM model described the “Envelope’s” as presenting non-linear and isotropic behaviors. The 3D geometrical modelling of the motion segment and the implant begins with the generation of a voxel-based model, obtained with a previously developed hexahedral FEM mesh of a motion segment and another for the prosthetic element, were used. The motion segment mesh - Figure 6.B.4 - was composed by five different structures: cortical bone, cancellous bone, annulus fibrosus, nucleus pulposus and cartilaginous endplate. The swelled “Ravioli” mesh - Figure 6.B.4 was only composed by the “Envelope”, while the core was left empty. A Fortran® code was applied to virtually generate the segmented 2D medical images and to reconstruct the 3D voxel-based geometric model. The detailed “Voxel searching” algorithm and the process of mesh generation of each implant are a matter of Nicast Ltd. responsibility, subjected to industrial confidentiality. Thus, none of these characteristics are addressed in this work.

---

<sup>xii</sup> More informations about the software in the Final Report of the NP Mimetic project.

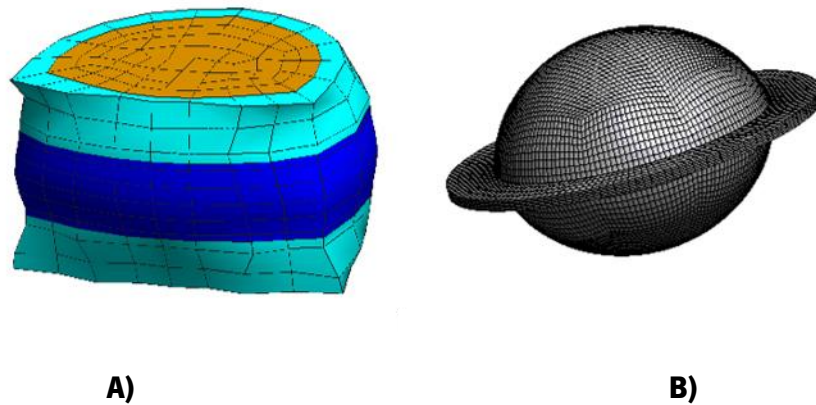


**Figure 6.B.4.** A) Motion segment mesh; B) Swelled implant mesh. Note: Images not scaled.

From the numerical model of “Ravioli”, the contact area was extrapolated using a linear regression ( $R^2=0.99$ ) to fit the data of the area for several compressive displacements imposed to a swelled 9 mm diameter “Ravioli” (Figure 6.B.5).

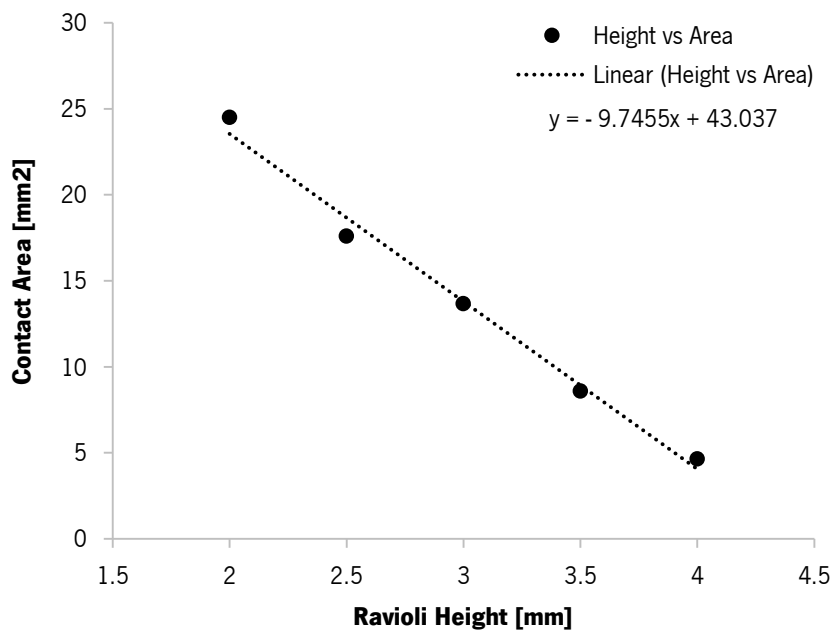


**Figure 6.B.5.** Linear regression of the contact area ( $R^2=0.99$ ) as function of the “Ravioli’s” height for a 9 mm diameter implant. This data was determined by a FEM model of “Ravioli”, produced by the CT2M researchers.

## 6.6. Results

### 6.6.1. Uniaxial Tensile Testing of the “Envelope”

The curves of the uniaxial test for both manufacturer (Nicast Ltd.) and this work (CT2M<sup>xiii</sup>) are described in Figure 6.B.6. The curves indicated a similar behaviour for the samples analyzed, for both sample dimensions - [40x20 mm] and [10x5 mm].

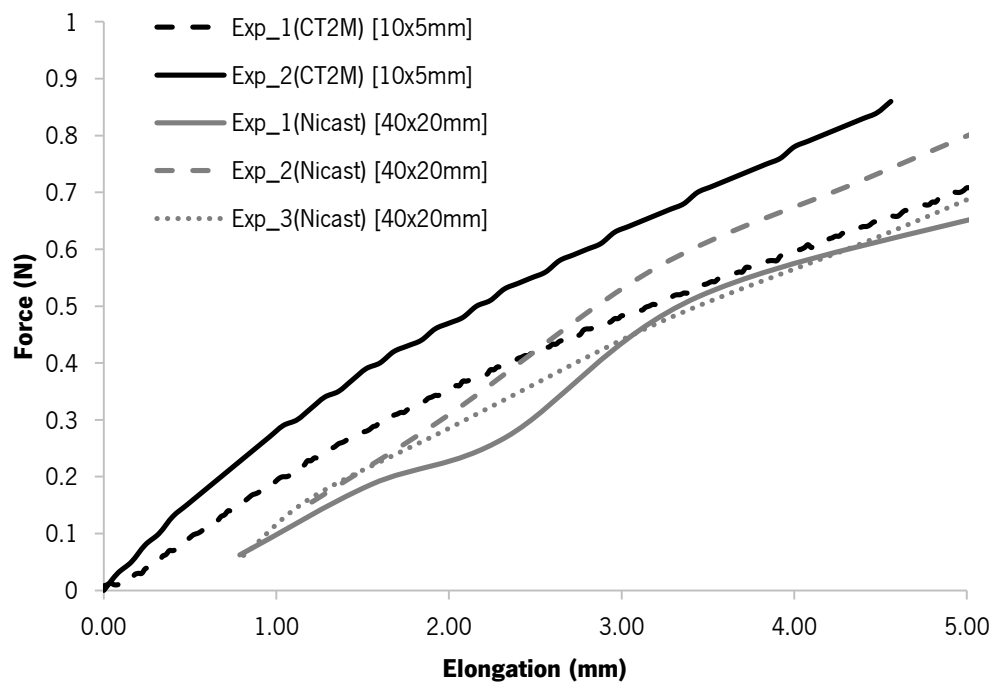


**Figure 6.B.6.** Curves of force (N) as function of the sample elongation (in mm) for both manufacturer (Nicast) and this work (CT2M), truncated at 5 mm elongation.

The results indicated no significant differences between the static stiffness coefficient ( $K_s$ ) of the tensile tests for both Nicast Ltd. and CT2M - Table 6.B.1.

<sup>xiii</sup> CT2M - Mechanical and Materials Technologies Centre – Department of Mechanical Engineering – University of Minho

**Table 6.B.1.** The static stiffness coefficient,  $K_s$  (in N/mm), obtained for the Env<sub>2</sub> by both Nicast Ltd. and CT2M.

$K_s$ (N/mm)	Nicast Ltd.	CT2M
<b>“Envelope”</b>	159.45 ± 22.35	149.03 ± 3.25

In order to eliminate the dependency of the specimen dimensions that occurs in a tensile force - elongation graph, this curve was converted into engineering stress and engineering strain - Figure 6.B.7.

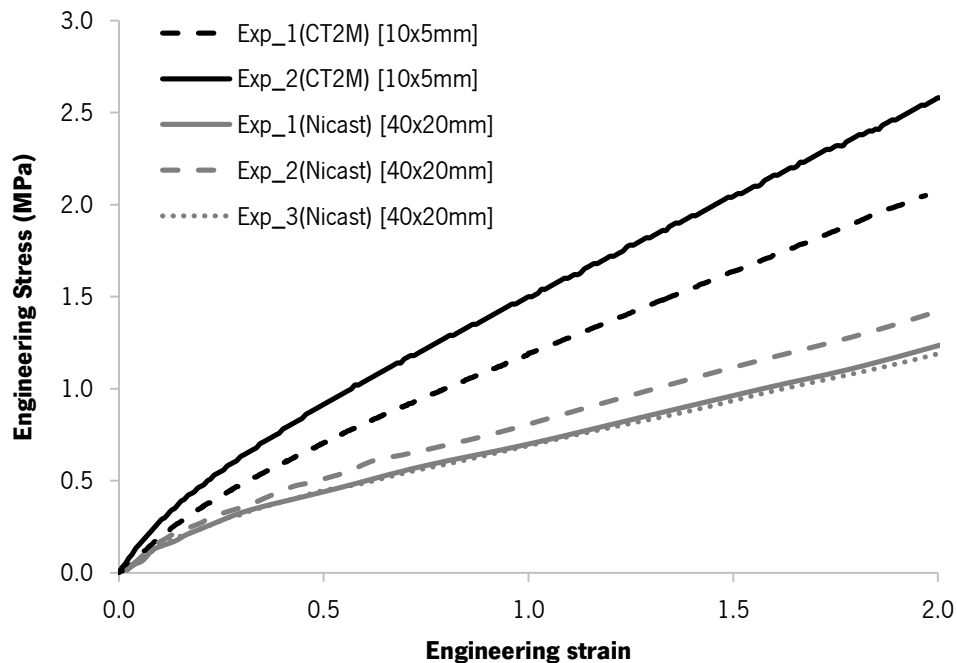


**Figure 6.B.7.** Curves of the nominal stress of the “Envelopes”, in MPa, as function of the engineering strain, for both manufacturer (Nicast) and CT2M work.

The elastic modulus or Young modulus ( $E$ , in MPa), in static conditions, was calculated as the slope of the Hookean region of the curves of engineering stress vs strain (from 0.5 to 2.0 of engineering strain;  $R^2 > 0.97$ ). The results revealed that the compressive modulus is significantly higher in the CT2M report - Table 6.B.2.

**Table 6.B.2.** Young modulus of the “Envelopes”, ( $E$ , in MPa) obtained by the Nicast Ltd. and CT2M for the Env<sub>2</sub>, in static conditions.

$E$ (MPa)	Nicast	CT2M	Mean $\pm$ S.D.
Envelope	0.54 $\pm$ 0.04	1.00 $\pm$ 0.09	0.73 $\pm$ 0.20

### 6.6.2. Cyclic Compression Tests and Percentage of Water Retention

The five cycles of loading-unloading revealed that all “Raviolis” reached the same load peaks when the samples are submitted to the maximum load (Figure 6.B.8, n=4). The value of the maximum peak oscillated between 2 N for the sample 3 and 3.5 N on the samples 1 and 4, respectively.

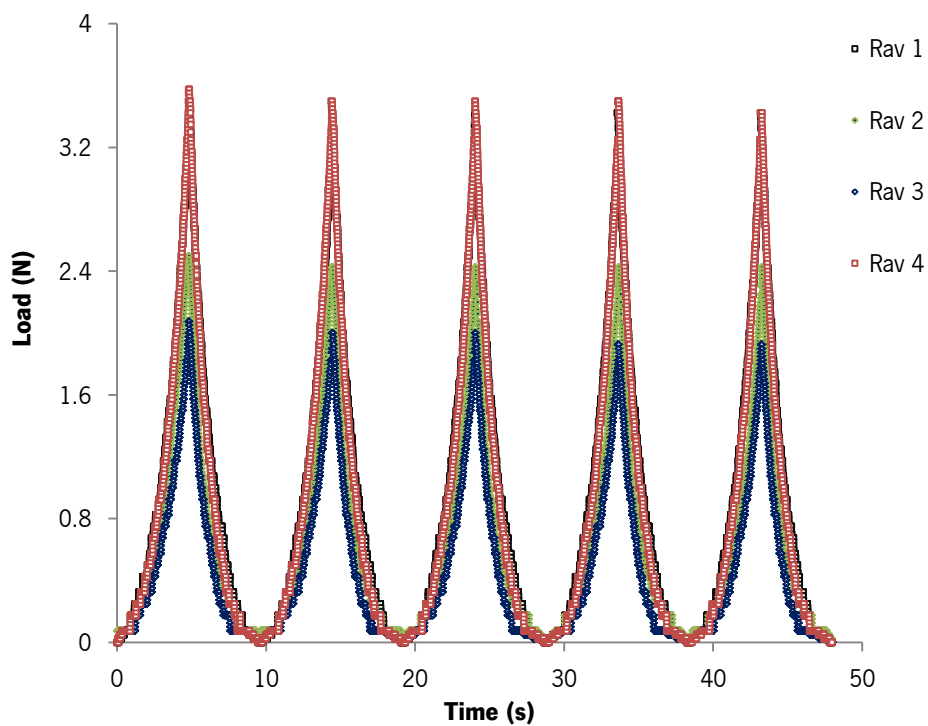


**Figure 6.B.8.** Load vs time curve of the five loading-unloading cycles for the four “Raviolis” used on the study.

The results of water retention showed no significant differences between “Raviolis”. The mean percentage of water retention is  $97.80 \pm 2.07$  (Table 6.B.3, n=4).

**Table 6.B.3.** Percentage of water retention (%WC) for all the samples tested, including the mean and the standard deviation (mean  $\pm$  S.D.)

“Ravioli” number	%WC
1	98.43
2	94.40
3	98.36
4	100
Mean $\pm$ S.D.	97.80 $\pm$ 2.07

### 6.6.3. Stress Relaxation Tests

The mathematical model presents a good fit for the experimental curve of the equilibrium stress-strain (Figure 6.B.9,  $R^2 > 0.93$ ,  $n=4$ ).

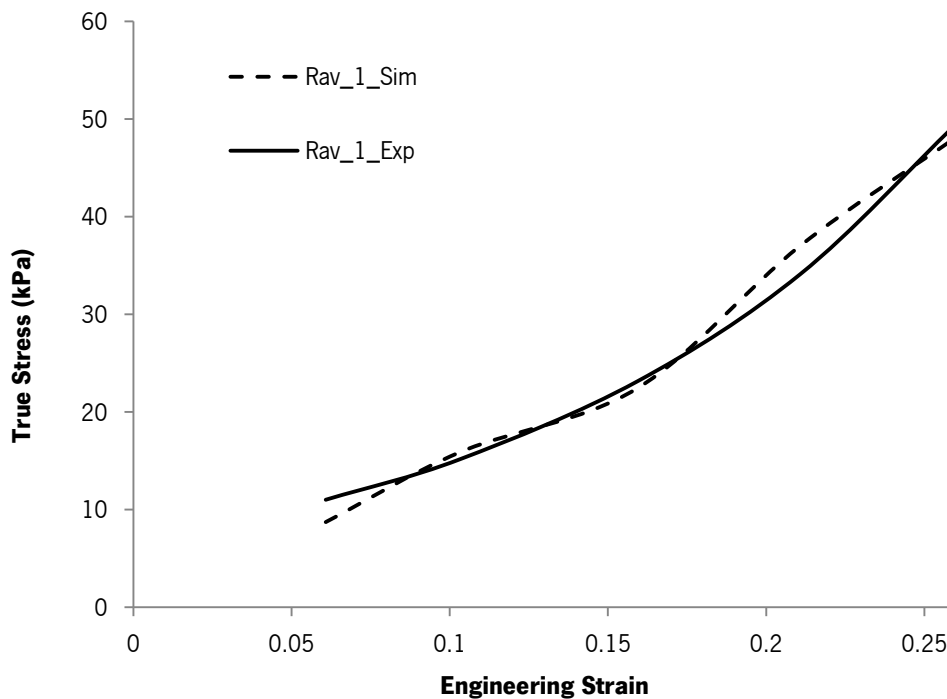


**Figure 6.B.9.** A generic example of the experimental curve of the true stress as function of the engineering strain (Rav\_1\_Exp) and the model adjust (Rav\_1\_Sim), with  $R^2 = 0.98$ .



The optimum set of constants  $A$  and  $\beta$  for the exponential function are  $22.63 \pm 6.72$  and  $7.00 \pm 0.79$ , respectively. Concerning to the parameters of the equilibrium stress-strain, the results are presented in Table 6.B.4.

The stress relaxation tests on “Raviolis” revealed a toe-modulus of  $8.32 \pm 2.21$  kPa, which is significantly higher than the reported for human NP and Hydrogel A ( $3.25 \pm 1.56$  kPa and  $2.82 \pm 1.19$ , respectively). However, no significant differences were found between the Hydrogels B and C and the “Ravioli”. Concerning to the linear-region modulus at 20% strain, the “Ravioli” presents a value of  $31.23 \pm 3.82$  kPa, which is significantly higher than the previous reported values. In terms of the percent relaxation, the “Raviolis” relaxed less than other HA-based solutions found in the literature (Table 6.B.4). However, no significant differences were found between the percent relaxation of the “Ravioli” and the NP ( $74.4 \pm 2.05\%$  for the “Ravioli” and  $65.77 \pm 11.30\%$  for the human NP).

**Table 6.B.4.** Mean and (standard deviation) for the unconfined compression equilibrium properties of the NP and several HA-based hydrogels solutions (Cloyd et al., 2007) as well as for the “Ravioli” (this study).

<b>Material</b>	<b>References</b>	<b>Toe modulus (kPa)</b>	<b>Linear modulus (kPa)</b>	<b>Relaxation (%)</b>
Human NP		3.25 (1.56)	5.39 (2.56)	65.77 (11.30)
Hydrogel A	Cloyd et al.	2.82 (1.19)	6.97 (2.10)	19.86 (6.38)
Hydrogel B	(2007)	7.91 (4.21)	21.90 (4.82)	13.89 (4.71)
Hydrogel C		8.37 (1.61)	14.47 (0.63)	30.67 (5.90)
Ravioli	This study	8.32 (2.21)	31.23 (3.82)	74.4 (2.05)

## **6.7. Discussion of the Mechanical and Material Parameters of the Final “Ravioli” Configuration**

Due to similarities in terms of composition, hydrogels have been considered as a suitable solution to replace a damaged NP (Strange and Oyen, 2012). These hydrogels should present a mechanical behaviour similar to the NP, in order to mimic its role on the intervertebral disc structure. Thus, a detailed description of the implants is critical to evaluate its potential to be an effective NP replacement solution, as well as to develop accurate finite element models of the hydrogels (Cloyd et al., 2007). In this investigation, the mechanical and material behaviour of the implants were assessed by the application of several tests, such as uniaxial tensile testing, cyclic compressive tests and stress relaxation tests.

The tensile tests are applied for several reasons namely in the selection of materials for engineering applications, in the determination of the benchmark tensile properties used in the material specifications and in the comparison between the mechanical response of new materials with pre-existent ones (Davis, 2004). In this work, the results of the uniaxial tensile tests were used to determine the tensile properties of the “Envelope” and to compare the values with the previous ones, reported by the manufacturer. The “Envelope” is subjected to tensile loads once placed into the intervertebral disc, which justifies the need of “Envelope” characterization using this kind of tests.

The uniaxial tensile experiments revealed no significant differences between  $K_s$  for both “Envelope” tests (manufacturer and CT2M) - Table 6.B.1. The results of the uniaxial test for both Nicast Ltd and CT2M indicated that the samples of “Envelope” with a relation 2:1 between height and length – in case [40x20 mm] and [10x5 mm], respectively - did not differ in terms of static stiffness coefficient.

Concerning to the static compressive modulus, the mean value is  $0.73 \pm 0.20$  MPa ( $n=5$ ), which is a typical value for an elastomer. The elastomers are characterized for being long-chain polymers with a compressive modulus as low as 1 MPa and high elastic extension. These materials are normally considered as incompressible or isochoric, with typical Poisson’s ratio

values of 0.4 - 0.5. Thus, a longitudinal elongation is normally compensated by a lateral contraction due to its high molecular mobility (Ashby, 2010).

Interestingly, the magnitude of stresses applied without reaching the “Envelope” yield or ultimate strength point is higher than the magnitude considered as physiological, indicating that there is no rupture in the normal *in vivo* range of stresses acting on the “Envelope”. However, significant differences were found between the static compressive modulus of the implant, provided by the manufacturer and the CT2M studies - Table 6.B.2. This divergence could be related to possible differences in the load cell used for the mechanical tests: due to technical limitations, only the 500 N with 0.1 N resolution was available to the mechanical test in the CT2M, while no information was given about the load cell used in Nicast test. The range of test loading was 0-1 N, which are under the minimum value that 500 N load cell is able to measure within its specifications. Thus, a load cell with lower loading capacity was strongly recommendable for these kinds of tests. Nonetheless, the results revealed that the “Envelope” is indicated to constrain the HydroMed core in terms of mechanical compliance and resistance to rupture, for the physiological range of values.

Several studies focused on the determination of the water content (Vernengo et al., 2008) and the swelling ratio (Eyholzer et al., 2011; Reza and Nicoll, 2010; Strange and Oyen, 2012) of different NP replacement solutions. However, it is also desirable to determine the water retention of the hydrogel after load application. Therefore, cyclic compressive tests were performed to evaluate the ability of the implant to retain water. The results indicated that the average percentage of water retention is around  $97.80 \pm 2.07$  (Table 6.B.3, n=4). Moreover, it was visible that the “Raviolis” reached the same peaks of load when the samples are submitted to cyclic values of strain. These results indicate that there is a detrimental water loss in the hydrogel after the application of physiological loading. Furthermore, the implant maintains its initial properties after the loading-unloading cycles. According with this information, the “Ravioli” can be considered as isochoric, since there was no volume variation during load application.

From this substantiation, it is clear that the implant does not completely mimize the NP function of successive water loss-gain during loading-unloading cycles. However, since the

cartilaginous endplate is normally damaged in a degenerative disc disease process, the fluid flow in the disc is already compromised when an implant is needed. Contrarily, the ability of water retention avoids the collapse of the disc structure and several other problems, such as the impingement of the posterior facet joints and facet joint syndrome, by maintaining the normal disc height during loading events (Vuono-Hawkins et al., 1995). Moreover, the HydroMed core amount could be manipulated and controlled during the process of manufacturing in order to reach the same physiological NP height, helping to maintain the normal dimensions of the disc.

The characterization of the loading acting on the NP is extremely difficult since several factors such as fluid flowing (Wang et al., 2011), swelling pressure (Sivan et al., 2014) or the type of confinement (Joshi et al., 2006) interfere on the measurement of its properties. Physiologically, the NP is loaded in both confined and unconfined compression configurations. Thus, tests in both conditions are essential to characterize the NP function as well as the implants specially designed to replace it.

On this study, the stress relaxation of the “Ravioli” was tested using unconfined tests. In addition to the implant limitations, these unconfined tests were selected since they allow comparing the obtained data with the previously reported in the literature. Concerning to the test results, the exponential function used to fit the experimental results has revealed a good fit ( $R^2 > 0.93$ ,  $n=4$ ), for the optimum set of parameters. Thus, this model showed to be indicated to “translate” the stress relaxation of this implant.

Previous reports have pointed the Poisson’s ratio, together with the modulus, as the essential parameters for selection of an NP implant (Cloyd et al., 2007). When a healthy NP expands laterally, the AF is submitted to circumferential stress. In fact, one of the most challenging tasks in the NP replacement is to keep the interaction between NP and AF. This stress-state is maintained by high Poisson’s ratio or swelling pressure (Cloyd et al., 2007). In the present study, the Poisson’s ratio was considered to be 0.45, a typical value for an incompressible material. This assumption was taken since the “Ravioli” showed to be isochoric, since there was no water loss after the application of physiological cycle loading.

Previous reports suggested that an appropriate material for the NP replacement should present a higher or equal stiffness than the healthy NP structure (Bao and Yuan, 2002). An implant with low stiffness could originate an underconstrained motion segment, induce the hypermobility and increase the stresses on adjacent discs (Cloyd et al., 2007). In this study, the stress relaxation tests on “Ravioli” had revealed that both toe and linear modulus are significantly higher than the reported for human NP, indicating that the “Ravioli” is a suitable option for the NP replacement.

In terms of the percentage of relaxation, the “Raviolis” relaxed less than other HA-based solutions found in literature (Table 6.B.4). However, no significant differences were found between the percent relaxation of the “Ravioli” and the NP ( $74.4 \pm 2.05$  % for the “Ravioli” and  $65.77 \pm 11.30$  for the human NP). Once again, these values support the idea that “Ravioli” presents adequate properties for the replacement of the NP.

Some limitations must be addressed to this work. First, the calculation of the contact area for each load imposed on the sample was performed using an FEM model, specially designed for this implant. Thus, this approach presents some limitations itself, since it is a numerical approximation. Second, the low number of implants tested; due to scarcity of “Raviolis” for mechanical testing could be a limitation for the statistical analysis. Third, the mechanical characterization of an implant should include the study of its properties under confined compression tests. However, due to the geometrical properties of the “Raviolis”, i.e. the welding, the confined tests could not be performed.

## **7. Effect of the Implant Insertion in the Motion Segment: a Load Relaxation Study**

*This chapter presents a compressive load relaxation test of a motion segment with the implant inserted on nuclear cavity. The load relaxation curves were then analyzed and compared with the typical load relaxation of a normal motion segment, in order to assess the effect of the implant in the motion segment behavior.*

### **7.1. Introduction**

The mechanical behaviour of the intervertebral disc (IVD) is time dependent, essentially due to the viscoelasticity of its compounds (both nucleus pulposus (NP) and annulus fibrosus (AF) and the osmotic regulation during loading-unloading processes (Huber et al., 2007). However, chemical, biological and mechanical changes within the IVD could induce degeneration on this complex structure. The NP is known to be the starting point of the degenerative process in the IVD, which consists on a loss in its proteoglycan concentration (Hukins, 2000; Roughley, 2004; Urban, 2000): the collagen fibres in the NP become gradually more fibrotic, promoting the IDP decrease and, consequently, a change on the disc biomechanics (Haefeli et al., 2006; Johannessen and Elliott, 2005).

The relation between the IVD biomechanics and the physiological modifications in the NP has been the target of several studies, including the assessment of changes associated to aging and degeneration (Ferguson and Steffen, 2003; Iatridis et al., 1997b; Massey et al., 2012; Thompson et al., 1990) pressurization (Schechtman et al., 2006), partial or total nucleotomy (Brinckmann and Horst, 1985; Johannessen et al., 2006; Markolf and Morris, 1974; Shea et al., 1994). The effect of compressive loading on the IVD after NP removal was also tested, revealing that this event promotes an increment on the disc deformation, radial bulging, and,

consequently, on the shear stress between the AF lamellae (Brinckmann and Horst, 1985; Cannella et al., 2008; Meakin and Hukins, 2000). Interestingly, the quantification of the amount of NP removed is closely related to the changes in the IVD behaviour (Cannella et al., 2008; Shea et al., 1994), since the discectomy provokes a IVD height reduction that is proportional to the volume of nucleus removed (Brinckmann and Grootenboer, 1991). Thus, the discectomy, known to be the most common treatment of degenerative disc disease for relatively young patients (25–40 years), is responsible of important biomechanical changes and, hypothetically, of long-term injuries in the spine (Boyd and Carter, 2006; Mochida et al., 2001).

New therapies, including tissue engineered NP structures (Mizuno et al., 2004; Séguin et al., 2004) and hydrogel-based constructs (Chou et al., 2009; Cloyd et al., 2007; Reza and Nicoll, 2010), aim to efficiently restore the structural and mechanical function of a normal IVD. However, the mechanics of these new options for NP replacement were not widely investigated, since the properties of these materials are normally measured after its production (Chou et al., 2009; Cloyd et al., 2007; Eyholzer et al., 2011; Vernengo et al., 2008), in a non-physiological state.

Few studies have examined the functional changes due to NP replacement solutions insertion in the disc. Bertagnoli et al. (2005) have studied the mechanical properties of hydrogel implants with a reinforced mesh layer. The results revealed that the implant withstands the axial compressive loads as well as the compressive fatigue test; in addition, no extrusion was detected in bending failure tests. Balkovec et al. (2013) have injected a thermo-reactive hydrogel in the annular access to evaluate the flexion and extension on the IVD. The results had shown that this hydrogel was able to restore the original angular stiffness of a cyclically fatigued *ex vivo* motion segment. However, both hydrogels were implanted through an incision or needle puncture, which could affect the annular stability on the mechanical *ex vivo* tests.

The stiffness is the primary parameter to be determined when the requirement is to evaluate how a material resists to deformation in response to an applied force. In the particular case of the IVDs, the stiffness quantification is crucial since changes on this value are normally related to lack of disc hydration (Costi et al., 2002) or disc degeneration (Zirbel et al., 2013). The

load relaxation tests are widely applied on IVDs (Huber et al., 2007; Iatridis et al., 1998; Johannessen et al., 2004; Yao and Gu, 2006). In fact, these tests describe how the materials relieve stress under constant strain, being an important tool for the characterization of the mechanical response of disc to deformation.

Thus, the goals of this section are: (1) to propose a new method to insert and retain the hydrogel - in case the “Ravioli”, the biomimetic prosthetic nucleus developed by the NP mimetic - in the nuclear cavity, during mechanical testing. It is expected that this method allows not only the evaluation the mechanical properties of the artificial NP in the motion segment, under axial compressive loads without any annular damage, but also to seal the cartilaginous endplate fracture for the hydrogel entrance, avoiding a possible material extrusion; (2) to assess the mechanical response of the structure motion segment with the “Ravioli” within. For that, the stiffness of both the motion segments with “Ravioli” inside (RMS) and control tests (CMS), consisting on an intact motion segment, were compared. The results of a load relaxation test were fit in a two exponential decay function and the parameters of this curve plus the coefficient of stiffness of RMS and CMS were compared. It was hypothesized that no significant differences would be found between parameters of load relaxation curve as well as for the stiffness coefficient for RMS and CMS.



## **7.2. Methods**

### **7.2.1. Motion Segment Collection and Preparation.**

A porcine lumbar spine, from a young cadaver - with approximately eighteen months-old - was collected from an abattoir. The spinal column was divided into motion segments (MSs), parallel to the mid-transverse plane of the disc Fig. 7.1 – A). In addition, all specimens were visually inspected before and immediately after the mechanical test. Care was taken to remove the surrounded tissues during dissection. The segments were stored at 4°C before testing, which were performed within 24 hours after dissection, in accordance with a protocol approved by the Institutional Human Tissue Committee (Campbell-Kyureghyan et al., 2011).

The specimens were immersed in a phosphate buffer saline solution (PBS 1X) before, during and after the mechanical test, to prevent the dehydration. The degeneration grade was assessed by Thompson five-category grading scheme (Thompson et al., 1990), after testing. All discs presented a level I of the Thompson degeneration scale.

### **7.2.2. Method for Insertion of the Implant in the Nucleus Pulposus Cavity**

The normal cartilaginous endplate (CEP), which is present on the upper and lower ends of the each IVD, consists of a mixture of uncalcified and calcified cartilage layers, with approximately 1 mm of thickness (Bae et al., 2013; Roberts et al., 1989). The CEP is the structure of the interface between the IVD and the vertebral body (Bogduk, 2005), and its functions are to act as a mechanical barrier and as a gateway for nutrient transport between the blood supply of the vertebral bodies and the avascular IVD tissues (Bae et al., 2013; Moon et al., 2013). Alterations in CEP could affect the IVD physiology, promoting the degenerative disc disease (Bae et al., 2013; Bogduk, 2005). With age, the CEP becomes sclerotic and the nutrition canals start to be obstructed. Consequently, the CEP loses vascular contact, becoming less permeable (Accadbled et al., 2008; Grignon et al., 2000; Roberts et al., 1996), which contributes to disc degeneration by reducing the diffusion of nutrients to the cells of the NP (Raj, 2008).

According to this, the “via” degenerated CEP should be considered as an alternative to insert possible substitutes of NP after discectomy since, once damaged, this structure was not able to perform its normal function anymore. In this study, the “Ravioli” was inserted in the NP cavity by a vertebral and CEP access. To implant the “Ravioli”, the motion segment (MS) was withdrawn from the PBS bath and a 4 mm-diameter perforation was carefully drilled longitudinally through vertebrae until a sudden change on structure resistance occurs. This change of resistance indicates the point of contact between the CEP and the NP.

The partial removal of the NP is a typical procedure in the implant insertion. Previous studies reported that the implantation of an NP prosthesis in partial nucleotomized segment led to restored disc height and to a stabilization of the mobility of the implanted segment to an physiological level (Goins et al., 2005). The maximum weight of “swelled Ravioli” in free swelling conditions was approximately 0.13 grams. Thus, an amount of approximately 0.1 grams of nuclear material was taken for the NP in order to ensure that the “Ravioli” expansion fill out the gap created by the removed NP.

The “Ravioli” was then placed in the NP cavity in dry configuration with an appropriated rod, in order to allow the swelling of the hydrogel in physiological conditions (Figure 7.1– B). The dry condition of implant consists on a 12.5 mg structure, with an inner diameter of 9 mm (more details are presented in Chapter 6). The “Ravioli” was properly folded in order to be inserted in NP cavity by the drilled vertebrae. After placing the implant, a cylindrical 4 mm-diameter cork piece was used to fill the drilled hole and its entrance, on the top of the MS, was closed with a fast drying silicone (Figure 7.1– C). The selection of cork as plug for the perforation in vertebral body was made according with its particular mechanical properties: first, the bending and progressive buckling of its cell walls structure makes the cork a relatively ductile material (Silva et al., 2005), being easily shaped to fit in the drilled hole of the MS; second, it does not interfere with the hydrogel swelling and it do not cause any disruption in the NP substitute.

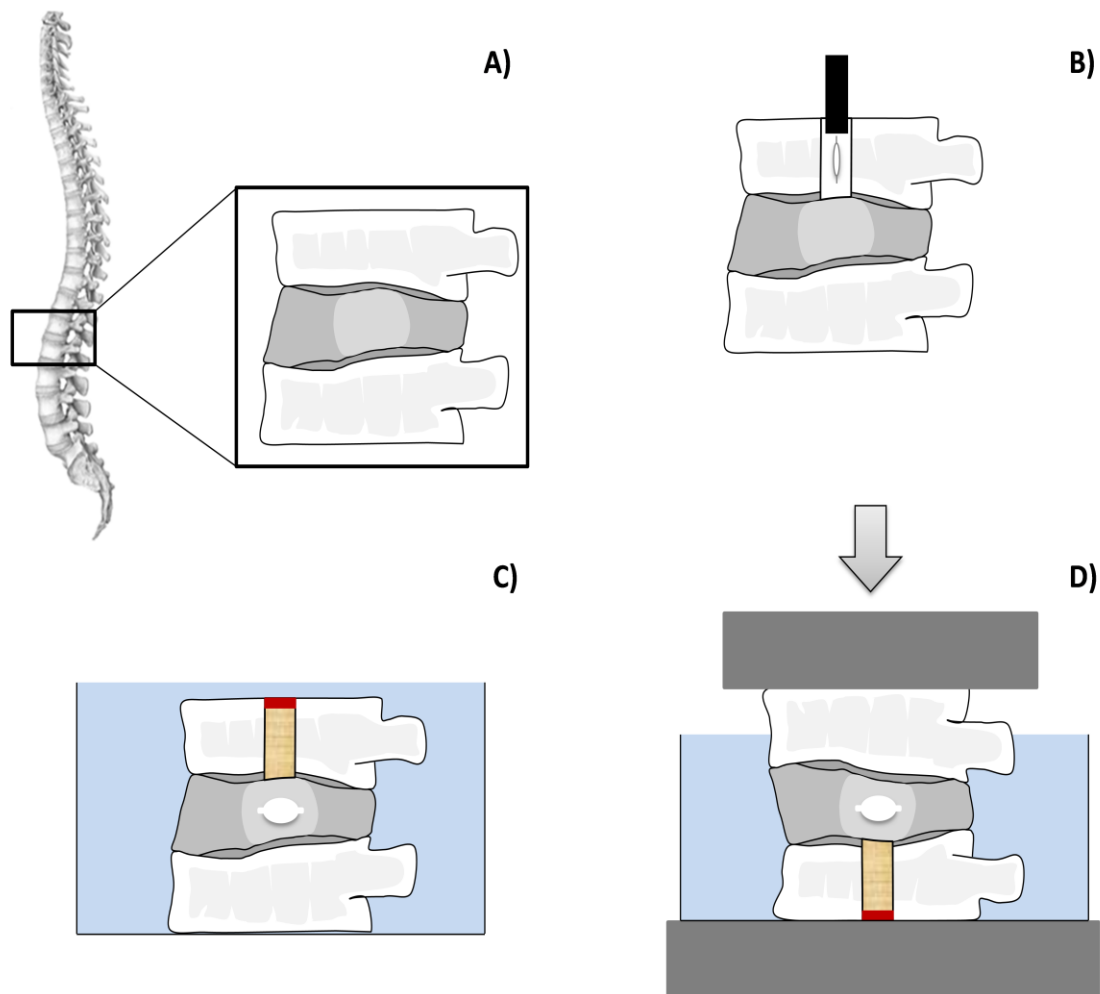


**Figure 7.1.** Schematic representation of the setup adopted to perform the mechanical test on the RMS (n=5): A) The motion segment was taken from the lumbar region of a porcine sample; B) After drill a hole in the top of the vertebra and CEP and removing of a prescribed amount of NP, a “Ravioli” in its initial configuration (dried) was inserted in the nuclear cavity using an appropriate rod; C) A cork plug (brown color) was placed in the vertebral hole to retain the “Ravioli” in the NP cavity and silicon (red color) was used on the top of MS to stick it to vertebrae.

Moreover, the whole structure was immersed in PBS (blue color in the image) during four hours, to allow the complete swelling of the hydrogel; D) Finally, the MS was placed on the mechanical tester, the Instron® 8874, after suffer a 180° rotation on the sagittal plane, to avoid the collapse of the cork structure. During the axial compressive mechanical test the IVD remained submersed in PBS to allow the “Ravioli” expansion. The control samples were tested in same configuration as the RMS (n=4).

### 7.2.3. Testing Equipment and Motion Segment Positioning.

The testing equipment consists of the previously described servo hydraulic testing system, Instron 8874, equipped with a 25 kN load cell (the Dynacell™ patented by Raymond et al. (2003)). The samples were placed on compression grips and aligned to minimize the effects of

bending/extension that could occur in a compression test with a misaligned sample. Thus, the samples were positioned in a center of a cast aluminum pot, parallel to the base. This pot was filled with PBS (1X), to keep the IVD entirely submersed (Figure 7.1– C). All tests were carried out at room temperature.

#### **7.2.4. Uniaxial Compressive Relaxation Tests**

During the load relaxation tests, the samples (n=5) were first submitted to a compressive pre-load of 30 N during 10 minutes, ensuring the contact with loading platen and helping on the minimization of errors due to post-mortem effects, such as the super hydration (Adams et al., 1996; Campbell-Kyureghyan et al., 2011). The load relaxation test was widely used to characterize mechanically the IVD response after a certain displacement (Iatridis et al., 1998; Johannessen et al., 2004; Yao and Gu, 2006). In this study, after load and displacement were set to zero, each sample was submitted to a compressive displacement of 1 mm, at a static strain rate –  $0.033 \text{ s}^{-1}$ . While the compressive displacement is considered to be a normal physiological value according with the height of the porcine IVD - no more than 20% of strain in the disc (Castro, 2013), the strain rate was chosen since it is considered as a physiological rate for the NP testing (Cloyd et al., 2007). A generic example of the axial compressive test input is showed in Figure 7.2. The compressive displacement of 1 mm was kept during 1 hour and the load as function of time was registered. One of the samples was discarded due to technical problems during the mechanical test. In addition, control tests (n=4) were performed in order to be compared with the results of the “Ravioli” insertion.

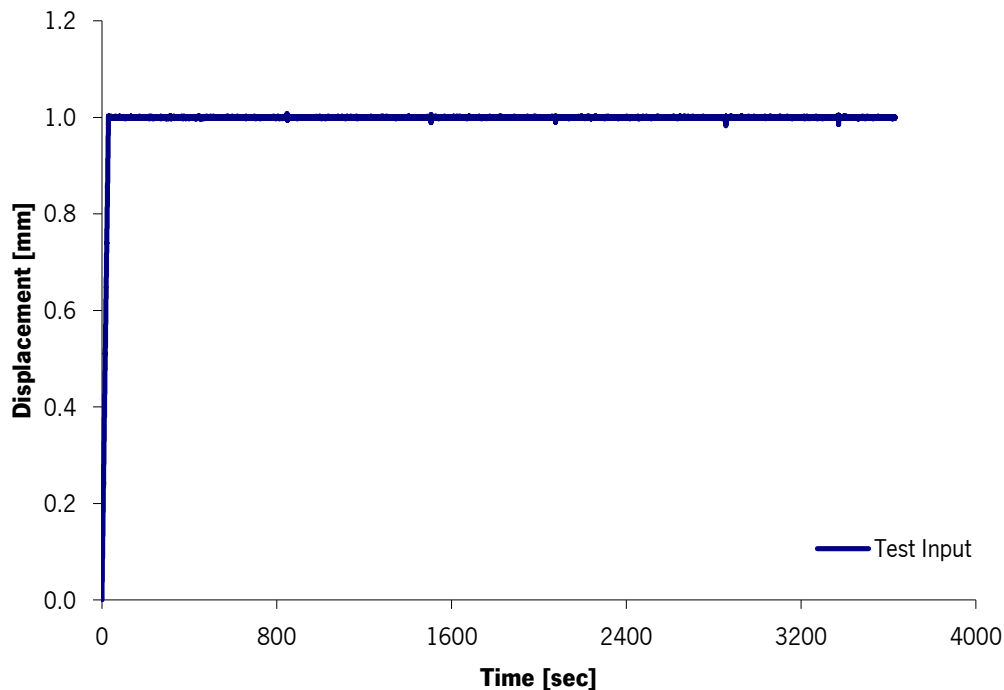


**Figure 7.2.** Load relaxation test input. A displacement of 1 mm at a strain rate of  $0.033 \text{ s}^{-1}$  was imposed to all samples – CMSs and RMSs.

### 7.2.5. Data Analysis

In a typical load-displacement curve of a biological material, there is an initial artifact, normally known as toe-region, likely caused by several facts such as the take-up of slack or the alignment or “seating” of the specimen. This artefact corresponds to a zone where a minimum load corresponds to a significant deformation in the sample. Although the application of the pre-load, the MSs in this study also present an initial toe-region, which was considered as corresponding to the first 0.5 mm of IVD displacement. Thus, to obtain correct value of stiffness coefficient, a linear regression was used in the Hookean region of the load-displacement curve - from 0.5 to 1 mm of displacement in the compressive test - in order to calculate the stiffness coefficient in both specimens, the CMS and the RMS.

Regarding load-relaxation curves, several exponential spring and dashpot models were considered for the data analysis. The experimental data, consisting on the values of force-time data from a load-relaxation test, were fitted in several mathematical models, including the

stretched exponential or Kohlrausch Williams Watts (KWW) function, since it was already applied in human lumbar disc tests (Johannessen et al., 2004; Sarver and Elliott, 2005; van der Veen et al., 2013). However, these models had revealed a weak correlation with the experimental data, due to the absence of clear distinction between a fast and slow decay. Thus, the best fit for the experimental data was found with a two-phase exponential decay. This two-phase model is typically used when the curve to be fitted is the result of the sum of a fast and slow exponential decay. This equation allowed predicting the force as a function of time in both CMS and RMS. The model is mathematically described by the Equation 7.1.

$$F(t) = F_{\infty} + S(F_0 - F_{\infty})e^{(-\tau_f \times t)} + (1 - S)(F_0 - F_{\infty})e^{(-\tau_s \times t)} \quad \text{Equation 7.1}$$

Where  $t$  represents the elapsed time;  $F_{\infty}$  represents the force (in Newton) at the equilibrium (i.e.  $F$  when the  $t$  tends to infinite);  $F_0$  is the initial force for  $t = 0$ ;  $R_f$  and  $R_s$ , expressed in  $s^{-1}$ , represent two rate constants: the fast and the slow rates respectively; finally, the  $S$  is the fraction of the span, from  $F_0$  to  $F_{\infty}$  accounted for by the faster of the two components. The parameters  $F_{\infty}$ ,  $R_f$ , and  $R_s$  and  $S$  were determined by the minimization of the sum of the squared error between the predicted and the experimental force, during load relaxation tests. According with these parameters, the values of the fast and the slow constants,  $\tau_f$  and  $\tau_s$  respectively (in seconds), were also determined as the reciprocal of the rate constants. In addition, the fast and slow half-life values,  $t_{f1/2}$  and  $t_{s1/2}$ , were considered as the ratio " $\ln 2 / k$ ". The half-life values have a particular meaning on the context of the problem: they represent the amount of time required for force to fall to half of its value as measured at the beginning of the time period, in both fast and slow decay periods.

In the end of each test, the final area was determined using specialized software - Image Pro Plus 4.6. Previous studies have shown that the post-mechanical testing measurements of area differed by no more than 10% of the initial area (Beckstein et al., 2008). Thus, it was assumed that the initial area,  $A_0$ , corresponds to the area measured after the end of testing plus a period of a four hours, necessary to reach the complete relaxation of the samples, for the range of values we applied to the MSs.

Finally, the swelling of the “Raviolis” on the inner region of the MS, was assessed after testing. The free-swelling was not quantitatively comparable with the “Ravioli” expansion in the nuclear cavity. On the one hand, the “Ravioli” presents a different osmotic pressure in these different conditions; on the other hand, the “Ravioli” needs to accommodate itself to the free space in the NP cavity during the swelling process, which is remarkably different than a free swelling process. For this work, it was defined that the minimal condition to consider the “Ravioli” as swelled was to reach the weight of 0.1 grams.

### **7.2.6. Statistical Analysis**

The raw data for each loading type was analysed using Graph Pad Prism 6.0. This software was used to determine the curves of best fit for each relaxation curves. In terms of statistical analysis, a *t-student* test with two-sample, with no adjustment, was used to characterize the significant differences between the CMSs and the RMSs, for all the constants and parameters determined experimentally. All statistical analysis was performed for a statistical significance level of  $p < 0.01$ .

### 7.3. Results

The results showed that the new method for the insertion of a new NP implant in the IVD is suitable to place and retain a hydrogel in the NP, without AF disruption, as well as it allowed the fulfillment of the pre-defined mechanical tests. All samples revealed that the cork did not collapse to the NP region and the silicon was able to completely contain the cork expansion under hydrated conditions. Moreover, the “Ravioli” had suffered swelling in three of four samples submitted to test (the “Ravioli” is considered as swelled when this structure expands on at least 0.1 gram of weight). The “Ravioli 2” (R2) was the unique structure which did not show significant swelling - Table 7.1. Furthermore, no collapse of the cork plug was found after the mechanical tests in each RMS.

The analysis of the mechanical response of the CMS and RMS was divided in two parts. Thus, in the first 30 seconds of testing, it was determined the static coefficient of stiffness ( $K_s$ ) for all samples, based on the linear region of load-displacement curve. As shown in the representative load-deformation curve presented in Figure 7.3, the region between 0.5 and 1 mm displacement was linear and well-described by a linear regression (mean  $R^2=0.99$ ,  $n=8$ ).

The mean value of  $K_s$  for the CMS is higher than the one determined for RMS. The magnitude of  $K_s$  of all samples varies between 1.7 N/m and 5.5 N/m. However, the results showed that the  $K_s$  does not present significant differences between the CMSs and the RMSs, for ( $p>0.01$ ). In Table 7.1 are presented the values of the  $A_0$  and the  $K_s$  for all motion segments, as well as the “Ravioli” swelling for each RMS sample.

Concerning to the load relaxation analysis, a two-phase exponential decay curve was fitted in the experimental results, in order to determine the relevant parameters. Thus, the parameters  $F_\infty$ ,  $C_f$  and  $C_s$  and  $S$  are responsible for the shape of the exponential curve as function of the elapsed time,  $t$ . The relaxation curves for the experimental tests and the exponential model adopted, for a representative sample of both CMS and RMS, are shown in Figure 7.4.



.The relaxation response and the corresponding two-phase exponential curve decay demonstrate that the exponential model fit well in both CMSs and RMSs relaxation data (mean  $R^2= 0.994$ ).

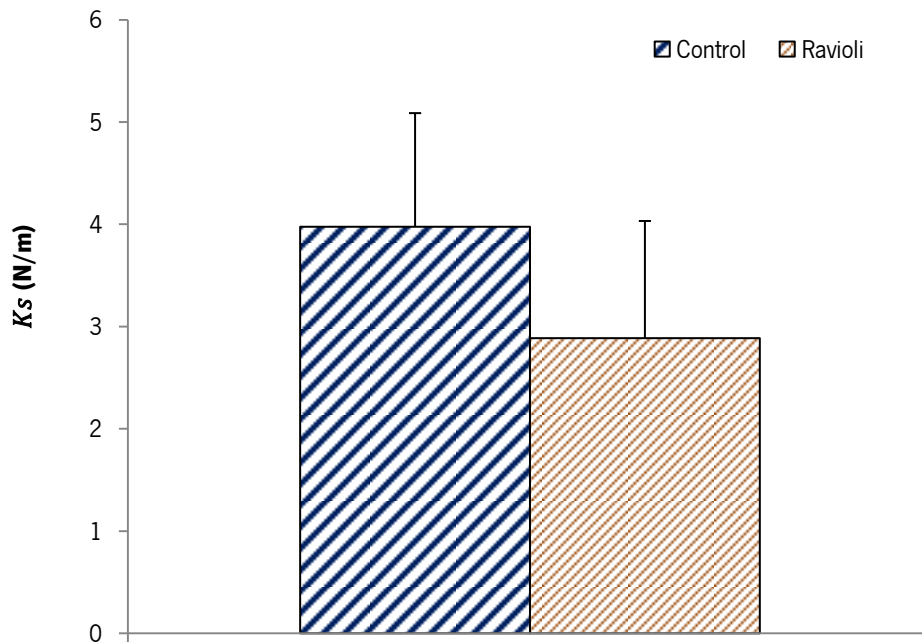


**Figure 7.3.** Mean value of the coefficient of stiffness ( $K_s$ ), in Newton per meter, for both CMS and RMS.

**Table 7.1.** Coefficient of stiffness ( $K_s$ , in Newton per meter) for the CMS and RMS, and the presence or absence of “Ravioli” swelling in the nuclear cavity of MS (“Yes” when it reached the minimum swelling, “No” for the cases where “Ravioli” did not expanded). Note: “N.A.” means “Not Applicable”.

	Sample	$K_s$ (N/m)	“Ravioli” Swelling
<b>CMS</b>	C1	2.9	N.A.
	C2	5.5	N.A.
	C3	2.9	N.A.
	C4	4.6	N.A.
<b>RMS</b>	Rav1	4.6	Yes
	Rav2	2.0	No
	Rav3	1.7	Yes
	Rav4	3.3	Yes

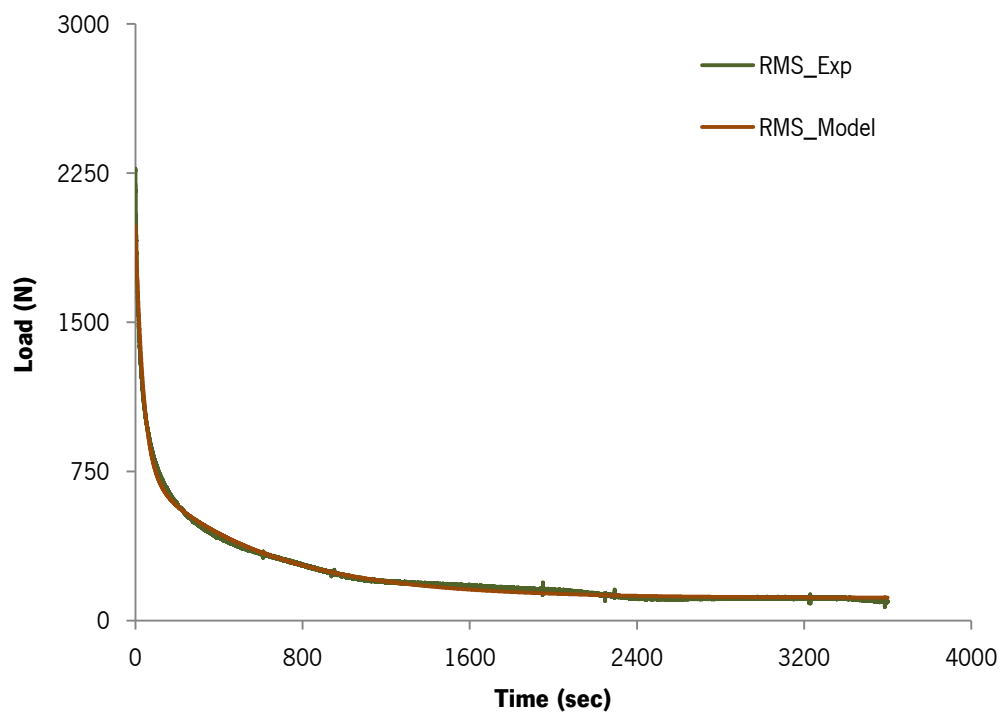
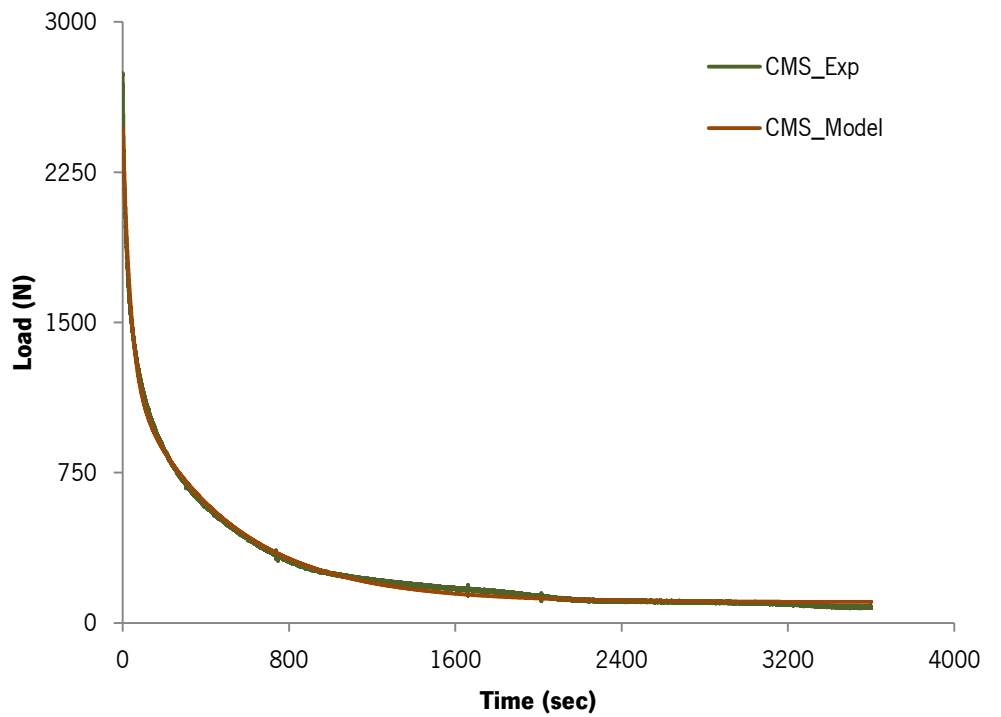


**Figure 7.4.** Load-relaxation curves for the experimental tests (green line) and the exponential model adopted (orange line), for a representative sample of both CMS and RMS.

Concerning to the parameters, the values are reported in Table 7.2. The results revealed that no significant differences were found between CMS and RMS, for all the relaxation parameters ( $p > 0.01$ ). The results also evidenced that the fast rate constant,  $R_f$ , is higher than the slow rate constant,  $R_s$ , for both CMS and RMS samples. Moreover, the mean value of the span fraction (S) – which corresponds to the faster decay, from  $F_0$  to  $F_\infty$  (in Newton), between the two components - is higher than 0.5, indicating that the fast response is predominant for the one hour test for both group of tests.

**Table 7.2.** Relaxation parameters (mean  $\pm$  standard deviation).

Parameter	CMS	RMS
$F_0$ (N)	1636 $\pm$ 627	2177 $\pm$ 686
$F_\infty$ (N)	98 $\pm$ 35	86 $\pm$ 20
$R_f$ (s <sup>-1</sup> )	2.3 E-02 $\pm$ 7.0E-03	2.5 E-02 $\pm$ 4.0E-03
$R_s$ (s <sup>-1</sup> )	1.6E-03 $\pm$ 3.0E-04	1.9 E-03 $\pm$ 2.0E-04
S	6.7 E-01 $\pm$ 5.0E-02	5.4 E-01 $\pm$ 4.0 E-02
$\tau_f$ (s)	42 $\pm$ 7.0	48 $\pm$ 17
$\tau_s$ (s)	520 $\pm$ 60	648 $\pm$ 111
$t_{f\frac{1}{2}}$	29 $\pm$ 5	34 $\pm$ 12
$t_{i\frac{1}{2}}$	360 $\pm$ 42	449 $\pm$ 77

#### **7.4. Discussion of the Effect of the Implant Insertion in a Motion Segment in terms of Load Relaxation**

The discectomy, which is the surgical procedure used to remove the NP from IVD, leads to posterior disc dysfunctions. Thus, the development of new techniques for NP replacement represents a promising way to eliminate or at least mitigate the clinical limitations induced by this procedure. One of the major focus in the NP replacement process is how to restore the biomechanical properties of a damaged disc (Zhou et al., 2014). Previous studies reported several hydrogels, such as photo-reactive nanomaterials (Eyholzer et al., 2011), self-curing polymers (Felt et al., 2001) or thermos-responsive polymers (Vernengo et al., 2008), that could mimic the swelling and the mechanical behaviour of the native human NP. However, these studies only evaluated the mechanical properties of these materials while they are not injected in the IVD. Thus, the behaviour of these biomaterials and the biomechanical response of the IVD once inserted in NP cavity are unknown.

However, some researchers have already investigated the change of the intervertebral disc stiffness at different loads after discectomy or after hydrogel injection. Shea et al., (1994) found that there are no significant differences in disc stiffness at 800 N in axial compression between intact and percutaneous discectomy. Cannella et al. (2008) showed that the IVD instability related to disc degeneration (which evolves an increment the range of motion) could be minimized using a synthetic hydrogel for the volume filling of the NP. Later, the studies performed by Balkovec et al. (2013) evidenced that an injectable hydrogel is able to restore the several characteristic IVD parameters such as the height of the IVD and the stiffness in porcine MS subjected to fatigue cycles.

Nevertheless the interesting results of these publications, all the discectomies evolved the disruption of the annular fibres. In addition, no information was given about how these hydrogels behave under the application of a load relaxation test, when inserted in the nuclear cavity. In the present study, a pioneer technique to insert and contain the new NP replacement solution *in vitro*, the “Ravioli”, was suggested. The load relaxation response was compared with a normal

disc (CMS), using load-displacement as well as the load relaxation curves of both CMS and RMSs.

The aim of this research was firstly, to demonstrate that this experimental procedure is able to insert and contain the NP implant *ex vivo* in the nuclear cavity, allowing also the fulfilment of compressive mechanical test; secondly, to confirm the hypothesis that the “Ravioli” is able to restore the stiffness and the loading relaxation responses of a damaged disc. This study demonstrated that the new technique of hydrogel insertion and retention in the NP cavity, without AF disruption, is suitable for both the introduction of an NP implant and for *ex vivo* evaluation of the mechanical behaviour of an NP substitute. Moreover, the analysis of the samples after mechanical testing revealed that the “Ravioli” had suffered a complete swelling in three of four samples submitted to test (Table 7.1), filling the gap left by the NP removal. The “Ravioli” swells, acquiring at least of 0.1 gram of weight when compared to the initial dry structure, which is assumed as reaching the complete swelling. The “Ravioli” R2 was the unique structure that did not suffer the expectable swelling. The post-test image analysis revealed that R2 presented a rupture in the “Envelope”, which possible occurred previously to the placement in the nuclear cavity.

An additional goal of this work is to determine if there are significant differences in terms of stiffness between the CMS and RMS. Thus, the coefficient of static stiffness ( $K_s$ ) was determined for the displacement period comprised between 0.5 and 1 mm, since it corresponds to the linear region of the curve load-displacement. The results revealed that the denucleated discs with hydrogel present the same magnitude for the  $K_s$  as the CMS, for quasi-static strain rates, indicating that the “Ravioli” insertion does not alter the normal value of the disc stiffness, under static condition. Interestingly, the stiffness of the sample that did not swell was similar to the ones that had expanded. This confirms the data from previous studies where it was hypothesized that stiffness did not change with the water content in the disc (van der Veen, 2009).

The mechanical loading acting on the IVD induces diurnal changes in dimensions and internal disc pressure *in vivo*. The changes in disc height are commonly attributed to the

combination of changes in the water content of NP and to creep deformation of the AF (Johannessen et al., 2004; Malko et al., 1999). Previous studies described these changes using a stretched exponential function, the Kohlrausch-Williams-Watts (KWW) function, or a Double-Voight (DV) model (Johannessen et al., 2004; van der Veen et al., 2013). However, although both KWW and DV models described well the behaviour of IVD for long term test (in the order of hours), these models revealed some difficult for the fitting in the typical duration tests, leading to under or overestimation of the model parameters (van der Veen et al., 2013).

While in the short-time strain of the IVD, the annular fibres are stretched and the fluids from the annular region are secreted, the long term response is ruled by viscoelastic phenomena and changes on fluid content in NP (McMillan et al., 1996; van der Veen, 2009). Therefore, to better simulate the load relaxation response of the IVD under axial compressive test, a two-phase exponential decay was used, in order to describe the combined behaviour of the IVD results as a sum of fast and slow responses. The advantage of this model is to present an excellent fit to the experimental data ( $R^2= 0.994$ ,  $n=8$ ), showing potential to correctly describe the relaxation of the IVD, for physiological time testing.

In this particular case, no differences were found between the RMS and the CMS on the load relaxation curve for one hour test ( $n=4$ ), indicating that the “Ravioli” could in fact mimic the behaviour of the NP, under a load relaxation test. Thus, the results demonstrated that the “Ravioli” insertion in the nuclear cavity presents a minimum effect on the relaxation parameters of the MS, suggesting that this hydrogel is a suitable option for the replacement of the relaxation capabilities of the IVD. The model also revealed a predominance of the fast response, since the mean value of the span fraction ( $S$ ) is higher than 0.5. These values were expected since the test only took one hour, being considered as a relatively fast test.

The disc mechanics is highly influenced by the fluid transport among the IVD structures (Ferguson et al., 2004). Moreover, the knowledge about the processes of disc hydration helps to better understand disc degeneration. The hydration levels in the IVD are essentially ruled by fixed charge density (Iatridis et al., 2003; Johannessen et al., 2004). However, the  $S$  value indicates that in these tests, the re-equilibrium of the osmotic pressure was predominantly governed by the

phenomenon of fluid flowing from the AF to the surrounding environment detrimental to the proteoglycan content change.

The time constants of the model,  $\tau_f$  and  $\tau_s$ , represent the time that a first order system requires to reach the 63% of the asymptotic value of the fast and slow component of the mechanical test after the application of a certain strain (van der Veen, 2009). Therefore, this parameter helps to describe the different test phases, the fast and the slow response. The results for the time constants revealed that is  $\tau_f$  approximately ten times lower than  $\tau_s$ , for both CMS and RMS. This is an expectable value since the fast response occurs during a lower period of time than the slow regime.

Notwithstanding the results for the “Ravioli” as a substitute for NP, the described approach has some limitations. First, it does not consider the effect of the NP removal on the load relaxation. Previous biomechanical tests had shown that the removal of the NP leads to an increase in mobility ranging from 38% to 100% compared with the intact spinal segment (Goins et al., 2005), originating annulus fissures and disc prolapse. In addition, the removal of the nucleus has been associated to outward bulging of the outer region of the AF, and to the inward bulging of the inner region to the center of the disc in axial loading tests (Meakin and Hukins, 2000). These factors are currently thought to be related to appearance of circumferential tears in the AF, further decreasing its resistance to shear forces (Di Martino et al., 2005). Thus, although it might be interesting the comparison with nucleotomized MS, it was decided do not include an MS without NP, since the nucleotomized state is considered to be non-relevant, due to the known “adverse effects” of the absence of NP in the normal behaviour of the disc. NP removal alters the distribution of circumferential and radial strains within the AF, causing the a considerable increment in circumferential strain in the posterolateral region, which could ultimately lead to annular tears (Showalter, 2015).

Second, the results are provided from an *ex vivo* mechanical test, which cannot be directly extrapolated for the response of this material *in vivo*. This response contains several more variables that were neglected or relativized in this study, such as the nutrition or the presence of the surrounding structures.

Third, this work does not quantify the long term response of the complex “Ravioli”-MS to loading as well as no image evaluation was performed during the mechanical test. It is well known that the long term response is of key importance to understand how this implantable material withstands to fatigue testing and how it resists to extrusion (Bertagnoli et al., 2005); moreover, the image analysis allows to understand “in loco” the reaction of the IVD to hydrogel placement and the biological and morphological changes on the inner structure of the IVD. Thus, for a better knowledge about the process of load relaxation, future investigations should include the evaluation of the image analyzes of the mechanical response of the “Ravioli” under loading and the long term response of the hydrogel.

Finally, this study used porcine lumbar spine for the “Ravioli” insertion and mechanical testing. Typically, the porcine cervical spine are considered as a reasonable analog to the human lumbar spine in what concerns to geometry, anatomy (Yingling et al., 1999), and function (Tampier et al., 2007). However, some differences can be found between the human and cervical porcine spines such as the large anterior processes and smaller pars interarticularis in porcine spines (Balkovec et al., 2013; Yingling et al., 1999). Moreover, the endplate areas are quite different: while in human CEPs the average area is around 1000 mm<sup>2</sup>, in the porcine cervical CEPs the area is around 500 mm<sup>2</sup> (Balkovec et al., 2013; Yingling et al., 1999). This particular study was performed with lumbar porcine discs which were already defined as considerable choice to study the benchmark values of IVD due to several characteristics, such as the average area of the CEP (around 1000 mm<sup>2</sup>) or the mechanical response to loading (see in Chapter 3). Nevertheless, the present experimental setup was successful in the purpose of characterize the stiffness and the load relaxation response of a motion segment with a “Ravioli” as a partial NP substitute. The hydrogel insertion technique is promising, especially when the requirements of NP replacement study evolved the preservation of an intact AF and the retention of the implant solution in the nuclear cavity. This simple approach helps to test the NPR solutions in-situ instead of the typical characterization measured after its production, outside its “working space”. Furthermore, the implant studied in the scope of this work, revealed evidences to be a good substitute of natural NP for both load-displacement and load relaxation test.





## 8. General Conclusions

*This chapter congregates and synthesizes the main findings of the present work. Furthermore, the outcomes of this work are analyzed and a critical review is included. Further improvements and future works are also suggested.*

### 8.1. Concluding Remarks

The topic of this thesis is to develop experimental procedures for the identification of materials properties of intervertebral disc (IVD) constituents in order to give a contribution for the development of a biomimetic substitute of the nucleus pulposus (NP).

Therefore, the goal of this research is to develop an experimental framework to study the mechanical specificities of IVD, in order to optimize both the accuracy of the computational models and the treatment strategies for back pain. This work also aims to give a contribution in the selection and the characterization of a long-term biomimetic substitute of NP, developed in the scope of the NP mimetic project. The attainment of this objective required the completion of four main experimental approaches, corresponding to four chapters.

In third chapter, the effect of quasi-static and cyclic compressive loading on the mechanical response of porcine intervertebral discs was determined in order to verify if porcine lumbar intervertebral discs are a suitable model to study the mechanical properties of human samples under these conditions. Moreover, this initially study also allow to perform some considerations about the processes of fluid flow in the porcine discs, according with the parameters obtained for a previously applied model (O'Connell et al., 2011). As general conclusion, the results of this chapter indicated that care must be taken on the direct mechanical behaviour comparison between porcine lumbar discs and human lumbar ones: they present different anatomical and physiological properties (Ryan et al., 2008), as well as relevant

differences in terms of quasi-static and dynamic response. However, several advantages are associated to the use of porcine samples: they are readily available, they are not subject to stringent regulations and the morphometric data for both porcine vertebrae and disc are described in detail, helping the researchers to choose the most appropriate experimental procedure (Busscher et al., 2010; Dath et al., 2007). All of these facts help to justify the use of these animals as model for the study of human spine behaviour.

For the designing of an efficient solution for NP replacement, it is essential to understand the behaviour of the intervertebral disc under variations in the internal disc pressure, as well as it is desirable the determination of the failure intradiscal pressure. Therefore, the fourth chapter of this thesis addresses the development of a methodology that allows applying increments in the intradiscal pressure. This approach presents the capacity to determine the compressive load throughout the variations in the intradiscal pressure as well as the ability to obtain the experimental values of the internal pressure that leads to disc failure. After ensure that this approach was able to measure the effect of the increments internal disc pressure on the relaxation rate of the motion segment, it was found that the effect of the increments on the intradiscal pressure on the relaxation rate is minimal during the initial steps of pressure increment. However, in the remaining steps of increment, a great variation in terms loading response as found, inducing severe oscillations on the relaxation rate.

The values of intradiscal pressure that leads to disc failure are a very specific characteristic, probably depending on constitutional factors and a range of features related with specimens particularities. From this research it was concluded that during overpressure events, there is redistribution of the internal pressure in the inner region of the multilayered annulus fibrosus (AF), suggesting that the collapse of the IVD structure is not a local but a generalized event. Moreover, it was found that the rupture in disc due to NP inflation in porcine samples could occur within the normal range of physiological intradiscal pressure for human samples. It was hypothesized that the use of different animal models, in special with a different aging, anatomy, composition and metabolism, could be responsible for the detected discrepancies. In addition, it was thought that the different techniques of measuring the failure pressure may also compromise the reliability of the results. As general idea, the replacement of the NP must be

selected according with the individual particularities of the damaged disc, as the magnitude of the values of intradiscal pressure that leads to disc rupture is dependent of several factors as the position of the disc in the spinal column and its geometry.

The computational and analytical models of the AF are essential tools for the development of new IVD implants. However, the accuracy of the computational and analytical models for the AF is strongly dependent on the material laws determined experimentally. The fifth chapter aimed to give a contribution for a better understanding of the mechanical behaviour of the reinforced-ground matrix of the AF, according with four regions. For that, each RGM region was submitted to unconfined uniaxial static and dynamic compressive tests, where a damaging strain is imposed. From the static tests it was shown, as expected, significant differences between the initial and repeated loading cycles, for the majority of analysed samples, indicating that damaging strains are related to a behavioural change in the AF. The unique exception arises from the samples of the anterior region, where the initial and repeated behaviour was revealed to be similar. It was also indicated that the anterior region was the most compliant region in the AF. All these results lead to the hypothesis that the reinforced-ground matrix (RGM) showed from the anterior region is more prepared to damaging compressive strains than the remaining RGM samples. In addition, the repeated loading tests demonstrated that RGM shows a significant drop in terms of stiffness, which is likely caused by an increment in the interlaminar separations. Thus, it was concluded that these AF damaging is likely preceded by a decreasing in the stiffness of the RGM and a consequent change on its mechanical behaviour.

The determination of the viscoelastic properties of the RGM is also essential as it allows a better comprehension about the dynamic behavior of this structure. Thus, from the dynamic test several viscoelastic parameters were obtained in order to assess the variations on the viscoelasticity of the RGM, according to the annular region and frequency. It was concluded that there is more prominent contribution of the elastic component for the mechanical response of the RGM than from the viscous one. It was found that the anterior region is the more viscous region in the AF. It is hypothesized that this anterior is more responsible for the energy storage than in the energy dissipation function of the IVD. Moreover, the local fibres-matrix or fibres-fibres interaction in the posterior and anterior regions of the RGM is frequency-dependent. A

possible explanation arises from the fact that a frequency higher than the characteristic frequency of the tissue could drive to a significant increase in the interstitial fluid pressure (Yao et al., 2002) and a structural “reorganization” of AF. This study also concluded that the propensity to imbibe fluid is different according to the annular regions which together with the irregular microstructure of the RGM, which might explain the regional differences in the AF in terms of viscoelastic properties. Thus, as conclusion of this work it is strongly recommended the use of different constitutive parameters for RGM, according to annular region.

An ideal solution to replace the NP must enclose the fulfillment of several requisites, including the ability to be implanted with a minimal invasive procedure; to retain large amount of water, providing an adequate swelling pressure under physiological loadings and; to withstand the complex mechanical loading acting on NP (Chan and Gantenbein-Ritter, 2012). Thus, the mechanical characterization of hydrogel-based solution, as well as its swelling pressure and the capacity to retain water after loading are therefore critical for the selection of proper NP replacement solution. The first aim of chapter six is to complement the manufacturer information about a developed hydrogel with potential to replace the NP - the “Ravioli”. This chapter also aims to help in the selection, among several options, of the most appropriate “Ravioli” configuration. As the “Ravioli” consists of two different structures (a nano-polymer based gel - the HydroMed core - with high water absorbing capacity, encapsulated by a nano-fibre film developed using electrospinning technology - the “Envelope”), different tests were performed. From the performed tests, it could be concluded that the HydroMed core presents a remarkable swelling capacity when immersed in aqueous environments. However, the presence of the “Envelope” is absolutely vital in the structure of the implant since it constrains the HydroMed core expansion, limiting the deformation of the gel, in both shape and volume. Moreover, the “Ravioli” is able to support the physiological stresses under quasi-static axial compressive loading mode. The biaxial tests also revealed that under physiological strains, a 0.2 mm-thickness “Envelope” is the most appropriate choice.

The second aim of chapter six was to assess the mechanical and material behaviour of the implants under the application of several tests, such as uniaxial tensile testing, cyclic compressive tests and stress relaxation tests. The uniaxial tensile tests showed that the

“Envelope” presents a Young’s modulus value that is typical of an elastomer. The results confirmed again that the “Envelope” is indicated to constrain the HM core in terms of mechanical compliance and resistance to rupture, for the physiological range of values. The stress relaxation tests revealed that both toe and linear modulus are significantly higher than the reported for human NP, indicating that the “Ravioli” behave within the established values for the NP replacement (Bao and Yuan, 2002). Cyclic compressive test were performed to evaluate the ability of the implant to retain water. According with these tests the “Ravioli” can be considered as isochoric, since there was no volume variation during load application. By maintaining the normal disc height during loading events, this ability of water retention avoids the collapse of the IVD structure and the impingement of the posterior facet joints and facet joint syndrome, (Vuono-Hawkins et al., 1995). It is also possible to manipulate the HydroMed core in order to reach the same physiological NP height, helping to maintain the normal dimensions of the IVD.

The characterization of the new implant also encloses the examination of the functional changes due to NP replacement solutions insertion in the disc. Chapter seven proposes a new method to insert and retain the implant in the nuclear cavity, during mechanical testing. Furthermore, it aims to assess the mechanical response of the structure motion segment with the implant placed in the nuclear cavity. This study demonstrated that the new technique of hydrogel insertion and retention in the NP cavity, without AF disruption, is suitable for both the introduction of a NP implant and for *ex vivo* evaluation of its mechanical behaviour. In addition, the results also evidenced that the “Ravioli” could mimic the behaviour of the NP under a load relaxation test, suggesting that this hydrogel is a suitable option for the replacement of the relaxation capabilities of the NP. Although showing promising results, the complete understanding about the process of load relaxation should include the evaluation of the image analyzes of the mechanical response of the “Ravioli” under loading and the long term response of the hydrogel. Moreover, the *in vivo* response should be studied as it contains several more variables that were neglected or relativized in this study, such as the nutrition or the presence of the surrounding structures.

In short, the experimental tests performed in this work have demonstrated to be an important tool to understand the properties of the intervertebral disc. The new set of results also

bring an important database for the upcoming developments in the implant designing, namely by the characterization of intervertebral disc structures under different conditions. This work also contributed for the selection and characterization of partial replacement implant, which could be considered a promising approach for a long-term replacement of the nucleus pulposus.

## **8.2. Future Works and Recommendations**

This work could be enriched by several additional improvements. In what concerns to the tests with the motion segments, although the option of the present work was to submit these structures to short term uniaxial compression, it would be interesting to include long term response of the motion segment. Ongoing research should also include the long term effect of the IVD hydration and the influence of the ligaments on the response of motion segment to quasi-static and dynamic load. The characterization of the mechanical response of the motion segments should encloses different types of loading profiles, such as multi-axial translational loadings or rotation, flexion and extension efforts. Alternative techniques such as ultrasonic tests (Kohlhauser et al., 2009) or quasi-static unloading experiments (Luczynski et al., 2012) should be also considered in the capture of the “truly” elastic behaviour of IVD.

Regarding to the experimental pressurization tests, the present work includes the relationship between internal disc pressure and load relaxation as well as it presents the values of internal disc pressure that leads to disc failure. Further experiments should contemplate the evaluation of the causal relationship between intradiscal pressure and disc height, in order to understand if the normal height on degenerated discs could be restored by the therapies based on the manipulation of intradiscal pressure (Vergroesen et al., 2014). For better understand the process of disc failure due to internal inflation, the phenomena occurring in annulus and in wall-endplate must be assessed, as the latter represents a critical point for disc rupture in compression (Adams, 2002; Schechtman et al., 2006). The inflation technique could be also associated to a microstructural analysis of the disc structure, helping to clarify the mechanisms of disc failure. Moreover, the data provided in this report is a result of inflation after pre-defined compression of the IVD; however, another types of efforts and loadings, such as flexion or rotation must be, together with disc inflation, should be considered in the rupture analysis.

This work also analyzes the mechanical response of the reinforced-ground matrix of the porcine annulus fibrosus to uniaxial compressive loads, in both dynamic and static configurations. This study could be enriched with biaxial and shear tests as they allow obtaining an additional amount of constitutive data about the mechanical behavior of the RGM. These tests could be also associated to microstructural analysis by means of image analysis as well as a follow-up of the fluid content in the RGM, in order to better understand the mechanical behavior of the annular matrix.

Finally, the characterization of the implant was assessed *ex-* and *in-situ*, i.e., the implant was tested alone and in the nucleus pulposus cavity. However, some improvements could be performed on the experimental approach. During the *ex situ* tests – Chapter 6, the calculation of the contact area of the implant during relaxation tests was assessed by the use of a previous developed Finite Element model. However, the implant could be immersed in an appropriate contrast dye and a precise image acquisition system could be coupled to the experimental test, allowing determining the implant dimensions. The implant core (without the “Envelope” encapsulation) should be also submitted to confined compression tests and the results should be compared with the reported in the literature for the nucleus pulposus characterization. This comparison would help on the clarification of the suitability of the Hydromed core as an efficient solution to substitute the nucleus pulposus function.

In what concerns to the *in situ* tests – Chapter 7, it would be interesting to include the analysis of the effect of the nucleus removal on the load relaxation. Ongoing studies should contain an additional group of samples, the motion segments without nucleus, and compare it with the results reported in this work. Several other mechanical tests could be also applied, such as different loading conditions and configurations, a long term evaluation and the image analysis during loading. Moreover, the mechanical response of the implant *in vivo* should be also assessed, as several variables were neglected or relativized in this study, such as the nutrition or the presence of the surrounding structures.

As general recommendations, the number of samples used during mechanical tests should be expanded to ensure the statistical significance of the results. Although the usage of animals as models for the study of the mechanical behavior of the disc is recognized as a



reasonable approach, it is also recommended the use of human samples for experimental tests, since they bring more precise information about its mechanical characteristics.

To sum up, the panoply of mechanical tests developed in this study contributed to significantly improve the knowledge about the mechanical behavior of the intervertebral disc and its structures as well as it gives valuable information about the viability of the use of an implant, specially designed to replace the nucleus pulposus. In addition, the suggested improvements could be taken in account in order to increase the accuracy and also to expand the outcomes of the present work. However due to lack of time and/or technical limitations, with was not possible to go ahead with this tasks that are strongly recommended in future researches in this field.

## Bibliography

- Acaroglu, E.R., Iatridis, J.C., Setton, L.A., Foster, R.J., Mow, V.C., Weidenbaum, M., 1995. Degeneration and aging affect the tensile behavior of human lumbar annulus fibrosus. *Spine (Phila. Pa. 1976)*. 20, 2690–2701.
- Accadbled, F., Laffosse, J.-M., Ambard, D., Gomez-Bouchet, A., de Gauzy, J.S., Swider, P., 2008. Influence of location, fluid flow direction, and tissue maturity on the macroscopic permeability of vertebral end plates. *Spine (Phila. Pa. 1976)*. 33, 612–619.
- Adams, M.A., 2002. *The Biomechanics of Back Pain*. Churchill Livingstone.
- Adams, M.A., Dolan, P., 2012. Intervertebral disc degeneration: evidence for two distinct phenotypes. *J. Anat.* 221, 497–506.
- Adams, M.A., Dolan, P., McNally, D.S., 2009. The internal mechanical functioning of intervertebral discs and articular cartilage, and its relevance to matrix biology. *Stress Int. J. Biol. Stress* 28, 384–389.
- Adams, M.A., Freeman, B.J.C., Morrison, H.P., Nelson, I.W., Dolan, P., 2000. Mechanical initiation of intervertebral disc degeneration. *Spine (Phila. Pa. 1976)*. 25, 1625–36.
- Adams, M.A., Green, T.P., 1993. Tensile properties of the annulus fibrosus. *Eur. Spine J.* 203–208.
- Adams, M.A., McNally, D.S., Dolan, P., 1996. “Stress” distributions inside intervertebral discs. The effects of age and degeneration. *J. Bone Joint Surg. Br.* 78, 965–72.
- Adams, M.A., Roughley, P.J., 2006. What is intervertebral disc degeneration, and what causes it? *Spine (Phila. Pa. 1976)*. 31, 2151–2161.
- Aladin, D.M.K., Cheung, K.M.C., Ngan, A.H.W., Chan, D., Leung, V.Y.L., Lim, C.T., Luk, K.D.K., Lu, W.W., 2010. Nanostructure of collagen fibrils in human nucleus pulposus and its correlation with macroscale tissue mechanics. *J. Orthop. Res.* 28, 497–502.
- Ala-Kokko, L., 2002. Genetic risk factors for lumbar disc disease. *Ann. Med.* 34, 42–47.
- Alini, M., Eisenstein, S.M., Ito, K., Little, C., Kettler, A.A., Masuda, K., Melrose, J., Ralphs, J., Stokes, I., Wilke, H.J., 2008. Are animal models useful for studying human disc disorders/degeneration? *Eur. Spine J.* 17, 2–19.

- Ambard, D., Cherblanc, F., 2009. Mechanical behavior of annulus fibrosus: a microstructural model of fibers reorientation. *Ann. Biomed. Eng.* 37, 2256–2265.
- Andersson, G.B., Schultz, A.B., 1979. Effects of fluid injection on mechanical properties of intervertebral discs. *J. Biomech.* 12, 453–8.
- Asano, S., Kaneda, K., Umehara, S., Tadano, S., 1992. The mechanical properties of the human L4-5 functional spinal unit during cyclic loading. The structural effects of the posterior elements. *Spine (Phila. Pa. 1976)*. 17, 1343–1352.
- Ashby, M.F., 2010. *Materials Selection in Mechanical Design*, Fourth Edition. Elsevier, 31-56.
- Ashley, G.W., Henise, J., Reid, R., Santi, D. V., 2013. Hydrogel drug delivery system with predictable and tunable drug release and degradation rates. *Proc. Natl. Acad. Sci. U. S. A.* 110, 2318–23.
- Ateshian, G.A., Warden, W.H., Kim, J.J., Grelsamer, R.P., Mow, V.C., 1997. Finite deformation biphasic material properties of bovine articular cartilage from confined compression experiments. *J. Biomech.* 30, 1157–64.
- Austen, S., Punt, I.M., Cleutjens, J.P.M., Willems, P.C., Kurtz, S.M., MacDonald, D.W., van Rhijn, L.W., van Ooij, A., 2012. Clinical, radiological, histological and retrieval findings of Activ-L and Mobidisc total disc replacements: a study of two patients. *Eur. Spine J.* 21 Suppl 4, S513–20.
- Bae, W.C., Statum, S., Zhang, Z., Yamaguchi, T., Wolfson, T., Gamst, A.C., Du, J., Bydder, G.M., Masuda, K., Chung, C.B., 2013. Morphology of the cartilaginous endplates in human intervertebral disks with ultrashort echo time MR imaging. *Radiology* 266, 564–74.
- Balkovec, C., Vernengo, J., McGill, S.M., 2013. The use of a novel injectable hydrogel nucleus pulposus replacement in restoring the mechanical properties of cyclically fatigued porcine intervertebral discs. *J. Biomech. Eng.* 135, 61004–5.
- Bao, Q.-B., Higham, P.A., 1993. Prosthetic nucleus for implanting disks, hydrogel beads and semipermeable cover. *WO Patent 1992010982*.
- Bao, Q.-B., Higham, P.A., 2001. Hydrogel intervertebral disc nucleus. *US Patent 5976186*.
- Bao, Q.-B., Songer, M., Pimenta, L., Werner, D., Reyes-Sanchez, A., Balsano, M., Agrillo, U., Coric, D., Davenport, K., Yuan, H., 2007. Nubac Disc Arthroplasty: Preclinical Studies and Preliminary Safety and Efficacy Evaluations. *SAS J.* 1, 36–45.

- Bao, Q.-B., Yuan, H.A., 2002. New technologies in spine: nucleus replacement. *Spine (Phila. Pa. 1976)*. 27, 1245–1247.
- Bass, E.C., Ashford, F.A., Segal, M.R., Lotz, J.C., 2004. Biaxial testing of human annulus fibrosus and its implications for a constitutive formulation. *Ann. Biomed. Eng.* 32, 1231–1242.
- Beckstein, J.C., Sen, S., Schaer, T.P., Vresilovic, E.J., Elliott, D.M., 2008. Comparison of animal discs used in disc research to human lumbar disc: axial compression mechanics and glycosaminoglycan content. *Spine (Phila. Pa. 1976)*. 33, E166–73.
- Bergmann, G. (ed., 2008). Charité Universitaetsmedizin Berlin “OrthoLoad”. URL [www.orthoload.com](http://www.orthoload.com)
- Bertagnoli, R., Sabatino, C.T., Edwards, J.T., Gontarz, G.A., Prewett, A., Parsons, J.R., 2005. Mechanical testing of a novel hydrogel nucleus replacement implant. *Spine J.* 5, 672–681.
- Best, B.A., Guilak, F., Setton, L.A., Zhu, W., Saed-Nejad, F., Ratcliffe, A., Weidenbaum, M., Mow, V.C., 1994. Compressive mechanical properties of the human anulus fibrosus and their relationship to biochemical composition. *Spine (Phila. Pa. 1976)*. 19, 212–21.
- Bogduk, N., 2005. *Clinical Anatomy of the Lumbar Spine and Sacrum*. Elsevier Health Sciences, 15-21.
- Bohlman, H.H., Emery, S.E., Goodfellow, D.B., Jones, P.K., 1993. Robinson anterior cervical discectomy and arthrodesis for cervical radiculopathy. Long-term follow-up of one hundred and twenty-two patients. *J. Bone Joint Surg. Am.* 75, 1298–1307.
- Bono, C.M., Garfin, S.R., 2004. History and evolution of disc replacement. *Spine J. Off. J. North Am. Spine Soc. North Am. Spine Soc.* 4, 145S–150S.
- Boxberger, J.I., Orlansky, A.S., Sen, S., Elliott, D.M., 2009. Reduced nucleus pulposus glycosaminoglycan content alters intervertebral disc dynamic viscoelastic mechanics. *J. Biomech.* 42, 1941–1946.
- Boyd, L.M., Carter, A.J., 2006. Injectable biomaterials and vertebral endplate treatment for repair and regeneration of the intervertebral disc. *Eur. Spine J.* 15 Suppl 3, S414–21.
- Brinckmann, P., Grootenboer, H., 1991. Change of disc height, radial disc bulge, and intradiscal pressure from discectomy. An in vitro investigation on human lumbar discs. *Spine (Phila. Pa. 1976)*. 16, 641–6.
- Brinckmann, P., Horst, M., 1985. The influence of vertebral body fracture, intradiscal injection,

- and partial discectomy on the radial bulge and height of human lumbar discs. *Spine (Phila. Pa. 1976)*. 10, 138–45.
- Bronner, F., Farach-Carson, M.C., Roach, H.I., 2010. *Bone and Development*. Springer Science & Business Media, 1-23.
- Brown, T., Robert, H.J., Yorra, A.J., 1957. Some Mechanical Tests on the Lumbosacral Spine with Particular Reference to the Intervertebral Discs. *J. Bone Joint Surg.* 39-A, 1135–1164.
- Busscher, I., Ploegmakers, J.J.W., Verkerke, G.J., Veldhuizen, A.G., 2010. Comparative anatomical dimensions of the complete human and porcine spine. *Eur. Spine J.* 19, 1104–14.
- Callaghan, J.P., McGill, S.M., 2001. Intervertebral disc herniation: studies on a porcine model exposed to highly repetitive flexion/extension motion with compressive force. *Clin. Biomech.* 16, 28–37.
- Campana, S., Charpail, E., de Guise, J. A., Rillardon, L., Skalli, W., Mitton, D., 2011. Relationships between viscoelastic properties of lumbar intervertebral disc and degeneration grade assessed by MRI. *J. Mech. Behav. Biomed. Mater.* 4, 593-9.
- Campbell-Kyureghyan, N.H., Yalla, S.V., Voor, M., Burnett, D., 2011. Effect of orientation on measured failure strengths of thoracic and lumbar spine segments. *J. Mech. Behav. Biomed. Mater.* 4, 549–557.
- Cannella, M., Arthur, A., Allen, S., Keane, M., Joshi, A., Vresilovic, E., Marcolongo, M., 2008. The role of the nucleus pulposus in neutral zone human lumbar intervertebral disc mechanics. *J. Biomech.* 41, 2104–2111.
- Cassidy, J.J., Hiltner, A., Baer, E., 2009. Hierarchical Structure of the Intervertebral Disc. *Connect Tissue Res.* 23, 75-88.
- Cassinelli, E.H., Kang, J.D., 2000. Current understanding of lumbar disc degeneration. *Oper. Tech. Orthop.* 10, 254–262.
- Castro, A., 2013. Development of a biomimetic finite element model of the intervertebral disc diseases and regeneration. Minho. PhD. thesis, University of Minho, Braga, Portugal.
- Castro, A.P.G., Wilson, W., Huyghe, J.M., Ito, K., Alves, J.L., 2014. Intervertebral disc creep behavior assessment through an open source finite element solver. *J. Biomech.* 47, 297–301.

- Cavalcanti, C., Correia, H., Castro, A., Alves, J.L., 2013. Constitutive modelling of the annulus fibrosus: Numerical implementation and numerical analysis. In: 2013 IEEE 3rd Portuguese Meeting in Bioengineering (ENBENG). IEEE, pp. 1–4.
- Cegoñino, J., Moramarco, V., Calvo-Echenique, A., Pappalettere, C., Pérez Del Palomar, A., 2014. A constitutive model for the annulus of human intervertebral disc: Implications for developing a degeneration model and its influence on lumbar spine functioning. *J. Appl. Math.* 2014.
- Chan, S.C.W., Ferguson, S.J., Gantenbein-Ritter, B., 2011. The effects of dynamic loading on the intervertebral disc. *Eur. Spine J.* 20, 1796-812.
- Chan, S.C.W., Gantenbein-Ritter, B., 2012. Intervertebral disc regeneration or repair with biomaterials and stem cell therapy - Feasible or fiction? *Swiss Med. Wkly.* 142.
- Cheung, J.T.-M., Zhang, M., Chow, D.H.-K., 2003. Biomechanical responses of the intervertebral joints to static and vibrational loading: a finite element study. *Clin. Biomech.* 18, 790–799.
- Ching, C.T.S., Chow, D.H.K., Yao, F.Y.D., Holmes, A.D., 2004. Changes in nuclear composition following cyclic compression of the intervertebral disc in an in vivo rat-tail model. *Med. Eng. Phys.* 26, 587–94.
- Cho, H., Park, S.-H., Lee, S., Kang, M., Hasty, K.A., Kim, S.-J., 2011. Snapshot of degenerative aging of porcine intervertebral disc: a model to unravel the molecular mechanisms. *Exp. Mol. Med.* 43, 334–340.
- Chou, A.I., Akintoye, S.O., Nicoll, S.B., 2009. Photo-crosslinked alginate hydrogels support enhanced matrix accumulation by nucleus pulposus cells in vivo. *Osteoarthr. Cartilage* 17, 1377–84.
- Claus, A., Hides, J., Moseley, G.L., Hodges, P., 2008. Sitting versus standing: does the intradiscal pressure cause disc degeneration or low back pain? *J. Electromyogr. Kinesiol.* 18, 550–8.
- Cloyd, J.M., Malhotra, N.R., Weng, L., Chen, W., Mauck, R.L., Elliott, D.M., 2007. Material properties in unconfined compression of human nucleus pulposus, injectable hyaluronic acid-based hydrogels and tissue engineering scaffolds. *Eur. Spine J.* 16, 1892–8.
- Colton, C., 1995. Implantable biohybrid artificial organs. *Cell Transplant.* 4, 415–436.
- Cortes, D.H., Elliott, D.M., 2012. Extra-fibrillar matrix mechanics of annulus fibrosus in tension and compression. *Biomech. Model. Mechanobiol.* 11, 781–90.

- Costi, J.J., Hearn, T.C., Fazzalari, N.L., 2002. The effect of hydration on the stiffness of intervertebral discs in an ovine model. *Test* 17, 446–455.
- Cripton, P. A, Dumas, G. A, Nolte, L.P., 2001. A minimally disruptive technique for measuring intervertebral disc pressure in vitro: application to the cervical spine. *J. Biomech.* 34, 545–9.
- Cunningham, B.W., 2004. Basic scientific considerations in total disc arthroplasty. *Spine J.* 4, S219–S230.
- Dath, R., Ebinesan, A.D., Porter, K.M., Miles, A.W., 2007. Anatomical measurements of porcine lumbar vertebrae. *Clin. Biomech. (Bristol, Avon)* 22, 607–13.
- Davis, J.R., 2004. *Tensile Testing*, 2nd Edition. ASM International.
- Delamarter, R.B., Bae, H.W., Pradhan, B.B., 2005. Clinical results of ProDisc-II lumbar total disc replacement: report from the United States clinical trial. *Orthop. Clin. North Am.* 36, 301–13.
- Dennison, C.R., Wild, P.M., Byrnes, P.W.G., Saari, A., Itshayek, E., Wilson, D.C., Zhu, Q.A., Dvorak, M.F.S., Cripton, P.A., Wilson, D.R., 2008. Ex vivo measurement of lumbar intervertebral disc pressure using fibre-Bragg gratings. *J. Biomech.* 41, 221–5.
- Denozière, G., Ku, D.N., 2006. Biomechanical comparison between fusion of two vertebrae and implantation of an artificial intervertebral disc. *J. Biomech.* 39, 766–775.
- Di Martino, A., Vaccaro, A.R., Lee, J.Y., Denaro, V., Lim, M.R., 2005. Nucleus pulposus replacement: basic science and indications for clinical use. *Spine (Phila. Pa. 1976)*. 30, S16–S22.
- Dolan, P., Luo, J., Pollintine, P., Landham, P.R., Stefanakis, M., Adams, M.A., 2013. Intervertebral disc decompression following endplate damage: implications for disc degeneration depend on spinal level and age. *Spine (Phila. Pa. 1976)*. 38, 1473–81.
- Ebara, S., Iatridis, J.C., Setton, L.A., Foster, R.J., Mow, V.C., Weidenbaum, M., 1996. Tensile properties of nondegenerate human lumbar annulus fibrosus. *Spine (Phila. Pa. 1976)*. 21, 452–461.
- Eberlein, R., Holzapfel, G., Schulze-Bauer, C., 2001. An Anisotropic Model for Annulus Tissue and Enhanced Finite Element Analyses of Intact Lumbar Disc Bodies. *Comput. Methods Biomech. Biomed. Engin.* 4, 209–229.

- Ellingson, A.M., Nuckley, D.J., 2012. Intervertebral disc viscoelastic parameters and residual mechanics spatially quantified using a hybrid confined/in situ indentation method. *J. Biomech.* 45, 491–6.
- Elliott, D.M., Setton, L.A., 2001. Anisotropic and Inhomogeneous Tensile Behavior of the Human Annulus Fibrosus: Experimental Measurement and Material Model Predictions. *J. Biomech. Eng.* 123, 256.
- Eyholzer, C., de Couraça, A.B., Duc, F., Bourban, P.E., Tingaut, P., Zimmermann, T., Månson, J.A.E., Oksman, K., 2011. Biocomposite hydrogels with carboxymethylated, nanofibrillated cellulose powder for replacement of the nucleus pulposus. *Biomacromolecules* 12, 1419–27.
- Felt, J.C., Rydell, M.A., Zdrahala, R.J., Arsenyev, A., 2001. Biomaterial system for in situ tissue repair. US Patent 6306177.
- Ferguson, S.J., Ito, K., Nolte, L.P., 2004. Fluid flow and convective transport of solutes within the intervertebral disc. *J. Biomech.* 37, 213–221.
- Ferguson, S.J., Steffen, T., 2003. Biomechanics of the aging spine. *Eur. Spine J.* 12 Suppl 2, S97–S103.
- Fujita, Y., Duncan, N.A., Lotz, J.C., 1997. Radial tensile properties of the lumbar annulus fibrosus are site and degeneration dependent. *J. Orthop. Res.* 15, 814–819.
- Galbusera, F., Schmidt, H., Noailly, J., Malandrino, A., Lacroix, D., Wilke, H.-J., Shirazi-Adl, A., 2011. Comparison of four methods to simulate swelling in poroelastic finite element models of intervertebral discs. *J. Mech. Behav. Biomed. Mater.* 4, 1234–41.
- Geisler, F.H., 2006. The CHARITÉ Artificial Disc: Design History, FDA IDE Study Results, and Surgical Technique. *Clin. Neurosurg.* 53, 223–228.
- Gloria, A., Causa, F., De Santis, R., Netti, P.A., Ambrosio, L., 2007. Dynamic-mechanical properties of a novel composite intervertebral disc prosthesis. In: *Journal of Materials Science: Materials in Medicine*. pp. 2159–2165.
- Goel, V.K., Ramirez, S.A., Kong, W., Gilbertson, L.G., 1995. Cancellous bone Young's modulus variation within the vertebral body of a ligamentous lumbar spine—application of bone adaptive remodeling concepts. *J. Biomech. Eng.* 117, 266–71.
- Goins, M.L., Wimberley, D.W., Yuan, P.S., Fitzhenry, L.N., Vaccaro, A.R., 2005. Nucleus pulposus replacement: an emerging technology. *Spine J.* 5, 317S–324S.



- Goto, K., Tajima, N., Chosa, E., Totoribe, K., Kubo, S., Kuroki, H., Arai, T., 2003. Effects of lumbar spinal fusion on the other lumbar intervertebral levels (three-dimensional finite element analysis). *J. Orthop. Sci.* 8, 577–584.
- Gregory, D.E., 2009. The Influence of the Tensile Material Properties of Single Annulus Fibrosus Lamellae and the Interlamellar Matrix Strength on Disc Herniation and Progress. PhD. thesis, University of Waterloo, Ontario, Canada.
- Grignon, B., Grignon, Y., Mainard, D., Braun, M., Netter, P., Roland, J., 2000. The structure of the cartilaginous end-plates in elder people. *Surg. Radiol. Anat.* 22, 13–19.
- Guerin, H.A.L., Elliott, D.M., 2006. Degeneration affects the fiber reorientation of human annulus fibrosus under tensile load. *J. Biomech.* 39, 1410–8.
- Guerin, H.L., Elliott, D.M., 2007. Quantifying the Contributions of Structure to Annulus Fibrosus Mechanical Function Using a Nonlinear , Anisotropic , Hyperelastic Model. *J. Orthop. Res.* 508–516.
- Guyer, R.D., Thongtrangan, I., Ohnmeiss, D.D., 2012. Outcomes of CHARITE Lumbar Artificial Disk versus Fusion: 5-Year Data. *Semin. Spine Surg.* 24, 32–36.
- Haefeli, M., Kalberer, F., Saegesser, D., Nerlich, A.G., Boos, N., Paesold, G., 2006. The course of macroscopic degeneration in the human lumbar intervertebral disc. *Spine (Phila. Pa. 1976)*. 31, 1522–31.
- Handa, T., Ishihara, H., Ohshima, H., Osada, R., Tsuji, H., Obata, K., 1997. Effects of hydrostatic pressure on matrix synthesis and matrix metalloproteinase production in the human lumbar intervertebral disc. *Spine (Phila. Pa. 1976)*. 22, 1085–1091.
- Hattori S., Oda H, Kawai S, U.-S., 1981. Cervical intradiscal pressure in movements and traction of the cervical spine. *Z. Orthop.* 19, 568–569.
- Heuer, F., Schmitt, H., Schmidt, H., Claes, L., Wilke, H.-J., 2007. Creep associated changes in intervertebral disc bulging obtained with a laser scanning device. *Clin. Biomech.* 22, 737–744.
- Hirsch, C., Nachemson, A., 1954. New observations on the mechanical behavior of lumbar discs. *Acta Orthop. Scand.* 23, 254–83.
- Holzappel, G. a, Schulze-Bauer, C. a J., Feigl, G., Regitnig, P., 2005. Single lamellar mechanics of the human lumbar anulus fibrosus. *Biomech. Model. Mechanobiol.* 3, 125–40.

- Hongo, M., Gay, R.E., Hsu, J.-T., Zhao, K.D., Ilharreborde, B., Berglund, L.J., An, K.-N., 2008. Effect of multiple freeze-thaw cycles on intervertebral dynamic motion characteristics in the porcine lumbar spine. *J. Biomech.* 41, 916–20.
- Hoogendoorn, R., 2008. Studies on the degeneration and regeneration of the intervertebral disc. PhD. thesis, Utrecht, Netherlands.
- Hsieh, A.H., Twomey, J.D., 2010. Cellular mechanobiology of the intervertebral disc: new directions and approaches. *J. Biomech.* 43, 137–45.
- Huang, R.C., Wright, T.M., Panjabi, M.M., Lipman, J.D., 2005. Biomechanics of nonfusion implants. *Orthop. Clin. North Am.* 36, 271–80.
- Huber, G., Morlock, M.M., Ito, K., 2007. Consistent hydration of intervertebral discs during in vitro testing. *Med. Eng. Phys.* 29, 808–13.
- Hukins, D.W.L., 2000. Relationship Between Structure and Mechanical Function of the Tissues of the Intervertebral Joint. *Integr. Comp. Biol.* 40, 42–52.
- Iatridis, J., Nicoll, S.B., Michalek, A.J., Walter, B., Gupta, M.S., 2013. Role of biomechanics in intervertebral disc degeneration and regenerative therapies: what needs repairing in the disc and what are promising biomaterials for its repair? *Spine J.* 13, 243–62.
- Iatridis, J.C., Laible, J.P., Krag, M.H., 2003. Influence of fixed charge density magnitude and distribution on the intervertebral disc: applications of a poroelastic and chemical electric (PEACE) model. *J. Biomech. Eng.* 125, 12–24.
- Iatridis, J.C., Maclean, J.J., Ryan, D.A., 2005. Mechanical damage to the intervertebral disc annulus fibrosus subjected to tensile loading. *J. Biomech.* 38, 557–565.
- Iatridis, J.C., Setton, L. a, Foster, R.J., Rawlins, B. a, Weidenbaum, M., Mow, V.C., 1998. Degeneration affects the anisotropic and nonlinear behaviors of human anulus fibrosus in compression. *J. Biomech.* 31, 535–44.
- Iatridis, J.C., Setton, L.A., Weidenbaum, M., Mow, V.C., 1997a. The viscoelastic behavior of the non-degenerate human lumbar nucleus pulposus in shear. *J. Biomech.* 30, 1005–1013.
- Iatridis, J.C., Setton, L.A., Weidenbaum, M., Mow, V.C., 1997b. Alterations in the mechanical behavior of the human lumbar nucleus pulposus with degeneration and aging. *J. Orthop. Res.* 15, 318–322.
- Iatridis, J.C., Weidenbaum, M., Setton, L.A., Mow, V.C., 1996. Is the nucleus pulposus a solid or

- a fluid? Mechanical behaviors of the nucleus pulposus of the human intervertebral disc. *Spine (Phila. Pa. 1976)*. 21, 1174–1184.
- lencean, S.M., 2000. Lumbar Intervertebral Disc Herniation Following Experimental Intradiscal Pressure Increase. *Acta Neurochir. (Wien)*. 142, 669–676.
- Indahl, A., Kaigle, A.M., Reikeräs, O., Holm, S.H., 1997. Interaction between the porcine lumbar intervertebral disc, zygapophysial joints, and paraspinal muscles. *Spine (Phila. Pa. 1976)*. 22, 2834–40.
- Izambert, O., Mitton, D., Thourot, M., Lavaste, F., 2003. Dynamic stiffness and damping of human intervertebral disc using axial oscillatory displacement under a free mass system. *Eur. Spine J.* 12, 562–6.
- Jacobs, W., Van der Gaag, N.A., Tuschel, A., de Kleuver, M., Peul, W., Verbout, A.J., Oner, F.C., 2012. Total disc replacement for chronic back pain in the presence of disc degeneration. *Cochrane database Syst. Rev.* 9, CD008326.
- Johannessen, W., Elliott, D.M., 2005. Effects of degeneration on the biphasic material properties of human nucleus pulposus in confined compression. *Spine (Phila. Pa. 1976)*. 30, E724–9.
- Johannessen, W., Vresilovic, E.J., Wright, A.C., Elliott, D.M., 2004. Intervertebral disc mechanics are restored following cyclic loading and unloaded recovery. *Ann. Biomed. Eng.* 32, 70–76.
- Johannessen, W., Vresilovic, E.J., Wright, A.C., Elliott, D.M., 2006. Disc mechanics with trans-endplate partial nucleotomy are not fully restored following cyclic compressive loading and unloaded recovery. *J. Biomech. Eng.* 128, 823–829.
- Joshi, A., 2004. Mechanical Behavior of the Human Lumbar Intervertebral Disc with Polymeric Hydrogel Nucleus Implant: An Experimental and Finite Element Study. PhD. thesis, Drexel University, Philadelphia, US.
- Joshi, A., Fussell, G., Thomas, J., Hsuan, A., Lowman, A., Karduna, A., Vresilovic, E., Marcolongo, M., 2006. Functional compressive mechanics of a PVA/PVP nucleus pulposus replacement. *Biomaterials* 27, 176–84.
- Kasra, M., Parnianpour, M., Shirazi-Adl, A., Wang, J.L., Gryn timer, M.D., 2004. Effect of strain rate on tensile properties of sheep disc anulus fibrosus. *Technol. Health Care* 12, 333–42.
- Kasra, M., Shirazi-Adl, A., Drouin, G., 1992. Dynamics of human lumbar intervertebral joints. Experimental and finite-element investigations. *Spine (Phila. Pa. 1976)*. 17, 93–102.

- Keller, T.S., Holm, S.H., Hansson, T.H., Spengler, D.M., 1990. 1990 Volvo Award in experimental studies. The dependence of intervertebral disc mechanical properties on physiologic conditions. *Spine (Phila. Pa. 1976)*. 15, 751–761.
- Keller, T.S., Spengler, D.M., Hansson, T.H., 1987. Mechanical behavior of the human lumbar spine. I. Creep analysis during static compressive loading. *J. Orthop. Res.* 5, 467–78.
- Klara, P.M., Ray, C.D., 2002. Artificial nucleus replacement: clinical experience. *Spine (Phila. Pa. 1976)*. 27, 1374–7.
- Klisch, S.M., Lotz, J.C., 1999. Application of a fiber-reinforced continuum theory to multiple deformations of the annulus fibrosus. *J. Biomech.* 32, 1027–36.
- Kohlhauser, C., Hellmich, C., Vitale-Brovarone, C., Boccaccini, A.R., Rota, A., Eberhardsteiner, J., 2009. Ultrasonic Characterisation of Porous Biomaterials Across Different Frequencies. *Strain* 45, 34–44.
- Korecki, C.L., MacLean, J.J., Iatridis, J.C., 2008. Dynamic compression effects on intervertebral disc mechanics and biology. *Spine (Phila. Pa. 1976)*. 33, 1403–1409.
- Kumaresan, S., Yoganandan, N., Pintar, F.A., 1999. Finite element analysis of the cervical spine: a material property sensitivity study. *Clin. Biomech. (Bristol, Avon)* 14, 41–53.
- Kuo, Y.-W., Wang, J.-L., 2010. Rheology of intervertebral disc: an ex vivo study on the effect of loading history, loading magnitude, fatigue loading, and disc degeneration. *Spine (Phila. Pa. 1976)*. 35, 743–752.
- Kurowski, P., Kubo, A., 1986. The relationship of degeneration of the intervertebral disc to mechanical loading conditions on lumbar vertebrae. *Spine (Phila. Pa. 1976)*. 11, 726–31.
- Le Huec, J.C., Mathews, H., Basso, Y., Aunoble, S., Hoste, D., Bley, B., Friesem, T., 2005. Clinical results of Maverick lumbar total disc replacement: two-year prospective follow-up. *Orthop. Clin. North Am.* 36, 315–22.
- Leahy, J.C., Hukins, D.W., 2001. Viscoelastic properties of the nucleus pulposus of the intervertebral disk in compression. *J. Mater. Sci. Mater. Med.* 12, 689–692.
- LeRoux, M.A., Guilak, F., Setton, L.A., 1999. Compressive and shear properties of alginate gel: effects of sodium ions and alginate concentration. *J. Biomed. Mater. Res.* 47, 46–53.
- Lewis, G., 2012. Nucleus pulposus replacement and regeneration/repair technologies: present status and future prospects. *J. Biomed. Mater. Res. B. Appl. Biomater.* 100, 1702–20.

- Li, S., Patwardhan, A.G., Amirouche, F.M., Havey, R., Meade, K.P., 1995. Limitations of the standard linear solid model of intervertebral discs subject to prolonged loading and low-frequency vibration in axial compression. *J. Biomech.* 28, 779–90.
- Lisi, A.J., O'Neill, C.W., Lindsey, D.P., Cooperstein, R., Cooperstein, E., Zucherman, J.F., 2006. Measurement of in vivo lumbar intervertebral disc pressure during spinal manipulation: a feasibility study. *J. Appl. Biomech.* 22, 234–9.
- Little, J.P., 2004. Finite Element Modelling Of Anular Lesions in the Lumbar Intervertebral Disc. PhD. thesis, Queensland University of Technology, Australia.
- Little, J.P., Adam, C.J., Evans, J.H., Pettet, G.J., Pearcy, M.J., 2007. Nonlinear finite element analysis of anular lesions in the L4 / 5 intervertebral disc. *J. Biomech.* 40, 2744–2751.
- Little, J.P., Pearcy, M.J., Tevelen, G., Evans, J.H., Pettet, G., Adam, C.J., 2010. The mechanical response of the ovine lumbar annulus fibrosus to uniaxial , biaxial and shear loads. *J. Mech. Behav. Biomed. Mater.* 3, 146–157.
- Lotz, J.C., 2004. Animal models of intervertebral disc degeneration: lessons learned. *Spine (Phila. Pa. 1976)*. 29, 2742–50.
- Luczynski, K., Dejaco, A., Lahayne, O., Jaroszewicz, J., Swieszkowski, W., Hellmich, C., 2012. MicroCT/Micromechanics-Based Finite Element Models and Quasi-Static Unloading Tests Deliver Consistent Values for Young's Modulus of Rapid-Prototyped Polymer-Ceramic Tissue Engineering Scaffold. *Comput. Model. Eng. Sci.* 8, 505-528
- Luczynski, K.W., Brynk, T., Ostrowska, B., Swieszkowski, W., Reihnsner, R., Hellmich, C., 2013. Consistent quasistatic and acoustic elasticity determination of poly-L-lactide-based rapid-prototyped tissue engineering scaffolds. *J. Biomed. Mater. Res. A* 101, 138–44.
- MacLean, J.J., Owen, J.P., Iatridis, J.C., 2007. Role of endplates in contributing to compression behaviors of motion segments and intervertebral discs. *J. Biomech.* 40, 55–63.
- Malandrino, A., Lacroix, D., Hellmich, C., Ito, K., Ferguson, S.J., Noailly, J., 2014. The role of endplate poromechanical properties on the nutrient availability in the intervertebral disc. *Osteoarthr. Cartilage* 22, 1053–60.
- Malandrino, A., Noailly, J., Lacroix, D., 2011. The effect of sustained compression on oxygen metabolic transport in the intervertebral disc decreases with degenerative changes. *PLoS Comput. Biol.* 7, e1002112.
- Malandrino, A., Noailly, J., Lacroix, D., 2013. Regional annulus fibre orientations used as a tool

- for the calibration of lumbar intervertebral disc finite element models. *Comput. Methods Biomech. Biomed. Engin.* 16, 923–928.
- Malko, J.A., Hutton, W.C., Fajman, W.A., 1999. An in vivo magnetic resonance imaging study of changes in the volume (and fluid content) of the lumbar intervertebral discs during a simulated diurnal load cycle. *Spine (Phila. Pa. 1976)*. 24, 1015–22.
- Marchand, F., Ahmed, A.M., 1990. Investigation of the laminate structure of lumbar disc annulus fibrosus. *Spine (Phila. Pa. 1976)*. 15, 402–10.
- Markolf, K.L., Morris, J.M., 1974. The structural components of the intervertebral disc. A study of their contributions to the ability of the disc to withstand compressive forces. *J. Bone Joint Surg.* 56, 675–687.
- Massey, C.J., van Donkelaar, C.C., Vresilovic, E., Zavaliangos, A., Marcolongo, M., 2012. Effects of aging and degeneration on the human intervertebral disc during the diurnal cycle: a finite element study. *J. Orthop. Res.* 30, 122–8.
- Masuoka, K., Michalek, A.J., MacLean, J.J., Stokes, I.A.F., Iatridis, J.C., 2007. Different effects of static versus cyclic compressive loading on rat intervertebral disc height and water loss in vitro. *Spine (Phila. Pa. 1976)*. 32, 1974–1979.
- McCullen, G.M., Yuan, H.A., 2003. Artificial disc: current developments in artificial disc replacement. *Curr. Opin. Orthop.* 14, 138–143
- McMillan, D.W., Garbutt, G., Adams, M.A., 1996. Effect of sustained loading on the water content of intervertebral discs: implications for disc metabolism. *Ann. Rheum. Dis.* 55, 880–7.
- McNair, C., Breakwell, L.M., 2010. (v) Disc degeneration and prolapse. *Orthop. Trauma* 24, 430–434.
- Meakin, J.R., Hukins, D.W.L., 2000. Effect of removing the nucleus pulposus on the deformation of the annulus fibrosus during compression of the intervertebral disc. *J. Biomech.* 33, 575–580.
- Menkowitz, M., Stieber, J.R., Wenokor, C., Cohen, J.D., Donald, G.D., Cresanti-Dakinis, C., 2005. Intradiscal pressure monitoring in the cervical spine. *Pain Physician* 8, 163–6.
- Mizuno, H., Roy, A.K., Vacanti, C.A., Kojima, K., Ueda, M., Bonassar, L.J., 2004. Tissue-engineered composites of annulus fibrosus and nucleus pulposus for intervertebral disc replacement. *Spine (Phila. Pa. 1976)*. 29, 1290–7; discussion 1297–8.

- Mochida, J., Toh, E., Nomura, T., Nishimura, K., 2001. The risks and benefits of percutaneous nucleotomy for lumbar disc herniation. A 10-year longitudinal study. *J. Bone Joint Surg. Br.* 83, 501–5.
- Moon, S.M., Yoder, J.H., Wright, A.C., Smith, L.J., Vresilovic, E.J., Elliott, D.M., 2013. Evaluation of intervertebral disc cartilaginous endplate structure using magnetic resonance imaging. *Eur. Spine J.* 22, 1820–8.
- Moore, M.K., Fulop, S., Tabib-Azar, M., Hart, D.J., 2009. Piezoresistive pressure sensors in the measurement of intervertebral disc hydrostatic pressure. *Spine J.* 9, 1030–4.
- Moore, R.J., 2000. The vertebral end-plate: what do we know? *Eur. Spine J.* 9, 92–6.
- Moore, R.J., 2006. The vertebral endplate: disc degeneration, disc regeneration. *Eur. Spine J.* 15 Suppl 3, S333–7.
- Moroney, S.P., Schultz, A.B., Miller, J.A., Andersson, G.B., 1988. Load-displacement properties of lower cervical spine motion segments. *J. Biomech.* 21, 769–79.
- Nachemson, A., 1963. The influence of spinal movements on the lumbar intradiscal pressure and on the tensile stresses in the annulus fibrosus. *Acta Orthop. Scand.* 33, 183–207.
- Nachemson, A., 1965. The effect of forward leaning on lumbar intradiscal pressure. *Acta Orthop. Scand.* 35, 314–28.
- Nachemson, A., Elfström, G., 1970. Intravital dynamic pressure measurements in lumbar discs. A study of common movements, maneuvers and exercises. *Scand. J. Rehabil. Med. Suppl.* 1, 1–40.
- Nerurkar, N.L., Elliott, D.M., Mauck, R.L., 2010. Mechanical design criteria for intervertebral disc tissue engineering. *J. Biomech.* 43, 1017–1030.
- Neumann, P., Beck, J., Steiner, M., Rempp, F., Fedder, H., Hemmer, P.R., Wrachtrup, J., Jelezko, F., 2010. Single-shot readout of a single nuclear spin. *Science* 329, 542–4.
- Niosi, C. a, Oxland, T.R., 2004. Degenerative mechanics of the lumbar spine. *Spine J.* 4, 202S–208S.
- O’Connell, G.D., Guerin, H.L., Elliott, D.M., 2009. Theoretical and uniaxial experimental evaluation of human annulus fibrosus degeneration. *J. Biomech. Eng.* 131, 111007.
- O’Connell, G.D., Jacobs, N.T., Sen, S., Vresilovic, E.J., Elliott, D.M., 2011. Axial creep loading and unloaded recovery of the human intervertebral disc and the effect of degeneration. *J.*

- Mech. Behav. Biomed. Mater. 4, 933–942.
- Okushima, H., 1970. Study on hydrodynamic pressure of lumbar intervertebral disc. *Nihon Geka Hokan*. 39, 45–57.
- Patwardhan, A.G., Havey, R.M., Meade, K.P., Lee, B., Dunlap, B., 1999. A Follower Load Increases the Load-Carrying Capacity of the Lumbar Spine in Compression. *Spine (Phila. Pa. 1976)*. 24, 1003-9.
- Pedley, D.G., Skelly, P.J., Tighe, B.J., 1980. Hydrogels in Biomedical Applications. *Br. Polym. J.* 12, 99–110.
- Péirié, D., Korda, D., Iatridis, J.C., 2005. Confined compression experiments on bovine nucleus pulposus and annulus fibrosus: sensitivity of the experiment in the determination of compressive modulus and hydraulic permeability. *J. Biomech.* 38, 2164–71.
- Pezowicz, C.A., Robertson, P.A., Broom, N.D., 2006. The structural basis of interlamellar cohesion in the intervertebral disc wall. *J. Anat.* 208, 317–30.
- Plasencia-Arriba, M.A., Maestre-García, C., 2007. New Horizons in the Treatment of Lumbar Disc Disease. *Rev. Española Cirugía Ortopédica y Traumatol. (English Ed.)* 51, 296–306.
- Pollintine, P., Van Tunen, M.S.L.M., Luo, J., Brown, M.D., Dolan, P., Adams, M.A., 2010. Time-dependent compressive deformation of the ageing spine: relevance to spinal stenosis. *Spine (Phila. Pa. 1976)*. 35, 386–394.
- Pospiech, J., Stolke, D., Wilke, H.J., Claes, L.E., 1999. Intradiscal pressure recordings in the cervical spine. *Neurosurgery* 44, 379–385.
- Race, A., Broom, N.D., Robertson, P., 2000. Effect of loading rate and hydration on the mechanical properties of the disc. *Spine (Phila. Pa. 1976)*. 25, 662–669.
- Raj, P.P., 2008. Intervertebral disc: Anatomy-physiology-pathophysiology-treatment. *Pain Pract.* 8, 18–44.
- Rawlinson, J.J., Punga, K.P., Gunsallus, K.L., Bartel, D.L., Wright, T.M., 2007. Wear simulation of the ProDisc-L disc replacement using adaptive finite element analysis. *J. Neurosurg. Spine* 7, 165–73.
- Ray, C.D., 2002. The PDN prosthetic disc-nucleus device. *Eur. Spine J.* 11 Suppl 2, S137–42.
- Raymond, D.L., Paul Derek, H., Bahra, C.S., 2003. Dynamic load cell apparatus. **US Patent 6508132**.



- Reza, A.T., Nicoll, S.B., 2010. Characterization of novel photocrosslinked carboxymethylcellulose hydrogels for encapsulation of nucleus pulposus cells. *Acta Biomater.* 6, 179–86.
- Roberts, S., Menage, J., Urban, J., 1989. Biochemical and structural properties of the cartilage end-plate and its relation to the intervertebral disc. *Spine (Phila. Pa. 1976).* 14, 166–174.
- Roberts, S., Urban, J.P., Evans, H., Eisenstein, S.M., 1996. Transport properties of the human cartilage endplate in relation to its composition and calcification. *Spine (Phila. Pa. 1976).* 21, 415–20.
- Ross, E.R.S., 2009. Revision in artificial disc replacement. *Spine J.* 9, 773–5.
- Roughley, P.J., 2004. Biology of intervertebral disc aging and degeneration: involvement of the extracellular matrix. *Spine (Phila. Pa. 1976).* 29, 2691–9.
- Rousseau, M.A., Bradford, D.S., Bertagnoli, R., Hu, S.S., Lotz, J.C., 2006. Disc arthroplasty design influences intervertebral kinematics and facet forces. *Spine J.* 6, 3, 258-66
- Ryan, G., Pandit, A., Apatsidis, D., 2008. Stress distribution in the intervertebral disc correlates with strength distribution in subdiscal trabecular bone in the porcine lumbar spine. *Clin. Biomech. (Bristol, Avon)* 23, 859–69.
- Sarver, J.J., Elliott, D.M., 2005. Mechanical differences between lumbar and tail discs in the mouse. *J. Orthop. Res.* 23, 150–155.
- Sato, K., Kikuchi, S., Yonezawa, T., 1999. In vivo intradiscal pressure measurement in healthy individuals and in patients with ongoing back problems. *Spine (Phila. Pa. 1976).* 24, 2468–74.
- Schechtman, H., Robertson, P.A., Broom, N.D., 2006. Failure strength of the bovine caudal disc under internal hydrostatic pressure. *J. Biomech.* 39, 1401–1409.
- Schmidt, H., Galbusera, F., Rohlmann, A., Shirazi-Adl, A., 2013. What have we learned from finite element model studies of lumbar intervertebral discs in the past four decades? *J. Biomech.* 46, 2342–55.
- Schollum, M.L., Robertson, P.A., Broom, N.D., 2009. A microstructural investigation of intervertebral disc lamellar connectivity: detailed analysis of the translamellar bridges. *J. Anat.* 214, 805–16.
- Schroeder, Y., Wilson, W., Huyghe, J.M., Baaijens, F.P.T., 2006. Osmoviscoelastic finite element model of the intervertebral disc. *Eur. Spine J.* 15 Suppl 3, S361–71.

- Schultz, A., Andersson, G., Ortengren, R., Haderspeck, K., Nachemson, A., 1982. Loads on the lumbar spine. Validation of a biomechanical analysis by measurements of intradiscal pressures and myoelectric signals. *J. Bone Joint Surg. Am.* 64, 713–20.
- Séguin, C.A., Grynepas, M.D., Pilliar, R.M., Waldman, S.D., Kandel, R.A., 2004. Tissue engineered nucleus pulposus tissue formed on a porous calcium polyphosphate substrate. *Spine (Phila. Pa. 1976)*. 29, 1299–307.
- Sélard, E., Shirazi-Adl, A., Urban, J.P.G., 2003. Finite element study of nutrient diffusion in the human intervertebral disc. *Spine (Phila. Pa. 1976)*. 28, 1945–1953; discussion 1953.
- Sen, S., Jacobs, N.T., Boxberger, J.I., Elliott, D.M., 2012. Human Annulus Fibrosus Dynamic Tensile Modulus Increases with Degeneration. *Mech. Mater.* 44, 93–98.
- Setton, L.A., D, P., Bonassar, L., Masuda, K., 2006. Chapter 62: Tissue engineering for regeneration and replacement of the intervertebral disc. In: Lanza R.P., Langer, R. and Vacanti, J.( eds ), *Principles of Tissue Engineering*. Academic Press , 4th edition . *Tissue Eng.* 1–35.
- Shahidi, M., Pichler, B., Hellmich, C., 2014. Viscous interfaces as source for material creep: A continuum micromechanics approach. *Eur. J. Mech. - A/Solids* 45, 41–58.
- Shankar, H., Scarlett, J.A., Abram, S.E., 2009. Anatomy and pathophysiology of intervertebral disc disease. *Reg. Anesth.* 67–75.
- Shea, M., Takeuchi, T.Y., Wittenberg, R.H., White, A.A., Hayes, W.C., 1994. A comparison of the effects of automated percutaneous discectomy and conventional discectomy on intradiscal pressure, disk geometry, and stiffness. *J. Spinal Disord.* 7, 317–25.
- Shim, V.P.W., Liu, J.F., Lee, V.S., 2006. A Technique for Dynamic Tensile Testing of Human Cervical Spine Ligaments. *Exp. Mech.* 46, 77–89.
- Shirazi-Adl, A., Ahmed, A.M., Shrivastava, S.C., 1986. A finite element study of a lumbar motion segment subjected to pure sagittal plane moments. *J. Biomech.* 19, 331–350.
- Shirazi-Adl, A., Parnianpour, M., 1993. Nonlinear response analysis of the human ligamentous lumbar spine in compression. On mechanisms affecting the postural stability. *Spine (Phila. Pa. 1976)*. 18, 147–58.
- Shiri, R., Karppinen, J., Leino-Arjas, P., Solovieva, S., Viikari-Juntura, E., 2010. The association between obesity and low back pain: a meta-analysis. *Am. J. Epidemiol.* 171, 135–54.

- Showalter, B., 2015. The Role of the Nucleus Pulposus in Human Intervertebral Disc Mechanical Function Quantified by Mechanical Loading and Non-Invasive Imaging. PhD. thesis, University of Pennsylvania, USA.
- Silva, S.P., Sabino, M.A., Fernandes, E.M., Correló, V.M., Boesel, L.F., Reis, R.L., 2005. Cork : properties, capabilities and applications. *Inter. Mater. Rev.*, 50, 6, 345–365.
- Silva-Correia, J., Correia, S.I., Oliveira, J.M., Reis, R.L., 2013. Tissue engineering strategies applied in the regeneration of the human intervertebral disk. *Biotechnol. Adv.* 31, 1514–31.
- Sivan, S.S., Roberts, S., Urban, J.P.G., Menage, J., Bramhill, J., Campbell, D., Franklin, V.J., Lydon, F., Merkher, Y., Maroudas, A., Tighe, B.J., 2014. Injectable hydrogels with high fixed charge density and swelling pressure for nucleus pulposus repair: biomimetic glycosaminoglycan analogues. *Acta Biomater.* 10, 1124–33.
- Skaggs, D.L., Weidenbaum, M., Iatridis, J.C., Ratcliffe, A., Mow, V.C., 1994. Regional variation in tensile properties and biochemical composition of the human lumbar annulus fibrosus [see comments]. *Spine (Phila. Pa. 1976)*. 19, 1310–1319.
- Smit, T.H., 2002. The use of a quadruped as an in vivo model for the study of the spine - biomechanical considerations. *Eur. Spine J.* 11, 137–44.
- Soltz, M.A., Ateshian, G.A., 2000. Interstitial fluid pressurization during confined compression cyclical loading of articular cartilage. *Ann. Biomed. Eng.* 28, 150–9.
- Spilker, R.L., Daugirda, D.M., Schultz, A.B., 1984. Mechanical response of a simple finite element model of the intervertebral disc under complex loading. *J. Biomech.* 17, 103–12.
- Stapleton, F., Stretton, S., Papas, E., Skotnitsky, C., Sweeney, D.F., 2006. Silicone hydrogel contact lenses and the ocular surface. *Ocul. Surf.* 4, 24–43.
- Steffen, T., Baramki, H.G., Rubin, R., Antoniou, J., Aebi, M., 1998. Lumbar intradiscal pressure measured in the anterior and posterolateral annular regions during asymmetrical loading. *Clin. Biomech. (Bristol, Avon)* 13, 495–505.
- Stokes, I.F., Laible, J.P., Gardner-Morse, M.G., Costi, J.J., Iatridis, J.C., 2011. Refinement of elastic, poroelastic, and osmotic tissue properties of intervertebral disks to analyze behavior in compression. *Ann. Biomed. Eng.* 39, 122–31.
- Strange, D.G.T., Oyen, M.L., 2012. Composite hydrogels for nucleus pulposus tissue engineering. *J. Mech. Behav. Biomed. Mater.* 11, 16–26.

- Tampier, C., Drake, J.D.M., Callaghan, J.P., McGill, S.M., 2007. Progressive disc herniation: an investigation of the mechanism using radiologic, histochemical, and microscopic dissection techniques on a porcine model. *Spine (Phila. Pa. 1976)*. 32, 2869–74.
- Thompson, J.P., Pearce, R.H., Schechter, M.T., Adams, M.E., Tsang, I.K., Bishop, P.B., 1990. Preliminary evaluation of a scheme for grading the gross morphology of the human intervertebral disc. *Spine (Phila. Pa. 1976)*. 15, 411–5.
- Tortora, G.J., Derrickson, B.H., 2008. *Principles of Anatomy and Physiology*. Wiley.
- Tsantrizos, A., Ordway, N.R., Myint, K., Martz, E., Yuan, H.A., 2008. Mechanical and Biomechanical Characterization of a Polyurethane Nucleus Replacement Device Injected and Cured In Situ Within a Balloon. *SAS J.* 2, 28–39.
- Umehara, S., Tadano, S., Abumi, K., Katagiri, K., Kaneda, K., Ukai, T., 1996. Effects of degeneration on the elastic modulus distribution in the lumbar intervertebral disc. *Spine (Phila. Pa. 1976)*. 21, 811–820.
- Urban, J.P., McMullin, J.F., 1988. Swelling pressure of the lumbar intervertebral discs: influence of age, spinal level, composition, and degeneration. *Spine (Phila. Pa. 1976)*. 13, 179–87.
- Urban, J.P.G., 2000. The Nucleus of the Intervertebral Disc from Development to Degeneration. *Integr. Comp. Biol.* 40, 53–61.
- Urban, J.P.G., Roberts, S., 2003. Degeneration of the intervertebral disc. *Arthritis Res. Ther.* 5, 120–130.
- van der Veen, A.J., 2009. Mechanical behaviour of the intervertebral disc under sustained compressive loading. PhD. thesis, VU University Medical Center, Amsterdam, The Netherlands.
- van der Veen, A.J., Bisschop, A., Mullender, M.G., van Dieën, J.H., 2013. Modelling creep behaviour of the human intervertebral disc. *J. Biomech.* 46, 2101–3.
- van der Veen, A.J., Mullender, M.G., Kingma, I., van Dieen, J.H., Van, J.H., Smit, T.H., 2008. Contribution of vertebral [corrected] bodies, endplates, and intervertebral discs to the compression creep of spinal motion segments. *J. Biomech.* 41, 1260–8.
- van Ooij, A., Oner, F.C., Verbout, A.J., 2003. Complications of artificial disc replacement: a report of 27 patients with the SB Charité disc. *J Spinal Disord Tech.* 16, 369-83.
- Veres, S.P., Robertson, P.A., Broom, N.D., 2010. The influence of torsion on disc herniation

- when combined with flexion. *Eur. spine J. Off. Publ. Eur. Spine Soc. Eur. Spinal Deform. Soc. Eur. Sect. Cerv. Spine Res. Soc.* 19, 1468–1478.
- Vergroesen, P.-P.A., van der Veen, A.J., van Royen, B.J., Kingma, I., Smit, T.H., 2014. Intradiscal pressure depends on recent loading and correlates with disc height and compressive stiffness. *Eur. Spine J.* 11, 2359-68
- Vernengo, J., Fussell, G.W., Smith, N.G., Lowman, A.M., 2008. Evaluation of novel injectable hydrogels for nucleus pulposus replacement. *J. Biomed. Mater. Res. B. Appl. Biomater.* 84, 64–9.
- Villarraga, M.L., Iannuzzi, A., 2009. *UHMWPE Biomaterials Handbook*. Elsevier.
- Virgin, W.J., 1951. Experimental properties into the physical properties on the intervertebral disc. *J. Bone Jt. Surg.* 33:B.
- Vogel, A., Pioletti, D.P., 2012. *Damping properties of the nucleus pulposus*. Clin. Biomech. (Bristol, Avon) 1–5.
- Vresilovic, E., Keane, M.F., Clemow, A.J.T., Smith, N.G., 2012a. Replacement or supplementation of a nucleus pulposus using a hydrogel. Patent US Patent 8118874.
- Vresilovic, E., Marcolongo, M.S., Lowman, A.M., Clemow, A.J.T., Keane, M.F., 2012b. Hydrogel balloon prosthesis for nucleus pulposus. US Patent 8287595.
- Vresilovic, E.J., Johannessen, W., Elliott, D.M., 2006. Disc mechanics with trans-endplate partial nucleotomy are not fully restored following cyclic compressive loading and unloaded recovery. *J. Biomech. Eng.* 128, 823–9.
- Vuono-Hawkins, M., Langrana, N.A., Parsons, J.R., Lee, C.K., Zimmerman, M.C., 1995. Materials and design concepts for an intervertebral disc spacer. II. Multidiameter composite design. *J. Appl. Biomater.* 6, 117–23.
- Wagner, D.R., Lotz, J.C., 2004. Theoretical model and experimental results for the nonlinear elastic behavior of human annulus fibrosus. *J. Orthop. Res.* 22, 901–909.
- Wang, J.L., Parnianpour, M., Shirazi-Adl, A., Engin, A.E., Li, S., Patwardhan, A., 1997. Development and validation of a viscoelastic finite element model of an L2/L3 motion segment. *Theor. Appl. Fract. Mech.* 28, 81–93.
- Wang, P., Yang, L., Hsieh, A.H., 2011. Nucleus pulposus cell response to confined and unconfined compression implicates mechanoregulation by fluid shear stress. *Ann. Biomed.*

Eng. 39, 1101–11.

Whatley, B.R., Wen, X., 2012. Intervertebral disc (IVD): Structure, degeneration, repair and regeneration. *Mater. Sci. Eng. C* 32, 61–77.

White, A.A., Panjabi, M.M., 1990. *Clinical Biomechanics of the Spine*. Lippincott Williams & Wilkins.

Wilke, H.J., Neef, P., Caimi, M., Hoogland, T., Claes, L.E., 1999. New in vivo measurements of pressures in the intervertebral disc in daily life. *Spine (Phila. Pa. 1976)*. 24, 755–762.

Wilson, W., Huyghe, J.M., van Donkelaar, C.C., 2007. Depth-dependent compressive equilibrium properties of articular cartilage explained by its composition. *Biomech. Model. Mechanobiol.* 6, 43–53.

Wu, H.C., Yao, R.F., 1976. Mechanical behavior of the human annulus fibrosus. *J. Biomech.* 9, 1–7.

Xi, L., Wang, T., Zhao, F., Zheng, Q., Li, X., Luo, J., Liu, J., Quan, D., Ge, J., 2014. Evaluation of an injectable thermosensitive hydrogel as drug delivery implant for ocular glaucoma surgery. *PLoS One* 9, e100632.

Yao, H., Gu, W.Y., 2006. Physical signals and solute transport in human intervertebral disc during compressive stress relaxation: 3D finite element analysis. *Biorheology* 43, 323–335.

Yao, H., Justiz, M.-A., Flagler, D., Gu, W.Y., 2002. Effects of Swelling Pressure and Hydraulic Permeability on Dynamic Compressive Behavior of Lumbar Annulus Fibrosus. *Ann. Biomed. Eng.* 30, 1234–1241.

Yingling, V.R., Callaghan, J.P., McGill, S.M., 1997. Dynamic loading affects the mechanical properties and failure site of porcine spines. *Clin. Biomech. (Bristol, Avon)* 12, 301–305.

Yingling, V.R., Callaghan, J.P., McGill, S.M., 1999. The porcine cervical spine as a model of the human lumbar spine: an anatomical, geometric, and functional comparison. *J. Spinal Disord.* 12, 415–23.

Zhang, Y., Drapeau, S., An, H.S., Markova, D., Lenart, B.A., Anderson, D.G., 2011. Histological features of the degenerating intervertebral disc in a goat disc-injury model. *Spine (Phila. Pa. 1976)*. 36, 1519–27.

Zhou, Z., Gao, M., Wei, F., Liang, J., Deng, W., Dai, X., Zhou, G., Zou, X., 2014. Shock absorbing function study on denucleated intervertebral disc with or without hydrogel injection through

static and dynamic biomechanical tests in vitro. *Biomed Res. Int.* 2014:461724.

Zimmerman, M.C., Vuono-Hawkins, M., Parsons, J.R., Carter, F.M., Gutteling, E., Lee, C.K., Langrana, N.A., 1992. The mechanical properties of the canine lumbar disc and motion segment. *Spine (Phila. Pa. 1976)*. 17, 213–20.

Zirbel, S. a, Stolworthy, D.K., Howell, L.L., Bowden, A.E., 2013. Intervertebral disc degeneration alters lumbar spine segmental stiffness in all modes of loading under a compressive follower load. *Spine J.* 13, 1134–47.

## Annexes

### Annex A: Calculation of the constants of the Table 2.4.

By the use of a DMA or a Mechanical spectrometer, in an oscillatory shear experiment, a sample, exposed to a sinusoidal strain ( $\gamma$ ) at an angular frequency of ( $\omega$ ), will present a gradual approach to a steady sinusoidal stress ( $\sigma$ ). The relation between these parameters is given by the Equations 8.1 and 8.2.

$$\gamma = \gamma_0 \sin \omega t \quad \text{Equation 8.1}$$

$$\sigma = \gamma_0 (G'(\omega) \sin \omega t + G''(\omega) \cos(\omega t)) \quad \text{Equation 8.2}$$

Where  $G'$  represents the shear storage modulus and  $G''$  represents the shear loss modulus. The complex shear modulus ( $G^*$ ) results from a real and an imaginary component, which evidences the intrinsic elastic and viscous nature of the material. Thus,  $G^*$  can be calculated by the Equation 9.3.

$$G^* = G' + iG'' \quad \text{Equation 8.3}$$

The method of  $\delta$  (phase shift angle),  $E'$  (storage modulus),  $E''$  (loss modulus) and  $\tan \delta$  (coefficient of friction) is detailed described in Chapter 5, Section 5.2.4.

The aggregate modulus,  $H_{A0}$ , and the zero-strain permeability,  $K_0$ , presented in Table 2.4, were previously described by Périé et al. (2005). These parameters describe the elastic behavior of the solid matrix and were determined used a non-linear regression of the Equation 8.4 to the equilibrium stress-stretch data:

$$\sigma = \frac{1}{2} H_{A0} \left( \frac{\lambda^2 - 1}{\lambda^{2\beta+1}} \right) e^{[\beta(\lambda^2-1)]} \quad \text{Equation 8.4}$$



While the parameters of the Equation 8.5 were determined by the non-linear regression for the Equation 8.6 to the experimental stress-relaxation, by means of the use of the difference scheme previously reported by Ateshian et al. (1997).

$$k = k_0 \left( \frac{\lambda - \phi_0^s}{1 - \phi_0^s} \right)^2 e^{[M(\lambda^2 - 1)/2]} \quad \text{Equation 8.5}$$

$$\frac{\delta \sigma^e}{\delta \lambda} \frac{\delta^2 u}{\delta z^2} = \frac{\lambda}{k} \frac{\delta u}{\delta t} \quad \text{Equation 8.6}$$

The parameters of the both Equations 8.5 and 8.6 were given by the work performed by Ateshian et al. (1997).

Concerning to the toe modulus ( $E_{toe}$ ), the static compressive modulus ( $E_s$ ) and the Poisson's ratio ( $\nu$ ) parameters, they were determined as described by Cloyd et al. (2007). Using the equation of the regression curve of the non-linear stress-strain at the end of each relaxation period, the toe-region modulus was calculated as the slope of this curve at 0% strain. The static compressive modulus was determined by means of the slope of the stress-strain curve at 20% strain. The Poisson ratio was calculated using the Equation 8.7.

$$\nu = -\varepsilon_1 / \varepsilon \quad \text{Equation 8.7}$$

Where the ( $\varepsilon_1$ ) represents the lateral strain, obtained as the change in diameter over the initial diameter of the cylindrical sample and the axial strain ( $\varepsilon$ ) was calculated by the change in cross-head displacement over initial height, obtained during the experimental tests.

The dynamic stiffness reported by Boxberger et al. (2009) was calculated as the quotient between the load ( $L_0$ ) and the displacement ( $d_0$ ) amplitudes in a dynamic compressive test (Equation 8.8).

$$K_d = L_0/d_0 \quad \text{Equation 8.8}$$

Finally, the damping capacity ( $DC$ ) was obtained by the Equation 8.9.

$$DC = \Delta W/W \quad \text{Equation 8.8}$$

Where  $\Delta W$  is the energy loss per loading cycle or hysteresis and  $W$  is the work input per loading cycle.

**Annex B: The engineering drawings for the testing devices that were specially designed and/or manufactured to carry out the experimental testing detailed in Chapter 4.**

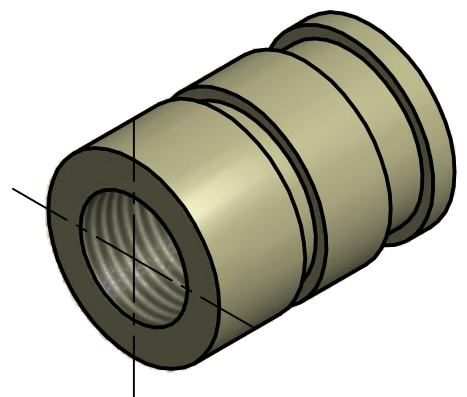
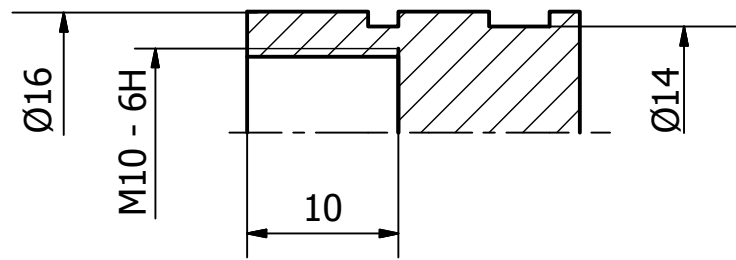
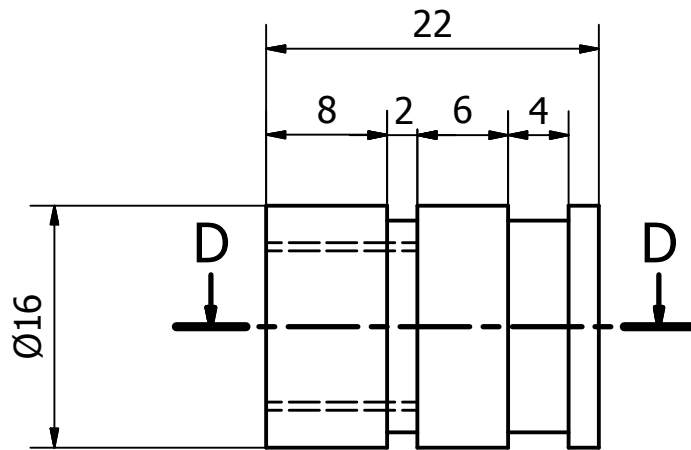
**B.1.** The technical drawing of the nylon piston (D1);

**B.2.** The technical drawing of the assembled piston (D2);

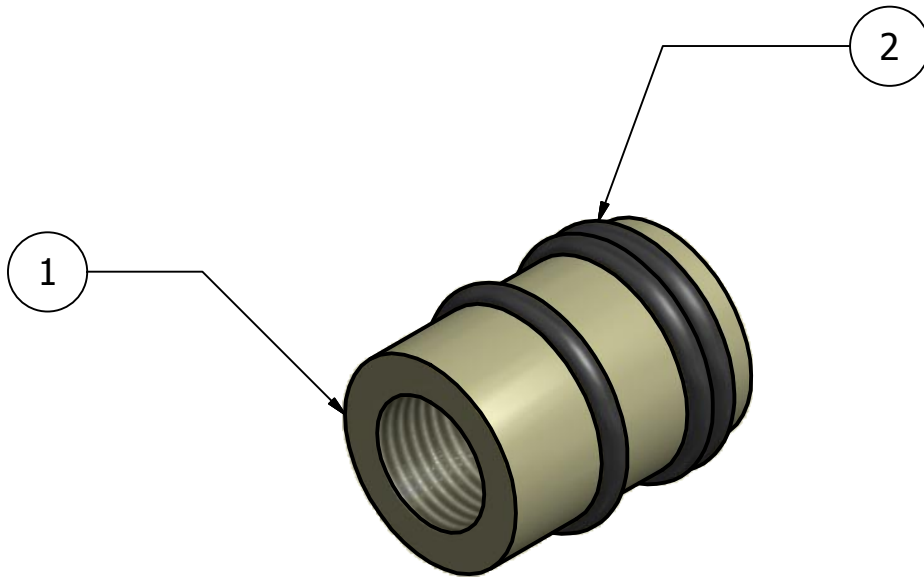
**B.3.** The technical drawing of the stainless steel hydraulic cylinder (D3).

**B.4.** The technical drawing of the stainless-steel basis for the motion segment placement (D4);

**B.5.** The technical drawing of the self-tapping screw (D5).



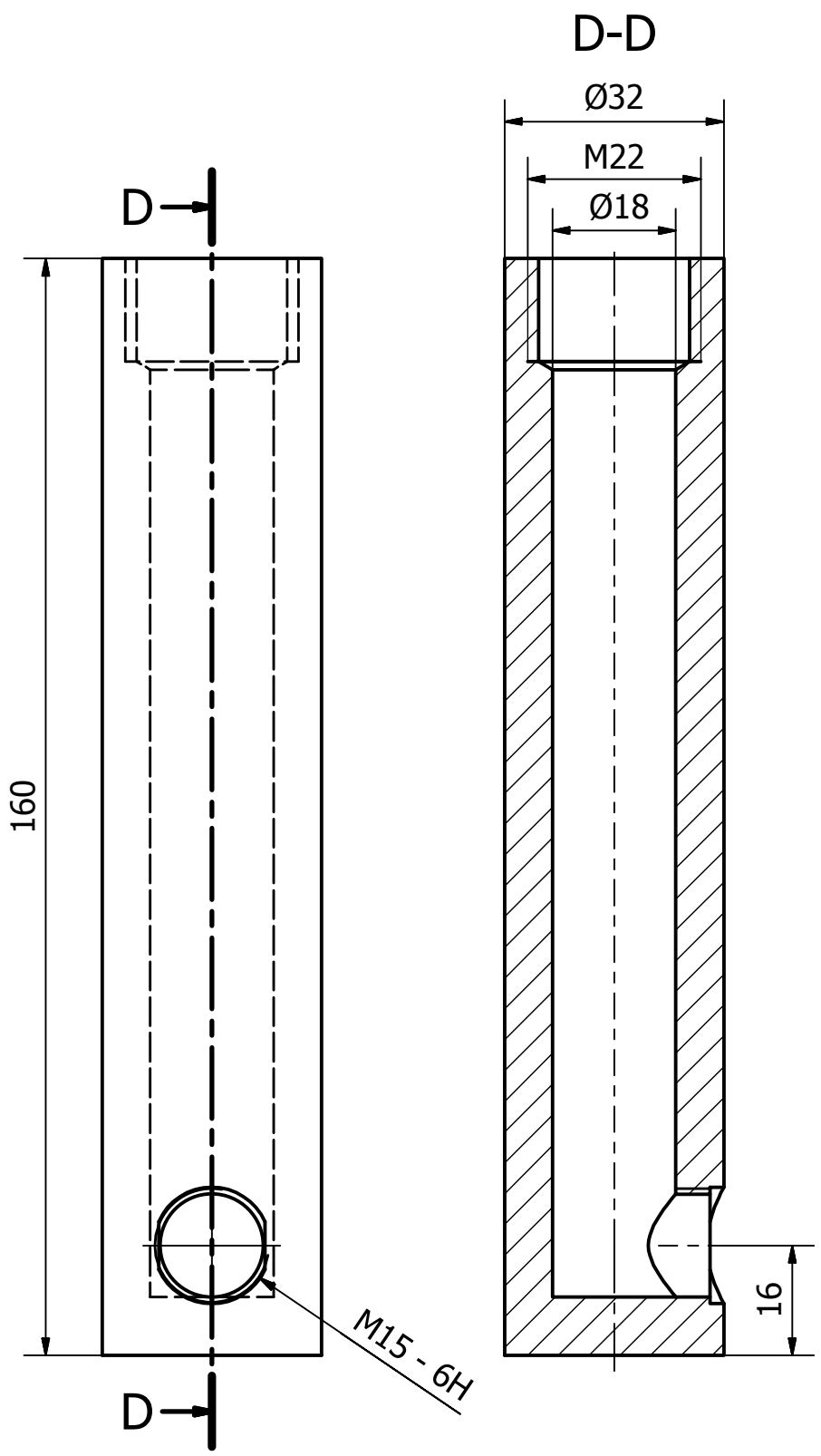
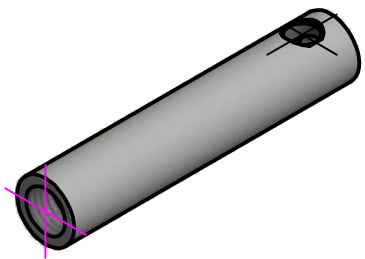
Projec.	28-10-2015	A. Araújo	PhD - Ângelo Araújo	CT2M - UMinho	
Desenh.	28-10-2015	A. Araújo			
Copiou	28-10-2015	A. Araújo			
Verific.	28-10-2015	M. Pinho			
Escala:	Nylon Piston			D1	
2 : 1					
Toler.					



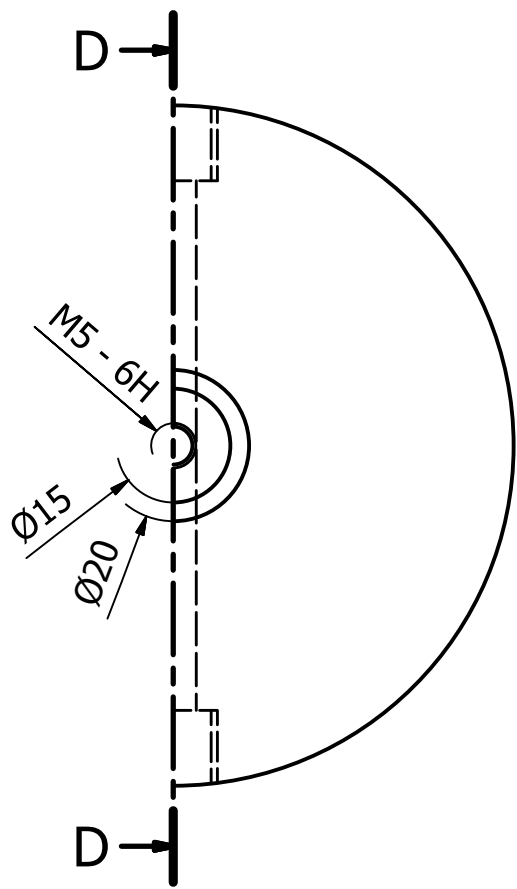
Parts List			
PART NUMBER	QTY	NAME	DESCRIPTION
1	1	Piston	D1
2	3	O-Ring	D2

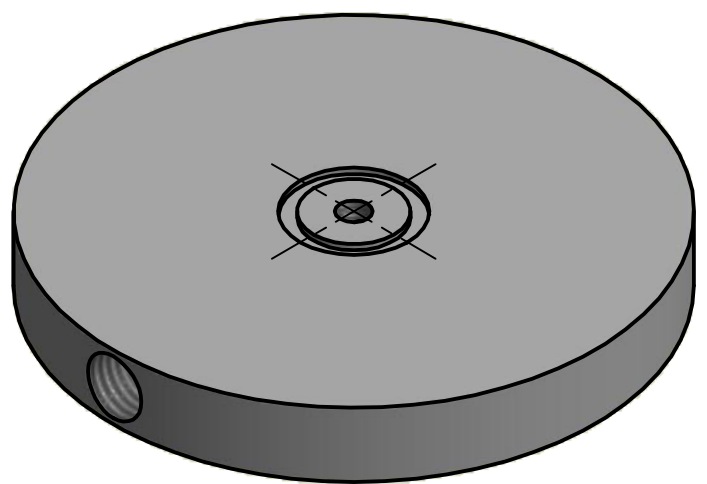
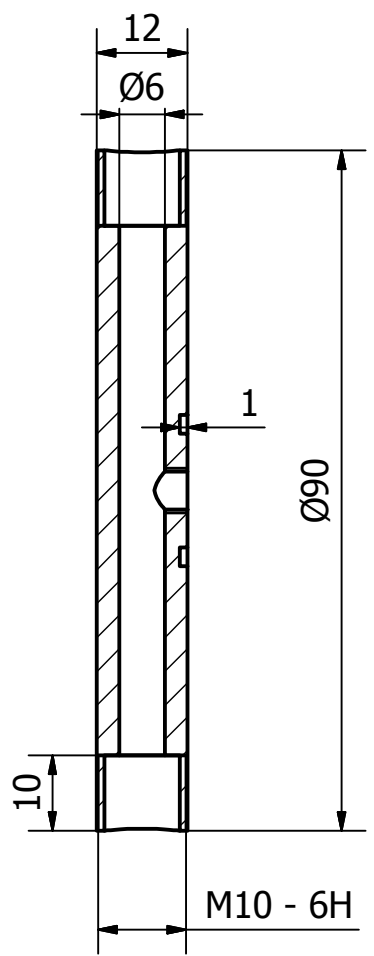
Projec.	28-10-2015	A. Araújo	PhD - Ângelo Araújo	CT2M - UMinho
Desenh.	28-10-2015	A. Araújo		
Copiou	28-10-2015	A. Araújo		
Verific.	28-10-2015	M. Pinho		
Escala:	Piston Assembly			
2 : 1				
Toler.				



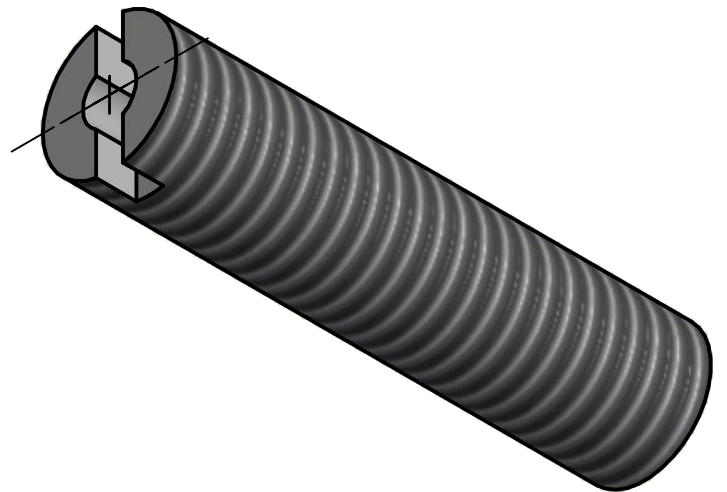
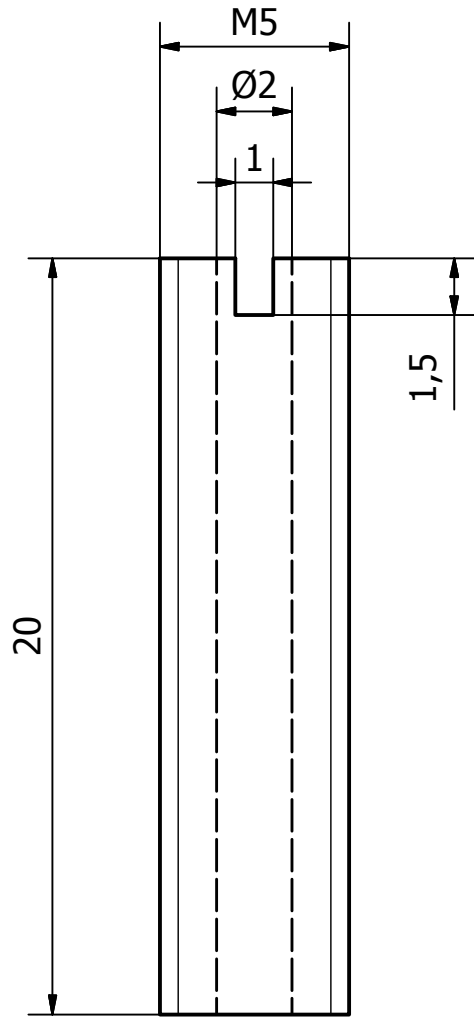
Projec.	28-10-2015	A. Araújo	PhD - Ângelo Araújo	CT2M - UMinho	
Desenh.	28-10-2015	A. Araújo			
Copiou	28-10-2015	A. Araújo			
Verific.	28-10-2015	M. Pinho			
Escala:	Stainless Steel Hydraulic Cylinder			D3	
1 : 1					
Toler.					



D-D



Projec.	28-10-2015	A. Araújo	PhD - Ângelo Araújo	CT2M - UMinho
Desenh.	28-10-2015	A. Araújo		
Copiou	28-10-2015	A. Araújo		
Verific.	28-10-2015	M. Pinho		
Escala:	Stainless Steel Basis			D4
1 : 1				
Toler.				



Projec.	28-10-2015	A. Araújo	PhD - Ângelo Araújo	CT2M - UMinho				
Desenh.	28-10-2015	A. Araújo						
Copiou	28-10-2015	A. Araújo						
Verific.	28-10-2015	M. Pinho						
Escala:	Self-tapping Screw			D5				
<b>5 : 1</b>								
Toler.								



**Annex C: The material and mechanical characteristics of the “Ravioli”, provided by the manufacturer - Nicast Ltd.)**

**C.1.** The final formulation of the Core-A, the Hydromed hydrogel.

<b>Hydrogel final characteristics</b>	
<b>Raw Material</b>	HM D650
<b>Solvent</b>	95% Et-OH
<b>Drying</b>	Few hours at 35°
<b>Free swelling (in water)</b>	900%

**C.2.** The tensile strength properties of the “Envelope” for the final configuration adopted – Env<sub>2</sub>, under different conditions (dry and wet).

<b>Env<sub>2</sub></b>	<b>Dry “Envelope”</b>	<b>Wet “Envelope”</b>
<b>Break Force [N]</b>	10.80	11.93
<b>Elongation at Break [mm]</b>	141.50	140.24
<b>Elongation at Break [%]</b>	253.75	250.59
<b>Ultimate Tensile Stress [MPa]</b>	3.73	3.88

**C.3.** The final parameters of the Raviolis given by the manufacturers (Nicast Ltd.).

<b>Ravioli Diameter (mm)</b>	<b>“Envelope” Thickness (mm)</b>	<b>Welding Beginning (mm)</b>	<b>Dry Core Weight Average (mg HM)</b>	<b>Core Weight after Swelling 24h Average (mg HM)</b>	<b>Height after Swelling 24h Average (mm)</b>
8	0.2	6.6	9.4	82	4.55
9	0.2	7.0	12.26	96	5.315
14	0.2	10.5	45	400	7.27

**C.4.** The expansion of the “Ravioli” and the unconfined compressive properties of the Ravioli, determined by the Nicast Lda.

<b>Core Weight (mg)</b>	<b>Ravioli Weight (mg)</b>	<b>Ravioli Weight after Swelling 24h (mg)</b>	<b>Ravioli Swelling in 24h (mg)</b>	<b>Break Force (N)</b>	<b>Compression at Break (N)</b>
40	62.3 ± 0.5	424.0 ± 7.9	1004.2 ± 20.4	178.3 ± 8.5	4.6 ± 0.3
60	82.3 ± 0.9	583.7 ± 13.8	935.6 ± 22.0	238.0 ± 32.6	6.0 ± 0.4
80	102.7 ± 3.3	745.0 ± 22.7	902.9 ± 25.3	78.3 ± 10.3	3.1 ± 0.2
100	124.7 ± 0.94	878 ± 10.8	853.3 ± 10.5	58.0 ± 17.0	2.8 ± 0.2

## **Annex D: Publications and Communications**

Araújo, A., Peixinho, N., Pinho, A. and Claro J.C.P., 2015. The mechanical response of the reinforced-ground matrix in the porcine annulus fibrosus to uniaxial compressive loading. In: *Materiais 2015 - XVII Conference of Sociedade Portuguesa dos Materiais*.

*The annulus fibrosus on the intervertebral disc presents a highly organized structure and composition, with nonlinear and anisotropic properties, which undergoes on an intricate combination of loads from several orientations during the daily routine. The purpose of this study is to determine the mechanical behaviour of the annular ground matrix under unconfined uniaxial compressive load and compared the response of annulus fibrosus to the application of both physiological and non-physiological strains. The results indicated that the analytical model presents an excellent fit on all the loading cycles applied on the samples ( $R^2 \geq 0.995$ ). It was found that there are significant differences between the loading the initial and the repeated loading cycles. The experimental data have confirmed that although the stiffness of the reinforced matrix generally decreases on repeated loading, this tissue still remains capable of withstand the mechanical loading. Thus, this event showed that even though the tissue had been subjected to a damaging strain, this structure is capable of withstand the compressive loading acting on disc. However, the mechanical properties of this tissue changed after the submitting this structure to injuring deformations; thus, its response to mechanical loading also alters after the application of non-physiological strains.*

Araújo, A., Peixinho, N., Pinho, A., Claro J.C.P, 2015. Comparison between the dynamic and initial creep response of porcine and human lumbar intervertebral discs. In: *IEEE 4th Portuguese Meeting on Bioengineering (ENBENG)*.

DOI: [10.1109/ENBENG.2015.7088868](https://doi.org/10.1109/ENBENG.2015.7088868)

*The study of mechanical properties of intervertebral disc (IVD) is important for the evaluation of disc implants. To determine these properties, several animal spine models were used. The goal of this work is to determine and compare the dynamic stiffness coefficient ( $K_d$ ) and initial*

*creep behavior of porcine intervertebral disc with the human ones. Porcine lumbar "motion segments" were subjected to 1200 cycles of axial compressive loading at 1 Hz, and a mean load of 500 N. The results were fitted with a mathematical model. The Kd values are in same magnitude as the previously reported for human. The model showed a good adjust to the initial creep behavior and the obtained parameters present the same magnitude as the human discs, with exception of time constant. This work revealed that porcine MS is an interesting model to study both the dynamic behavior and initial creep response of human disc.*

Araújo, A., Peixinho, N., Pinho, A., Claro J.C.P., (Accepted on 15/01/2015). Quasi-static and Dynamic Properties of the Intervertebral Disc: Experimental Study and Model Parameters Determination for the Porcine Lumbar Motion Segment. In: Acta of Bioengineering and Biomechanics.

DOI: [10.5277/ABB-00153-2014-0](https://doi.org/10.5277/ABB-00153-2014-0)

*The study of axial loading is essential to determine the properties of intervertebral disc. The objectives of this work are (1) to quantify the mechanical properties of porcine lumbar intervertebral discs under static and cyclic compressive loading and (2) to determine the parameters of a five-parameter rheological model for porcine and compare them with those obtained for human lumbar intervertebral discs. Thus, the porcine lumbar motion segments were subjected to quasi-static and dynamic compression tests. The quasi-static tests were used to obtain the static stiffness coefficient at different strain rates, while the data from the cyclic compressive tests were used to both determine the dynamic stiffness coefficient and to be fitted in a 5-parameter model, in order to simulate the creep response of the porcine intervertebral discs. The results demonstrated that dynamic stiffness coefficient of porcine discs is between four and ten times higher than the static stiffness coefficient, depending on load applied. The parameters of the rheological model suggested a low permeability of nucleus and endplate during the fast response of porcine discs. In addition, the fast response in terms of displacement is four times higher than those documented for human discs. This*

*study revealed that care must be taken on the comparison between porcine and human discs, since they present different behaviour under quasi-static and dynamic compressive loading.*

Araújo, A., Peixinho, N., Pinho, A., Claro J.C.P., 2014. Novel Methodology to Assess the Relaxation Rate of the Intervertebral Disc by Increments on Intradiscal Pressure. In: Applied Mechanics and Materials, Vol. 664, pp. 379-383.

DOI: [10.4028/www.scientific.net/AMM.664.379](https://doi.org/10.4028/www.scientific.net/AMM.664.379)

*The Intervertebral Disc is subjected to several types of loading during daily routine events. However, the overloading on this structure induces higher Intradiscal Pressure, which could cause severe damage on its structure. This study describes a new approach to that allows monitorize and pressurize nuclear region of the IVD, with a cartilaginous endplate access, by the insertion of an external fluid, while a Motion Segment (MS-assembly composed by vertebra-disc-vertebra) is compressed at a physiological load. This methodology includes the use of a pneumatic structure that applies a certain pressure on the hydrostatic system, forcing a fluid to enter into the MS through a screw, with a drilled hollow along its entire length. Preliminary results indicated that this methodology presents high potential to efficiently pressurize the IVD, providing a useful tool to better understand the response of this structure under pressure.*

Araújo, A., Peixinho, N., Pinho, A., Claro J.C.P., 2015. On the experimental intradiscal pressure measurement techniques: a review. In: New Trends in Mechanism and Machine Science - Mechanisms and Machine Science, Vol. 24, pp. 243-250.

DOI: [10.1007/978-3-319-09411-3\\_26](https://doi.org/10.1007/978-3-319-09411-3_26)

*The intradiscal pressure has been essential for prevent the spinal complaints by forming a basis for clinical advice to promote the correct sitting postures. As a consequence, it is evident the need of an accurate method for measure the intradiscal pressure, to better understand the disc response to hydorstatic pressure fluctuations. Numerous reviews regarding disc mechanics are available, including intradiscal pressure benchmarks; however,*

*an analysis on the techniques of intradiscal pressure measurement is needed. Therefore, this review will remain focused on the methodologies adopted for measure the intradiscal pressure in several conditions: for different daily activities, under external loads and for values where occurs annulus fibrosus disruption. The importance of the intradiscal pressure on disc function will be discussed as well as the some guidelines for design new measurement techniques will be defined.*

Araújo, A., Peixinho, N., Pinho, A., Claro J.C.P., 2013. A novel methodology for measure the intradiscal pressure and height disc variation of intervertebral disc under compression. In: 5<sup>o</sup> Congresso Nacional de Biomecânica.

*The intervertebral disc is subjected to several types of loading during daily routine events. However, the overloading on this structure induces higher intradiscal pressure, which could cause severe damage on its structure. This study describes a new methodology to monitor both IDP and height disc variation by applying external pressure, while a motion segment (assembly composed by vertebrae-disc-vertebrae) compressed at a physiological load.*

Araújo, A., Peixinho, N., Pinho, A., 2012. Stress characterization of intervertebral disc on radial direction: an experimental approach. Proceedings of European Society of Biomechanics (Poster Presentation), Vol. 45, Suppl. 1, pp. S620.

DOI: [http://dx.doi.org/10.1016/S0021-9290\(12\)70621-8](http://dx.doi.org/10.1016/S0021-9290(12)70621-8)